Technical Report CERC-89-9
April 1996

US Army Corps of Engineers
Waterways Experiment Station

Coastal Engineering Research Program

SBEACH: Numerical Model for Simulating Storm-Induced Beach Change

Report 4
Cross-Shore Transport Under Random Waves and Model Validation with SUPERTANK and Field Data

by *Randall A. Wise, S. Jarrell Smith, WES*
Magnus Larson, University of Lund

Prepared for Headquarters, U.S. Army Corps of Engineers

Coastal Engineering Research Program

Technical Report CERC-89-9
April 1996

SBEACH: Numerical Model for Simulating Storm-Induced Beach Change

Report 4
Cross-Shore Transport Under Random Waves and Model Validation with SUPERTANK and Field Data

by Randall A. Wise, S. Jarrell Smith

U.S. Army Corps of Engineers
Waterways Experiment Station
3909 Halls Ferry Road
Vicksburg, MS 39180-6199

Magnus Larson

Department of Water Resources Engineering
Lund Institute of Technology
University of Lund
Box 118, Lund, Sweden S-221 00

Report 4 of a series

Approved for public release; distribution is unlimited

Prepared for U.S. Army Corps of Engineers
Washington, DC 20314-1000

Under Work Unit 32530

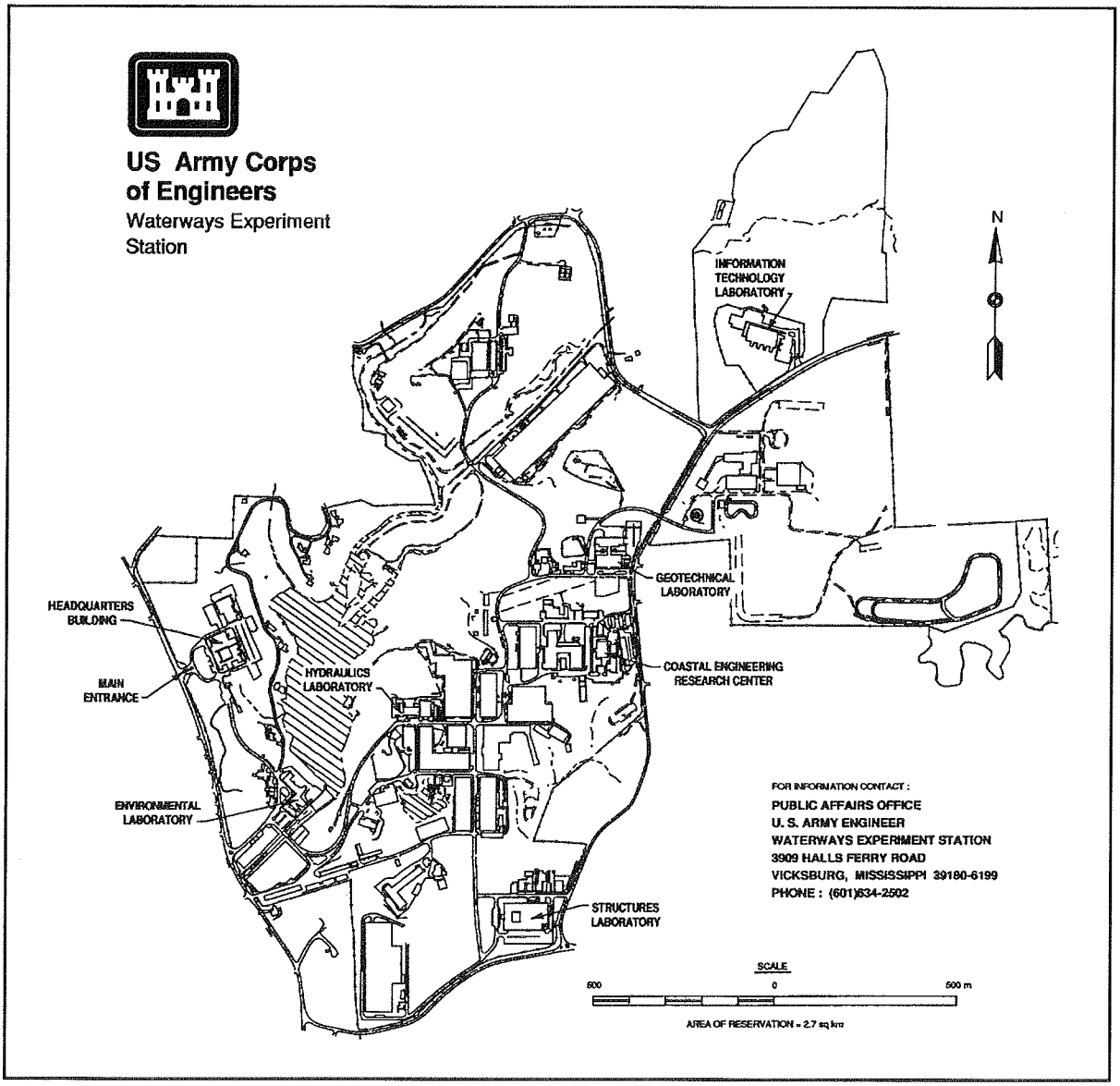

Waterways Experiment Station Cataloging-in-Publication Data

Wise, Randall A.

SBEACH : numerical model for simulating storm-induced beach change. Report 4, Cross-shore transport under random waves and model validation with SUPERTANK and field data / by Randall A. Wise, S. Jarrell Smith, Magnus Larson ; prepared for U.S. Army Corps of Engineers.

266 p. : ill. ; 28 cm. — (Technical report ; CERC-89-9 rept.4)

Includes bibliographic references.

Report 4 of a series.

1. SBEACH (Computer program) 2. Beach erosion — Mathematical models. 3. Sediment transport — Mathematical models. 4. Storm surges — Mathematical models. I. Smith, S. Jarrell. II. Larson, Magnus. III. United States. Army. Corps of Engineers. IV. U.S. Army Engineer Waterways Experiment Station. V. Coastal Engineering Research Center (U.S. Army Engineer Waterways Experiment Station) VI. Coastal Engineering Research Program (U.S.) VII. Title. VIII. Title: Numerical model for simulating storm-induced beach change. IX. Title: Cross-shore transport under random waves and model validation with SUPERTANK and field data. X. Series: Technical report (U.S. Army Engineer Waterways Experiment Station) ; CERC-89-9 rept.4.
TA7 W34 no.CERC-89-9 rept.4

Contents

List of Figures

List of Tables

Preface

This study was conducted at the Coastal Engineering Research Center (CERC), U.S. Army Engineer Waterways Experiment Station (WES), Vicksburg, MS, and the Department of Water Resources Engineering (DWRE), Institute of Science and Technology, University of Lund (UL), Lund, Sweden. Work at WES was authorized as part of the Civil Works Research and Development Program by Headquarters, U.S. Army Corps of Engineers (HQUSACE), and was performed under the Calculation of Cross-Shore Sediment Transport and Beach Profile Change Work Unit 32530, Shore Protection and Restoration Program, CERC. Messrs. John H. Lockhart, Jr., Barry W. Holliday, and Charles Chesnutt were HQUSACE Technical Monitors. Ms. Carolyn M. Holmes was CERC Program Manager.

This study was performed and the report prepared over the period 21 October 1992 through 15 September 1995. Dr. Magnus Larson, UL, and Mr. Randall A. Wise, Coastal Processes Branch (CPB), Research Division (RD), CERC, who was Principal Investigator (PI) of the Calculation of Cross-Shore Sediment Transport and Beach Profile Change Work Unit, developed the enhancements to the Storm-induced BEAch CHange (SBEACH) model presented in this report. Mr. Wise, and Mr. S. Jarrell Smith, CPB, RD, conducted the model evaluation studies. Mr. Peter J. Neilans, CPB, RD assisted in running model simulations during the model evaluation studies. This report was written by Mr. Wise, Dr. Larson, and Mr. Smith. Ms. Holley Messing, Civil Engineer Technician, CPB, RD, generated most of the figures presented herein and assisted with preparation of the final document. Mr. Mark Gravens, CPB, RD, Ms. Julie Rosati, CPB, RD, Mr. Neilans, and Mr. Bruce A. Ebersole, Chief, CPB, RD, provided technical review of this report.

Work at CERC was performed under the general supervision of Dr. James R. Houston and Mr. Charles C. Calhoun, Jr., Director and Assistant Director, respectively, of CERC, and the administrative supervision of Mr. H. Lee Butler, Chief, RD, and Mr. Ebersole, Chief, CPB.

At the time of publication of this report, Director of WES was Dr. Robert W. Whalin. Commander was COL Bruce K. Howard, EN.

1 Introduction

Beaches erode and accrete in response to varying waves, water levels, and currents in the nearshore zone. During storms, catastrophic beach and dune erosion can occur in a matter of hours, resulting in significant shoreline recession and damage to property and upland resources. Consequently, protection of upland infrastructure against storm erosion, flooding, and wave attack is a primary concern in the field of coastal engineering. Beach nourishment has become a preferred method of providing such protection, and many beach-fill projects have been designed and constructed in the past several years. Effective design of beach fills for shore protection requires an understanding of and the capability to predict sediment transport processes that control beach response to storms. Numerical modeling of beach evolution is a powerful technique that can be applied to assist in project design. Numerical models provide a framework for predicting project response, objectively evaluating design alternatives, and analyzing data to develop an understanding of coastal processes. The Storm-induced BEAch CHange (SBEACH) numerical model has been developed as an engineering tool for simulating beach profile evolution in response to storms.

This report is fourth in a series describing development of the SBEACH model. The first report in the SBEACH series (Larson and Kraus 1989a) describes initial model development including formulation of the approach, empirical foundation of the model, and initial tests and verification with large-scale laboratory data and limited field data. The second report (Larson, Kraus, and Byrnes 1990) describes the numerical solution procedure and includes model verification and sensitivity tests using field data and hypothetical cases. Model capabilities and limitations are also discussed. The third report (Rosati et al. 1993) serves as the User's Manual and provides guidance for model application. The User's Manual discusses model input/output, interface operation, and model calibration. A set of tutorial exercises is included to give step-by-step instruction in model operation. The objective of the present report is to describe recent model enhancements that have been developed to improve calculation of sediment transport under random waves. Also, a comprehensive evaluation of model capabilities in predicting beach and dune erosion is presented using high-quality laboratory

and field data of beach profile change. A brief overview of the SBEACH model is provided below as background for the present study.

Overview of SBEACH

SBEACH is an empirically based numerical model for simulating two-dimensional cross-shore beach change. The model was initially formulated using data from prototype-scale laboratory experiments and further developed and verified based on field measurements (Larson and Kraus 1989a; Larson, Kraus, and Byrnes 1990) and sensitivity testing (Larson and Kraus 1989b, 1991). SBEACH calculates mesoscale beach profile change (Larson and Kraus 1994,1995) with emphasis on beach and dune erosion and bar formation and movement. The model is intended for predicting short-term profile response to storms.

A fundamental assumption of the SBEACH model is that profile change is produced solely by cross-shore processes, resulting in a redistribution of sediment across the profile with no net gain or loss of material. Longshore processes are considered to be uniform and neglected in calculating profile change. This assumption is expected to be valid for short-term storm-induced profile response on open coasts away from tidal inlets and coastal structures. In calculating beach profile change, the model assumes that cross-shore sediment transport is produced by breaking waves and changes in water level. SBEACH includes an internal wave model which calculates the cross-shore variation in wave height and water level setup across the beach profile. With information from the wave model, cross-shore sediment transport rates are calculated using relationships derived from empirical analysis of laboratory and field data of beach profile change. The wave model and sediment transport relationships previously used in SBEACH were developed based on monochromatic waves. In the present version of the SBEACH model, wave transformation and sediment transport rates are calculated using random wave properties to improve prediction of profile change in field applications.

SBEACH requires data typically available in engineering studies to calculate beach profile response. For project applications, primary input to SBEACH includes time histories of wave height, wave period, and total water elevation (tide and surge); pre- and post-storm beach profile survey data; and median sediment grain size. Optionally, wave direction and wind speed and direction can also be specified. Sampling intervals of input wave and water level time histories usually range from 1 to 4 hr. Input required for model configuration includes parameters such as grid size, time-step, and transport rate coefficient. Typical values of model grid size and time-step are 3 m and 5 min, respectively. The model operates through a user interface which facilitates data input, model execution, and analysis of model results.

A principal application of SBEACH is in the design of beach fills. SBEACH is used to calculate beach profile response of alternative design configurations to storms of varying intensity. Model predictions of beach erosion are used to estimate with- and without-project storm damages over the project design life. In the design process, storm erosion, flooding, and wave damage estimates are utilized in economic analyses to compare total project costs and total project benefits (including storm damage reduction benefits) for each design alternative. The design alternative which maximizes net project benefits is typically selected. Thus, accurate model prediction of beach and dune erosion in response to storms is important in defining and optimizing both the physical performance and economic feasibility of beach-fill projects. In the present study, predictive capabilities of SBEACH are evaluated using field data to provide a level of confidence in model results for project applications.

Scope of Report

Chapter 1 provides an introduction and brief overview of the SBEACH model. Chapter 2 describes the development and implementation of the random wave model included in SBEACH. Chapter 3 discusses the formulation of sediment transport relationships for random waves and describes a dune overwash algorithm that has been developed to improve prediction of dune erosion during extreme events. In Chapter 4, SBEACH is applied using large-scale laboratory data from the SUPERTANK project (Kraus and Smith 1994) to evaluate model predictions for various wave and water level conditions and beach configurations. Chapter 5 includes case studies of beach and dune erosion for several sites and storm conditions to evaluate model predictions in the field. Chapter 6 provides concluding observations from the study.

Simulation results for SUPERTANK case studies and for field case studies are presented in Appendixes A and B, respectively. Appendix C provides the notation for signs and symbols used in this report.

2 Random Wave Model

An important factor influencing beach profile change is the degree of randomness in the incident wave field. Monochromatic waves are characterized by a single offshore wave height and period. As individual waves in a monochromatic wave field propagate shoreward, they break at a common point on the profile corresponding to the breaking depth. Such uniform breaking conditions produce a pronounced bar and trough on the beach profile. In contrast, a random wave field consists of individual waves with different height and period that break at varying locations across the profile. The more evenly distributed forcing of random waves tends to produce a profile with less pronounced morphological features as compared to monochromatic waves (Larson and Kraus 1994). Also, in a random wave field, individual waves that are potentially constructive or destructive to the beach may exist simultaneously, which make it more difficult to assess the net effect on the profile evolution.

The effect of randomness on beach profile change is particularly important in the field, where seas are characterized by random waves. Previously, the SBEACH profile change model utilized a monochromatic wave model to represent random wave processes. This approach provided reasonable results as a first approximation. However, in order to achieve a more realistic description of beach profile change under random waves, a random wave model is required. This chapter presents the random wave model (Larson 1995) that has been implemented in SBEACH.

Modeling Approach and Assumptions

Several models have been proposed for describing wave decay in the surf zone, differing mainly in the formulation of the energy dissipation due to breaking and whether they were developed for monochromatic or random waves (Battjes and Janssen 1978; Thornton and Guza 1983; Svendsen 1984; Dally, Dean, and Dalrymple 1985). The models for random waves transform a representative statistical wave height across shore, typically the root-mean-square (rms) wave height, and require some assumptions to be made about the probability distribution function (pdf) for the waves in the surf zone. Another

class of models include those that were originally based on the study of monochromatic waves and have been modified to simulate transformation of random waves by using a wave-by-wave approach or Monte Carlo simulation technique (Dally 1990, 1992; Larson and Kraus 1992). The Monte Carlo simulation technique involves transforming many individual wave components from a random wave distribution, and determining the wave characteristics across the surf zone by superposition of the individual wave components. This technique has been verified with high-quality field data and has the inherent advantage of not requiring an assumption about the shape of the pdf in the surf zone. However, Monte Carlo simulations require transforming a large number of individual waves or representative wave components to achieve a reliable estimate of wave statistics in the surf zone. This approach is not well suited for time-dependent beach erosion models such as SBEACH, because of the extensive number of wave calculations that would be required at each model time-step.

Similar to the Monte Carlo simulation technique, the present random wave model assumes that wave properties at any point across the profile may be obtained by individually transforming a large number of waves and adding the effects of each single wave component. However, the present model is formulated using statistical relationships such that transformation of only a single representative wave height is required. As the representative wave height is transformed across shore, the fractions of broken, unbroken, and reformed waves are determined and used in the calculation to represent random wave properties. This formulation provides for a realistic description of random waves while at the same time requiring only a single wave transformation. Given the same incident wave conditions, this semi-analytic model reproduces macroscale features of wave height transformation across the surf zone, including breaking and reformation, in agreement with the Monte Carlo approach that involves transformation of many individual waves (Larson 1995).

The model assumes that a random wave field is characterized at some point offshore by a pdf for the wave height, a peak spectral wave period, and a mean incident wave angle. Thus, it is assumed that the sea is narrow-banded in frequency and direction, and that the randomness of the sea enters only through the chosen pdf for the wave height. The offshore point where the wave height pdf is defined is assumed to be at a depth where wave breaking is negligible.

Theoretical Development

Wave height distribution

Seaward of the surf zone, where no wave breaking occurs, the variation in wave height is assumed to follow a Rayleigh distribution (Longuet-Higgins

1952). The probability density function for the Rayleigh distribution is given in terms of the rms wave height H_{rms} according to

$$p(H)dH = \frac{2H}{H_{rms}^2} e^{-\left(\frac{H}{H_{rms}}\right)^2} dH \tag{1}$$

where $p(H)$ is the probability density of a given wave height H. The integrated form of Equation 1 gives the distribution function

$$F(H) = 1 - e^{-\left(\frac{H}{H_{rms}}\right)^2} \tag{2}$$

where $F(H)$ denotes the probability that a given wave has a height below a certain value H. Figure 1 displays a plot of the probability density and distribution function for a Rayleigh distribution, with the wave height normalized by H_{rms}.

For a wave field with a total number of waves N, the rms wave height at a given location on the profile is defined by

$$H_{rms}^2 = \frac{1}{N}\sum_{i=1}^{N} H_i^2 \tag{3}$$

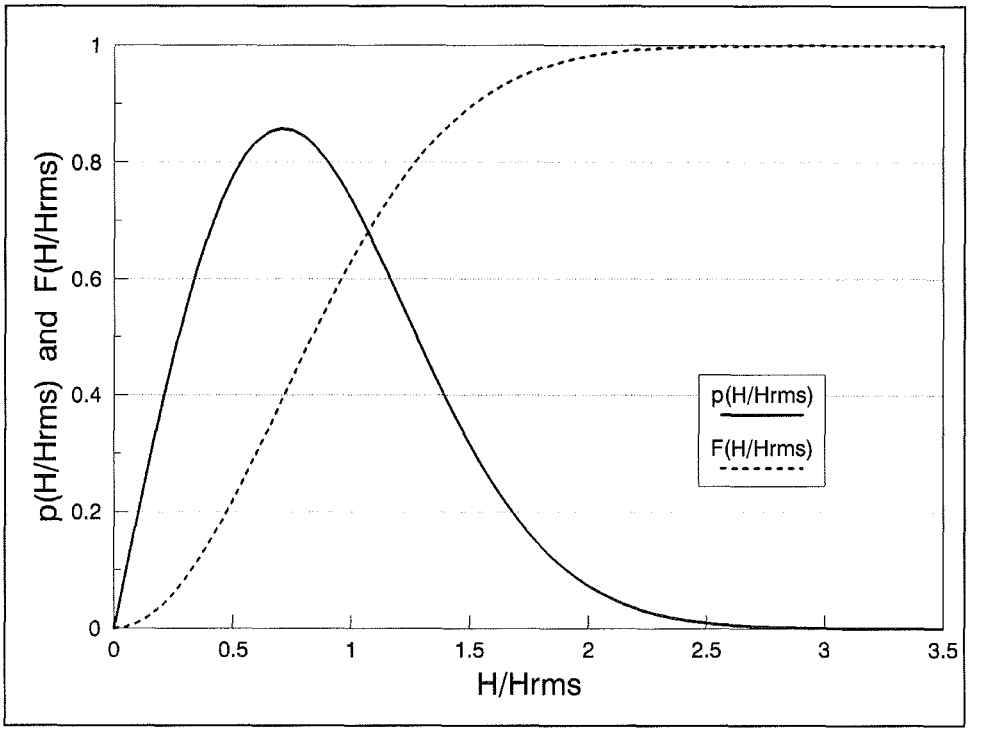

Figure 1. Probability density and distribution function for a Rayleigh distribution

where H_i is the height of the i-th individual wave. Seaward of wave breaking, all individual waves in a Rayleigh-distributed wave field are described by Equation 1, given a value of H_{rms}. However, as the waves propagate onshore, the higher waves experience depth-limited breaking, and a Rayleigh distribution is less suited for characterizing the random variation in wave height. In order to account for changes in wave height distribution produced by breaking waves, Equation 3 is expressed as

$$H_{rms}^2 = \frac{1}{N}\sum_{i=1}^{N} H_i^2 = \frac{1}{N}\sum_{i=1}^{n(x)} H_i^2 + \frac{1}{N}\sum_{i=1}^{m(x)} H_i^2 \tag{4}$$

where n is the number of nonbroken waves and m is the number of broken waves at a given location x on the profile. In Equation 4, H_{rms} is the rms wave height for both broken and nonbroken waves.[1] The number of broken and nonbroken waves ($m + n$) at each location on the profile is equal to the total number of waves N in the wave field (i.e., the number of waves is conserved across the profile).

The fraction of broken waves is defined as $\alpha = m/N$, and the fraction of nonbroken waves is given by $n/N = (N - m)/N = 1 - \alpha$. The following definitions are introduced

$$H_n^2 = \frac{1}{n}\sum_{i=1}^{n(x)} H_i^2 \tag{5}$$

$$H_m^2 = \frac{1}{m}\sum_{i=1}^{m(x)} H_i^2 \tag{6}$$

where H_n and H_m are the rms wave heights for nonbroken and broken waves, respectively. Using α together with Equations 5 and 6, Equation 4 is expressed in the form

$$H_{rms}^2 = (1 - \alpha)\, H_n^2 + \alpha\, H_m^2 \tag{7}$$

In the general case, nonbroken waves consist both of unbroken waves and waves that were broken but have re-formed at some seaward point. To account for wave re-formation, the number of unbroken waves at a specific location x is defined as u and the number of re-formed waves is defined as r, with the number of nonbroken waves given as $n = u + r$. The total number of waves remains constant at $N = u + r + m$. Using these definitions, Equation 4 is modified to yield

---

[1] The following terminology is employed in this report regarding wave breaking: unbroken refers to waves that have never broken, whereas nonbroken waves include both unbroken and re-formed waves.

$$H_{rms}^2 = \frac{1}{N}\sum_{i=1}^{u(x)} H_i^2 + \frac{1}{N}\sum_{i=1}^{r(x)} H_i^2 + \frac{1}{N}\sum_{i=1}^{m(x)} H_i^2 \quad (8)$$

Defining the fraction of unbroken and reformed waves as $\beta = u/N$ and $\mu = r/N$, respectively, Equation 8 may be written

$$H_{rms}^2 = \beta H_u^2 + \mu H_r^2 + \alpha H_m^2 \quad (9)$$

where H_u and H_r are the rms wave heights for unbroken and re-formed waves, respectively. It is noted that, by definition, the sum of unbroken, re-formed, and broken wave fractions ($\beta + \mu + \alpha$) is equal to 1. Using Equation 9, all waves are described throughout the surf zone in terms of an rms wave height.

Governing equations and model formulation

Dally, Dean, and Dalrymple (1985) proposed a model to describe wave decay in the surf zone assuming that energy dissipation due to wave breaking is proportional to the excess energy flux beyond a stable energy flux which is dependent on water depth. The Dally model has been extensively verified for a variety of wave conditions, including laboratory and field situations and regular and irregular waves (Dally, Dean, and Dalrymple 1985; Ebersole 1987; Larson and Kraus 1989a; Dally 1990, 1992; Larson and Kraus 1992). An appealing feature of the model is the demonstrated reliability of its empirical coefficient values, making the model quite robust and suitable for engineering application. Also, the capability of the model to describe wave re-formation makes it useful in calculating cross-shore sediment transport and beach profile change for barred profiles.

Dally's breaker decay model forms the basis of the monochromatic wave model originally included in SBEACH (Larson and Kraus 1989a). To determine profile change under random waves, the original version of SBEACH used the significant wave height H_s as a representative measure of incident wave conditions. The wave height was treated as a regular wave and transformed across the profile using the monochromatic wave model to determine the cross-shore variation of wave energy dissipation, water level setup, and net sediment transport rates. The basic theory used to develop the monochromatic wave model is modified to include random waves as presented below.

Assuming a Rayleigh distribution at some point offshore and representing this distribution with a collection of N waves, nonbroken waves are transformed according to

$$\frac{d}{dx}\left(F_i \cos\theta\right) = 0 \quad (10)$$

and broken waves are transformed according to

$$\frac{d}{dx}\left(F_i \cos\theta\right) = \frac{\kappa}{d}\left(F_i - F_{st}\right) \tag{11}$$

where F_i is the energy flux for the i-th individual wave, θ the mean incident wave angle, d the total water depth ($d = h + \eta$; where h is the still-water depth and η the wave setup), F_{st} the stable wave energy flux, and κ an empirical energy decay parameter (set to 0.15). The wave energy flux is expressed as

$$F_i = \frac{1}{8}\rho g H_i^2 C_g \tag{12}$$

in which ρ is the density of water, g the acceleration of gravity, and C_g the group speed defined by

$$C_g = \frac{1}{2}\left[1 + \frac{\frac{4\pi d}{L}}{\sinh\left(\frac{4\pi d}{L}\right)}\right] C \tag{13}$$

where L is the wavelength and C the wave phase speed. The wave phase speed is determined through the dispersion relationship

$$C = C_o \tanh\left(\frac{2\pi d}{L}\right) \tag{14}$$

where

$$C_o = \frac{gT}{2\pi} \tag{15}$$

in which C_o is the wave phase speed in deep water and T is the peak wave period.

The stable wave energy flux F_{st} included in Equation 11 corresponds to a stable wave height H_{st} at which breaking ceases, where H_{st} is expressed in terms of water depth according to

$$H_{st} = \Gamma d \tag{16}$$

in which Γ is an empirical stable wave height coefficient (set to 0.4). Thus, F_{st} is expressed as

$$F_{st} = \frac{1}{8}\rho g (\Gamma d)^2 C_g \tag{17}$$

Using Equations 12 and 17, and dividing by $1/8\rho g$, Equations 10 and 11 are expressed as

$$\frac{d}{dx}\left(H_i^2 C_g \cos\theta\right) = 0 \tag{18}$$

$$\frac{d}{dx}\left(H_i^2 C_g \cos\theta\right) = \frac{\kappa}{d}\left(H_i^2 C_g - \Gamma^2 d^2 C_g\right) \tag{19}$$

Summing Equations 18 and 19 separately for all waves at a specific location x gives

$$\sum_{i=1}^{n(x)} \frac{d}{dx}\left(H_i^2 C_g \cos\theta\right) = 0 \tag{20}$$

$$\sum_{i=1}^{m(x)} \frac{d}{dx}\left(H_i^2 C_g \cos\theta\right) = \sum_{i=1}^{m(x)} \frac{\kappa}{d}\left(H_i^2 C_g - \Gamma^2 d^2 C_g\right) \tag{21}$$

Equations 20 and 21 are combined to yield

$$\sum_{i=1}^{N} \frac{d}{dx}\left(H_i^2 C_g \cos\theta\right) = \sum_{i=1}^{m(x)} \frac{\kappa}{d}\left(H_i^2 C_g - \Gamma^2 d^2 C_g\right) \tag{22}$$

where $N = n + m$ is used on the left side of the equation.

Since N is a constant and C_g and d are functions of x only, Equation 22 may be rearranged to yield

$$\frac{d}{dx}\left(C_g \cos\theta \sum_{i=1}^{N} H_i^2\right) = \frac{\kappa}{d} C_g \left(\sum_{i=1}^{m(x)} H_i^2 - \Gamma^2 d^2 \sum_{i=1}^{m(x)} 1\right) \tag{23}$$

Each term in Equation 23 is divided by N which gives

$$\frac{d}{dx}\left(C_g \cos\theta \frac{1}{N} \sum_{i=1}^{N} H_i^2\right) = \frac{\kappa}{d} C_g \left(\frac{1}{N} \sum_{i=1}^{m(x)} H_i^2 - \Gamma^2 d^2 \frac{m}{N}\right) \tag{24}$$

where it was noted that the last sum in Equation 23 is equal to m. Utilizing the definitions of rms wave height given in Equations 3 and 6, Equation 24 can be expressed as

$$\frac{d}{dx}\left(H_{rms}^2 C_g \cos\theta\right) = \frac{\kappa}{d} C_g \left(\alpha H_m^2 - \alpha \Gamma^2 d^2\right) \tag{25}$$

where α is the fraction of broken waves, as before, given by $\alpha = m/N$. Equation 7 is rearranged to obtain the following expression

$$\alpha\ H_m^2 = H_{rms}^2 - (1 - \alpha)\ H_n^2 \tag{26}$$

which is substituted into Equation 25 to yield

$$\frac{d}{dx}\left(H_{rms}^2 C_g \cos\theta\right) = \frac{\kappa}{d}\left[H_{rms}^2 C_g - (1-\alpha) H_n^2 C_g - \alpha \Gamma^2 d^2 C_g\right] \tag{27}$$

Introducing the rms energy flux and a definition of the stable energy flux for irregular waves, Equation 27 can be written in a form equivalent to Equation 11

$$\frac{d}{dx}(F_{rms}\cos\theta) = \frac{\kappa}{d}(F_{rms} - F_{stab}) \tag{28}$$

where

$$F_{rms} = \frac{1}{8}\rho g H_{rms}^2 C_g \tag{29}$$

$$F_{stab} = \frac{1}{8}\rho g\left[(1-\alpha)H_n^2 + \alpha\Gamma^2 d^2\right]C_g \tag{30}$$

If all waves are broken (i.e., $\alpha = 1$, and $H_n = 0$) Equation 27 reduces to the original breaker decay model proposed by Dally, Dean, and Dalrymple (1985).

Equation 27 can be solved for H_{rms} by employing a numerical finite difference technique. To solve the equation, the rms of the nonbroken waves H_n must be specified at each point across shore together with the fraction of broken waves α. This specification is straightforward for a beach profile with depth that increases monotonically with distance offshore; however, for a non-monotonic beach profile, such as a barred profile, an empirical closure relationship must be added to model wave re-formation. In the following two sections, the irregular breaker decay model represented by Equation 27 will be developed first for a monotonic profile and then for a non-monotonic profile. For the latter case, an empirical equation is introduced to describe wave re-formation.

Wave decay over a monotonic profile

For a beach profile with depth that increases monotonically with distance offshore, α and H_n may be computed directly with the assumption that a Rayleigh distribution is valid at some point seaward of the surf zone where wave breaking is negligible. In this case, the Rayleigh pdf is transformed from the offshore point to the point of interest and truncated at a wave height corresponding to the local incipient breaking wave height. A monotonic profile will never allow wave re-formation, and the fraction of broken waves will increase monotonically as the waves propagate onshore. Thus, the number of unbroken and nonbroken waves will be equal at each point across the surf zone.

Shoaling a Rayleigh pdf from an offshore point x_{off} to a point x closer to shore, neglecting wave breaking, yields the following relationship between the rms wave heights at the two locations

$$H_x^2 = \frac{C_{goff}}{C_g}\frac{\cos\theta_{off}}{\cos\theta}H_{off}^2 \tag{31}$$

where H is the rms wave height ignoring wave breaking, and the subscripts x and *off* refer to the respective locations. As previously discussed, it is assumed that wave breaking is negligible at x_{off}. At some inshore point x where wave breaking becomes significant, Equation 31 will predict an unrealistically high rms wave height. Therefore, energy dissipation due to wave breaking and associated wave height decay are included in the wave transformation calculations as follows.

Assuming that individual waves break when a fixed ratio between wave height and water depth $\gamma_b = 0.78$ is exceeded, the fraction of broken waves at x may be determined from the Rayleigh distribution according to (compare Equation 2)

$$\alpha = e^{-\left(\frac{\gamma_b d}{H_x}\right)^2} \tag{32}$$

where d is the water depth and H_x is the rms wave height at x neglecting wave breaking. The rms wave height for unbroken waves H_n may be derived by integrating the truncated Rayleigh pdf

$$H_n^2 = \frac{\int_0^{\gamma_b d} H^2 p(H)\, dH}{\int_0^{\gamma_b d} p(H)\, dH} \tag{33}$$

where $p(H)$ is the Rayleigh pdf given by Equation 1. Substituting Equation 1 into Equation 33 and solving yields

$$H_n^2 = \frac{1}{1 - \alpha}\left[H_x^2 - \alpha\left(H_x^2 + \gamma_b^2 d^2\right)\right] \tag{34}$$

Using Equation 34 to replace H_n in Equation 27 produces the following equation valid for a monotonic beach

$$\frac{d}{dx}\left(H_{rms}^2 C_g \cos\theta\right) = \frac{\kappa}{d}\left[H_{rms}^2 C_g - (1 - \alpha) H_x^2 C_g + \alpha d^2\left(\gamma_b^2 - \Gamma^2\right) C_g\right] \tag{35}$$

The rms wave height H_{rms} is the only unknown in Equation 35, whereas H_x and α are calculated explicitly at each point across shore from Equations 31 and 32, respectively.

Wave decay over a non-monotonic profile

If the profile depth does not increase monotonically with distance offshore, such as along a barred beach profile, H_n and α in Equation 27 cannot be calculated directly from the Rayleigh pdf. A predictive equation is needed to determine the number of waves that re-form along negatively sloping sections of the beach. Given an equation for calculating the fraction of waves

re-forming at a specific location, the reformed wave height can be estimated based on the stable wave energy flux given by Equation 16 and transformed as a nonbroken wave until it reaches a smaller depth and breaks again. Such an equation is developed and included in the following formulation.

As before, the random wave model given by Equations 28-30 is solved to yield H_{rms}; however, since in this case H_{rms} represents unbroken, re-formed, and broken waves, writing F_{stab} in a slightly different form is more convenient. Using Equation 9 rather than Equation 7 in the derivation of Equation 28, F_{stab} may be expressed as

$$F_{stab} = \frac{1}{8}\rho g\left[\beta H_u^2 + \mu H_r^2 + \alpha \Gamma^2 d^2\right] C_g \tag{36}$$

Thus, before H_{rms} is calculated, the fractions of unbroken and re-formed waves (β and μ), as well as the respective rms wave heights (H_u and H_r), must be predicted. It is noted that the fraction of broken waves α is given by the relation $\alpha = 1 - \beta - \mu$.

When a negative slope is encountered, wave re-formation occurs and μ increases. The fraction of unbroken waves remains fixed and is determined from Equation 32 by using properties at the smallest depth d_{sm} seaward of the studied point (truncation of the Rayleigh pdf). The rms wave height for the unbroken waves H_u is calculated by integrating the truncated Rayleigh pdf to yield

$$H_u^2 = \frac{1}{\beta}\left[H_x^2 - \alpha_{sm}\left(H_x^2 + \frac{\gamma_b^2 d_{sm}^2 C_{gsm}\cos\theta_{sm}}{C_g \cos\theta}\right)\right] \tag{37}$$

where

$$\alpha_{sm} = e^{-\left(\frac{\gamma_b d_{sm}}{H_{xsm}}\right)^2} \tag{38}$$

and H_x is given by Equation 31. The subscript sm refers to the point x_{sm} having the smallest depth seaward of the studied point. The fraction of unbroken waves β at any point on the profile is given by

$$\beta = 1 - \alpha_{sm} \tag{39}$$

Several different formulations of a predictive equation for determining the amount of waves that reform along negative slopes were investigated, and the following equation was chosen to model the effect of wave re-formation

$$\mu = \alpha_{sm} - \alpha_o\left(\frac{F_{rms} - F_{stab}}{F_{rms,o} - F_{stab,o}}\right)^{\lambda} \tag{40}$$

where

$$\alpha_o = \alpha_{sm} - \mu_o \tag{41}$$

The parameter λ is an empirical wave re-formation coefficient and the subscript o refers to the point x_o where wave re-formation starts. Equation 40 is valid for F_{rms} greater than F_{stab} and implies that all waves that are broken at x_o re-form as F_{rms} approaches F_{stab}. When F_{rms} falls below F_{stab}, energy dissipation ceases and no broken waves exist. In Equation 41, μ_o is the fraction of re-formed waves at x_o which exist from a re-formation point further offshore ($\mu_o = 0$ at the seaward-most re-formation point). Thus, multiple points of wave re-formation (i.e., multiple bars) can be treated using Equation 40. The parameter λ included in Equation 40 controls how rapidly wave re-formation occurs along negatively sloping sections of the beach, where a large λ produces more rapid wave re-formation. Through comparision with data and sensitivity testing (Larson 1995), a value of $\lambda = 0.5$ was found to yield reasonable results, and this value is used in the present model.

To calculate the rms height of the re-formed waves H_r, an empirical pdf for re-formed waves is constructed by calculating the fraction of waves that re-form at each point using Equation 40 and calculating the associated wave height using Equation 16. The pdf is transformed as the waves propagate onshore and H_r is determined at each point across the profile from the pdf. As the reformed waves experience shoaling again, they will eventually break, and this is described in the model by truncating the pdf for the re-formed waves at $\gamma_b d$ (waves with heights above this threshold become broken waves again). It is noted that the equations developed for a non-monotonic profile reduce to those for a monotonic profile when no wave re-formation occurs (i.e., $\mu = 0$).

Wave Model Validation

Detailed testing and evaluation of the random wave model were performed by Larson (1995). Two cases included in the study are presented here to illustrate model capabilities in predicting random wave transformation over barred profiles. The selected cases involve comparisons with laboratory data from the SUPERTANK project (Kraus, Smith, and Sollitt 1992) and field data from the DELILAH project (Smith, Larson, and Kraus 1993).

The SUPERTANK project was conducted to investigate cross-shore hydrodynamic and sediment transport processes using the large wave tank at Oregon State University, Corvallis, OR. The project included measurement of random wave transformation across a barred sandy beach profile. Figure 2 displays the calculated and measured H_{rms} together with the surveyed beach profile for run A0517A from the SUPERTANK project. This run involved incident random waves with an rms wave height of 0.57 m and a peak period of 3 sec. The beach profile included a bar with a crest located at a water depth of about 0.6 m. Although only the two shoreward-most gauges appear to have been influenced by wave breaking, the wave model reproduces the measured rms wave height decay, as shown in Figure 2.

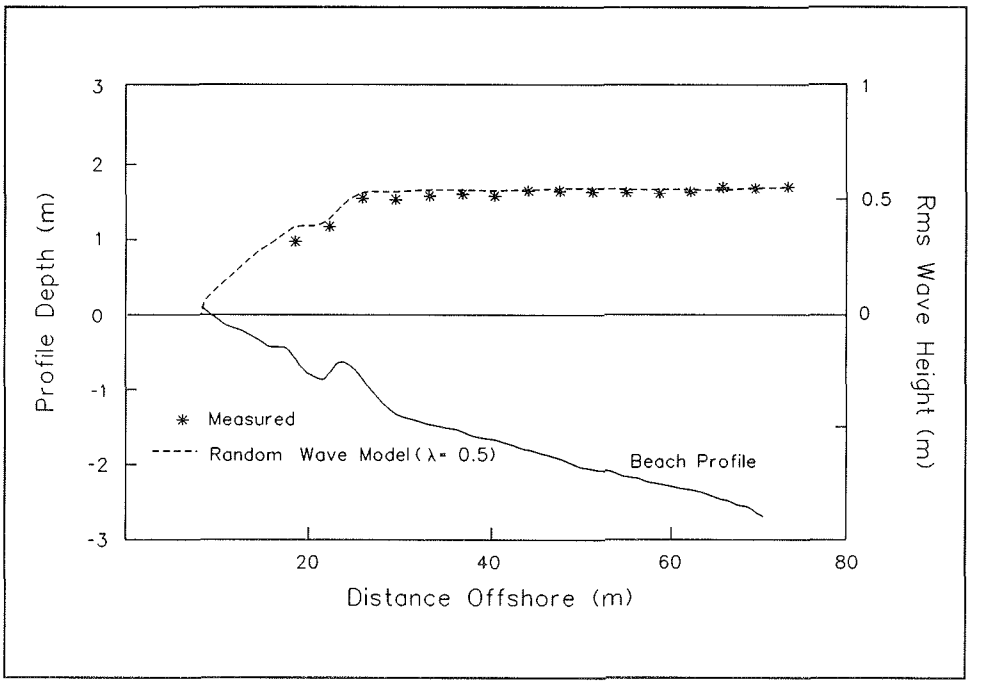

Figure 2. Calculated and measured rms wave height together with the beach profile for SUPERTANK run A0517A

The DELILAH field data collection project was conducted in October 1990 on the barred nearshore bathymetry at the U.S. Army Engineer Waterways Experiment Station, Coastal Engineering Research Center, Field Research Facility located at Duck, NC, facing the Atlantic Ocean on a sandy barrier island beach. Data collection included offshore wave information (at a depth of 8 m) and measurements of wave transformation across the barred profile. Figure 3 displays calculation results for case 1000 from the DELILAH project. Incident waves for this case had an rms height of about 0.71 m and a peak period of about 9.7 sec. As shown in the figure, the random wave model well reproduces the measured rms wave height decay. Also included in the figure are calculated results obtained using a complete Monte Carlo simulation approach involving transformation of 1,500 individual waves. The random wave model predictions are virtually identical to those of the Monte Carlo approach, indicating that the single wave approach used in the random wave model provides equally good results as the computationally intensive wave-by-wave approach.

Model Implementation in SBEACH

The SBEACH model was initially modified to include the random wave model described above and random wave sediment transport formulas (discussed in Chapter 3). The modified version of SBEACH was tested using

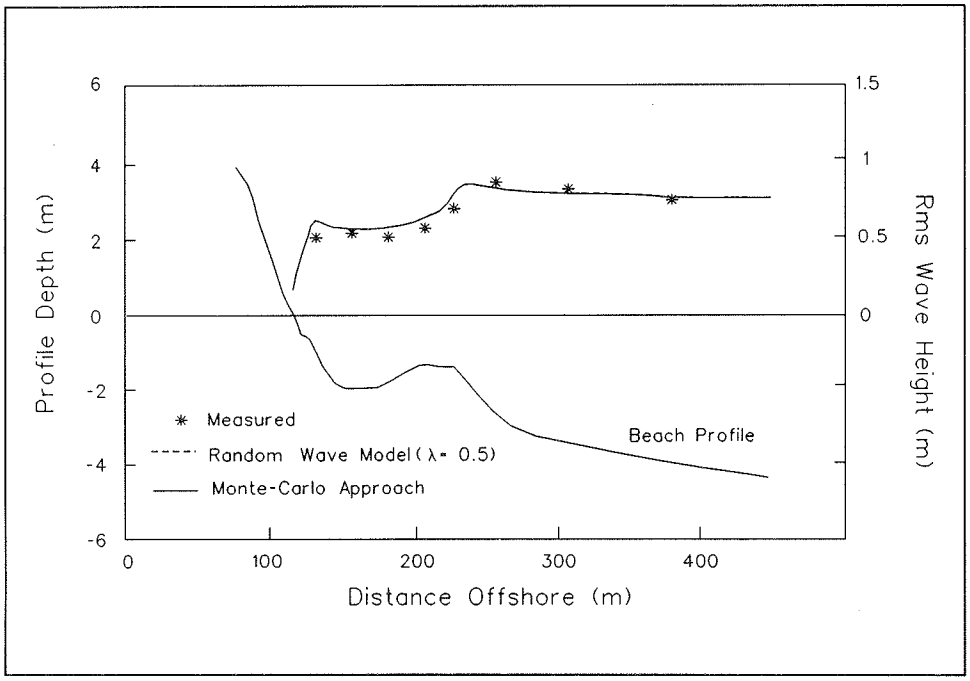

Figure 3. Calculated rms wave height for the random wave model and the Monte Carlo approach, together with measured wave height and beach profile for DELILAH case 1000

beach profile change data from the SUPERTANK project (Larson 1994, 1996). Results from this evaluation indicated good agreement between model predictions and laboratory measurements of beach profile change. In preliminary tests with field data sets, however, the model consistently underestimated erosion. It was reasoned that the unsatisfactory agreement with the field data was associated with using the rms wave height rather than the significant wave height in calculating energy flux and dissipation, water level setup, and sediment transport rates (the original version of SBEACH used significant wave height to compute these parameters for field applications).

For a Rayleigh distribution of wave heights, the relation between significant wave height and the rms wave height is given by

$$H_s = 1.416\ H_{rms} \tag{42}$$

Given the same incident waves, the flux F_s associated with the significant wave height is approximately twice the rms flux F_{rms} since wave energy flux is proportional to the square of the wave height. Therefore, it is reasonable to conclude that applying rms flux in a sediment transport model originally developed and calibrated based on significant flux will generally result in underprediction of wave energy-related quantities. In the field, such differences are magnified due to large incident wave heights; whereas the differences become less apparent in the lab where wave heights are smaller.

To improve model results for field applications, the random wave model is modified to compute wave parameters based on significant energy flux of the incident waves as discussed below.

The wave energy flux equation (Equation 28) is expressed in terms of the significant energy flux F_s according to

$$\frac{d}{dx}(F_s \cos\theta) = \frac{\kappa}{d}(F_s - F_{stabs}) \tag{43}$$

where

$$F_s = \frac{1}{8}\rho g H_s^2 C_g \tag{44}$$

For the general case of a non-monotonic profile, the stable wave energy flux (Equation 36) is modified to yield

$$F_{stabs} = \frac{1}{8}\rho g\left[\beta(f_s H_u)^2 + \mu(f_s H_r)^2 + \alpha\Gamma^2 d^2\right]C_g \tag{45}$$

The parameters β, μ, α, H_u, and H_r are calculated as before, and the factor f_s is included to convert from rms wave height to significant wave height for unbroken waves and re-formed waves. Here it is assumed that the pdf of the reformed waves is similar in shape to the pdf of the unbroken waves so that a single conversion factor can be used. The stable energy flux for broken waves (last term in Equation 45) is not multiplied by a conversion factor because it is defined uniquely based on local water depth and is not a function of the wave height distribution.

Seaward of wave breaking, the factor f_s is equal to the ratio of significant wave height to rms wave height for the entire Rayleigh distribution and is given by $f_s = 1.416$ (see Equation 42). In the surf zone where some fraction of waves are breaking, f_s can be estimated from the truncated Rayleigh distribution which describes the fraction of unbroken waves. The value of f_s in the surf zone is derived as follows.

At a given point on the profile, the fraction of unbroken waves is expressed in terms of the breaking wave height H_b and the rms wave height of the entire Rayleigh distribution assuming no wave breaking H_x

$$\beta = 1 - e^{-\left(\frac{H_b}{H_x}\right)^2} \tag{46}$$

The rms wave height of the unbroken waves H_u is expressed in terms of β, H_b, and H_x (compare Equation 34)

$$H_u = \left\{\frac{1}{\beta}\left[1 - (1-\beta)\left(1 + \frac{H_b^2}{H_x^2}\right)\right]\right\}^{\frac{1}{2}} H_x \tag{47}$$

From Equation 2, the threshold wave height H_t that is greater than 2/3 of the unbroken waves is calculated as

$$H_t = \left[- \ln\left(1 - \frac{2}{3}\beta\right)\right]^{0.5} H_x \tag{48}$$

The average of the highest 1/3 of the unbroken waves (i.e., the significant wave height for unbroken waves H_{us}) is derived from the following equation

$$H_{us} = \frac{\int_{H_t}^{H_b} Hp(H)dH}{\int_{H_t}^{H_b} p(H)dH} \tag{49}$$

where $p(H)$ is given by Equation 1. The integral in the numerator of Equation 49 must be solved numerically since no analytical solution exists. The integral in the denominator represents the fraction of total waves having a height between H_t and H_b and is equal to $\beta/3$. Employing Equations 47 and 49, f_s is determined according to

$$f_s = \frac{H_{us}}{H_u} \tag{50}$$

Figure 4 displays a plot of f_s as a function of the breaking wave height H_b normalized by H_x. Also shown in Figure 4 are plots of the fraction of unbroken waves β and the normalized significant wave height for unbroken waves H_{us}. For large values of H_b/H_x (corresponding to large depths), β approaches 1.0 indicating that few waves are broken, and f_s approaches 1.416 corresponding to the value for the full Rayleigh distribution. As H_b/H_x decreases, both β and H_{us} approach zero as all waves become broken. The curve $f_s(H_b/H_x)$ shown in Figure 4 is stored as a data array in the random wave model and is used to compute the significant wave height for unbroken and re-formed waves at each point across the profile.

Calculation of Wave-Related Parameters

The random wave model in SBEACH solves the conservation of wave energy flux equation (as given by Equations 43-45) to compute wave height decay across the surf zone. Wave- and wind-induced water level setup are included in the calculation by solving the cross-shore momentum equation given by

$$\rho g d \frac{d\eta}{dx} = - \frac{dS_{xx}}{dx} - C_D \rho_a |W| W \cos\varphi \tag{51}$$

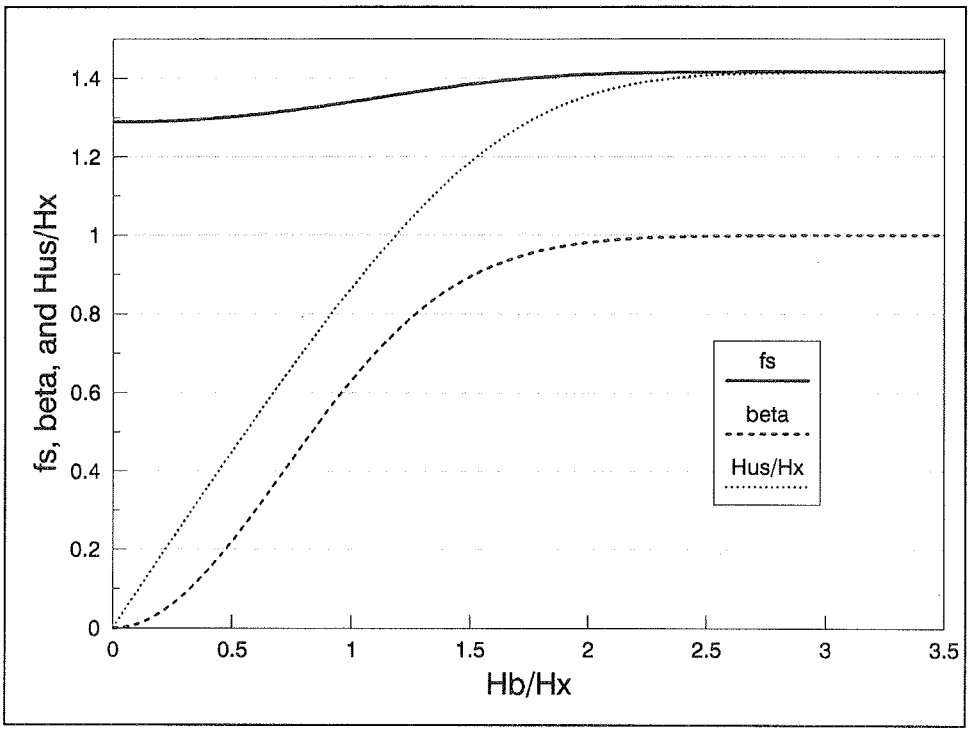

Figure 4. Plot of significant wave conversion factor, fraction of unbroken waves, and significant unbroken wave height as functions of breaking wave height

where η is the water level displacement, S_{xx} the cross-shore component of radiation stress, C_D the wind drag coefficient, ρ_a the density of air, W the wind velocity, and φ the wind direction. The radiation stress S_{xx} is given by linear wave theory as

$$S_{xx} = \frac{1}{8}\rho g H_s^2 \left[\frac{C_g}{C}(\cos^2\theta + 1) - \frac{1}{2}\right] \tag{52}$$

where H_s is determined across the profile using the random wave model. The wind drag coefficient is calculated based on an expression developed by the WAMDI Group (1988)

$$C_D(W) = \begin{cases} 1.2875\,10^{-3}, & |W| < 7.5\,m/\text{sec} \\ (0.8 + 0.065|W|)\,10^{-3}, & |W| \geq 7.5\,m/\text{sec} \end{cases} \tag{53}$$

If wind data are not available, wind speed is set to zero and the setup calculation is performed using radiation stress only.

Energy dissipation due to breaking waves D, which is used in SBEACH to compute cross-shore sand transport rates, is given by

$$D = \frac{1}{d}\frac{d}{dx}\left(F_s \cos\theta\right) \tag{54}$$

Using Equation 43, the following relationship for D is obtained

$$D = \frac{\kappa}{d^2}\left(F_s - F_{stabs}\right) \tag{55}$$

The values of F_s and F_{stabs} are determined from the random wave model and D is calculated across the profile.

Input data requirements of the random wave version of SBEACH are identical to those of the previous monochromatic version (see Rosati et al. 1993). Basic hydrodynamic input includes time series of significant wave height, peak wave period, and water level. Optionally, wave angle and wind speed and direction can be also be specified. Computations of random wave parameters are performed across the profile at each time-step based on input wave and water level information. The resulting wave parameters are used to calculate sediment transport rates as discussed in the next chapter.

3 Cross-Shore Transport Under Random Waves

The SBEACH profile change model utilizes a mesoscale approach to calculate sediment transport across the profile, where the direction and rate of sediment transport are expressed in terms of wave, profile, and sediment properties. In the initial development of SBEACH, Larson and Kraus (1989a) investigated the cross-shore transport rate under monochromatic waves by inferring the transport rate distribution from consecutively measured beach profiles in large wave tank (LWT) experiments. The profile was divided into different zones of cross-shore transport based on characteristics of the hydrodynamics across the profile (Miller 1976; Svendsen, Madsen, and Buhr Hansen 1978; Skjelbreia 1987). Sediment transport relationships were developed for each of four principal transport zones including: (a) pre-breaking zone, (b) breaker transition zone, (c) broken wave zone, and (d) swash zone. The sediment transport relationships were implemented in SBEACH with a monochromatic wave model being used to delineate the zones of transport. For random waves, the relationships for calculating the direction and rate of sediment transport must be modified to represent transport under broken and unbroken waves which exist simultaneously across the profile.

In this chapter, cross-shore sediment transport relationships derived from the monochromatic LWT data are reviewed. The monochromatic transport relationships are modified for random waves to develop transport relationships (Larson 1994, 1996) included in the present version of SBEACH. Also, an algorithm developed for SBEACH to simulate dune erosion produced by overwash is discussed.

Review of Monochromatic Transport Relationships

Transport direction

A large number of criteria have been developed for predicting the general response of a beach profile to incident waves (Waters 1939; Rector 1954; Iwagaki and Noda 1962; Dean 1973; Sunamura and Horikawa 1974; Larson

and Kraus 1989a; Kraus, Larson, and Kriebel 1991). In most of these studies, the response of the beach was classified into two different shapes typically referred to as bar/berm profiles (other common descriptions include: bar/step, storm/normal, erosional/accretionary, dissipative/reflective, winter/summer). The evolution of a particular beach profile shape is closely related to the properties of the transport rate distribution, where bar profiles are generally produced by offshore transport and berm profiles by onshore transport. Thus, criteria determined from the overall profile response have often been employed to predict the direction of the cross-shore transport.

The following criterion for distinguishing between the development of bar/berm profiles was proposed by Larson and Kraus (1989a) and included in SBEACH based on experiments with monochromatic waves in the LWT

$$\frac{H_o}{L_o} = M\left(\frac{H_o}{wT}\right)^3 \tag{56}$$

where H_o is the deepwater wave height, L_o the deepwater wavelength, T the wave period, w the sediment fall speed. The value of the empirical coefficient M was determined to be 0.00070 based on the LWT data. If the left side of Equation 56 (corresponding to wave steepness) is less than the right side (corresponds to dimensionless fall speed), then offshore transport or erosion is predicted; otherwise onshore transport or accretion occurs. Kraus, Larson, and Kriebel (1991) applied Equation 56 to random waves by using the mean height as the characteristic wave measure, and also evaluated other dimensionless parameter combinations for distinguishing profile response.

Transport under broken waves

The largest rates of cross-shore transport typically occur under broken waves where the transfer of organized wave energy to turbulence provides work for suspending and transporting sediment. The details of sediment transport under broken waves are too complex to be resolved at present, and models developed to predict the transport rate employ simplified descriptions. A classification of such models with reference to the simplifications involved is given (going from the less to the more detailed approach):

a. *Energy dissipation models*. The transport rate is related to the wave energy dissipation and no attempt is made to resolve the circulation pattern in the surf zone.

b. *Energetics models*. The transport rate is related to the velocity at a selected reference level above bottom; thus, the local velocity has to be predicted in the surf zone at this level.

c. *Concentration-velocity models*. The transport rate is obtained from integrating the product of the predicted mean concentration and velocity profile through the water column.

Transport rate formulas based on energy dissipation have been successfully employed in engineering numerical models of profile response (Kriebel and Dean 1985; Kriebel 1986; Larson and Kraus 1989a; Larson, Kraus, and Byrnes 1990). Such formulas are compatible with the requirements of engineering numerical models, which often have to be employed with a minimum of input data.

Kriebel and Dean (1985) suggested the following relationship for the cross-shore transport rate q based on wave energy dissipation

$$q = K(D - D_{eq}) \tag{57}$$

where D is the energy dissipation, D_{eq} the equilibrium energy dissipation, and K an empirical coefficient. Larson and Kraus (1989a) modified Equation 57 to include a slope term

$$\begin{aligned} q &= K\left[D - \left(D_{eq} - \frac{\epsilon}{K}\frac{dh}{dx}\right)\right] \qquad D > D_{eq} - \frac{\epsilon}{K}\frac{dh}{dx} \\ q &= 0 \qquad\qquad\qquad\qquad\qquad\quad D \le D_{eq} - \frac{\epsilon}{K}\frac{dh}{dx} \end{aligned} \tag{58}$$

where h is the still-water depth and ϵ is an empirical coefficient. The slope term was introduced to account for the effect of gravity in limiting the steepness of the beach profile and to improve numerical stability in the vicinity of the breakpoint bar. The application of Equations 57 and 58 in predicting transport magnitude and direction has varied slightly. During storm conditions, when D is expected to be much greater than D_{eq}, Equations 57 and 58 will predict similar values of the transport rate. When D is less than D_{eq}, Equation 57 yields a negative transport rate, implying onshore transport of material. However, it has been shown in LWT data that accretion often occurs when D is greater than D_{eq} (Larson and Kraus 1989a), making Equation 57 unsuitable for predicting such events. Equation 58 provides an improved capability in predicting the transport rate under accretionary conditions based on analysis of the LWT data. This equation was implemented in SBEACH to calculate the magnitude of transport under broken waves, with the transport direction determined from Equation 56. In Equation 58, D_{eq} effectively functions as a "threshold" below which the influence of broken waves on transport is considered negligible.

Transport under nonbroken waves

In analysis of profile evolution in LWT data, Larson and Kraus (1989a) showed that, seaward of the breakpoint, the transport rate decayed exponentially with distance offshore according to

$$q = q_b e^{-\lambda_1 (x - x_b)} \tag{59}$$

where q_b is the transport rate at the breakpoint, x_b the location of the break point, and λ_1 an empirical coefficient characterizing the rate of decay (see Larson and Kraus 1995 for a physically based motivation of Equation 59). A similar equation was formulated to model the transport rate in the breaker transition zone, between the breakpoint and the plunge point

$$q = q_p e^{-\lambda_2 (x - x_p)} \tag{60}$$

where q_p is the transport rate at the plunge point, x_p the location of the plunge point, and λ_2 an empirical coefficient. The breakpoint corresponds to the point of incipient wave breaking, and the plunge point corresponds to the point where waves become fully broken.

The decay coefficient in Equation 59 was empirically derived in terms of the median grain size D_{50} and breaking wave height H_b

$$\lambda_1 = m_* \left(\frac{D_{50}}{H_b} \right)^{0.47} \tag{61}$$

where m_* is an empirical coefficient. For the breaker transition zone, limited data suggested that

$$\lambda_2 = 0.2 \lambda_1 \tag{62}$$

Equations 59 and 60 were shown to satisfactorily fit both erosional and accretionary cases, but the value of of m_* was generally smaller for accretionary waves. To calculate transport under nonbroken waves, the value of q_p is first determined at the offshore boundary of the surf zone using Equation 58, and then the exponential decay rates are applied seaward in the respective zones.

Transport in the swash

Larson and Kraus (1989a) found that for a majority of the LWT experiments, the shape of the net transport rate on the foreshore could be approximated by a simple linear decay with distance. Based on these findings, the following equation was implemented in SBEACH to calculate the transport rate in the swash zone

$$q = q_s \frac{x - x_r}{x_s - x_r} \tag{63}$$

where q_s is the transport rate at the shoreward boundary of the surf zone located at x_s, and x_r is the location of the runup limit. A linear decay in transport as predicted by Equation 63 implies that the foreshore advances/recedes uniformly with equal volume change at all points across the foreshore.

Transport Relationships for Random Waves

The relationships for cross-shore transport under monochromatic waves are generalized to random waves by treating the random wave field as a collection of individual waves. A criterion for predicting net transport direction is developed based on the assumption that the random wave field follows a Rayleigh distribution in deep water. Under the assumption of linearity in transport and no wave-wave interactions, the transport rate produced by random waves is obtained by computing the transport rate for each individual wave and averaging over all waves according to

$$q = \frac{1}{N} \sum_{i=1}^{N} q_i \tag{64}$$

where q is the average transport rate at x, N is the number of individual waves, and q_i the transport rate for wave i at x.

Transport direction

Assuming that the criterion for monochromatic waves given by Equation 56 can be applied to determine the direction of transport for each individual wave in a random wave field, the critical deepwater wave height H_{oc} that separates erosion and accretion is given by

$$H_{oc} = \sqrt{\frac{1}{M} \frac{(wT)^3}{L_o}} \tag{65}$$

Thus for an individual wave with deepwater wave height H_o, erosion is predicted when H_o is greater than H_{oc}, and accretion occurs otherwise. For a Rayleigh distribution of wave heights, accretionary and erosional waves exist simultaneously, and the net effect is estimated by summing the effects of individual waves. Because the magnitude of transport is determined as a function of wave energy dissipation, only waves that are broken are included in the sum.

At a given location on the profile, the fraction δ_e of the broken waves which are erosional is determined from the Rayleigh pdf and given by

$$\delta_e = \frac{e^{-\left(\frac{H_{oc}}{H_{rmso}}\right)^2}}{e^{-\left(\frac{H_{bo}}{H_{rmso}}\right)^2}} \qquad \delta_e \le 1 \tag{66}$$

where H_{rmso} is the deepwater rms wave height and H_{bo} the wave height at incipient breaking transformed seaward to deep water. Equation 66 is obtained by dividing the fraction of waves which are greater than H_{oc} in deep water by the fraction of all broken waves. The transformed breaking wave height H_{bo} is given by

$$H_{bo}^2 = (\gamma_b d)^2 \frac{C_g}{C_{go}} \frac{\cos\theta}{\cos\theta_o} \tag{67}$$

where wave refraction is included and the subscript o denotes deepwater conditions (compare Equation 31).

By substituting the expression for H_{oc} from Equation 65 into Equation 66, the following result is obtained

$$\delta_e = \frac{e^{-\frac{1}{M}\frac{H_{rmso}}{L_o}\left(\frac{wT}{H_{rmso}}\right)^3}}{e^{-\left(\frac{H_{bo}}{H_{rmso}}\right)^2}} \qquad \delta_e \le 1 \tag{68}$$

Thus, the fraction of the breaking waves that are erosional is predicted using a similar set of parameters as for distinguishing profile response under monochromatic waves (Equation 56), with the deepwater wave steepness and dimensionless fall speed expressed in terms of H_{rmso} as the characteristic wave height. Note that both Equations 66 and 68 are valid for H_{bo} less than or equal to H_{oc}. When H_{bo} is greater than H_{oc}, all broken waves are erosional and, by definition, $\delta_e = 1$.

Equation 68 predicts the portion of the broken waves that are erosional at points across the profile, but does not determine the net direction of transport. A simple approach for arriving at a predictive equation for the transport direction on the basis of Equation 68 is to assume that at a certain depth each individual broken wave transports an equal magnitude of sediment. Such an assumption is in agreement with Dean (1977), who postulated that the local wave height and, hence, the wave energy dissipation depend only on water depth. Assuming that transport is proportional to energy dissipation, this implies that every broken wave at a specific depth will transport the same amount of sediment.

Given δ_e as the fraction of broken waves that are erosional, the fraction of accretionary waves is defined as $\delta_a = 1-\delta_e$. Assigning each individual broken wave equal weight and summing to determine the net direction yields

$$\xi = \delta_e - \delta_a = 2\delta_e - 1 \qquad -1 \le \xi \le 1 \tag{69}$$

where ξ is a transport function that gives the net direction and a weight that accounts for the variability in wave height defined by the Rayleigh pdf. Substituting Equation 68 for δ_e in Equation 69 yields

$$\xi = 2\frac{e^{-\frac{1}{M}\frac{H_{rmso}}{L_o}\left(\frac{wT}{H_{rmso}}\right)^3}}{e^{-\left(\frac{H_{bo}}{H_{rmso}}\right)^2}} - 1 \qquad -1 \le \xi \le 1 \tag{70}$$

Net erosion occurs when ξ is positive, whereas net accretion is predicted when ξ is negative. The magnitude of the transport function depends on the number of erosional versus accretionary waves. When the broken waves are either all erosional or all accretionary, ξ equals 1.0 and -1.0, respectively. For an equal number of erosional and accretionary waves, ξ equals zero, resulting in no net transport.

Transport under broken waves

To describe transport under broken waves, Equation 58 is employed to determine the transport rate of each individual wave in the random wave field and substituted into Equation 64 to yield the following expression for the average transport rate for all broken waves

$$q = \frac{1}{N}\sum_{i=1}^{N} K\left[D_i - \left(D_{eq} - \frac{\epsilon}{K}\frac{dh}{dx}\right)\right] \tag{71}$$

where N is a large number of waves, and K and ϵ are empirical transport coefficients from the monochromatic transport relationship.

Because only broken waves contribute to the transport, the number of waves N included in the summation in Equation 71 can be replaced by the number of broken waves m

$$q = \frac{1}{N}\sum_{i=1}^{m} K\left[D_i - \left(D_{eq} - \frac{\epsilon}{K}\frac{dh}{dx}\right)\right] \tag{72}$$

A certain number of the broken waves m_e will be erosional and the remainder m_a will be accretionary, where $m = m_e + m_a$. Separating erosional and accretionary waves in Equation 72 yields

$$q = \frac{1}{N}\sum_{i=1}^{m_e} K\left[D_i - \left(D_{eq} - \frac{\epsilon}{K}\frac{dh}{dx}\right)\right] - \frac{1}{N}\sum_{i=1}^{m_a} K\left[D_i - \left(D_{eq} - \frac{\epsilon}{K}\frac{dh}{dx}\right)\right] \tag{73}$$

where offshore transport is regarded as positive. Since the quantity within the parentheses of Equation 73 is constant for all waves at a specific location, Equation 73 can be rearranged to yield

$$q = \frac{1}{N}\sum_{i=1}^{m_e} K D_i - \frac{1}{N}\sum_{i=1}^{m_a} K D_i - K\left(D_{eq} - \frac{\epsilon}{K}\frac{dh}{dx}\right)\frac{m_e - m_a}{N} \quad (74)$$

The factor included in the right-hand term of Equation 74 may be expressed as

$$\frac{m_e - m_a}{N} = \frac{m_e - m_a}{m}\frac{m}{N} = \xi\alpha \quad (75)$$

where $(m_e\text{-}m_a)/m$ is identified as ξ, and m/N is equal to the fraction of broken waves α as defined in Chapter 2. Following the assumption that each broken wave at a specific water depth transports the same magnitude of sediment, the wave energy dissipation terms in Equation 74 can be written

$$\frac{1}{N}\sum_{i=1}^{m_e} KD_i - \frac{1}{N}\sum_{i=1}^{m_a} K D_i = \frac{m_e - m_a}{m}\frac{K}{N}\sum_{i=1}^{m} D_i = \xi\frac{K}{N}\sum_{i=1}^{m} D_i \quad (76)$$

Substituting Equations 75 and 76 into 74, the following expression is obtained

$$q = K\xi\left[D - \alpha\left(D_{eq} - \frac{\epsilon}{K}\frac{dh}{dx}\right)\right] \quad (77)$$

where D is the average energy dissipation per unit water volume. Similar to the transport rate equation for monochromatic waves, the expression within the brackets must be positive for transport to occur, otherwise the transport rate is set to zero. To compute the transport rate, the value of D is determined from the random wave model according to Equation 55. The appearance of the function ξ in Equation 77 weighs the influence of erosional versus accretionary waves on the transport rate and determines the net direction of transport.

In the general case, both erosional and accretionary transport are predicted by Equation 77. In the present model validation, however, the focus is on profile change produced by erosion. Accretionary profile change is not emphasized for two reasons. First, engineering applications of the model, which involve short-term prediction of profile response to storms, typically require that the most eroded condition of the beach be determined. For such applications, modeling of post-storm recovery produced by accretion is not desirable, because the final predicted profile would not represent the most eroded condition. Second, model predictions of accretion have been validated only to a limited extent in field applications. In general, accretion is driven primarily by nonbroken waves and occurs over a longer term which is not consistent with the theory and assumptions of profile change included in the

present model. Further research is required to develop improved engineering methods for predicting accretionary profile change.

Transport under nonbroken waves

The transport rate seaward of the breakpoint of an individual wave is assumed to decay exponentially with distance according to the monochromatic relationship given by Equation 59. Applying Equation 64 to sum for all waves in the random wave field, the contribution to the transport rate from nonbroken waves is given by

$$q = \frac{1}{N} \sum_{i=1}^{n} q_{bi} \, e^{-\lambda_i (x - x_{bi})} \tag{78}$$

In Equation 78, n is the number of nonbroken waves at x, x_{bi} the location of the breakpoint for wave i, q_{bi} the transport rate at incipient breaking for wave i, and λ_i the exponential decay coefficient, where q_{bi} and λ_i are evaluated at x_{bi}. Equation 78 sums up the contributions to the transport rate from all waves that break inshore of x. The coefficient λ_i is determined as a function of the median grain size and incipient breaking wave height as for monochromatic waves (Equation 61). Unlike the formulation for monochromatic waves, a separate relationship for transitioning waves is not employed, as it is assumed that the difference in decay rate between pre-breaking and transitioning waves will have a much smaller influence on profile change under random waves due to the occurrence of multiple breakpoints across the profile.

Equation 78 is more easily solved from a numerical standpoint by dividing the profile shoreward of the studied point x into a number of grid cells n_s and adding the contribution of incipient breaking waves at each cell to the transport rate at x. Such a method to approximate Equation 78 yields

$$q = \sum_{j=1}^{n_s} q_{bj} \, e^{-\lambda_j (x - x_{bj})} \Delta \alpha_j \tag{79}$$

where $\Delta\alpha_j$ represents the increase in the fraction of broken waves in cell j. In Equation 79, q_{bj} and λ_j are estimated at all shoreward locations using Equations 77 and 61, respectively.

Transport in the swash

Sediment transport in the swash zone was previously computed in SBEACH assuming a linear decay in the transport rate (Equation 63). In this section, a modified form of the transport rate equation is derived based on a schematic description of swash zone transport properties. The net transport rate on the foreshore is primarily a function of the local beach slope, sediment

characteristics, and the wave (bore) properties in the swash. On beaches with coarser sediment, such as gravel or shingle beaches, the sediment characteristics are of pronounced importance because of percolation. On fine-grained beaches percolation effects are minor since the material is typically saturated and the downward transport of water during a swash cycle is small. Percolation effects will be neglected here, and it is assumed that no water is lost during a swash cycle.

A general expression for the sediment transport on a sloping beach under waves is

$$q = B_1 \tau_b^{3/2} \tan\beta_l \tag{80}$$

where τ_b is the time-averaged bottom shear stress, $\tan\beta_l$ the local beach slope, and B_1 a coefficient that encompasses sediment properties, such as grain size and density, as well as an empirical multiplier. Madsen (1991, 1993) derived Equation 80 to predict bed load under nonbroken waves and Watanabe (1982, 1985) has employed a similar expression for the total transport under both broken and nonbroken waves. In some studies a critical shear stress for incipient motion has been included in Equation 80; however, in many cases this value is much smaller than τ_b and may be neglected.

Equation 80 is used here to derive the approximate shape of the transport rate distribution in the swash zone, whereas the magnitude of the transport is determined by the conditions at the shoreward boundary of the surf zone. In order to apply Equation 80 on the foreshore, the local, time-averaged shear stress due to the swash must be specified. The shear stress is assumed to be related to the velocity according to

$$\tau_b = \frac{1}{2} f \rho u_s^2 \tag{81}$$

where f is a friction coefficient, ρ the water density, and u_s the time-averaged velocity in the swash, taken to be uniform through the water column. Thus, Equation 80 can be written in terms of the local swash velocity

$$q = B_2 u_s^3 \tan\beta_l \tag{82}$$

where B_2 is a new coefficient that is determined primarily by the sediment properties.

In order to employ Equation 82 to calculate transport rates, an estimate of the local velocity in the swash is required that represents the net effect of the uprush and backwash. To compute local velocities, a detailed model of the swash dynamics is needed that involves a high-resolution description in time and space. Such a detailed model is not compatible with the present modeling approach. Also, because the application of Equation 82 involves large uncertainties in relating q to u_s, the value of computing u_s in great detail is questionable.

A simple estimate of u_s is made here to evaluate the transport rate in Equation 82. If the velocity of the bore that travels up the foreshore is u_{bs} at x_s immediately before a swash cycle begins, the velocity of the bore front u_b is estimated as

$$u_b^2 \sim u_{bs}^2 - 2g\Delta h \tag{83}$$

where g is the acceleration of gravity and Δh is the elevation difference between the center of the bore at x_s and at a specific point on the foreshore. The proportionality in Equation 83 results from treating the front of the bore as a mass of water moving up the foreshore (compare Shen and Meyer 1962, Waddell 1973), or from employing the Bernoulli equation between x_s and x for a water particle on the surface of the bore front. If friction and turbulent losses are neglected, the proportionality expressed in Equation 83 may be replaced with an equal sign.

Although the bottom friction is the main agent for transporting the sediment through τ_b it is assumed here that the decrease in velocity on the foreshore is mainly determined by the transformation of kinetic energy to potential energy and not by energy loss. Furthermore, the representative local velocity regarding sediment transport at a point on the foreshore is taken to be proportional to the speed of the bore front when it passes that point. Thus, substituting Equation 83 into Equation 82 and combining all proportionality multipliers into one coefficient B_3 yields

$$q = B_3\left(u_{bs}^2 - 2g\Delta h\right)^{3/2} \tan\beta_l \tag{84}$$

The transport at x_s is expressed as

$$q_s = B_3\left(u_{bs}^2\right)^{3/2} \tan\beta_s \tag{85}$$

where $\tan\beta_s$ is the local beach slope at x_s. By dividing Equation 84 by 85, the shape of the transport rate distribution on the foreshore is obtained.

$$\frac{q}{q_s} = \left(1 - \frac{2g\Delta h}{u_{bs}^2}\right)^{3/2} \frac{\tan\beta_l}{\tan\beta_s} \tag{86}$$

Equation 86 is valid for elevations on the foreshore for which $2g\Delta h$ is less than u_{bs}^2. The limit where $2g\Delta h = u_{bs}^2$ is assumed to correspond to the runup limit Z_R. Equation 86 can thus be written in terms of Z_R.

$$\frac{q}{q_s} = \left(1 - \frac{\Delta h}{Z_R}\right)^{3/2} \frac{\tan\beta_l}{\tan\beta_s} \tag{87}$$

For a plane-sloping foreshore described by

$$\Delta h = m_{fs}\left(x_s - x\right) \qquad x<x_s \tag{88}$$

where $m_{fs}=\tan\beta_l$ is the constant foreshore slope, Equation 87 is reduced to

$$q = q_s \left(\frac{x - x_r}{x_s - x_r} \right)^{3/2} \tag{89}$$

Equation 89 is similar to the linear transport relationship given by Equation 63, with the decay term raised to a power of 3/2. Although the foreshore is generally not constant in slope, an advantage of employing Equation 89 over Equation 87 is that the transport rate is expressed in terms of profile distance x and is more straightforward to implement from a numerical standpoint. Also, Equation 89 is consistent with the observations in the LWT where the transport rate decayed with distance. The relative influence of local slope variations on the transport rate is estimated in the model by multiplying Equation 89 by a slope factor

$$f_{slope} = \frac{\tan\beta_l}{\tan\beta_o} \tag{90}$$

where $\tan\beta_l$ is the local slope at x and $\tan\beta_o$ is a representative constant slope for the foreshore. Using the factor given by Equation 90, steeper slopes produce an increase in the rate of erosion and gentler slopes result in a decrease. As the local slope approaches the representative slope, the slope factor goes to 1.0 corresponding to no effect on the transport rate. For negative slopes, the slope factor is set to zero to prevent local changes in transport direction which could result in numerical instability.

To calculate transport in the swash zone, the transport rate q_s is determined at the shoreward boundary of the surf zone x_s using Equation 77, and Equation 89 is applied landward. The shoreward boundary of the surf zone corresponds to the point on the profile where the water depth is equal to a user-specified parameter *DFS* defined as the depth of the foreshore. The landward boundary of transport on the foreshore x_r is defined by the limit of runup given by

$$Z_R = 1.47 H_{rmso} \left(\frac{\tan\beta_o}{\sqrt{H_{rmso}/L_o}} \right)^{0.79} \tag{91}$$

where H_{rmso} is the deepwater rms wave height, L_o the deepwater wavelength, and $\tan\beta_o$ the representative slope of the foreshore. Equation 91 was derived by Larson and Kraus (1989a) based on empirical analysis of LWT data.

Dune Overwash Algorithm

In applying beach profile response tools for design and evaluation of shore protection projects, engineers are required to simulate a wide range of conditions. Of particular importance in beach fill design is the need to predict beach profile response to storms characterized by high waves and water levels. Often, these extreme storms produce dune overwash and foreshore

profile inundation. Therefore, in developing a profile change model suitable for engineering use, provision must be made for the model to handle overwash conditions.

Background of development

Prior to development of the present overwash algorithm, SBEACH handled overwash conditions by applying the swash zone transport relation given by Equation 63 and setting the runup limit at the landward boundary of the calculation grid. This procedure resulted in offshore transport of sand up and over the landward side of the dune, which is an unrealistic description of overwash processes. Limitations of this simple approach in modeling dune overwash were recognized. Because of a lack of data quantifying dune overwash processes, however, improved methods could not be formulated and verified in a practical manner.

Recently, an extensive beach-fill monitoring program supported by the U.S. Army Corps of Engineers and the State of Maryland provided a high-quality data set describing beach profile change at Ocean City, MD (Stauble et al. 1993). As part of the monitoring program, profile surveys were made periodically and after severe storm events at several locations along the project reach. Waves and water level information were collected by nearshore gauges. Analysis of profile and storm data collected through the monitoring program prompted the development of the present overwash algorithm.

During 2-5 January 1992, a strong northeaster struck Ocean City, MD. The impact of the storm on the Ocean City beach-fill project is documented in a special issue of the journal *Shore and Beach* (Vol. 61, No. 1, 1993). Following the storm, an emergency assessment of the beach-fill project performance was conducted. As part of the emergency assessment, numerical simulations of profile response to the storm were performed using the SBEACH model together with pre-storm profile survey data and storm wave and water level information. Post-storm profile measurements were not yet available at the time. Preliminary simulation results showed little erosion of the dune, whereas site inspections indicated that significant erosion had occurred, with the dune being totally removed at some locations. It was reasoned that the high waves and water levels associated with the storm produced significant dune overwash which was not being simulated properly by the model.

Based on results of the emergency assessment, SBEACH was modified to include a simple overwash algorithm. The preliminary overwash algorithm produced results which were in qualitative agreement with site inspections. After post-storm profile survey data were obtained, dune overwash and erosion produced by the storm were quantified and the algorithm was re-examined and improved. The overwash algorithm was calibrated to the data set and the results showed that the observed dune overwash and foreshore

erosion were well reproduced (Kraus and Wise 1993). The improved overwash algorithm was tested further in a second study using additional profile lines and multiple storms at Ocean City. As in the first study, the calculated results well reproduced the measured dune and foreshore profile response (Wise and Kraus 1993). The overwash algorithm was further refined based on additional tests and included in the present random wave version of SBEACH.

Calculation procedure

Although the overwash algorithm was developed and calibrated using a limited number of storm and profile data, the calculation procedures were formulated in a generalized manner so that the algorithm could be applied over a range of conditions. Four basic principles of operation were posited in formulating the present overwash algorithm: (a) overwash occurs if the calculated limit of runup exceeds the dune crest, (b) overwash causes landward movement of sediment up and over the dune crest, (c) the magnitude of onshore transport occurring during overwash is a function of the extent by which calculated runup exceeds the dune crest and is related to wave bore properties at the dune crest, and (d) the landward limit of overwash depends on subaerial profile volume and geometry in a similarity relationship.

Based on the first principle of operation, the overwash algorithm becomes operative when the predicted runup elevation (given by Equation 91) exceeds the elevation of the dune crest located at x_{dc}. If the still-water level (tide plus surge) exceeds the dune crest, then the overwash algorithm is deactivated and profile inundation occurs. In the case of profile inundation, the dune is essentially treated as an underwater bar, and transport is calculated using the surf zone transport relationship.

According to the formulation of swash zone transport given by Equation 89, the transport rate decays with landward distance from the surf zone. For erosional transport, this assumption produces offshore movement of material across the entire swash zone. However, following the second principle postulated above, overwash produces onshore transport of sediment over the dune. Therefore, the distribution of the swash zone transport rate is modified during calculation of overwash to provide onshore movement of sediment at the dune according to

$$q = q_{dc} + (q_s - q_{dc})\left(\frac{x - x_{dc}}{x_s - x_{dc}}\right)^{3/2} \qquad x_{dc} < x < x_s$$

$$q = q_{dc}\frac{x - x_r}{x_{dc} - x_r} \qquad x_r < x < x_{dc} \tag{92}$$

where the maximum rate of onshore transport q_{dc} (<0) is assumed to occur at the location of the dune crest x_{dc}. In Equation 92, the shape of the transport rate distribution between the surf zone and the dune crest is similar to that used in the standard calculation of swash zone transport. Landward of the dune crest, the transport rate is assumed to decay linearly from the maximum rate of onshore transport q_{dc} to zero at the position of the landward boundary of transport x_r. The use of a linear decay rate with distance landward of the dune crest rather than a decay to the power of 3/2 provided better agreement with data. Employing different transport decay rates on either side of the dune crest can be supported by considering the differences in physical processes. On the seaward face of the dune, transport is driven by the combined effects of the bore uprush and downrush; whereas on the landward face, transport is driven by unidirectional bore overwash with no return flow. Thus, it is reasonable to assume that transport rate characteristics are somewhat different on either side of the dune crest.

The distribution of transport rates given by Equation 92 provides a smooth transition from offshore (positive) to onshore (negative) transport while maintaining a simple description of overwash consistent with existing swash zone sediment transport calculation procedures. It is noted that although the transport rate shifts from an offshore to an onshore direction at some point seaward of the dune crest, the transport rate gradient remains positive, producing a net removal of sand along the entire seaward face of the dune. Landward of the dune crest, the transport rate gradient is negative, producing deposition of sediment.

To calculate overwash using Equation 92, the transport rate at the seaward boundary of the swash zone q_s and the location of the boundary x_s are determined as for the standard swash zone transport calculation. The magnitude of the maximum rate of onshore transport q_{dc} is determined based on properties of the overwash bore. The depth of the overwash bore at the dune crest is estimated by

$$d_{dc} = d_s\left(\frac{x_{dc} - x_{r*}}{x_s - x_{r*}}\right) \tag{93}$$

where d_s is the water depth at the landward boundary of the surf zone and x_{r*} is the location of the calculated runup limit that would occur on a hypothetical profile extending landward of the dune crest with constant slope of $\tan\beta_o$. The value of x_{r*} is given by

$$x_{r*} = x_{swl} - \frac{Z_R}{\tan\beta_o} \tag{94}$$

where x_{swl} is the location where the still-water level intersects the beach profile, Z_R is the limit of runup given by Equation 91, and $\tan\beta_o$ is the representative foreshore slope. Equation 93 assumes that the bore depth decays linearly with distance landward from the surf zone.

Given the bore depth at the dune crest, the velocity of the bore at the dune crest is estimated by

$$u_{dc} = 2(g d_{dc})^{1/2} \tag{95}$$

where g is the acceleration of gravity. Equation 95 was developed by Le Méhauté (1976) using the method of characteristics to represent the velocity of a bore that would result from the breaking of a dam. Here it is assumed that the relationship between velocity and depth similarly describes an overwash bore (Holland, Holman, and Sallenger 1991).

Assuming that the transport rate is proportional to the bore velocity cubed (compare Equation 82), q_{dc} is given by

$$q_{dc} = - B_* u_{dc}^3 \tag{96}$$

where B_* is an empirical coefficient. A negative sign is included in Equation 96 to indicate onshore transport. In principle, the value of B_* depends on sediment properties and other properties of the foreshore profile. Developing a detailed expression for B_* to account for such dependencies would require an extensive empirical analysis. To simplify the application of Equation 96 and to reduce the number of empirical parameters which must be specified by the user, B_* is assumed to be proportional to the transport rate coefficient K. Relating B_* to K as a first approximation is convenient since K is the primary calibration coefficient controlling the magnitude of transport rates across other portions of the profile. In calibrating the overwash algorithm, various values of B_* were tested by multiplying K by different factors of ten. Reasonable agreement was obtained using the relation

$$B_* = 10^2 K \tag{97}$$

The transport relationship described by Equations 93-96 was developed to satisfy the third principle of operation regarding the magnitude of onshore transport occurring during overwash. As the predicted runup extends farther inland from the dune crest, the depth of the bore over the dune will increase, which in turn will produce higher rates of onshore transport. On the other hand, when the predicted runup limit corresponds exactly to the position of the dune crest (x_{r*} equals x_{dc}), q_{dc} goes to zero and the sediment transport calculation given by Equation 92 reduces to the standard methodology used when no overwash is predicted.

In the standard calculation of swash zone transport, the location of the landward boundary of transport x_r is defined by the predicted limit of runup. During overwash, a different definition is required, because the predicted runup elevation exceeds the maximum profile elevation. In the present overwash algorithm, the value of x_r appearing in Equation 92 is determined using the following procedure.

The limit of runup Z_R and extent of potential runup x_{r*} are calculated from Equations 91 and 94 based on a hypothetical foreshore profile which extends beyond the dune crest with constant slope $\tan\beta_o$. The profile volume (per unit width of beach) above still-water level which is traversed by the runup is determined for the hypothetical constant slope profile and given according to

$$V_r = \frac{1}{2}(x_{swl} - x_{r*})Z_R \tag{98}$$

The profile volume above still-water level of the actual profile is then calculated incrementally, starting at x_{swl} and moving landward. The landward boundary of transport x_r is assumed to correspond to the point on the actual profile where the total volume above still-water level equals V_r. This calculation procedure was developed as a simple method of taking into account subaerial profile volume and geometry in determining the landward limit of overwash. For higher elevations behind the dune crest, the landward extent of overwash will be smaller; whereas for lower elevations, overwash will extend further inland.

4 SUPERTANK Case Studies

The purpose of this chapter is to assess the performance of SBEACH in modeling profile changes measured during the SUPERTANK project. The SUPERTANK data set includes a collection of high-density, high-quality wave and profile measurements for a variety of wave conditions and profile configurations. These data provided an excellent opportunity to assess SBEACH's performance in modeling profile changes in a controlled environment under various testing conditions. SBEACH was first applied to the SUPERTANK test cases using default calibration parameter values. The model was then calibrated to a single case and applied to the remaining cases to determine calculation improvements gained through model calibration. Model performance is assessed through visual inspection of results and by employing statistical measures of agreement between calculations and data.

SUPERTANK Data Set

The SUPERTANK study was undertaken in August/September 1992 at the O. H. Hinsdale Wave Research Laboratory, Oregon State University. The study was a multi-institutional effort to obtain detailed information pertaining to surf-zone processes. A product of the study was an extensive data set of wave transformation, velocities, profile surveys, and sediment transport measurements across the beach profile for each test case.

The channel used in the SUPERTANK study was 104 m long, 3.7 m wide, and 4.6 m deep. On one end of the tank was a digitally controlled hydraulic wave generator capable of generating random or monochromatic waves. The wave generator faced a 76-m beach profile constructed of 600 m^3 of sand. Sand for the profile was obtained from the Oregon coast and had a median grain size of 0.22 mm. Data collected during the SUPERTANK study were gathered by a dense array of wave gauges, current meters, sediment concentration profilers, pressure gauges, video cameras, and other instruments. Further details of the SUPERTANK project are presented in Kraus and Smith (1994). A summary of the data sets collected at SUPERTANK is provided by Smith and Kraus (1995).

For the purposes of this study, the numerous tests conducted in the SUPERTANK study were reduced to a group of test cases suitable for use in evaluating the performance of SBEACH. This group consisted of tests simulating equilibrium erosion, dune erosion, erosion at a seawall, berm flooding, foredune erosion, and erosion of both narrow-crested and broad-crested mounds. Tests involved both random and monochromatic waves, and in each case the corresponding wave model was used in the SBEACH simulations. A summary of test conditions for the selected case studies is given in Appendix A. Larson (1994, 1996) used the random wave model and transport relationships outlined in Chapters 2 and 3 to calculate profile evolution for some of the SUPERTANK tests discussed in this chapter. Results from these studies demonstrated good agreement between model predictions and measurements of profile change. In these previous studies, H_{rms} was employed as the characteristic wave height in the random wave model, whereas in the present study, H_s is employed as discussed in Chapter 2. Because of the application of different characteristic wave heights, calculation results and optimal values of model transport coefficients vary between the studies.

Measuring Model Performance

Visual inspection of model results provides a good indication of model performance. Visual inspection alone, however, is somewhat subjective and does not provide a quantitative measure of model performance. Although difficulties arise in assigning an absolute measure of performance to a numerical model, it is relatively easy to compare statistics between the computed and measured values describing a specific aspect of the system being modeled. In this study, the performance of SBEACH is evaluated through both visual inspection and statistical comparison of model results and data.

Measures of performance used for analysis of the SUPERTANK cases are based on the statistical fit of the calculated profile to the measured profile for a given simulation. These measures of performance include an rms parameter (*RMS*) and a residual parameter (*Res*). *RMS* is a measure of the rms difference between the measured and calculated profiles and is given by:

$$RMS = \sqrt{\frac{1}{N_p} \sum_{j=1}^{N_p} (y_m - y_c)^2} \tag{99}$$

The residual is given by:

$$Res = \frac{\sum_{j=1}^{N_p} \sqrt{(y_m - y_c)^2}}{\sum_{j=1}^{N_p} \sqrt{(y_i - y_m)^2}} \tag{100}$$

where

y_i = initial profile elevation
y_m = measured final profile elevation
y_c = calculated final profile elevation
N_p = number of points across the profile

RMS gives a measure of the average absolute difference between the calculated elevations and the measured elevations. The residual, *Res*, is similar to a parameter used by Zheng and Dean (1995) and provides a relative measure of the difference between the measured and calculated profiles as compared to the amount of actual change that has occurred over a given range of the profile. For instance, a *Res* value of 0.33 indicates that the difference between the calculated profile and final measured profile is 1/3 of the total change between the initial and final measured profiles. Smaller values of *RMS* and *Res* correspond to a better fit. An analysis program was developed for this study to obtain the values of *RMS* and *Res* across any specified range of the beach profile.

Default Simulations

The SBEACH model was first applied to the SUPERTANK test cases using default values of the calibration parameters. Default calibration parameter values have been established based on previous model tests and applications with various laboratory and field data (Larson and Kraus 1989a; Larson, Kraus, and Byrnes 1990; Rosati et al. 1993).

Calibration parameters

The parameters that are used in calibrating SBEACH are the transport rate coefficient (K), the coefficient for the slope-dependent transport term (ϵ), and the depth of the foreshore (DFS) which corresponds to the landward end of the surf zone. Each parameter has an effect on various aspects of beach profile change as modeled in SBEACH.

The transport rate coefficient, K, influences the rate at which transport occurs when the energy dissipation per unit volume is greater than the equilibrium energy dissipation per unit volume. Model calculations typically

show greater sensitivity to the transport rate coefficient than to the other calibration parameters, and the transport rate coefficient is used as the primary calibration parameter. The default value for K is 1.75 x 10^{-6} m^4/N.

The slope-dependent coefficient, ϵ, influences the slope of the profile. This parameter is included in the surf zone transport equation to account for changes in the transport rate produced by local variations in profile slope. Lower values of ϵ result in steeper nearshore profiles and steeper bars, whereas higher values of ϵ result in profiles with gentler slopes and flatter bars. The default value for ϵ is 0.002 m^2/s.

The parameter *DFS* defines the landward end of the surf zone on the modeled profile and affects the magnitude of transport in the swash zone. A higher value of *DFS*, corresponding to a greater depth at the boundary between the surf and swash zones, typically increases transport rates in the swash zone, producing more erosion at the foreshore. Conversely, lower values of *DFS* typically decrease foreshore erosion. The default value of *DFS* is 0.3 m.

Other parameters that affect the profile response are the median sediment grain size and the avalanching angle. The median grain size is a key parameter in calculation of the transport rate and is included in the fundamental theory of SBEACH in determining the equilibrium energy dissipation. A reliable estimate of the median grain size is necessary for accurate results from the model. Median grain size represents a physical characteristic of the beach sediment and should not be used as a calibration parameter. However, in cases where there is uncertainty in the value of median grain size or where large variations in grain size are known to exist across the profile, sensitivity of model results to a range of values should be examined.

The avalanching angle defines the steepest subaerial beach profile slope that can develop in the model before avalanching occurs. Factors such as grain size and degree of sediment compaction influence the profile slope at which avalanching occurs. Maximum profile steepness can vary from site to site and is best approximated by examining historical profile records. In applying the model to a particular data set, the value of the avalanching angle should be selected to best represent steep slopes which may exist on the pre- and post-storm foreshore profile such as at a dune scarp.

Results of default simulations

Default simulations were executed by inputting the initial and final profiles, wave data, and water level data into the configuration and other supporting files and running SBEACH. Model results were then analyzed to determine the previously described measures of performance. Appendix A presents a comprehensive view of model results for all cases. Selected results which are representative of the default simulations are discussed below.

Equilibrium erosion. The equilibrium erosion cases were the first tests performed during SUPERTANK. The initial profile was a planar beach and was subjected to varying wave conditions including both random and monochromatic waves. Table A1 summarizes the input wave conditions for each case. The first few equilibrium tests produced significant erosion at the foreshore and development of an offshore bar. During later tests, the amount of erosion decreased as the profile approached an equilibrium shape.

Figure 5 shows the initial, calculated, and measured profiles for the first case, P1A.[1] The test resulted in removal of material from the upper profile and deposition in an offshore bar. Although the calculated results show similar trends compared to the measurements, the model overpredicted the amount of erosion at the foreshore. Offshore movement of the bar was overestimated, and the model did not reproduce the shape of the bar-trough system. Similar characteristics were observed in model results for other equilibrium cases involving random waves.

Figure 6 shows model results for an equilibrium erosion case that involved a series of monochromatic waves. For this case the initial beach profile was near equilibrium and little change occurred in the nearshore profile. In the offshore, a deep trough formed under the influence of the monochromatic waves. Although the trough feature was not reproduced, the model correctly predicted little change in the nearshore. Figure 7 shows another case involving monochromatic waves, in which more profile change was observed. For this case, SBEACH overestimated the amount of foreshore erosion. The location of the bar was fairly well modeled, although details of the bar and trough development were not predicted.

The equilibrium cases show that for both random and monochromatic waves, SBEACH tended to overpredict erosion using default calibration parameter values. However, in cases where the profile was already at or near equilibrium and little profile change occurred, the model predicted little change. These observations suggest that the model accurately represents the equilibrium profile shape, but approaches equilibrium too rapidly indicating that the default value of K is too high for these cases.

Dune erosion. The dune erosion cases involved constructing a dune in the wave tank and subjecting this dune to erosive wave conditions, including an increase in water level. Case P5A involved erosion of a dune constructed with loosely packed sand, whereas case P6A involved running similar wave conditions on a compacted dune.

---

[1] In all figures displaying SUPERTANK results, the vertical datum corresponds to the water level at the start of the test. The water level was held constant during each test, except where noted in Table A1.

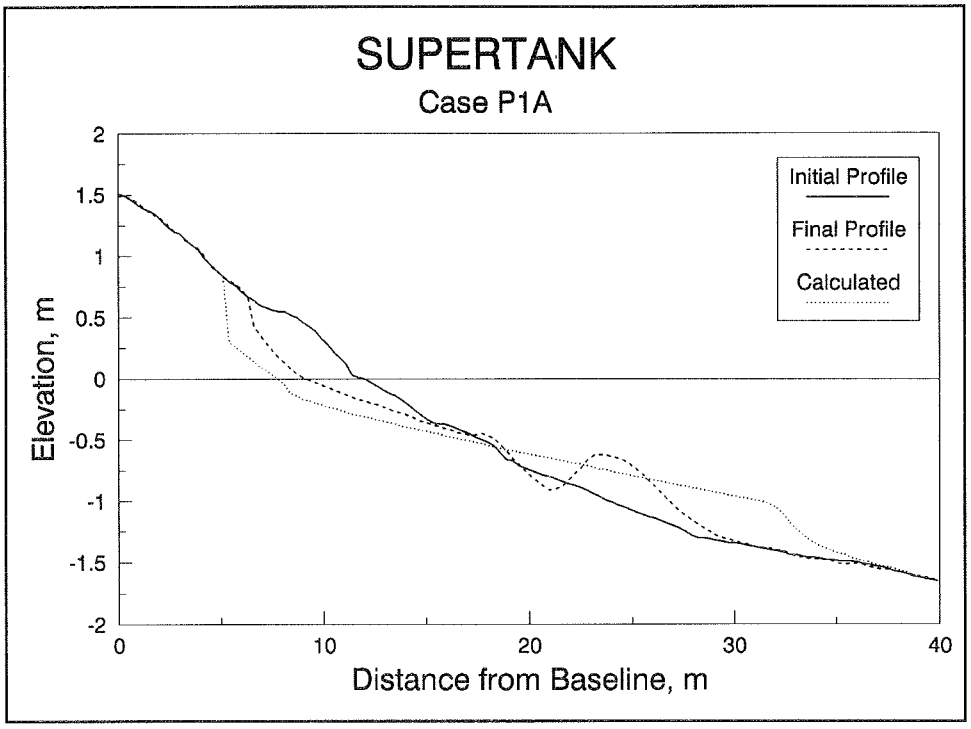

Figure 5. Result of default simulation, SUPERTANK case P1A

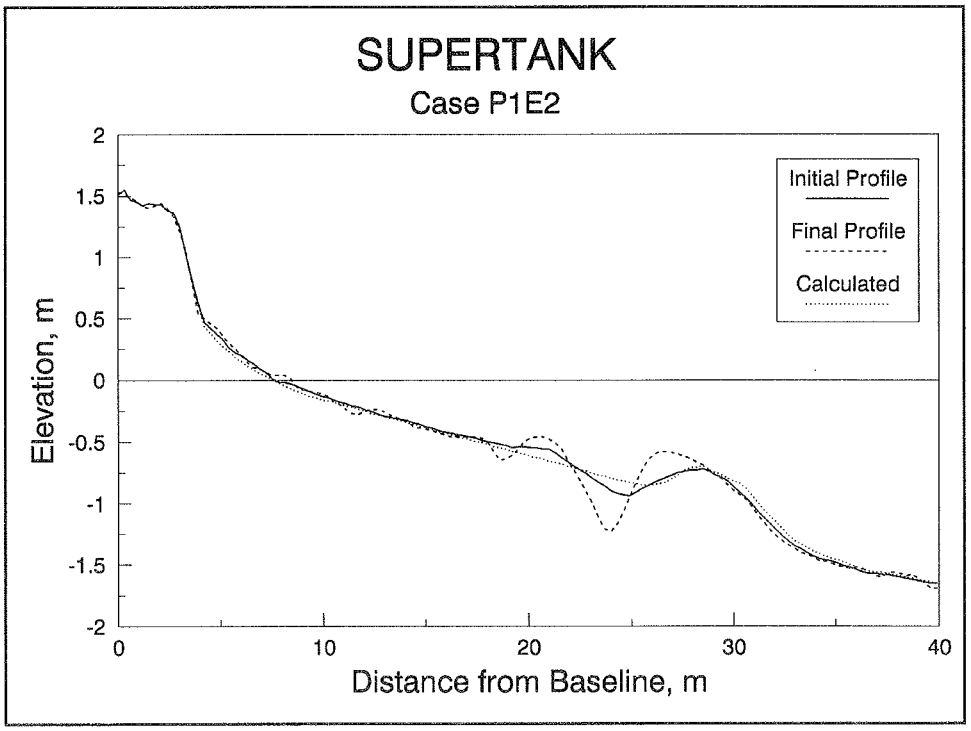

Figure 6. Result of default simulation, SUPERTANK case P1E2

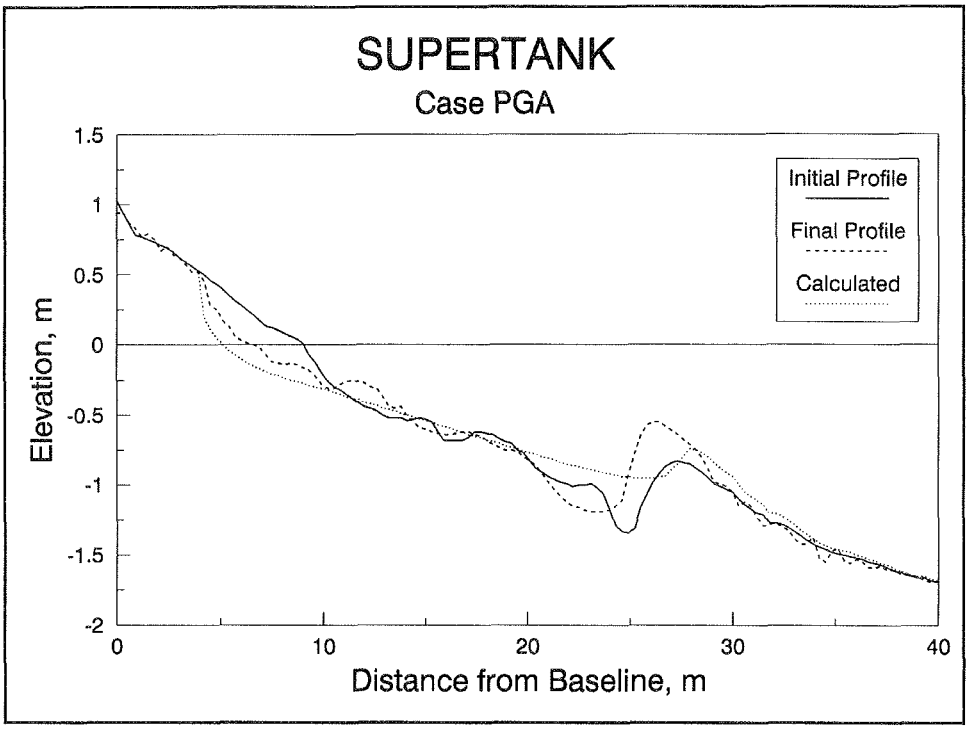

Figure 7. Result of default simulation, SUPERTANK case PGA

Simulation of the loosely packed dune test resulted in good agreement with measured erosion at the foreshore and dune, as shown in Figure 8. As observed in the equilibrium erosion cases, the modeled bar feature was situated some distance offshore from the measured bar. Figure 9 shows simulation results for the compacted dune. Although the shape of the compacted dune was well reproduced, SBEACH overpredicted the amount of erosion. The difference in model predictions between the two dune cases might be expected due to greater erosion resistance associated with the compacted sediment which is not accounted for in SBEACH.

Foredune erosion. This test case was designed to reproduce overwash of a foredune that may occur during a severe storm surge. As shown in Figure 10, SBEACH performed well in modeling the overtopping and complete erosion of the foredune. The final slope of the eroded profile was well reproduced. The model correctly predicted no erosion of the larger dune feature located behind the eroded foredune. The overwash algorithm included in the model overpredicted the amount of sediment that was transported onshore over the foredune crest.

Berm flooding. The berm flooding test cases were designed to replicate erosion associated with a storm surge that floods a berm located on the beach profile. Simulation results for both berm flooding test cases show reasonable agreement with the data as displayed in Figures 11 and 12.

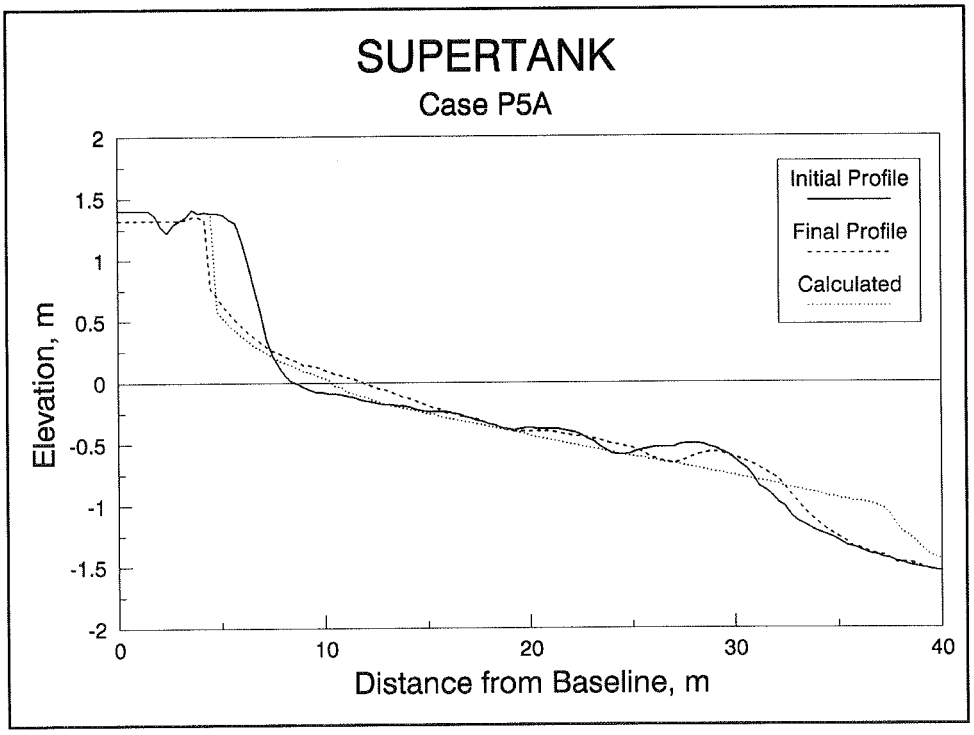

Figure 8. Result of default simulation, SUPERTANK case P5A

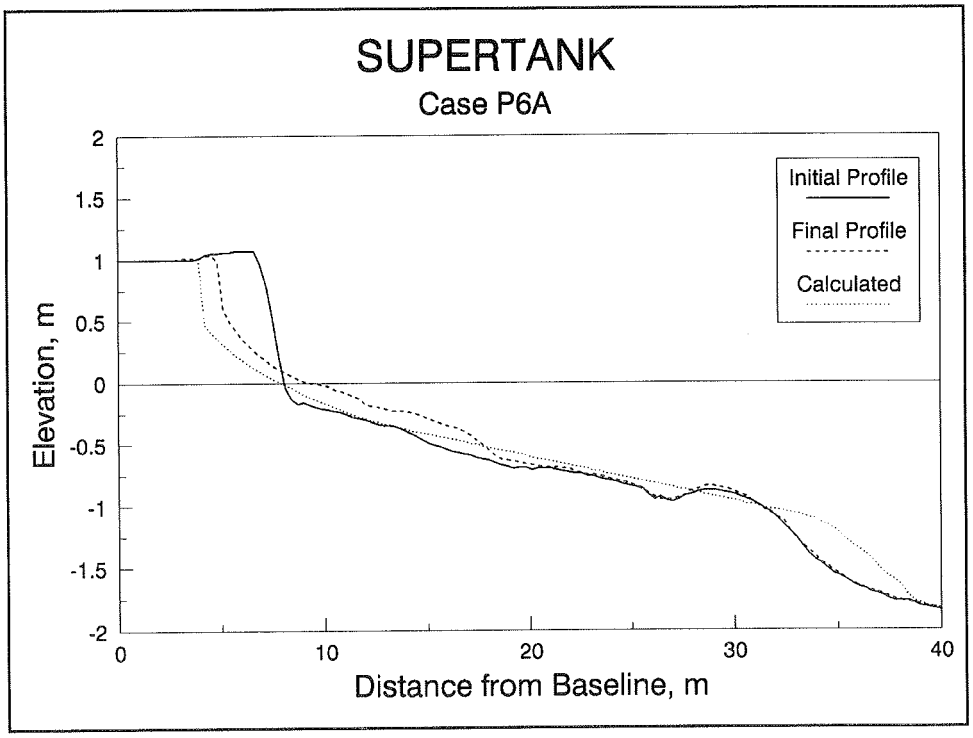

Figure 9. Result of default simulation, SUPERTANK case P6A

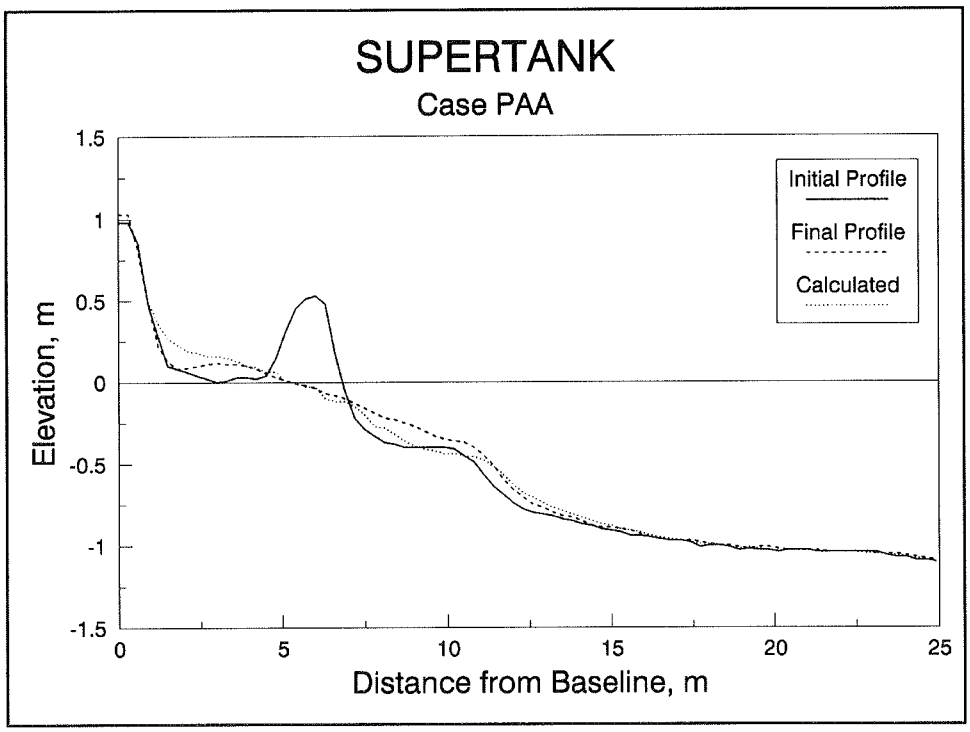

Figure 10. Result of default simulation, SUPERTANK case PAA

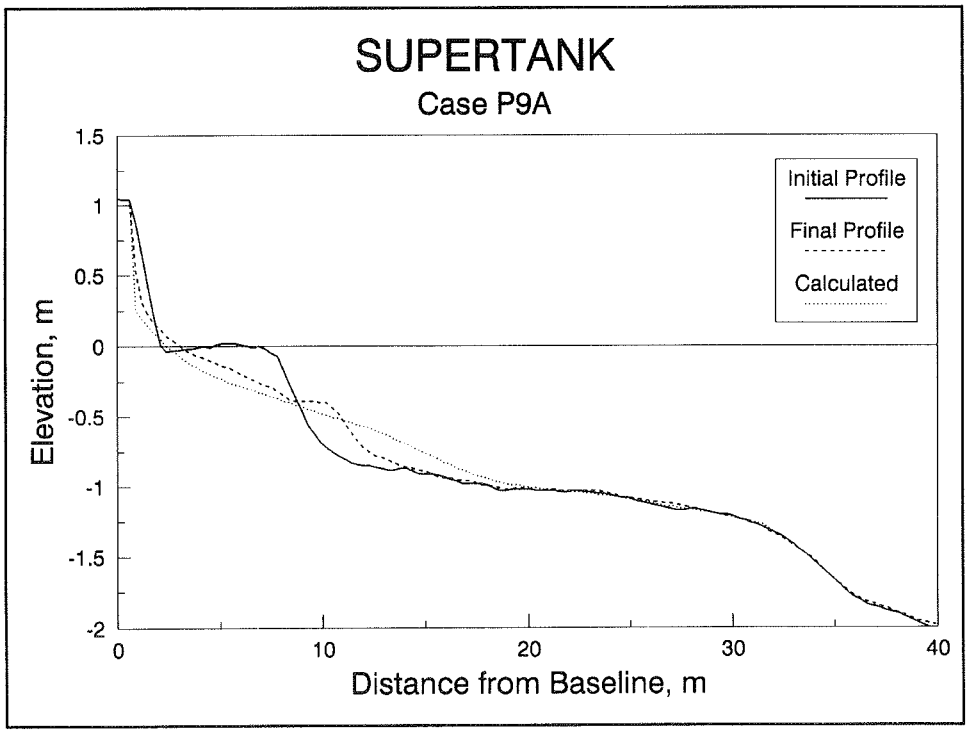

Figure 11. Result of default simulation, SUPERTANK case P9A

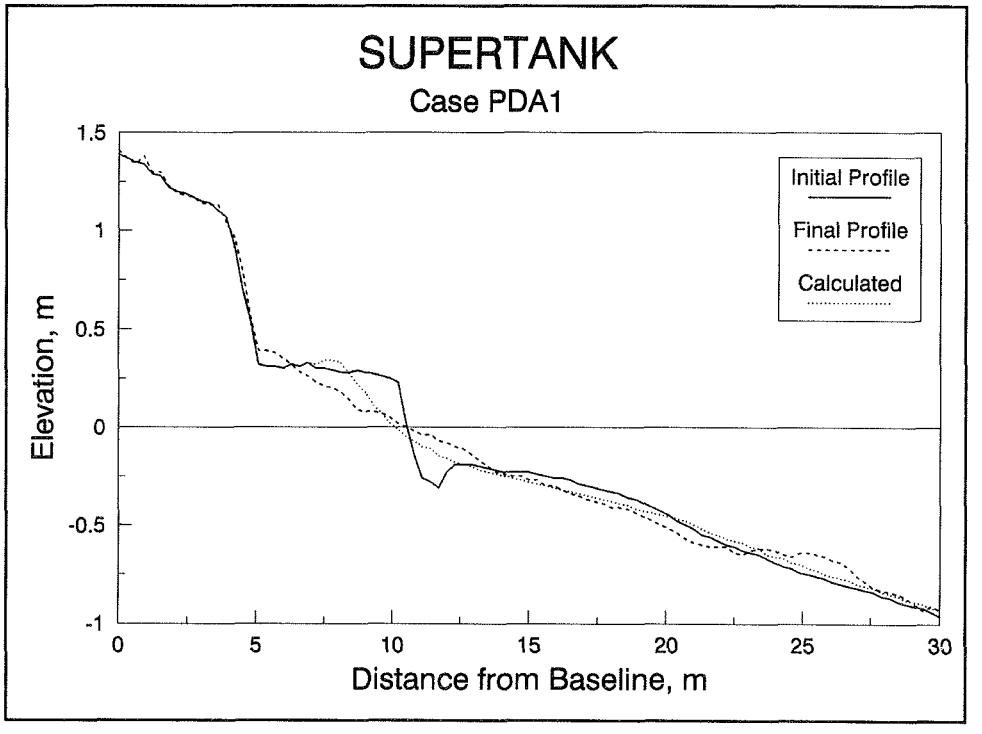

Figure 12. Result of default simulation, SUPERTANK case PDA1

In the first case, P9A, the berm was completely flooded and a portion of the dune behind the berm eroded. SBEACH correctly predicted the occurrence of dune erosion, but overestimated the amount of erosion at the berm and base of the dune (Figure 11). In the second berm flooding case, PDA1, the profile was subjected to a similar wave climate as P9A, but the water level was decreased by 0.6 m prior to the test. The decrease in water level resulted in a corresponding decrease in berm erosion with no erosion of the dune. Model results also show a decrease in berm erosion and no dune erosion. However, the model underestimated the magnitude of berm erosion observed in the laboratory data (Figure 12).

Seawall. The seawall studies at SUPERTANK were designed to provide insight into erosional processes at the base of a seawall. Three seawall tests were run, each with a different configuration.

For case P7D, a seawall was placed just above the still-water level on a gradually sloping profile. The seawall was flooded during the course of the test by raising the water depth by approximately 0.45 m. Wave action produced local deposition of sediment at the base of the seawall and formed a bar feature in the offshore region of the profile. Otherwise, no significant changes were observed across the nearshore profile.

The SBEACH simulation did not reproduce deposition at the seawall, and predicted more erosion of the initial profile than was observed, as shown in Figure 13. The calculated profile showed offshore deposition of the eroded material in three distinct bars. The largest bar was located offshore of the measured bar, while two smaller inner bars were located in the vicinity of the measured bar. The different bar features are probably associated with the rise in water level during the simulation. These results suggest that as the water level increased, the model moved toward an equilibrium state faster than what was evidenced by the measured profiles. Such response indicates that the default value of the transport rate coefficient, K, is too high in this case. This observation is consistent with the previously discussed results in which the model overestimated erosion.

The initial profile for the seawall case P8A1 was constructed by removing some of the material from in front of the seawall and placing it seaward on the profile. The resulting terraced profile allowed waves to break closer to the seawall, attacking the wall more directly than the previous case (Kraus and Smith 1994). The still-water level was held constant during this test at an elevation such that the base of the seawall was flooded to a depth of approximately 0.5 m. Contrary to expectations, the terraced profile test did not result in any significant scour at the seawall. A prominent bar with a deep trough formed at the offshore limit of the terraced portion of the profile (Figure 14).

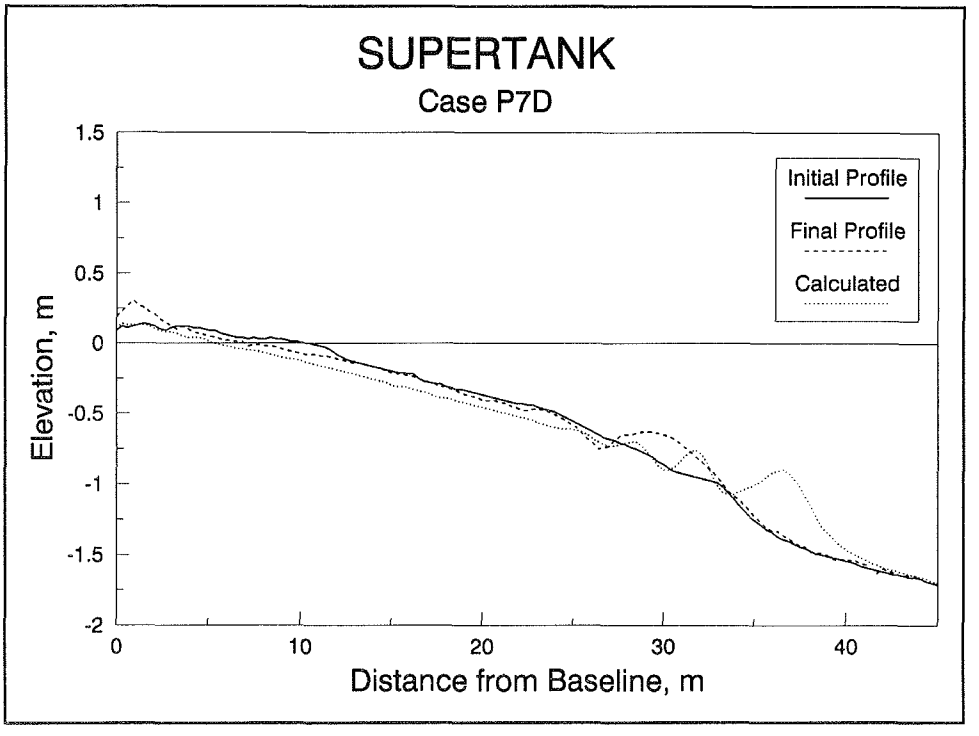

Figure 13. Result of default simulation, SUPERTANK case P7D

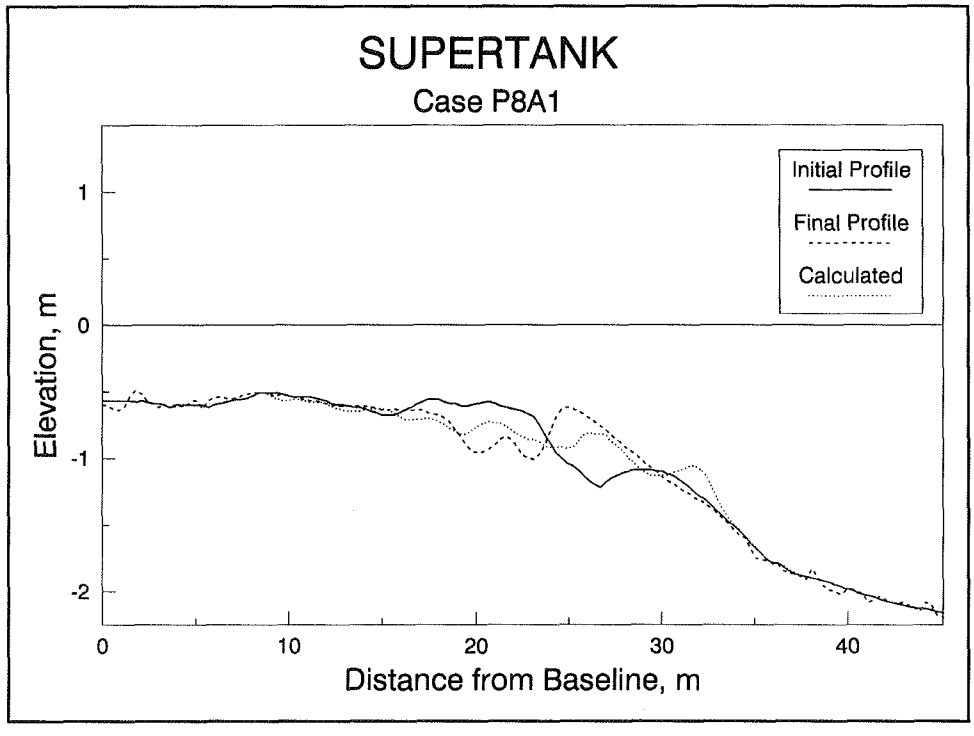

Figure 14. Result of default simulation, SUPERTANK case P8A1

As shown in Figure 14, SBEACH correctly predicted the absence of erosion at the seawall. The model also predicted the formation of a bar at the observed location, but did not reproduce the details of the bar and trough shape.

In the final seawall case (PCA), a sloping profile was constructed in front of the seawall. During the test the still-water level was raised from 0.15 to 0.45 m above the base of the wall. Unlike the previous cases, this test produced a prominent scour hole at the seawall. The observed scour hole was localized, with most of the erosion occurring close to the base of the seawall. Material eroded from the base of the seawall was deposited offshore in a fairly uniform manner with no distinct bar formation.

SBEACH predicted scour at the seawall, but not to the depth that was observed in the measurements. Modeled results also differed in nature from the laboratory observations in that the erosion occurred across a wider region of the profile (Figure 15). Similar to observations, SBEACH predicted fairly uniform deposition of the eroded material across the offshore profile with no formation of a distinct bar.

Narrow-crested mound. For this set of test cases, a narrow-crested mound was constructed in the offshore region of the profile. Wave breaking at the mound caused a significant amount of energy dissipation, reducing the amount

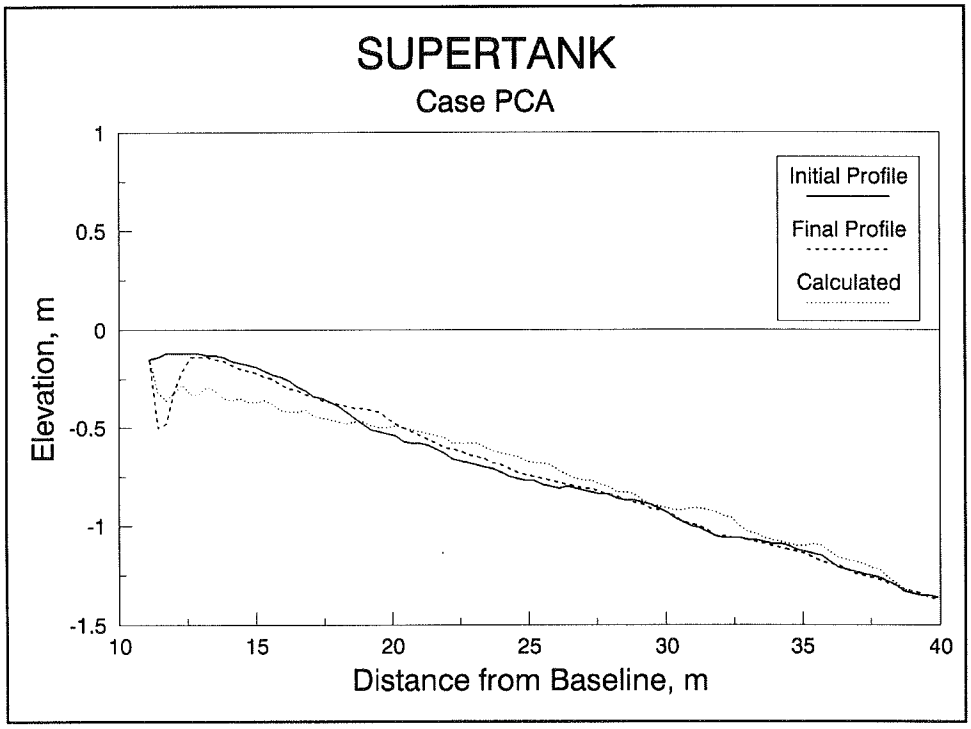

Figure 15. Result of default simulation, SUPERTANK case PCA

of incident wave energy that reached the foreshore. Tests were run with both random and monochromatic waves.

Figure 16 shows the results for the random wave case, PJA. Waves in this test case produced significant erosion at the mound. Erosion was greater on the shoreward side of the mound with some sediment being transported down the shoreward-facing slope. As illustrated in Figure 16, SBEACH overestimated erosion of the mound, with the entire mound crest being uniformly lowered. The model also overestimated the amount of erosion on the foreshore as may be expected considering the lowering of the mound crest. Both the model predictions and data show little change in the middle portion of the profile, implying wave re-formation occurred between the mound and the nearshore.

Figure 17 shows the results for the monochromatic wave test (case PJC). As illustrated in the figure, the uniform breakpoint of the monochromatic waves produced an increase in elevation of the mound crest corresponding to the formation of an offshore bar. A nearshore bar also formed from deposition of eroded foreshore sediment. In contrast to the observed profile changes, the model predicted little change in shape of the offshore mound. Foreshore erosion was reproduced fairly well, but the location of the nearshore bar was situated further offshore.

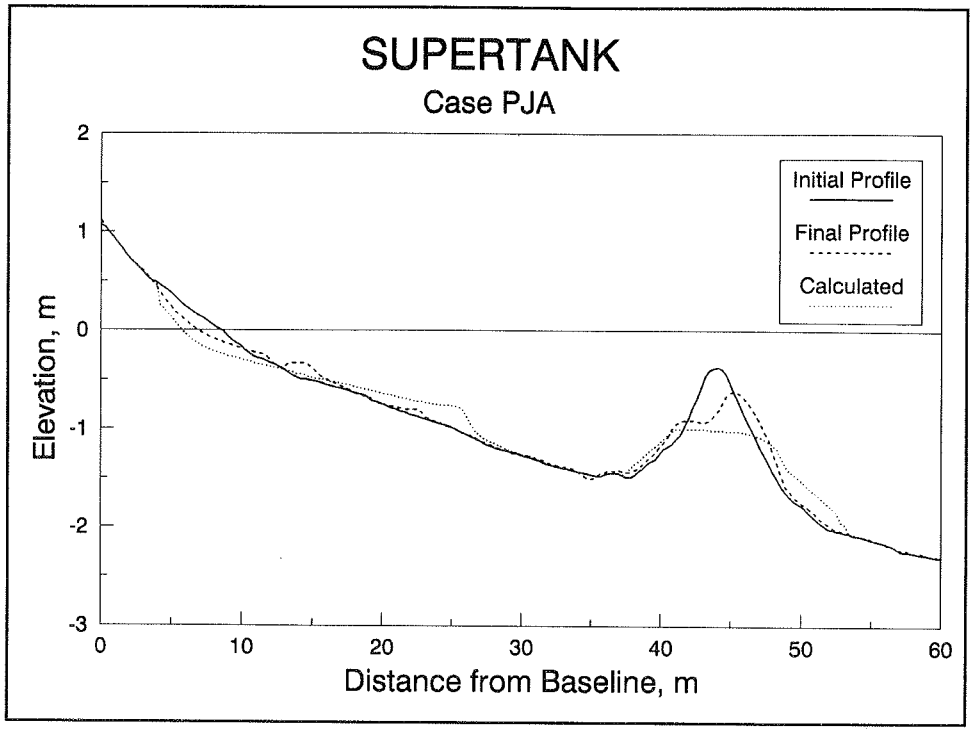

Figure 16. Result of default simulation, SUPERTANK case PJA

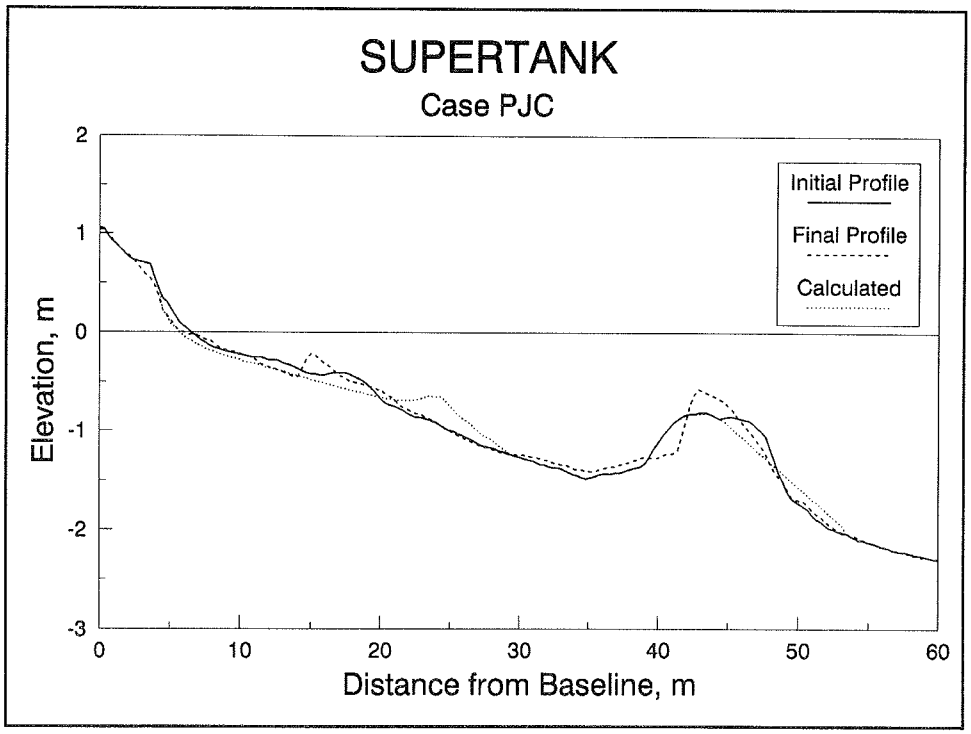

Figure 17. Result of default simulation, SUPERTANK case PJC

Broad-crested mound. SUPERTANK cases PKA and PKC involved erosion of a broad-crested offshore mound under random and monochromatic waves, respectively. The mound was constructed at approximately the same depth and location on the profile as the narrow-crested mound, and similar wave conditions were used.

As shown in Figure 18, the random wave test (case PKA) produced a trough at the offshore end of the mound, with material being deposited on the offshore slope of the mound. Little profile change was observed elsewhere. The SBEACH simulation eroded the entire mound to an elevation approximately 0.3 m below the initial mound, with most of the eroded material from the SBEACH simulation being deposited across the offshore slope of the mound. As a result of the lower mound height, the simulation allowed more wave energy to reach the foreshore, causing erosion to be overestimated at the foreshore.

The monochromatic wave test (case PKC) produced a trough on the offshore end of the broad-crested mound and reduced the height of the entire mound crest, as observed in Figure 19. The sediment removed from the mound was deposited in a bar at the offshore end of the mound crest. Model simulation of the test case produced slightly more lowering of the mound than was observed. Also, formation of a bar at the offshore end of the mound was

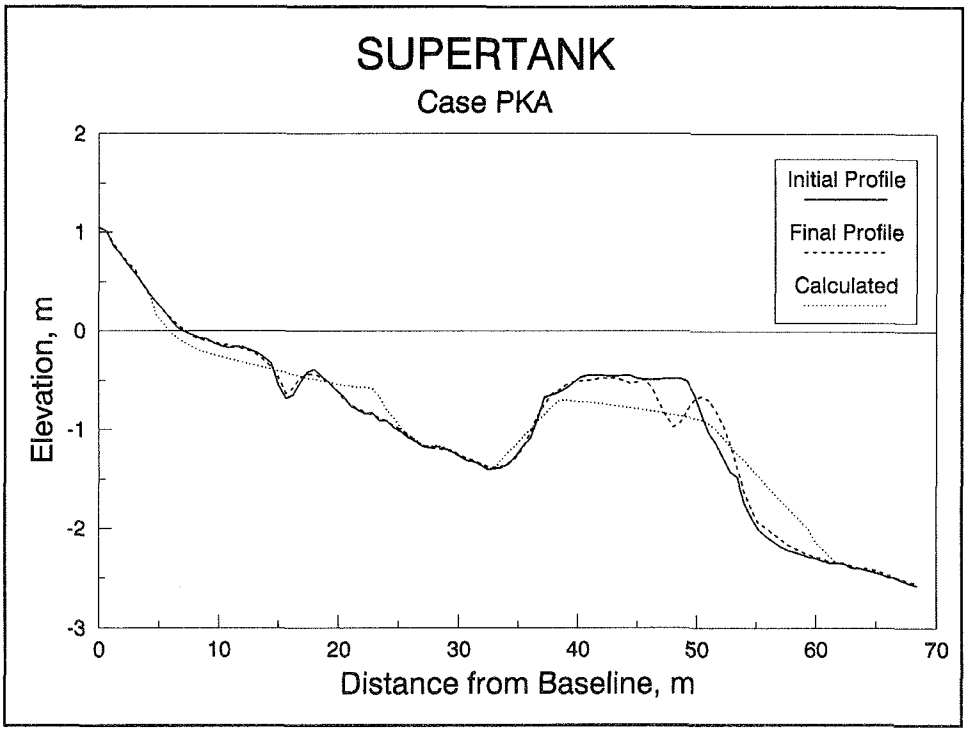

Figure 18. Result of default simulation, SUPERTANK case PKA

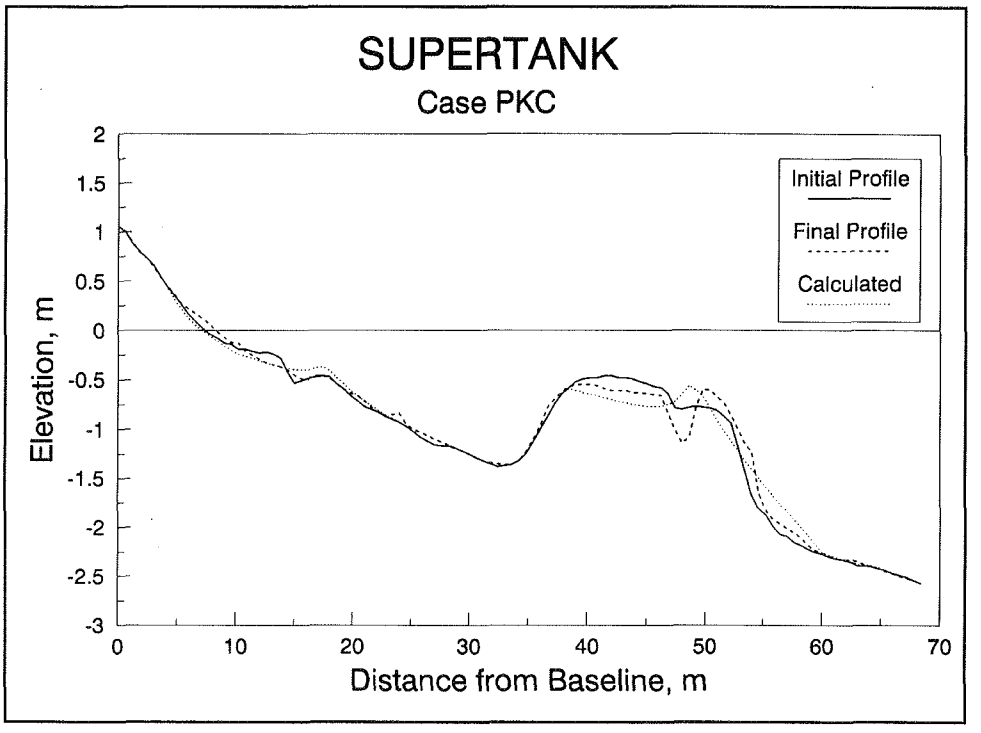

Figure 19. Result of default simulation, SUPERTANK case PKC

predicted, but the observed trough was not reproduced. SBEACH predicted erosion at the foreshore, whereas slight accretion was observed in the data.

For both the narrow- and broad-crested mound cases, SBEACH tended to erode and flatten the shape of the mound to a greater degree than was observed. The reduction of the mound height in the numerical simulation allowed more wave energy to pass across the mound, resulting in more erosion at the foreshore.

Summary

Model simulations using default calibration parameters qualitatively reproduced the measured profile response for most cases. In general the model predicted changes in profile morphology including areas of erosion and deposition. From a quantitative standpoint, however, the model tended to overestimate the magnitude of profile changes including erosion at the foreshore, offshore movement of the bar, and lowering of the offshore mound crest. Calibration of the model was performed to improve agreement between calculations and measurements.

Calibration

In order to best simulate all test cases, a representative test case was identified for calibration. The test case selected as most representative for the remaining profiles was case P5A, a dune erosion case. Case P5A involved a combination of significant erosion of the foreshore and dune, erosion related to water level rise, and development and movement of an offshore bar. This combination of effects presented an opportunity to adjust the calibration parameters to a representative collection of processes that dominate a significant number of the SUPERTANK test cases.

Calibration procedure

The calibration procedure started by simulating the selected calibration case using default parameters. Upon review of the results from the default simulation, conclusions were made regarding which calibration coefficients required modification and whether the values of the coefficients needed to be increased or decreased from the default values. Results from the changes in each calibration parameter were recorded and an iterative procedure was used to obtain the best fit of the calculated profile to the measured profile. The calibration process continued until no further improvements were gained by varying the calibration parameters.

Various methods are available for evaluating improvements gained through modifying calibration coefficient values. The simplest is visual inspection. The initial, final, and calculated profiles may be plotted to identify the portion of the calculated profile that does not match the final measured profile. With a basic understanding of the effects of the calibration parameters on the modeled profile, the user can make necessary modifications.

In addition to the method of visual inspection, statistical measures such as those given by Equations 99 and 100 can be used during calibration. Statistical measures allow the user to discern improvements that may be difficult to evaluate visually. An instance in which this type of comparison is useful is when improvements at one location on a profile are gained at the expense of another location. The statistical method of comparison provides an objective measure of the overall improvement along the profile and allows the best fit to be selected.

For calibration to case P5A, both visual inspection and statistical parameters were used to obtain the best simulated fit of the profile. Visual inspection was used to identify the appropriate parameter to be adjusted, whereas the statistical comparison allowed for fine-tuning of the individual calibration parameters. Improvements in the modeling of case P5A resulting from calibration are shown in Figure 20. In this figure, it can be seen that a much improved fit at the bar location was achieved in exchange for a slight

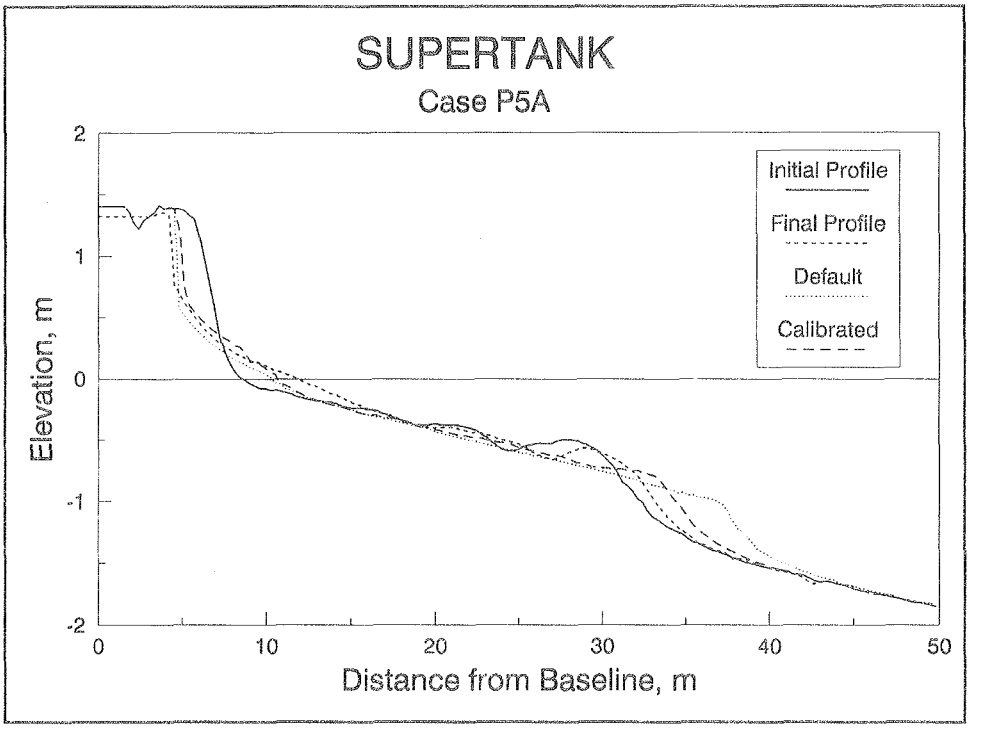

Figure 20. Comparison between results of default and calibrated simulations for SUPERTANK case P5A

compromise in the fit at the foreshore and dune. The parameters resulting from the calibration procedure for case P5A are given in Table 1. After calibration parameters for the representative case (P5A) were chosen, the parameters were used in subsequent model runs for the remaining test cases.

Table 1
Default and Calibrated Calibration Parameters for Case P5A

Parameter	Default Value	Calibrated Value
Transport rate coefficient, *K*	1.75 x 10^{-6} m^4/N	0.55 x 10^{-6} m^4/N
Slope-dependent coefficient, ϵ	0.002 m^2/sec	0.003 m^2/sec
Depth of the foreshore, *DFS*	0.3 m	0.15 m

Results of calibrated simulations

Simulation results using the calibration parameter values derived from case P5A were distinctly split between random wave cases and monochromatic wave cases. The random wave cases indicated significant improvements when

using the calibration parameters from case P5A. However, simulation of the monochromatic cases with the calibration parameters from case P5A produced unsatisfactory agreement.

Random wave test cases. The rms and residual parameters given by Equations 99 and 100 were calculated across the entire profile for the default and calibrated simulations. The parameters were also computed across portions of the profile corresponding to the nearshore and bar regions. The nearshore region was defined as the portion of the profile between the shoreward boundary and the point of transition from erosion to deposition on the measured profile. The bar region included the area of offshore deposition and the region of bar and trough formation and movement. The nearshore and bar regions were identified for each case based on visual inspection of the initial and final measured profiles. Separate analysis of the nearshore region was performed since prediction of erosion at the shore is the model result used most often in project applications. The bar region was also analyzed to provide insight into model predictions of bar formation and movement. Table A2 presents results of the statistical calculations for each case.

For the default simulations of random wave cases, the average value of the residual parameter in the nearshore region was 2.32 before calibration. After calibration, the average value of the residual for all cases decreased to 0.87, indicating improved agreement. An average residual of 0.87 may still seem fairly high. However, a significant portion of the higher residual values were for cases in which the actual profile change and absolute error in prediction (as measured by the rms parameter) were small. In fact, the average value of *RMS* for the calibrated simulations was 6.0 cm in the nearshore region, indicating an average error of 6.0 cm in predicting nearshore profile elevation.

Figure 21 presents the improvement in the nearshore residual for each random wave test case. Figure 22 presents the changes in absolute error in the nearshore for each random wave test case. Both of these figures show that consistent improvement was achieved through calibration to the random wave cases. Individual improvements in the profiles of the calibrated cases are shown for an equilibrium erosion case (P1A), a berm flooding case (PDA1), a seawall case (P7D), and a mound case (PKA) in Figure 23. In each case, the calibrated simulation provided improved agreement.

Although model calibration provided significant improvements in calculated results for most cases, all differences between the predicted and measured profiles were not eliminated. For example, SBEACH still did not reproduce details of bar and trough systems such as the one for case P1D shown in Figure 24. Also, in the foreshore dune erosion case, PAA, the lower transport rate coefficient resulted in incomplete erosion of the foredune and underestimation of offshore transport and overwash of the eroded material (Figure 25).

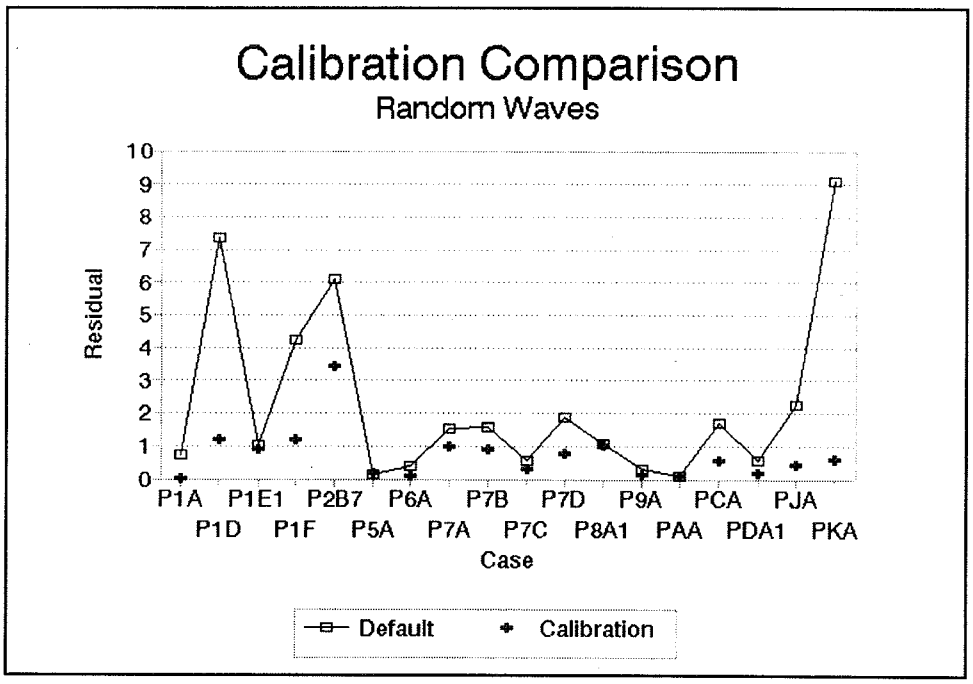

Figure 21. Comparison between residuals of default and calibrated SUPERTANK simulations

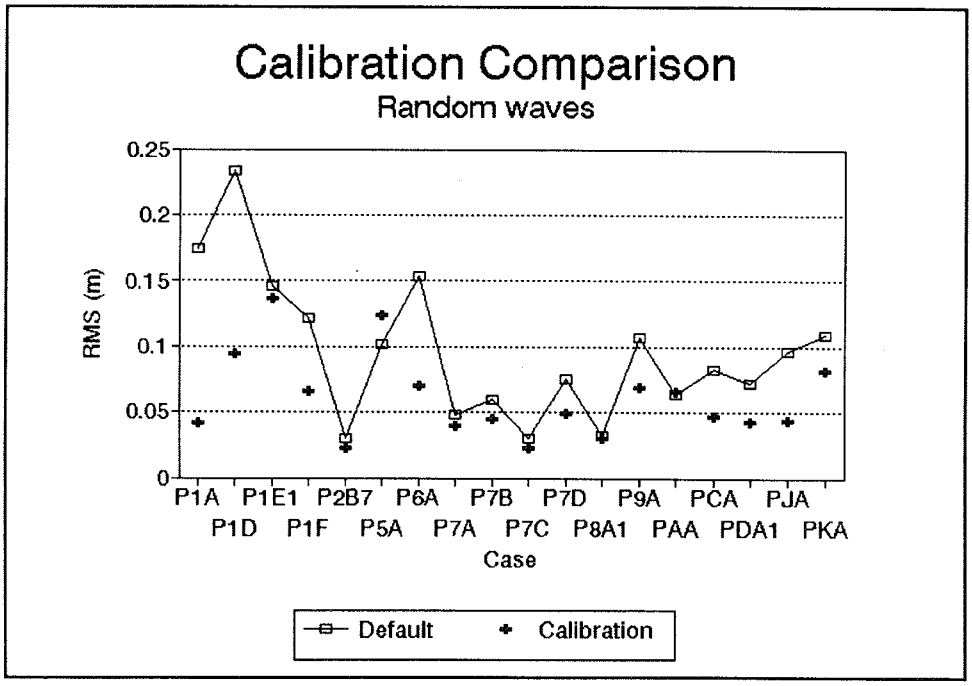

Figure 22. Comparison between RMS error of default and calibrated SUPERTANK simulations

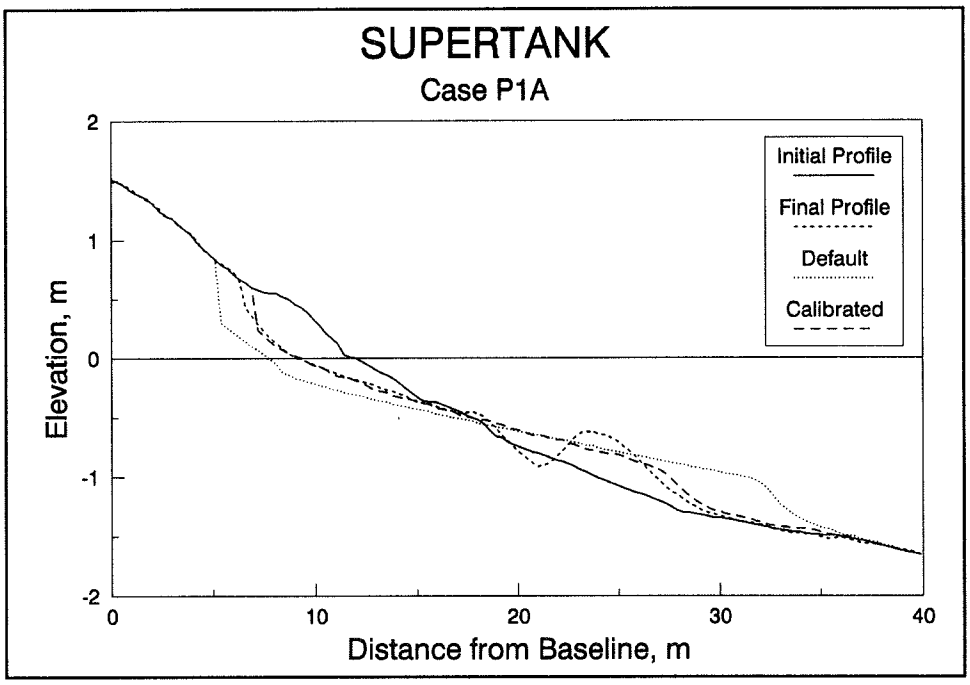

a. Case P1A

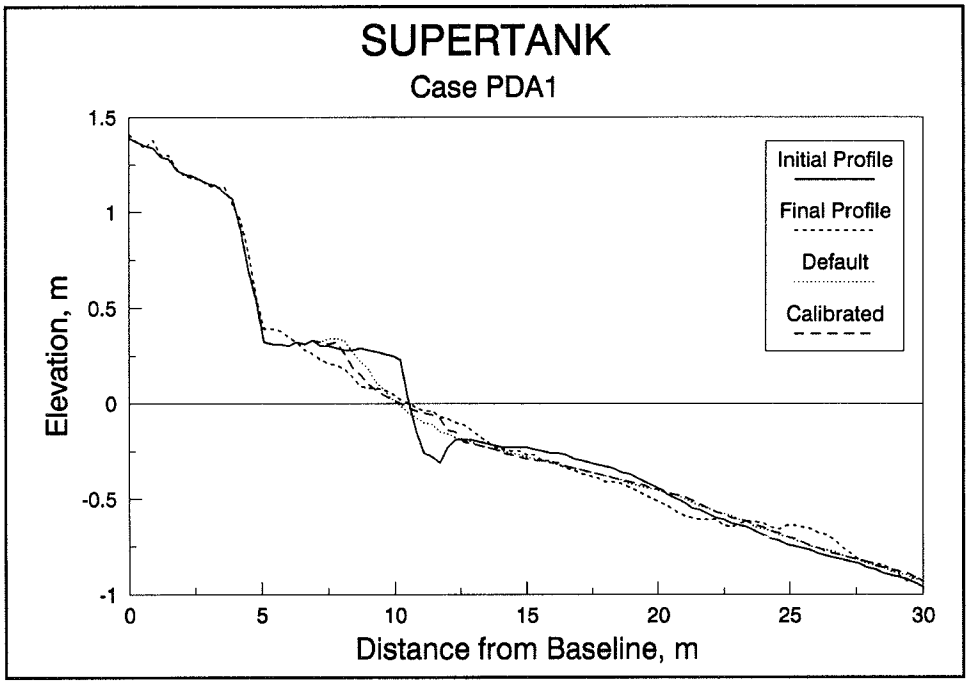

b. Case PDA1

Figure 23. Comparisons of selected default and calculated SUPERTANK profiles (Continued)

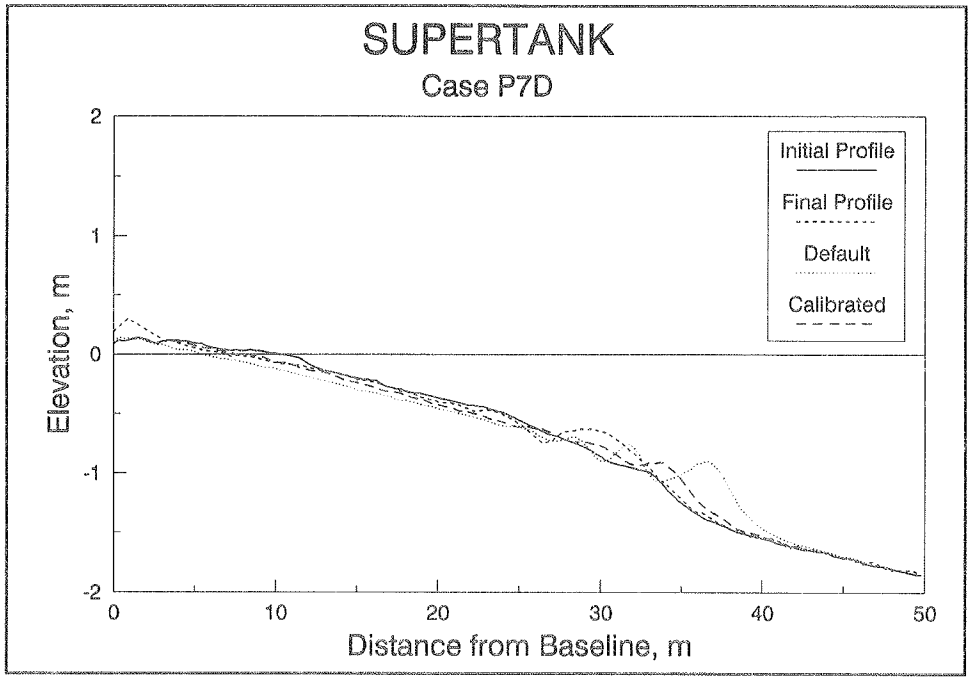

c. Case P7D

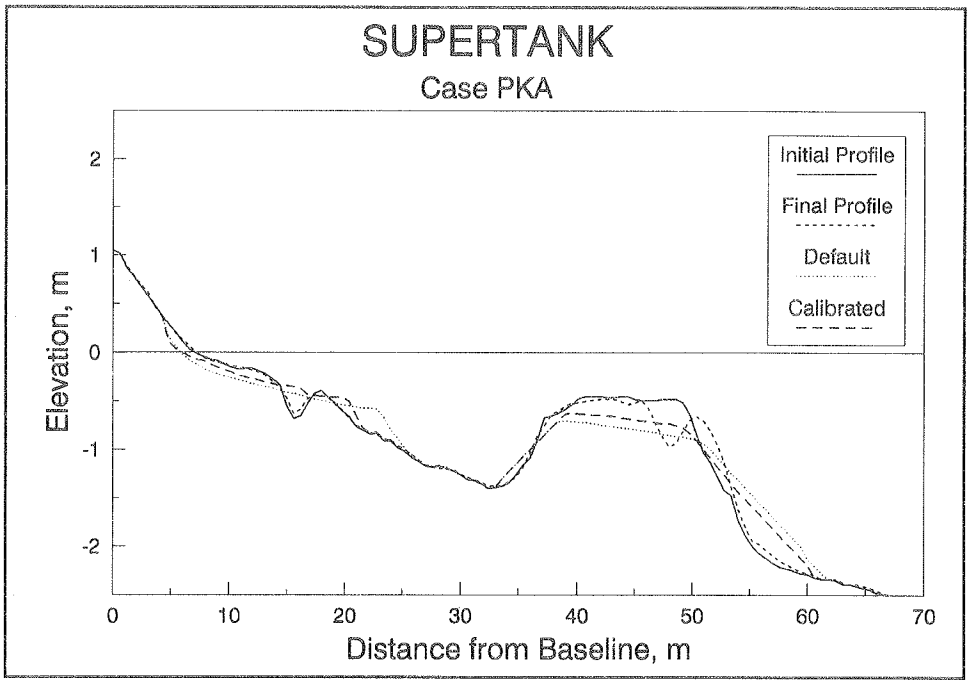

d. Case PKA

Figure 23. (Concluded)

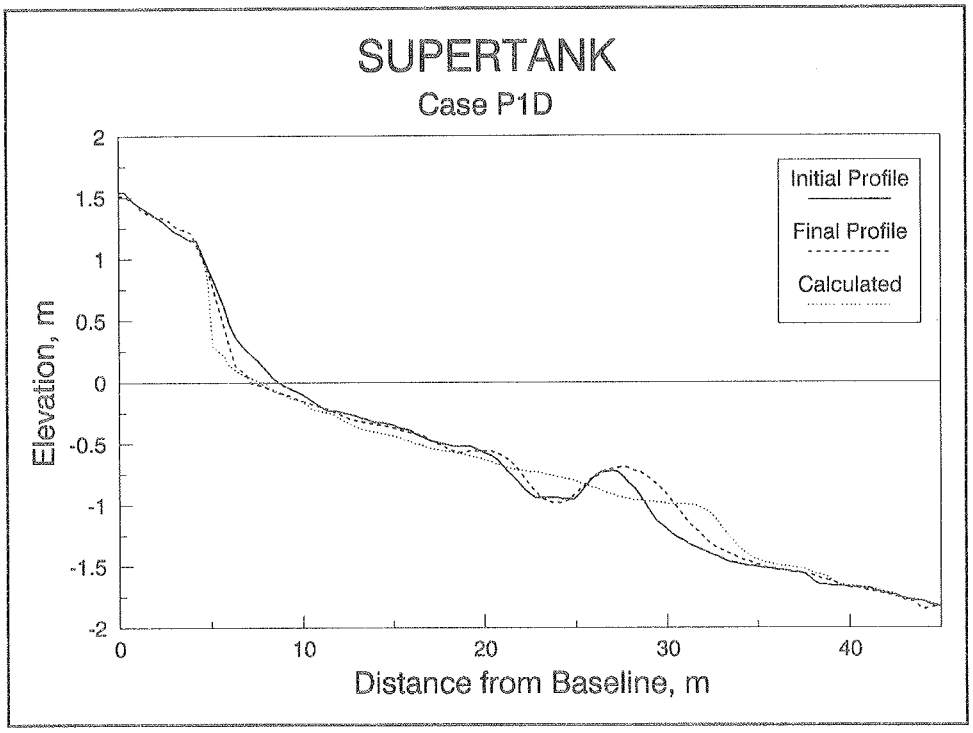

Figure 24. Result of calibrated simulation, SUPERTANK case P1D

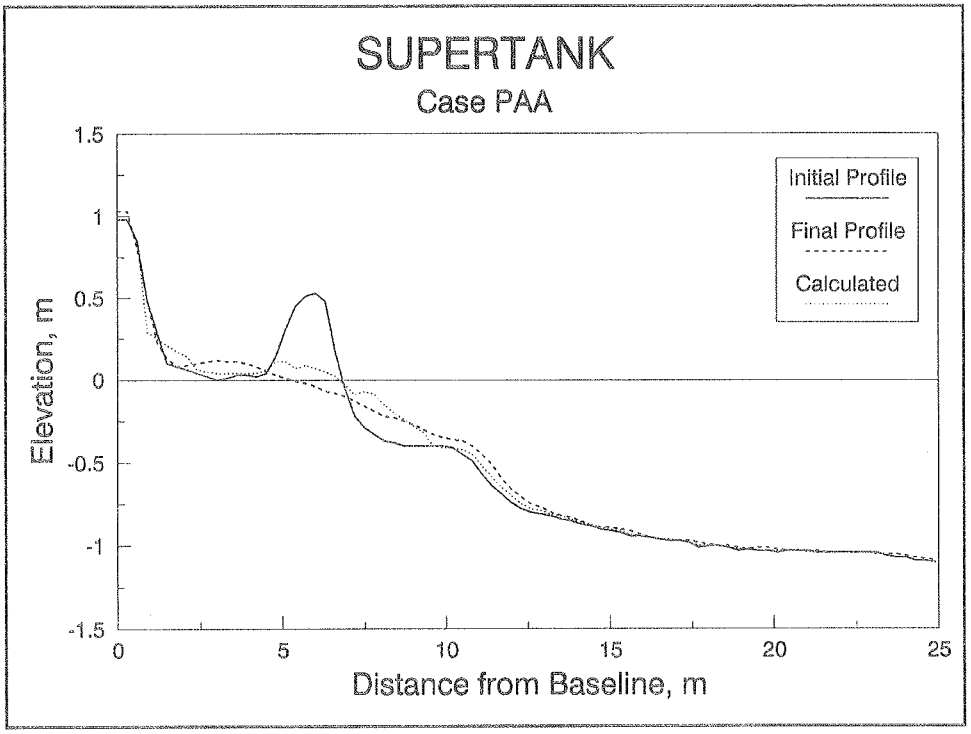

Figure 25. Result of calibrated simulation, SUPERTANK case PAA

Monochromatic test cases. The calibration to case P5A resulted in consistent improvements for almost all cases run with random waves. However, nearly all of the monochromatic wave cases showed worse agreement using the calibration parameter values derived from the calibration to case P5A. Figure 26 shows a plot of nearshore residuals for the monochromatic wave cases both before and after calibration to case P5A. Nearly all of the monochromatic cases calibrated to the random test case resulted in excessive foreshore erosion and produced profile slopes that were milder than those measured in the laboratory. The distinct differences between the results of the random wave cases and the monochromatic wave cases prompted a separate calibration to a monochromatic wave case.

Monochromatic calibration. The calibration for the monochromatic wave cases followed the guidelines outlined for calibration of the random wave cases. Case PGA was selected as the representative case for the monochromatic calibration. The calibration parameter values resulting from the monochromatic calibration are given in Table 2. The transport rate coefficient, K, was reduced slightly from the previous calibration. The slope term coefficient ϵ was also reduced, while the depth of the foreshore *DFS* was increased. The decrease in K reduced the amount of calculated foreshore erosion, resulting in a better fit to the measured data. By decreasing the value of ϵ, the slope of the profile increased, to better fit the profile slope of case PGA. An increase in *DFS* provided better agreement of profile change at

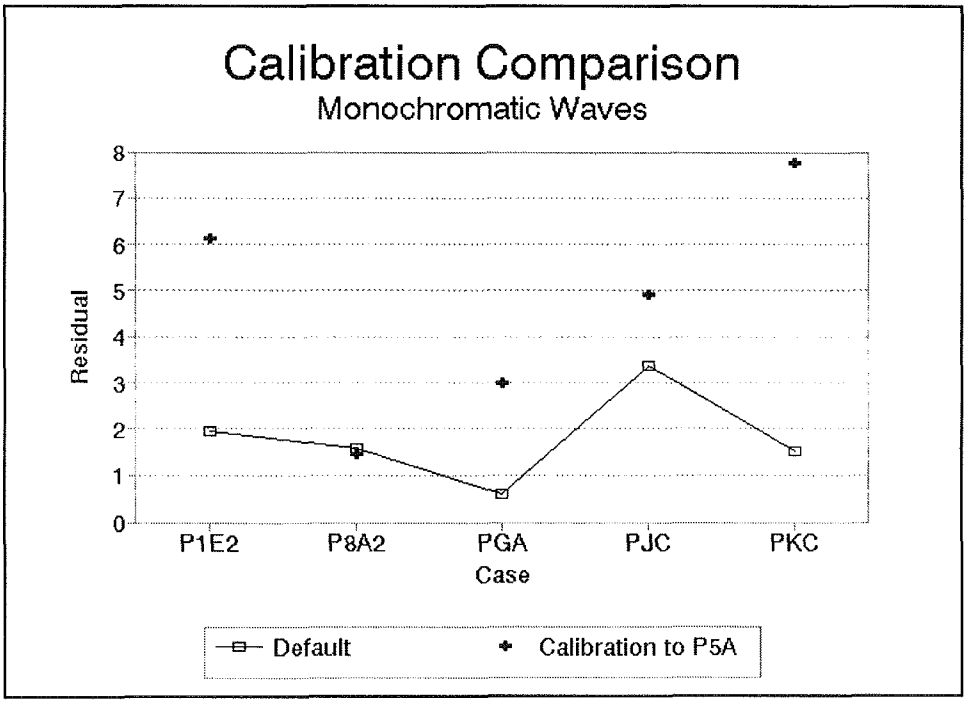

Figure 26. Comparisons of residuals between default and P5A calibration (monochromatic cases)

Table 2
Parameters for Monochromatic Case Calibration

Parameter	Monochromatic Calibration Values
Transport rate coefficient, K	0.50×10^{-6} m^4/N
Slope-dependent coefficient, ϵ	0.001 m^2/sec
Depth of the foreshore, *DFS*	0.25 m

the foreshore. Improvements gained through calibration to case PGA are shown in Figure 27.

The monochromatic calibration yielded significant improvements for the monochromatic test cases. Figure 28 shows that in all cases the monochromatic calibration improved model performance, as measured by the nearshore residual, over both the default parameters and the random wave calibration parameters. This implies that separate calibrations are necessary when employing SBEACH to simulate profile response under random waves versus monochromatic waves.

Summary

Calibration to the dune erosion case, P5A, greatly improved the model results for the random wave cases over the results obtained using the default parameters. The fact that improvements using the calibrated parameters were consistent among random wave cases (nearly all cases improved over the default runs) indicates that a single calibration can be applied to simulate a wide variety of cases with acceptable results. Extending this observation to field applications suggests that use of a single calibration at a given site should provide reasonable results for a variety of beach configurations and storm conditions.

Applying the random wave calibration parameters to the monochromatic wave cases resulted in unsatisfactory agreement with the data. By performing a separate calibration for the monochromatic tests, model results were in much closer agreement with the laboratory data. This indicates that separate calibrations should be performed when applying SBEACH to simulate profile change under random waves versus monochromatic waves.

Profile Evolution

The frequency of SUPERTANK profile surveys provided a unique opportunity to observe the evolution of a profile as it eroded. This portion of

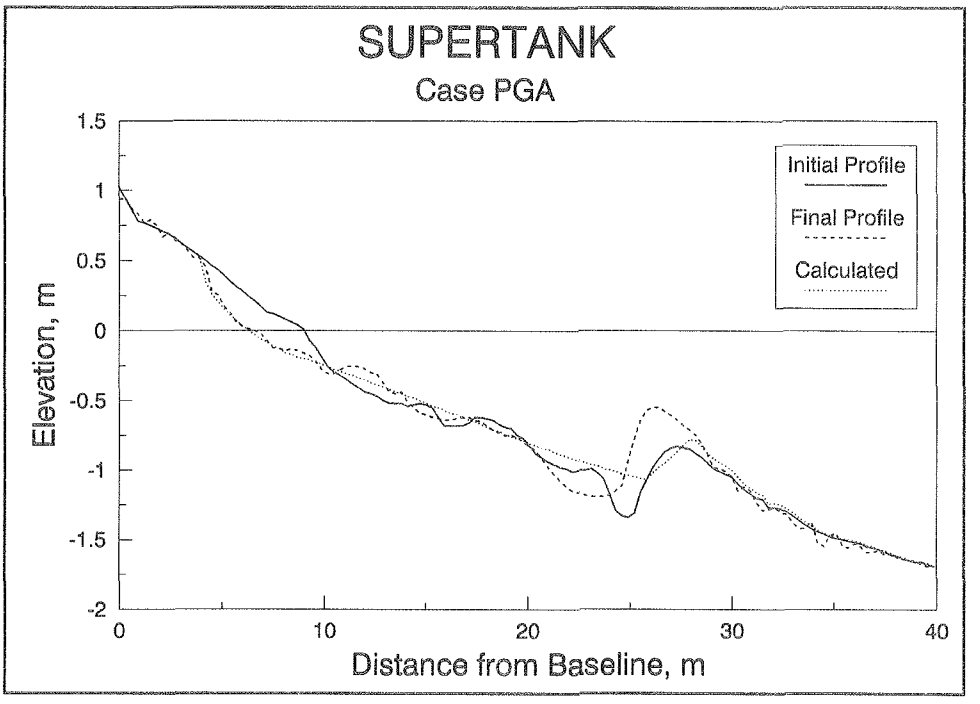

Figure 27. Result of simulation of monochromatic calibration, SUPERTANK case PGA

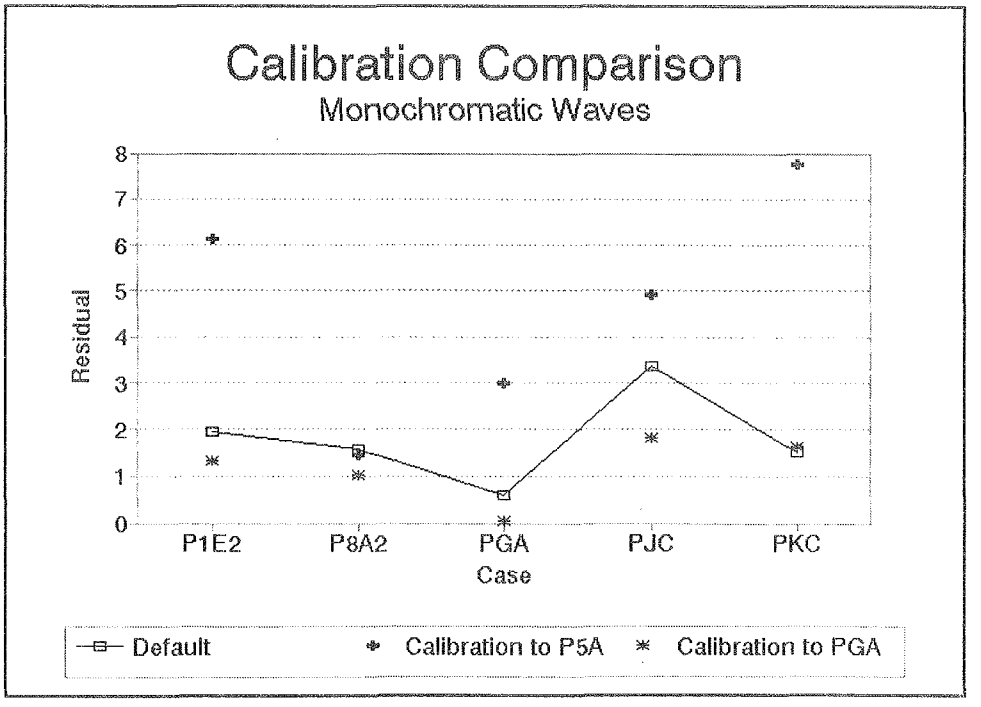

Figure 28. Comparisons of residuals between default, P5A calibration; and PGA calibration (monochromatic cases)

the study focused on the capability of the calibrated model to simulate temporal characteristics of profile response for two SUPERTANK cases involving equilibrium erosion (case P1A) and dune erosion (case P5A).

Case P1A

In modeling temporal profile response, the calculated profile was output at each time during the simulation that an intermediate profile survey was made during the laboratory test. Comparison of calculated and measured profile change is given in Figure 29 at three time intervals for the calibrated simulation of case P1A. The temporal response was well modeled although there is a slight lag in the calculation of erosion at the foreshore.

The sensitivity of the time response to changes in the transport rate coefficient K was investigated. Figure 30 shows the time variation in residual of the entire profile for different simulations of case P1A using various values of K. Higher values of K provided better agreement early in the simulation while lower values provided best agreement over the entire simulation period.

Case P5A

A similar analysis was performed for the dune erosion case, P5A. As shown in Figure 31, the calculated profile followed the observed profile fairly well in the early part of the simulation. At the end of the test, the calculated dune erosion began to lag the data. Increasing K improved the prediction of final dune erosion, but also resulted in worse agreement in the simulation of the bar. This suggests that in some applications there is a trade-off in the present model in accurately simulating dune erosion versus bar formation and movement. This trade-off could be related to inadequacies of the simplified approach in modeling swash zone transport and dune erosion processes under certain conditions.

Hannover Laboratory Data

In addition to the SUPERTANK laboratory data, a single data set from a laboratory study conducted at the University of Hannover, Germany, was used to evaluate the SBEACH model. The median grain diameter of the sediment used in the experiment was 0.33 mm. Random waves with a significant height of 1.5 m and a peak spectral period of 6 sec were used in the tank to bring the constructed dune profile to equilibrium. Additional information on the laboratory study is presented by Dette and Uliczka (1986).

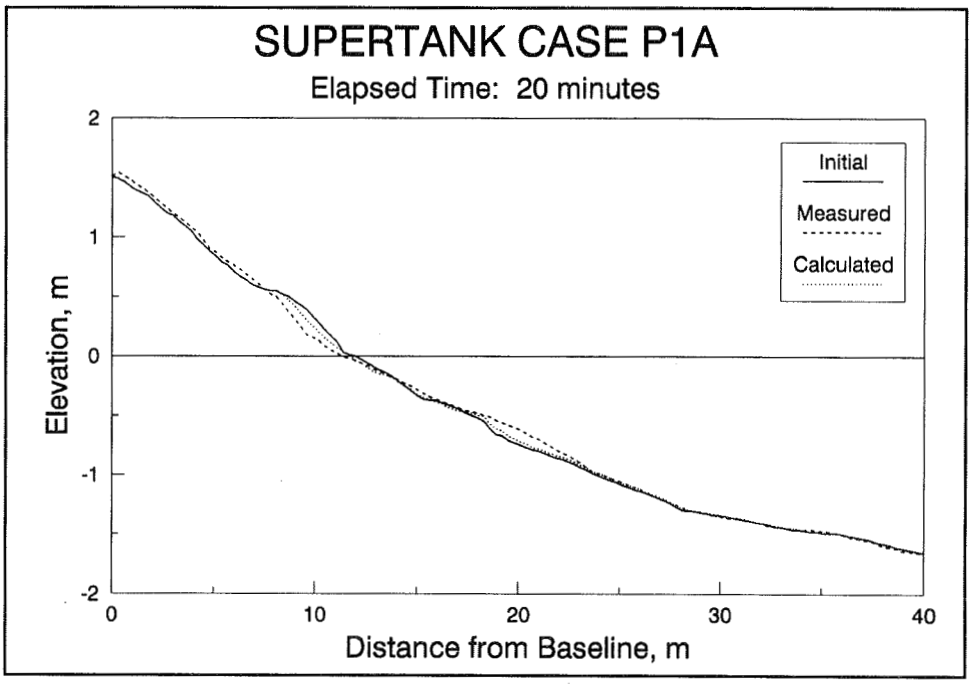

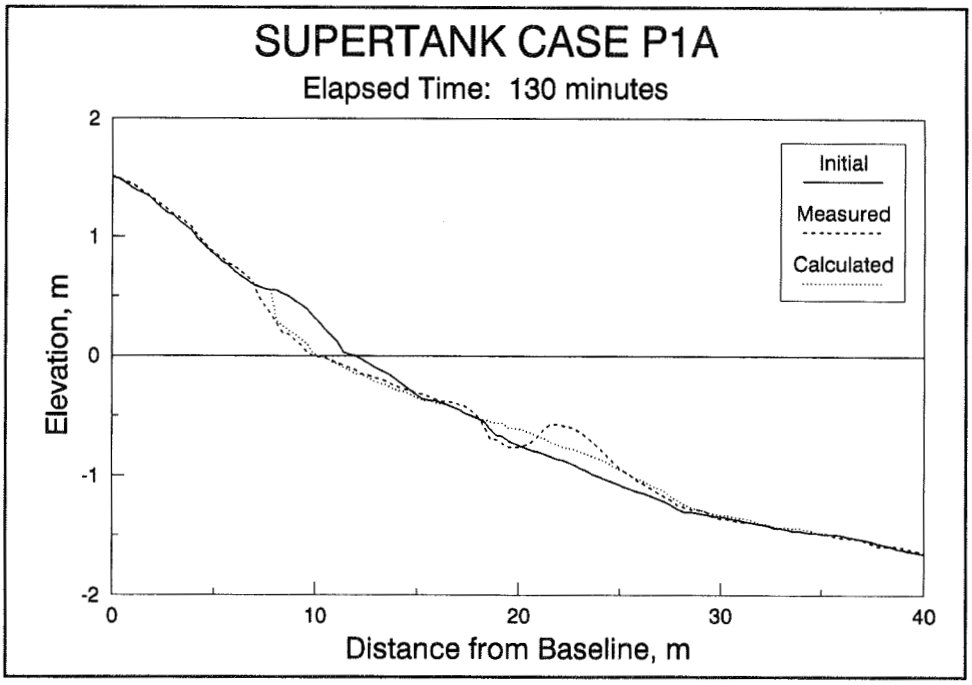

Figure 29. Measured and simulated time-series evolution of SUPERTANK Case P1A (Continued)

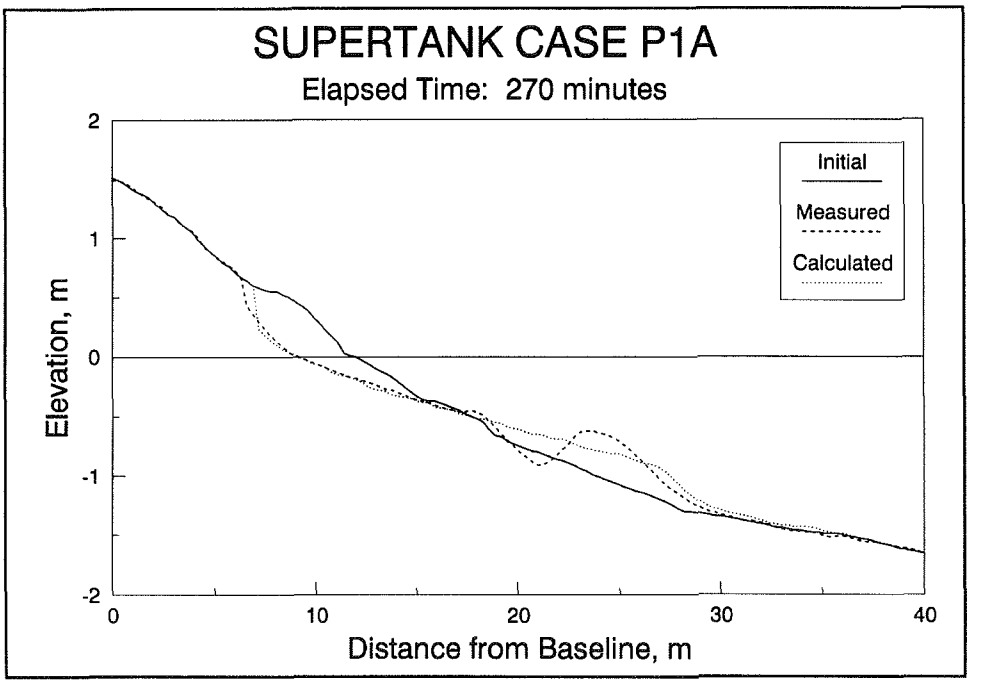

Figure 29. (Concluded)

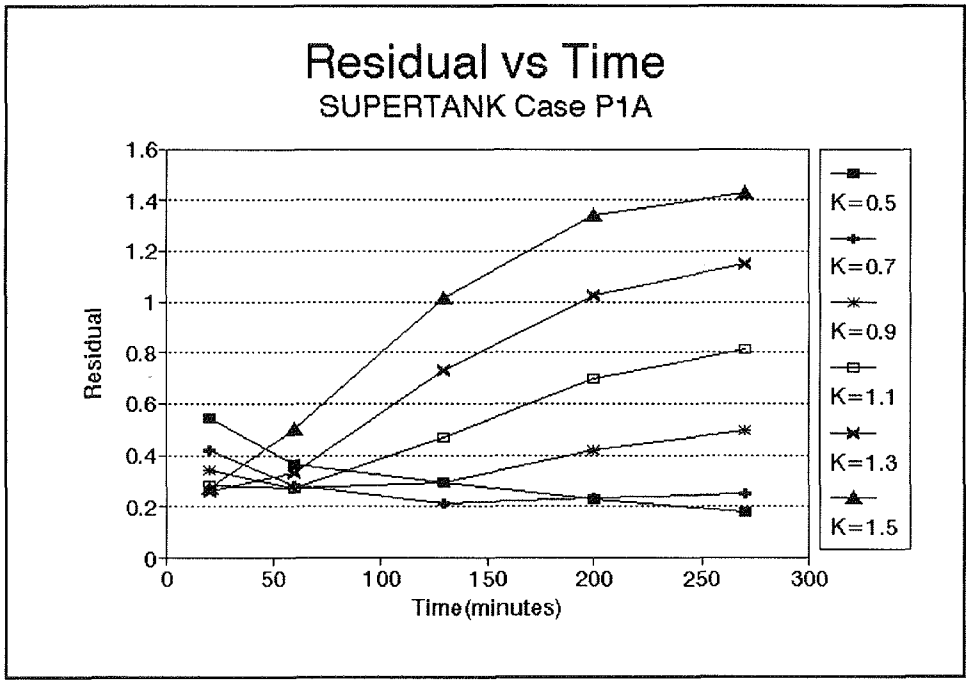

Figure 30. Residual vs. time for a range of K (transport rate coefficient) values

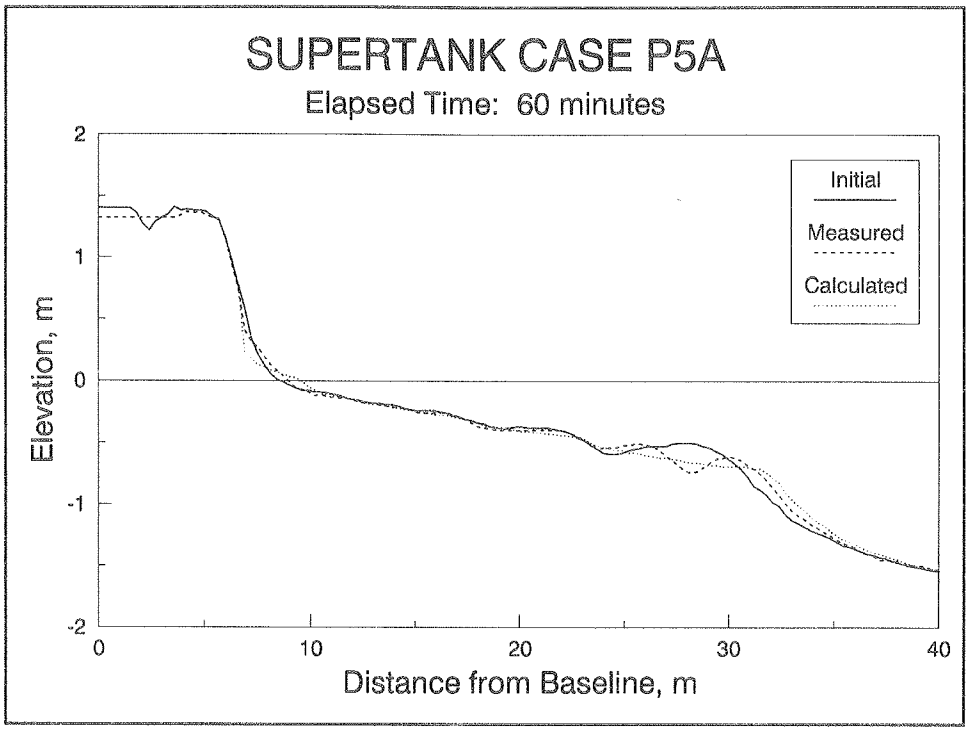

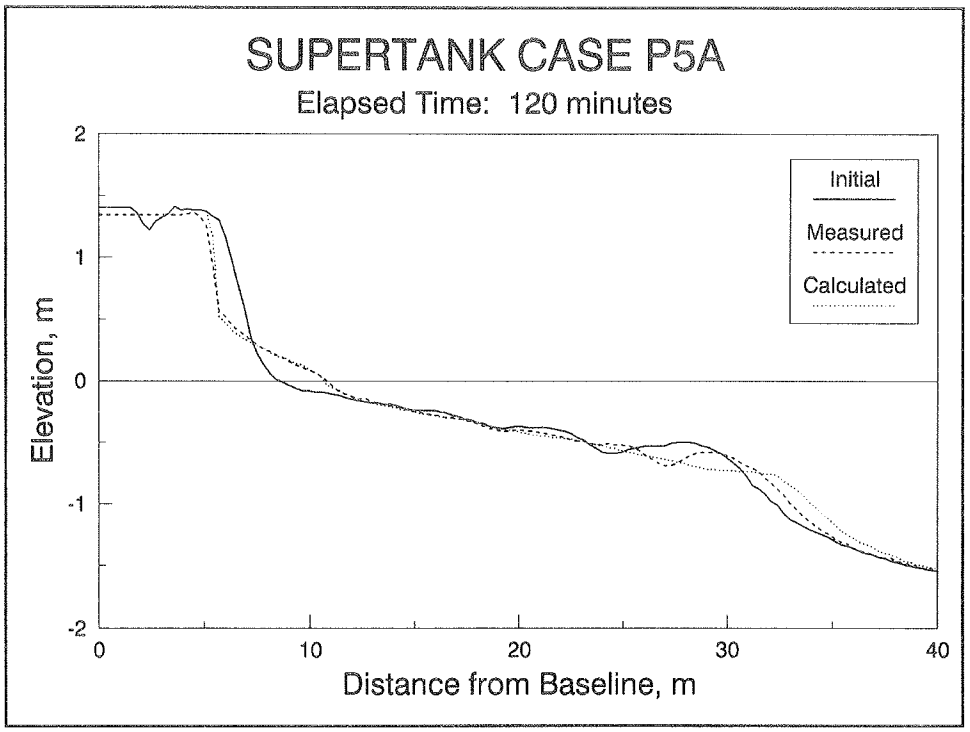

Figure 31. Measured and simulated time-series evolution of SUPERTANK Case P5A (Continued)

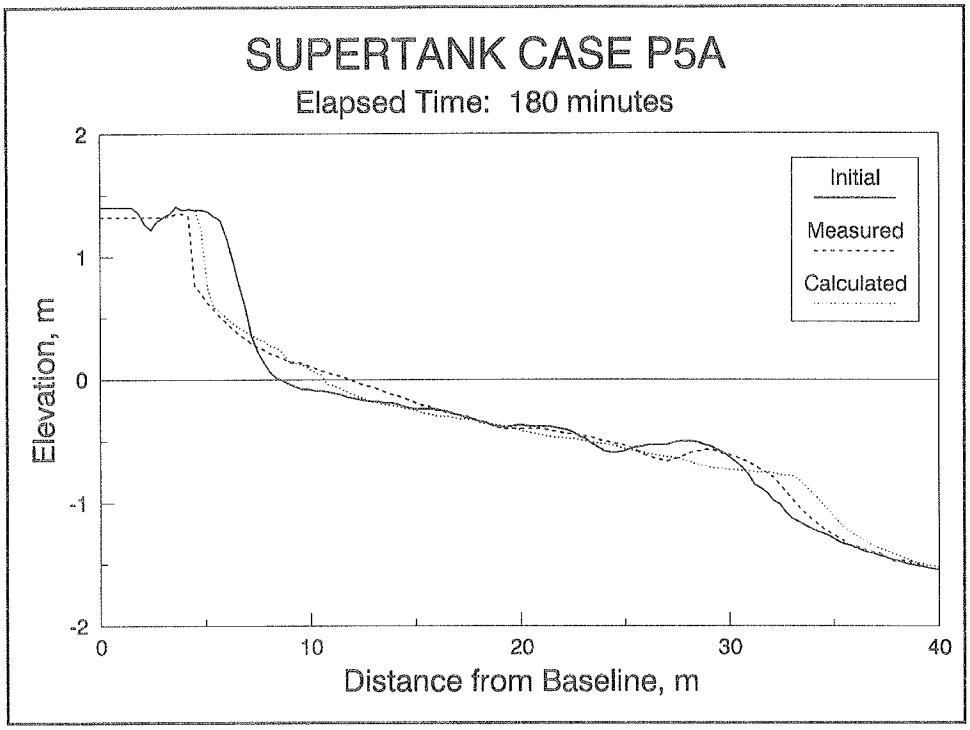

Figure 31. (Concluded)

Using default values for the calibration parameters, the SBEACH model reproduced the measured erosion fairly well with a slight overestimation of foreshore erosion and offshore movement of sediment (Figure 32). Following calibration of the model to the data, agreement between the measured and calculated profiles improved. With a decrease in the value of K to 1.20×10^{-6} m^4/N in the calibrated case, the predicted erosion at the dune came more in line with the data, as evident in Figure 33. The decrease in K also reduced the volume of sediment that was transported offshore. The value of ϵ was changed from the default value of 0.002 m^2/sec to 0.005 m^2/sec to produce a flatter profile.

The amount of erosion in the Hannover test was greater than that observed in the SUPERTANK tests, indicating the initial profile was in greater disequilibrium. Also, larger incident wave heights were used in the Hannover test, implying more energetic conditions. These factors may explain why a higher value of K was required for the Hannover test as compared to the SUPERTANK cases. This limited comparison suggests that K may be a function of the scale of profile change as well as wave conditions.

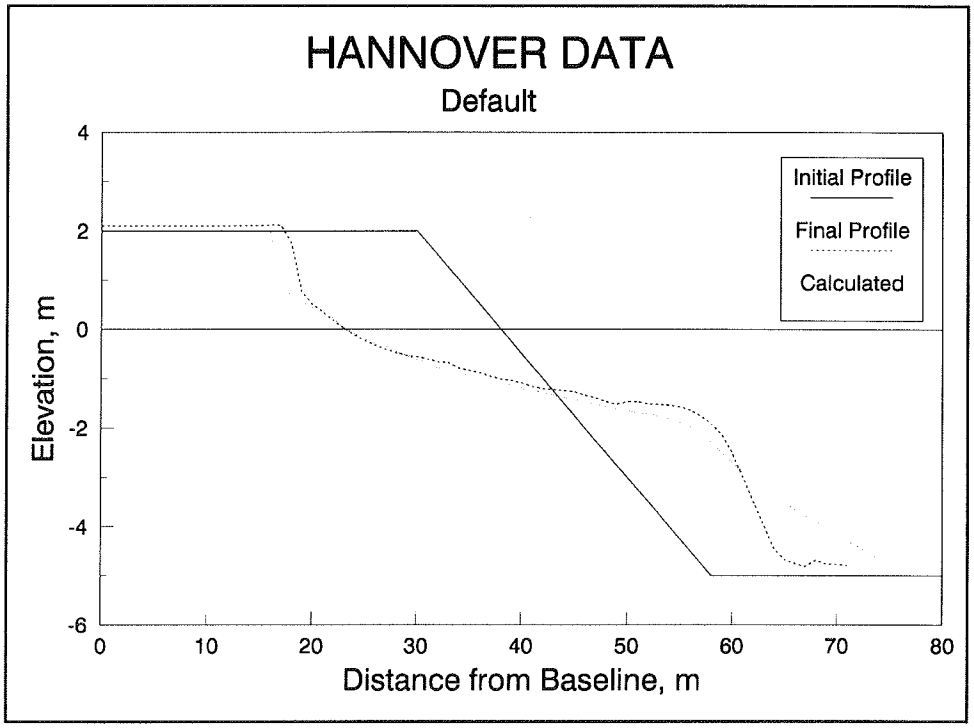

Figure 32. Result of default simulation of Hannover laboratory data

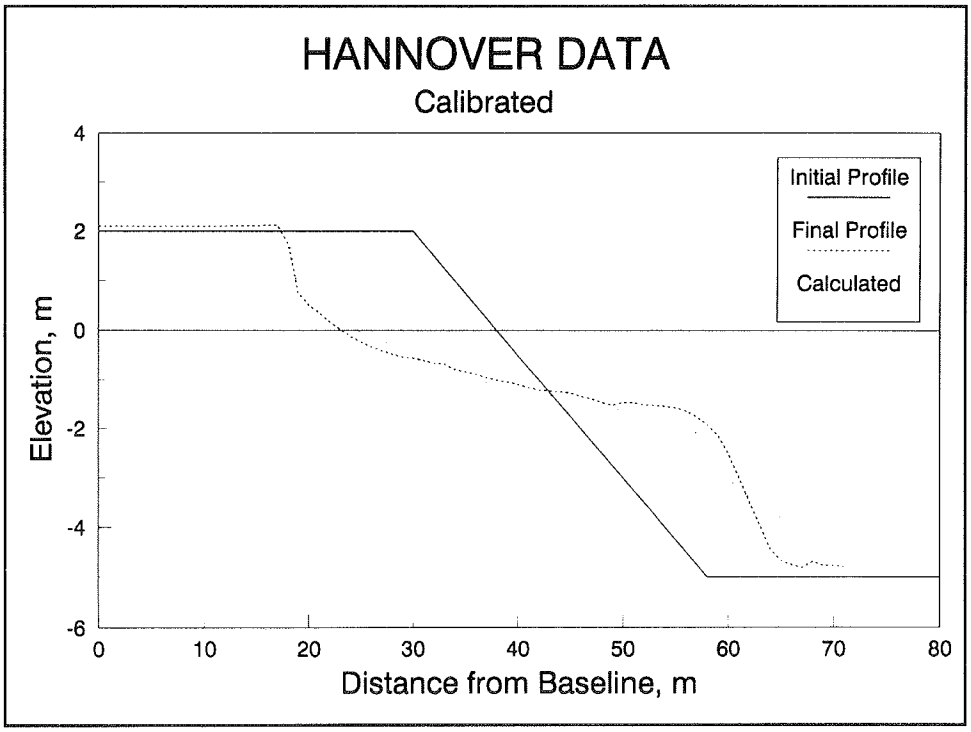

Figure 33. Result of calibrated simulation of Hannover laboratory data

Summary of Laboratory Simulation Results

In the presentation of results for the various test cases, certain trends and tendencies of SBEACH were observed. These observations are summarized by topic in the following section.

Model performance

In general, SBEACH performed reasonably well in simulating the variety of test cases included in the SUPERTANK data set. Although the default simulations tended to overestimate erosion, improved results were obtained through model calibration. A single calibration provided improved agreement for nearly all random wave cases. A separate calibration was required for the monochromatic wave cases. Equilibrium erosion, dune erosion, and nearshore berm erosion were generally well simulated. SBEACH was less successful in simulating certain aspects of profile change for the seawall and offshore mound cases.

Foreshore and dune

In engineering practice, the main focus of profile modeling is the response of the foreshore and dune. In the SUPERTANK simulations, application of default calibration parameters resulted in overprediction of observed foreshore erosion in most cases. This may be explained by the fact that the default parameters were derived primarily for field applications in which the surf zone is more energetic and the scale of profile change is larger than that observed at SUPERTANK. Lower values of the transport rate coefficient were required to simulate the lower energy regime of the wave flume. Following model calibration, improved agreement was achieved at the foreshore for most cases. In some cases, such as the foredune erosion test, somewhat poorer agreement at the foreshore was observed following calibration. This observation suggests that the simplified methods of calculating foreshore and dune erosion require improvement to provide equally good results of dune and berm erosion for different beach configurations and storm conditions using a single calibration. Also, the results for the compacted versus loosely packed dune cases indicate sediment compaction is an important factor influencing erosion. Further research is required to account for effects of sediment compaction in the model.

Simulation of the seawall cases showed that the model was able to qualitatively represent the observed profile changes in front of the seawall. However, the results indicate that improvements are required to accurately reproduce details of erosion and scour occurring in front of a seawall.

Bar and offshore mound

Using the default calibration parameters, SBEACH overestimated the offshore movement of the bar, particularly in the random wave cases. Following calibration, model calculations more closely matched the location of the observed bar, although details of the bar and trough development were not reproduced. For most test cases, the accuracy of the model in simulating offshore profile change and bar development was considered acceptable for use in engineering applications, which typically focus more on the foreshore. The model was less successful in reproducing profile changes for the offshore mound tests. In these cases, overprediction of mound erosion affected profile response at the foreshore, where erosion was also overestimated. These results suggest further study is required to improve model simulation of profile change of offshore mounds.

Profile evolution

The frequency of profile measurements collected during the SUPERTANK study allowed a unique opportunity to assess the model's ability to simulate the temporal changes of the beach profile under erosive wave conditions. Overall, this evaluation showed reasonable agreement between the calculations and data. There was a slight lag of foreshore erosion observed in the calibrated model. This lag became more pronounced with attempts to better match the location of the bar by decreasing the transport rate coefficient, K. Conversely, attempts to better match the response at the foreshore by increasing K resulted in poorer agreement between the modeled and measured profile at the bar. This suggests that improvements could be made in calculation of swash zone transport to better correlate the time scale and magnitude of foreshore response with that of the subaqueous profile.

5 Field Case Studies

The purpose of this chapter is to evaluate the capability of SBEACH to reproduce storm-induced profile change measured in the field. Several field sites and storm events were selected for study, based on quality and availability of data. The model was first applied to all cases using default calibration parameter values. The model was then calibrated to a single profile for each site and applied to the remaining profiles at the site. Evaluation of model performance focuses on simulation of erosion at the foreshore and dune.

Field Data

Data requirements for application of SBEACH to field cases are similar to those for laboratory studies. Minimum data requirements include beach profile surveys, wave and water level information, and sediment grain size information. Ideally, the data set includes beach profiles surveyed immediately before and after the storm, and time histories of storm waves and water levels measured by wave and tide gauges located at the study site. Often, however, the best available data include profile surveys which were performed some time before and after the storm. Such profile data may record beach change produced by longer term processes not related to the storm as well as effects of post-storm beach recovery. In many cases, wave or tide gauge data are not available and, alternatively, hindcast information is used to estimate storm conditions. The quality and accuracy of data being input to the model should be considered when evaluating model results. Also, the degree to which measured profile change satisfies basic model assumptions, such as longshore uniformity of sediment transport, must be considered in the analysis.

Field cases selected for this study were the best available records of storm-induced profile response suited for application and evaluation of SBEACH. The field case studies include Ocean City, MD (a series of storms from October 1991 - January 1992); Manasquan/Point Pleasant Beach, NJ (March 1984 storm); Dewey Beach/Rehoboth Beach, DE (December 1992 storm); and Debidue Beach/Myrtle Beach, SC (Hurricane Hugo, September 1989).

Measuring Model Performance

In development of the measures of model performance for field cases, emphasis was placed on modeling the response of the dune and foreshore. Profile response at the foreshore and dune is important in engineering applications of the model, where model estimates of erosion are used to determine the effects of storms on structures and property adjacent to the shoreline. For this study, measures of performance were selected based on types of information that a field engineer requires in the assessment of storm damage. These measures include volume change at the foreshore, recession of a specified contour, and landward storm intrusion (Figure 34).

Volume change

Volume change at the foreshore is computed as the net gain or loss in volume per unit beach width above some specified elevation. In this study, the reference elevation for volume calculations was set to the National Geodetic Vertical Datum (NGVD) which approximately corresponds to mean sea level at the selected field sites. The measure of volume change is useful in identifying how effective SBEACH models erosion of the subaerial beach, which is important in defining volume requirements for beach-fill operations. Volume change is not always a reliable measure of model accuracy in predicting storm erosion, however. Some post-storm measured profiles include berm features indicating that a significant amount of beach recovery occurred between the end of erosive wave conditions and the time of the post-storm survey. In such cases, calculation of volume change with the data could underestimate the amount of erosion that was produced by the storm and

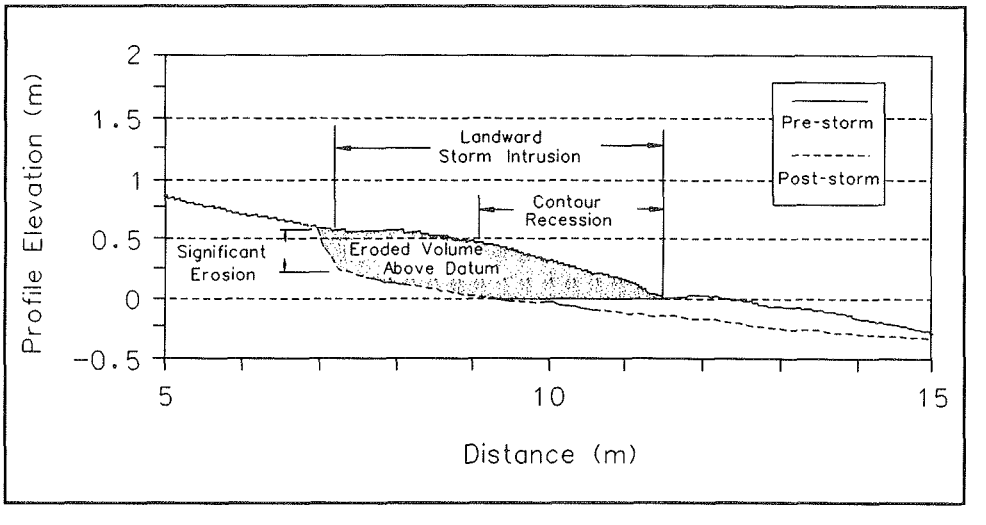

Figure 34. Definition of model performance measures at the foreshore

predicted by SBEACH. Thus, the presence of post-storm recovery berms must be considered when evaluating model performance with this measure.

Contour recession

Measuring the horizontal recession of a specified contour allows an assessment of how well SBEACH models the erosion of a given feature (such as a dune or berm) on the beach profile. Contour recession also provides information on the loss of beach width resulting from a storm. For this study, a representative beach contour located between the reference elevation (NGVD) and the dune crest was identified for each field case. Recession of the selected contour from its initial position on the profile was determined from the data and compared with simulation results.

Landward storm intrusion

Another measure of beach profile change at the foreshore is the extent of landward storm intrusion. Landward storm intrusion is defined as the landward limit of some specified depth of profile erosion. In this study, an erosion depth of 0.3 m was employed for all cases. The measure of storm intrusion is often employed in beach-fill design to quantify the landward extent of potential structural damage caused by erosion and undermining. All measures of landward storm intrusion presented in this report are referenced to the horizontal position of the vertical datum (NGVD) on the initial beach profile.

General Procedure

Evaluation of model performance in simulating beach erosion followed a general procedure for each field case study. Model simulations were first performed using default calibration parameter values. The model was then calibrated to a single representative beach profile and applied to the remaining profiles. Default and calibrated model results were compared with data using visual inspection and the measures of performance described previously.

Default simulations

The field case studies began with default simulations of beach profile response for all profiles and storms at each study site, using the default values of the calibration parameters (K = 1.75 x 10^{-6} m^4/N, ϵ = 0.002 m^2/s, and DFS = 0.3 m). Input to the model included the pre-storm beach profile, median sediment grain size, and time histories of wave conditions and water levels.

Model calibration

Upon completion of the default simulations, a representative profile for each field site was selected and SBEACH was calibrated to the profile. Factors considered in selecting a representative profile included profile shape, mass conservation during the storm, relative position along the beach, proximity to coastal structures, and accuracy of default simulation results with respect to other profiles.

Model calibration followed a procedure similar to that used for the laboratory case studies. The calibration parameters were adjusted systematically to improve agreement between the simulated and measured profiles. Calibration efforts focused on achieving best agreement at the foreshore, while providing reasonable results in the offshore portion profile. Visual inspection and statistical measures were employed to determine the optimum calibration. The calibrated model was applied to the remaining profiles of each corresponding case study.

The time interval of measured wave information used in the simulations varied in range from 1 to 4 hours. Wave input to the model was interpolated between measured values at each model time-step. During calibration, the influence of temporal variability in wave height was investigated by randomly varying the input wave height at each time-step within a small predefined percentage of the interpolated value (e.g., within ± 10 percent). This technique has been used in previous field studies to better represent the natural time variation of wave conditions (Larson, Kraus, and Byrnes 1990). The method enables simulation of smoother, more realistic profile features as observed in the field. No wave variability was employed in the default simulations.

Comparison of default and calibrated simulations

The measures of performance outlined in this chapter were applied to the simulation results to quantify model performance using default parameters and improvements gained through calibration. In addition to quantitative measures, visual inspection of the profiles was used to assess the general performance of the model. Appendix B presents a full record of measured and simulated results for all profiles and storms examined in the field case studies. A summary of the analysis for each case is presented below.

Ocean City, MD

From late October 1991 to early January 1992, the beach at Ocean City, MD, was impacted by a series of severe storms. The series of storms, which included the 30 October 1991 "Halloween storm," 11 November 1991 storm,

and 4 January 1992 storm, caused extensive erosion of the constructed foreshore and dune at Ocean City. A major beach nourishment project had just been completed at Ocean City as a joint effort of the U.S. Army Corps of Engineers, the state of Maryland, Worcester County, and the Town of Ocean City (Grosskopf and Stauble 1993). As part of the project monitoring effort, sled surveys were performed to collect beach profile data at ten locations along the shoreline. These profile data enabled the analysis of the erosional effects of the series of storms. Measurements of local wave conditions and water levels from an offshore gauge together with grain size distribution measurements provided a comprehensive set of high-quality data for application of SBEACH. Figures 35-37 present the wave and water elevation time histories recorded by the offshore gauge and used as input to SBEACH for each storm. The wave gauge was located outside the surf zone at a depth of approximately 10 m. Based on results of sediment analyses performed during the monitoring program, a median sediment grain size of 0.35 mm was selected as a representative value for all beach profiles. Further details on the beach-fill project and monitoring program at Ocean City are provided by Stauble et al. (1993). Impacts of the storms at Ocean City are discussed in a special issue of *Shore and Beach* (Vol. 61 No. 1, 1993).

Default simulations

Halloween storm. As shown in Figure 35, the Halloween storm produced high waves and water levels at Ocean City for approximately 4 days, with a peak significant wave height of about 3 m and a peak water elevation of about 1.5 m NGVD. Data for six profile lines were available to model the beach response to the storm. Pre-storm profiles were collected in June 1991 and post-storm surveys were performed shortly after the storm. The June surveys were assumed to well represent the condition of the upper beach profile prior to the storm, as no other significant erosion events occurred between June and October. Figure 38 presents the total volume change per unit beach width calculated between surveys for each profile. Five profiles exhibited a net loss of material while one profile gained material. The fact that mass was not conserved across the profiles indicates that material was redistributed by longshore processes between surveys. It is reasoned that the longshore processes primarily affected the subaqueous profile, and changes on the upper beach profile and dune were caused mainly by cross-shore processes during the storm. Thus, model results are expected to produce better agreement on the upper beach profile than on the offshore portion of the profile.

Results of default simulations provided reasonable agreement with the data for all but one of the profiles. Figure 39 shows calculation results for profile 63 (denoting the profile at 63rd Street) where good agreement was obtained above the vertical datum. Below datum, the measured profile exhibits a convex shape with a nearshore step, whereas the calculated profile shows a more concave shape with a bar situated offshore. The measured

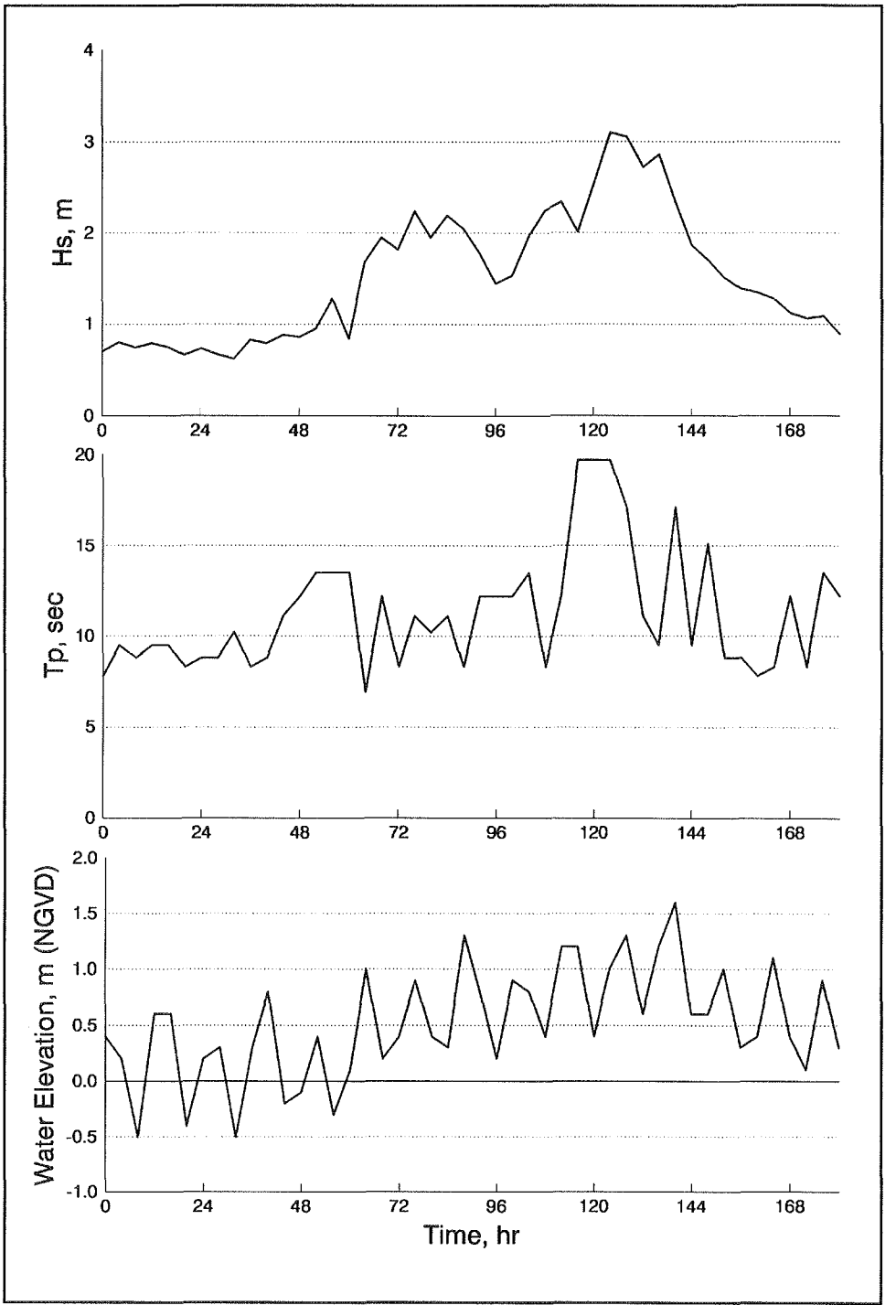

Figure 35. Wave height, wave period, and water elevation time-histories for the Halloween 1991 storm, Ocean City, MD

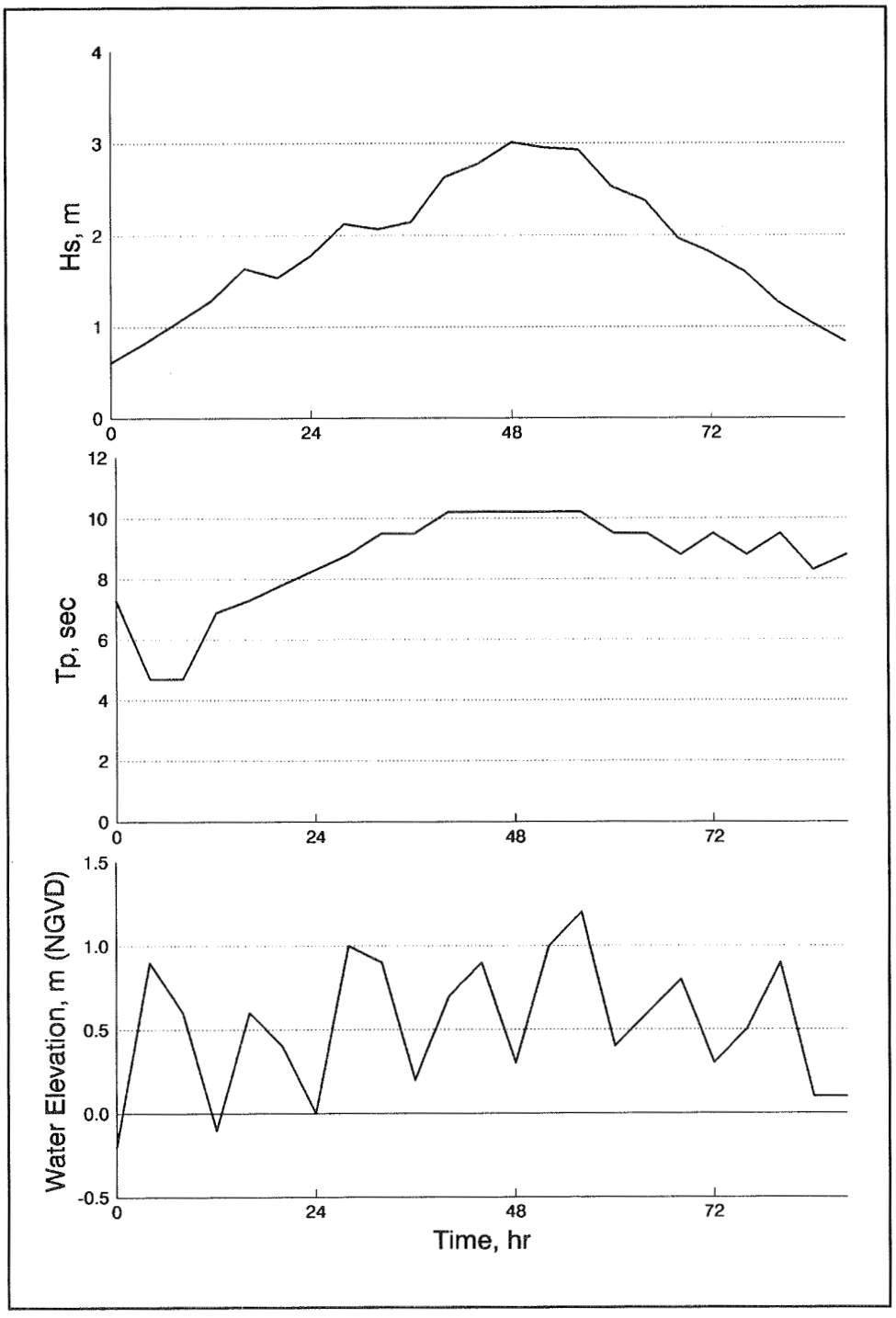

Figure 36. Wave height, wave period, and water elevation time-histories for the 11 November 1991 storm, Ocean City, MD

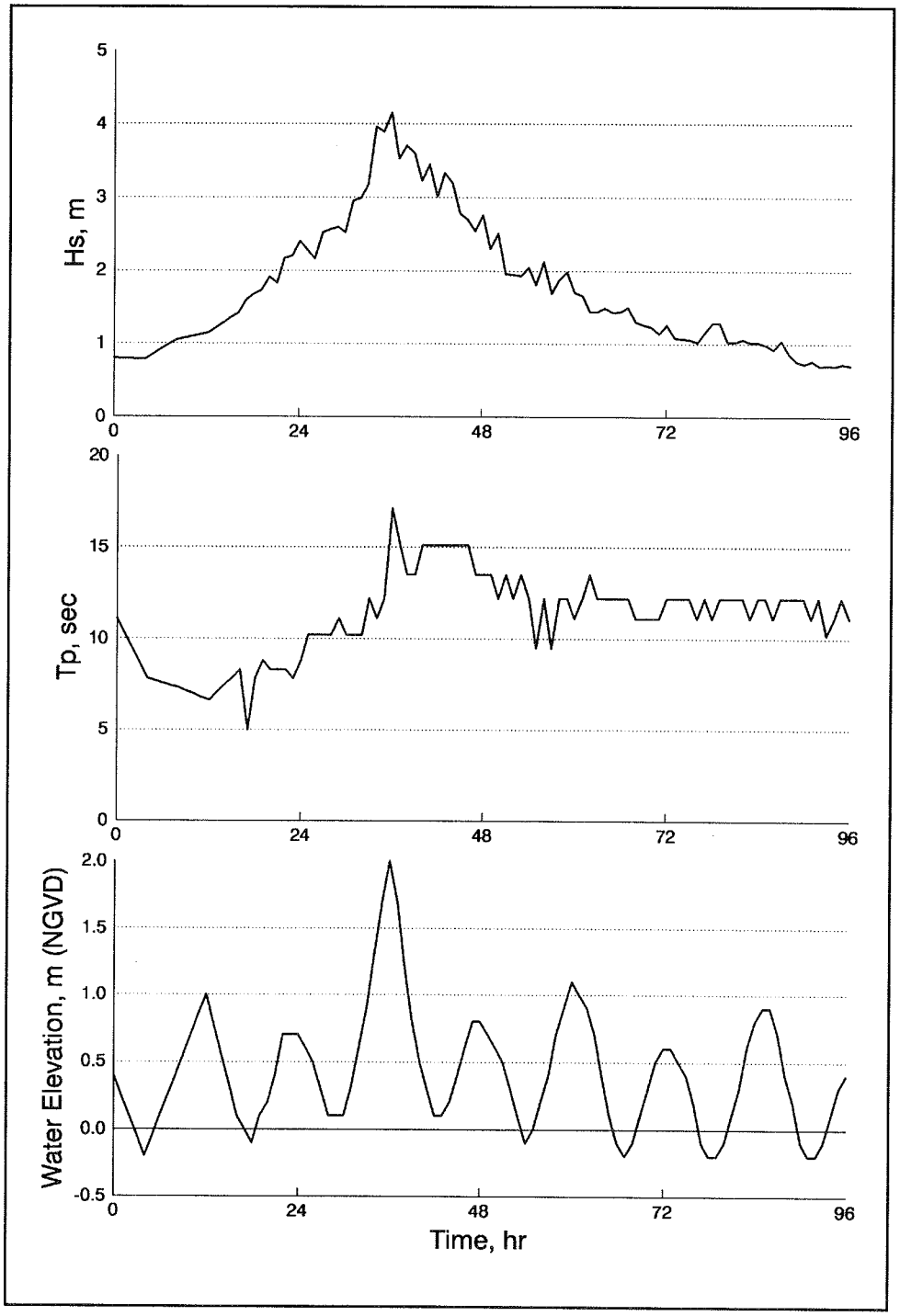

Figure 37. Wave height, wave period, and water elevation time-histories for the 4 January 1991 storm, Ocean City, MD

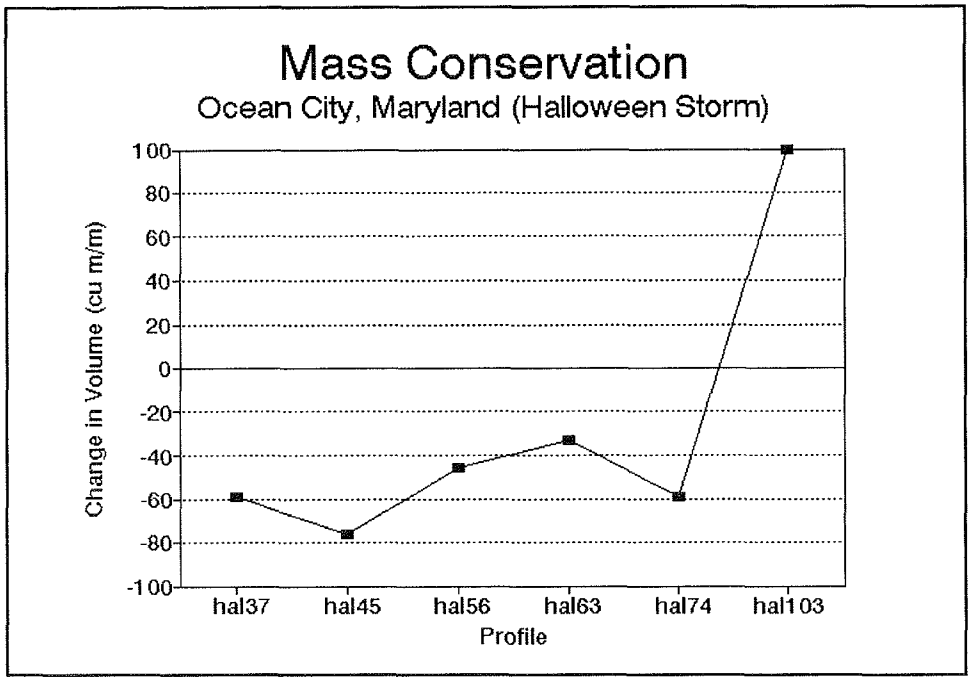

Figure 38. Conservation of mass between beach profile surveys for the Halloween storm, Ocean City, MD

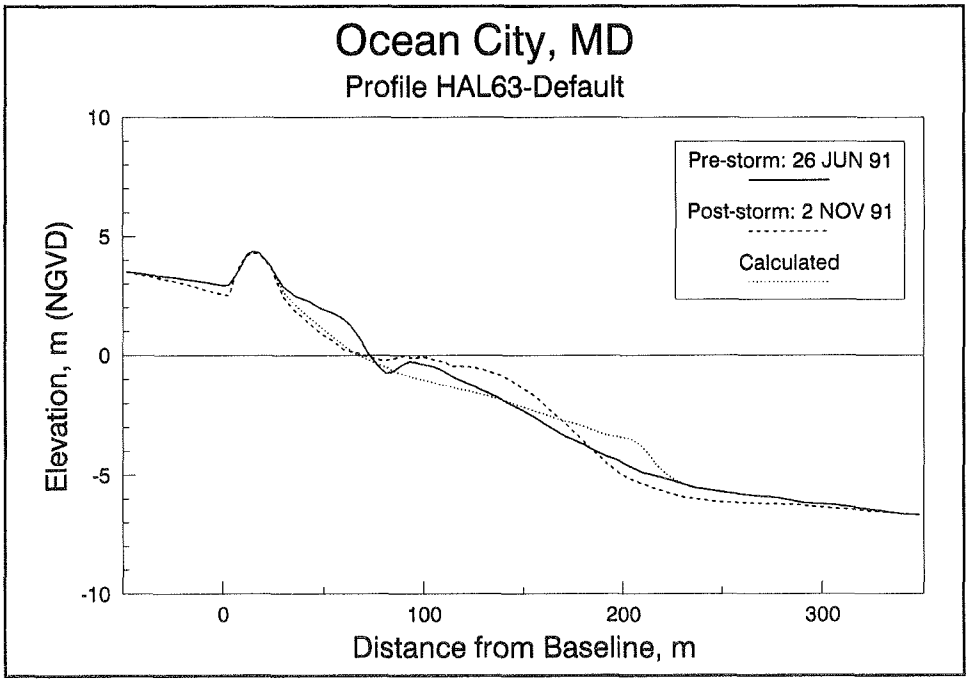

Figure 39. Result of default simulation of the Halloween storm for profile 63, Ocean City, MD

beach step may be attributed to onshore movement of material from the bar during the waning storm conditions, resulting in recovery of the beach profile prior to the surveys. Another example of default simulation results is shown in Figure 40 for profile 103. In this case, the model significantly overpredicted erosion at the foreshore. This overprediction is likely due to the large amount of volume that was gained on the measured profile. The offshore limit of deposition is well matched for this case. Simulation results for the remaining profiles are included in Appendix B.

November-January storms. The November-January (NJ) cases involved a combined simulation of the 11 November 1991 storm and the 4 January 1992 storm. The combination of storms was necessary because beach profile data were not available between the two events. Figures 36 and 37 show the time-histories of wave and water level information for the storms. As observed in the figures, high waves and water levels lasted approximately 3 days for both storms. The November storm had a peak significant wave height of about 3 m and water elevation of about 1.2 m NGVD. The January storm was much more severe, with a peak wave height and water level of 4 m and 2 m NGVD, respectively. Of the three storms included in the study, the January storm produced the most damage to the upper beach due to the high surge.

The beach profiles measured after the Halloween storm served as pre-storm profiles for the NJ storm set. Beach surveys performed shortly after the January storm provided post-storm profiles for comparison with model results.

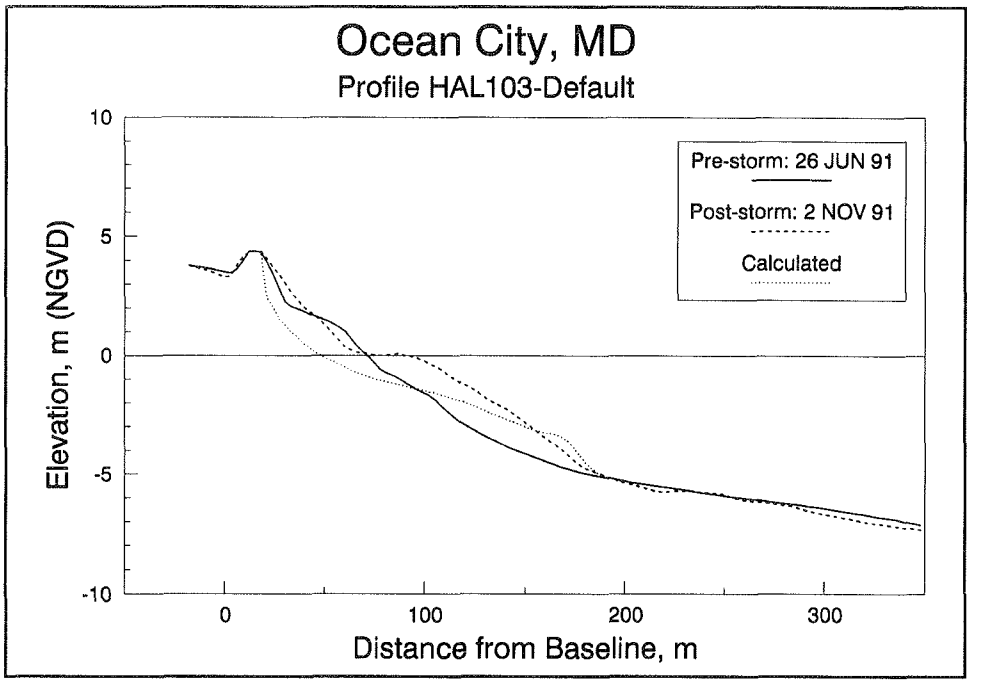

Figure 40. Result of default simulation of the Halloween storm for profile 103, Ocean City, MD

Figure 41 shows the degree to which mass was conserved between the pre- and post-storm surveys. A large gain in material was observed on profiles 37 and 103; whereas, mass was conserved reasonably well on the other profiles.

Measured beach response to the NJ storm series shows that four of the six profiles experienced overwash of the dune, and SBEACH produced dune overwash in each of the four cases. Figure 42 shows calculation results for profile 45, where the magnitude of overwash and dune recession were well modeled with the default parameters. It is noted that although substantial erosion occurred at the dune, erosion on the lower foreshore profile was minimal. Simulation results for profile 63 are shown in Figure 43. In this case, the model underestimated the amount of overwash and dune retreat observed on the measured profile. As with profile 45, no erosion occurred at the shoreline for this case. Another example from the NJ storm set is shown in Figure 44 for profile 56. In this case, little change was observed across the entire subaerial profile in both the measured and modeled results. These results indicate that the subaerial beach at profile 56 was near equilibrium for these storm conditions.

October-January storms. The October-January (OJ) cases involved simulation of the entire series of all three storms for four profile lines which did not have intermediate profile data available between the storms. For these cases, pre-storm profiles were available from the June 1991 surveys and post-

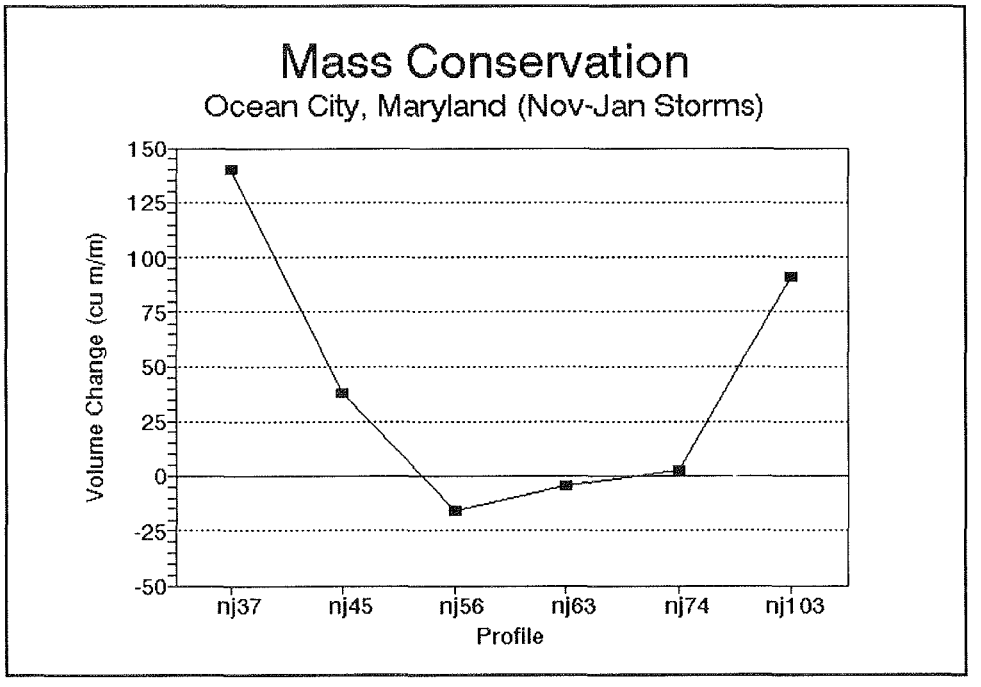

Figure 41. Conservation of mass between beach profile surveys for the NJ storm series, Ocean City, MD

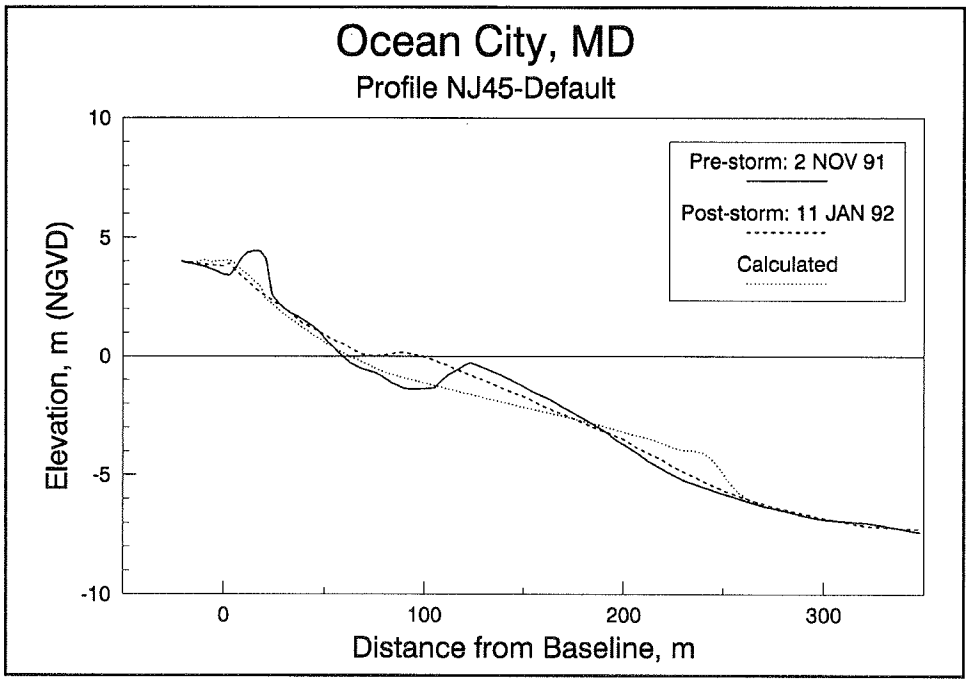

Figure 42. Result of default simulation of the NJ storm series for profile 45, Ocean City, MD

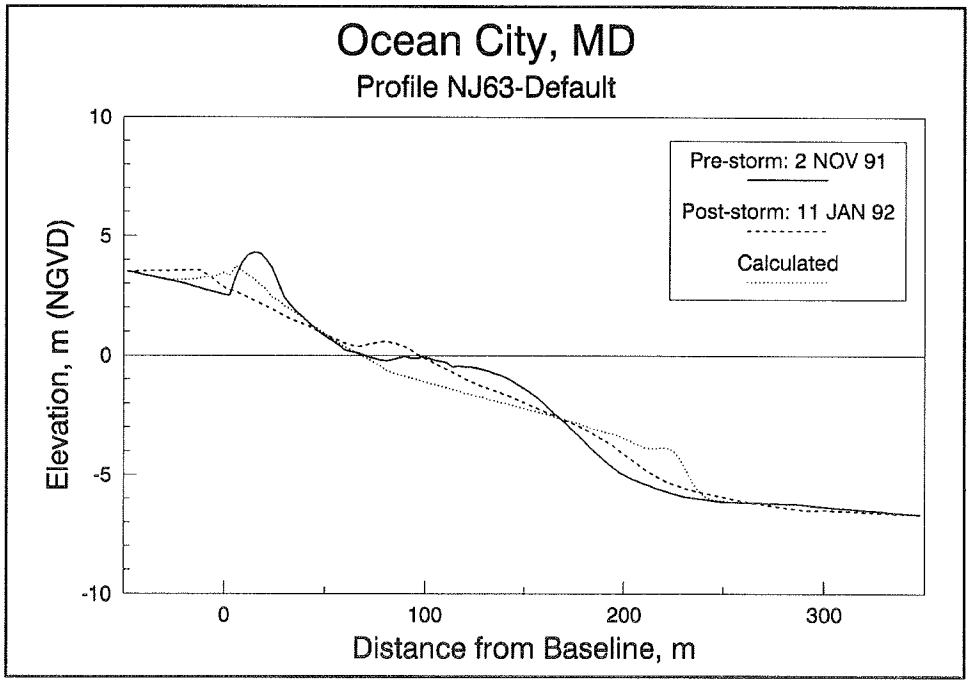

Figure 43. Result of default simulation of the NJ storm series for profile 63, Ocean City, MD

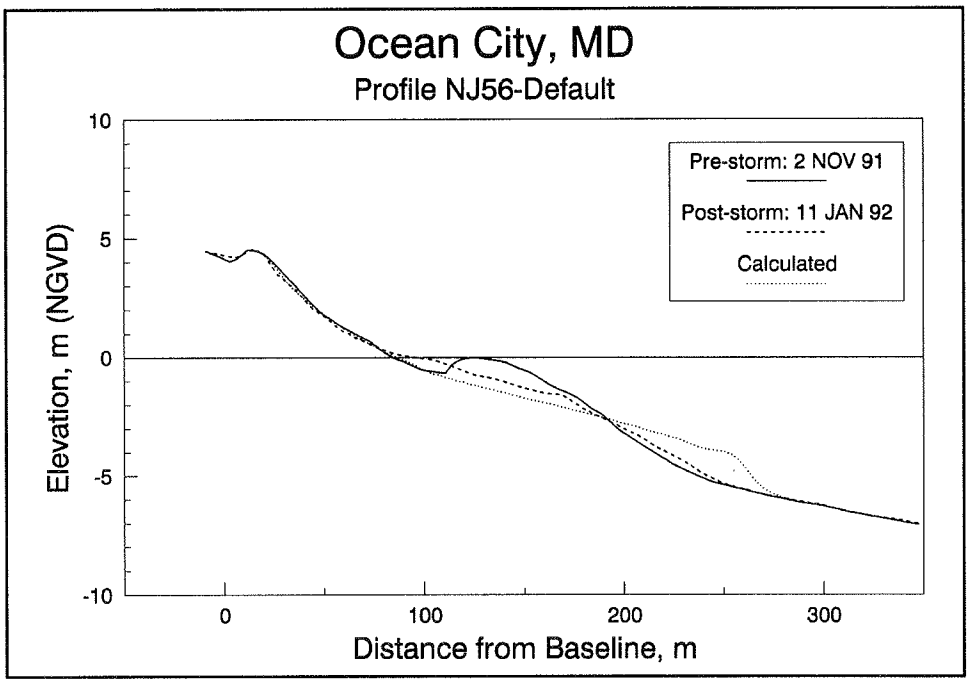

Figure 44. Result of default simulation of the NJ storm series for profile 56, Ocean City, MD

storm profiles were obtained from the surveys performed after the January storm. Figure 45 shows total volume changes between surveys for the four profiles. Profile 92 gained a substantial amount of volume, whereas material was better conserved across the other profiles.

Figure 46 shows default simulation results for profile 86 of the OJ storm set. Measured dune recession and overwash are well matched by the model. The calculation shows deposition of eroded material further offshore than observed in the data; however, the berm feature located at the shoreline of the post-storm measured profile implies beach recovery occurred prior to the survey. Simulation results for profile 81 are shown in Figure 47. In this case, the model underestimated erosion on the upper profile. As the eroding dune migrated landward during the calculation, the overwash algorithm produced a slight increase in elevation of the dune crest not observed in the data.

Model calibration

In general, the default simulations produced reasonable agreement with the data, although in some cases the model under- or overestimated erosion. To improve calculation results, the model was calibrated to profile 81 of the OJ test cases. This case was selected because it involved all three storms, exhibited reasonable conservation of mass between profile surveys, and resulted in poorer agreement at the dune among the default simulations.

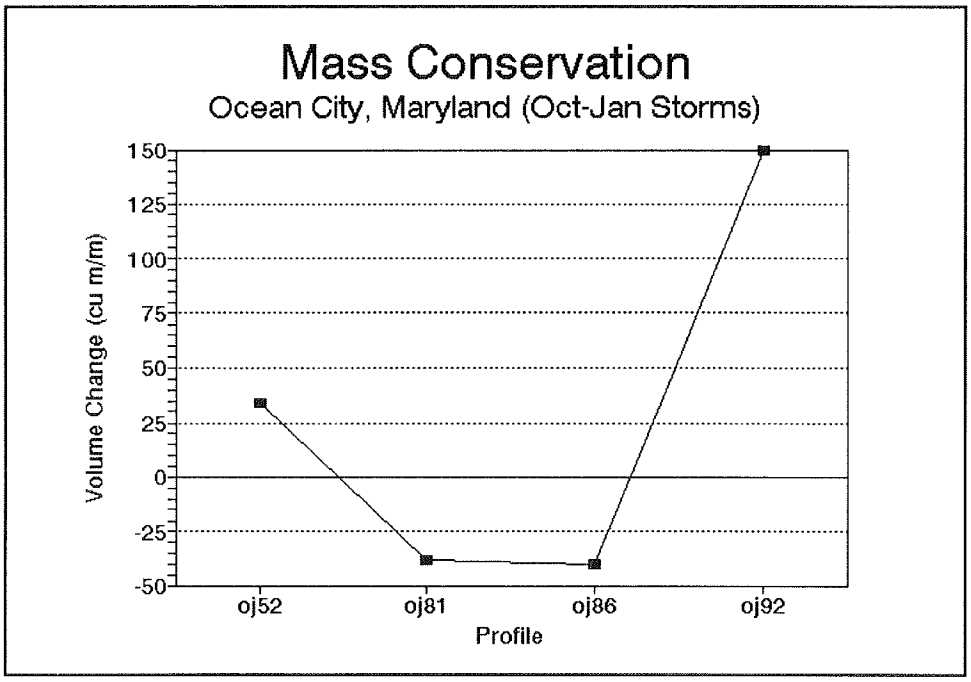

Figure 45. Conservation of mass between beach profile surveys for the OJ storm series, Ocean City, MD

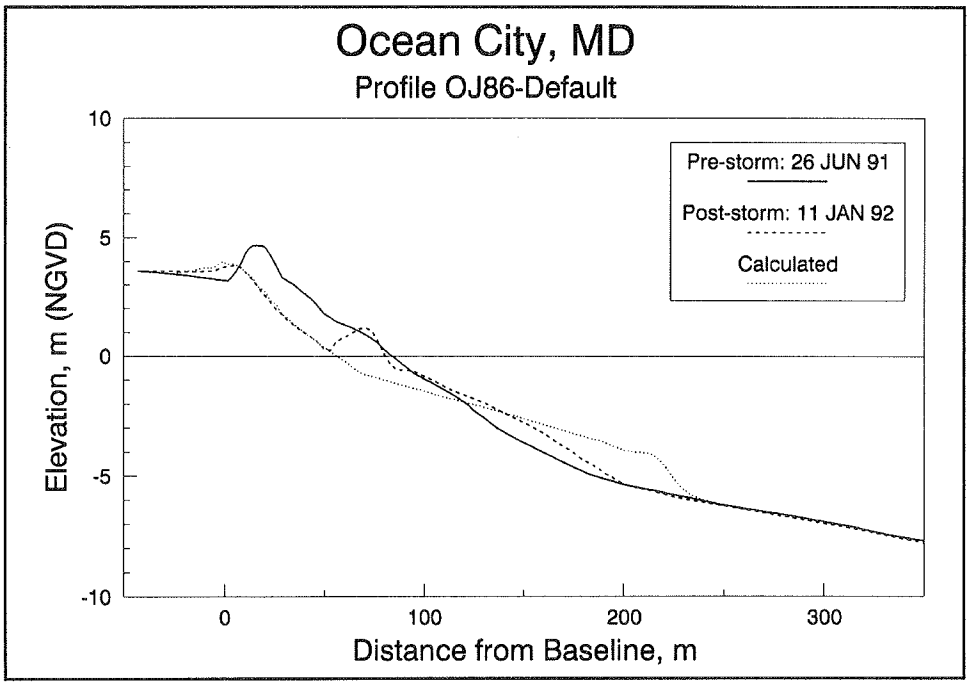

Figure 46. Result of default simulation of the OJ storm series for profile 86, Ocean City, MD

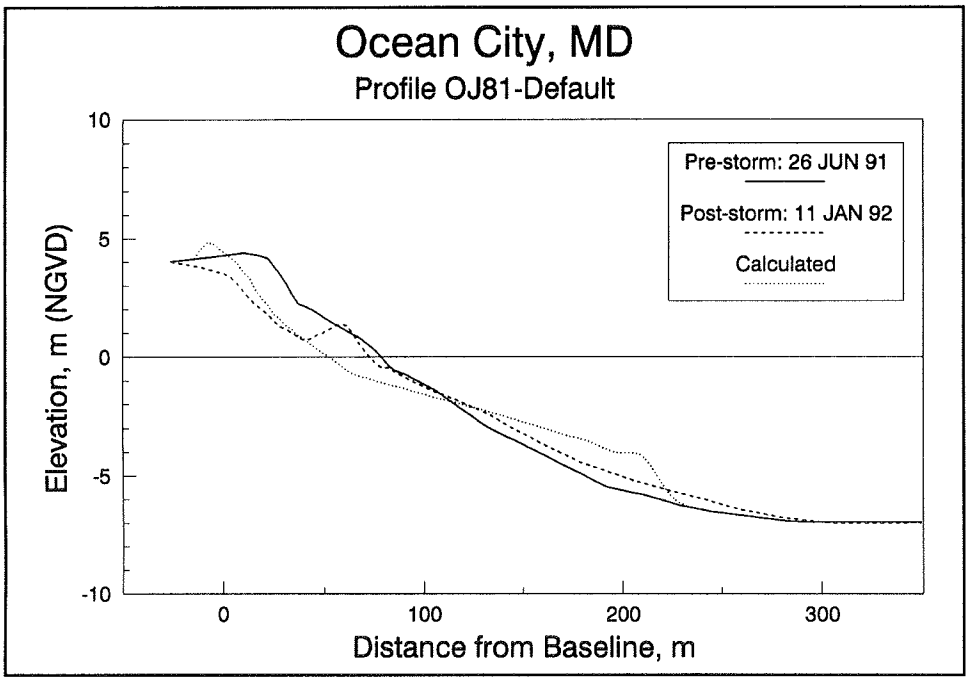

Figure 47. Result of default simulation of the OJ storm series for profile 81, Ocean City, MD

Improved agreement was achieved for profile 81 by decreasing K from 1.75×10^{-6} m^4/N to 1.5×10^{-6} m^4/N, increasing ϵ from 0.002 m^2/s to 0.005 m^2/s, and increasing *DFS* from 0.30 m to 0.50 m. Wave height variation within ± 10 percent was employed in the calibration run. Figure 48 shows a comparison of the default simulation and calibrated results together with the measured profile. The calibrated run better matched the recession and slope of the foreshore, but the overwash algorithm still produced a mound of deposition at the dune crest which was not observed in the data. Better modeling of overwash for this case was obtained in a previous application of a developmental version of SBEACH (Wise and Kraus 1993) in which $H_{1/10}$ rather than H_{rms} was used to calculate the landward limit of runup and overwash. In subsequent development of the overwash algorithm and analysis with other data, the use of $H_{1/10}$ proved to overestimate runup and overwash in most cases, and the model was modified to employ the rms wave height in calculating the runup limit (Equation 91). A probable reason that better agreement was achieved with use of $H_{1/10}$ for this case, as well as for profiles 63 and 74, is that these profiles are located in the area of an erosional "hotspot" along the shoreline (Stauble and Kraus 1993). The hotspot may be related to the focusing of wave energy by a shoreface-attached shoal which could produce locally higher runup. Although exact agreement with the measured response is not achieved with the present model, Figure 48 demonstrates that with calibration, improved results were obtained over the default simulation.

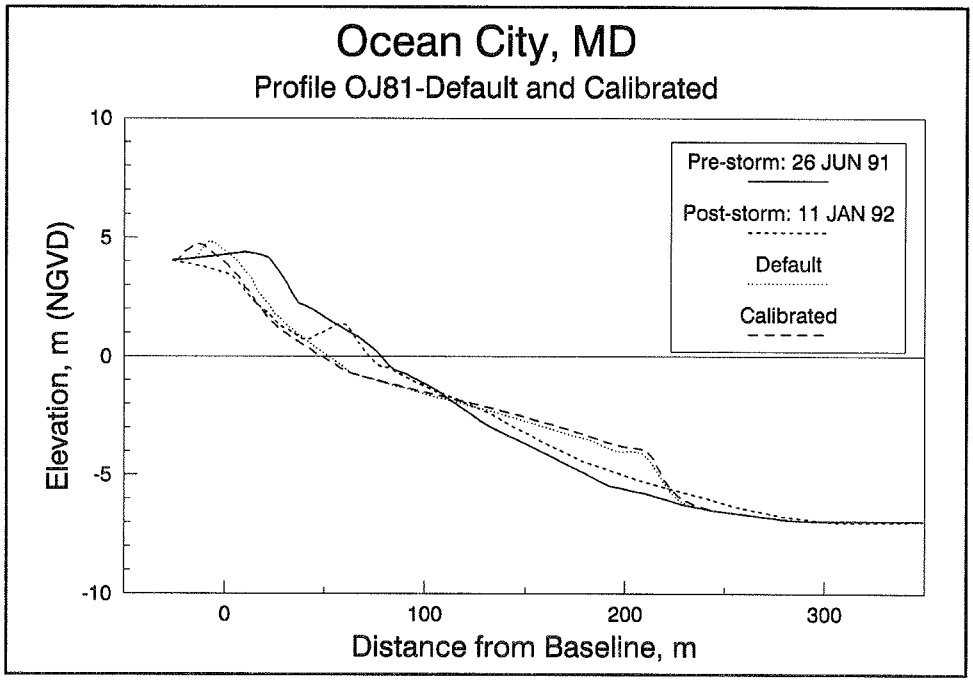

Figure 48. Results of default and calibrated simulations of the OJ storm series for profile 81, Ocean City, MD

Calibrated simulations

Simulations of the Halloween storm and the NJ and OJ storm groups were performed using the calibration parameters selected above. Simulation results for all cases are presented in Appendix B. The calibrated runs are summarized below by storm group.

Halloween storm. Based on visual inspection of results, the calibrated runs produced improved agreement over the default simulations for the Halloween storm profiles. An example of improvement is provided in Figure 49 which shows a comparison of default and calibrated results for profile 45. Although the amount of foreshore erosion was still underestimated for this case, the calibrated results were closer to the measurements. To quantify improvements gained through calibration, the measures of performance described above were calculated for default and calibrated runs. Figure 50 compares volume change above NGVD for the measured, default simulated, and calibrated profiles for each case. Although the default simulations generally underestimated loss of volume, the measured trends were followed except for profile 103. The calibrated simulations produced closer agreement with the data. It is noted that profile 103 exhibited a large net increase in total profile volume between surveys, which may explain why no loss of material occurred above NGVD for this case. Figure 51 shows

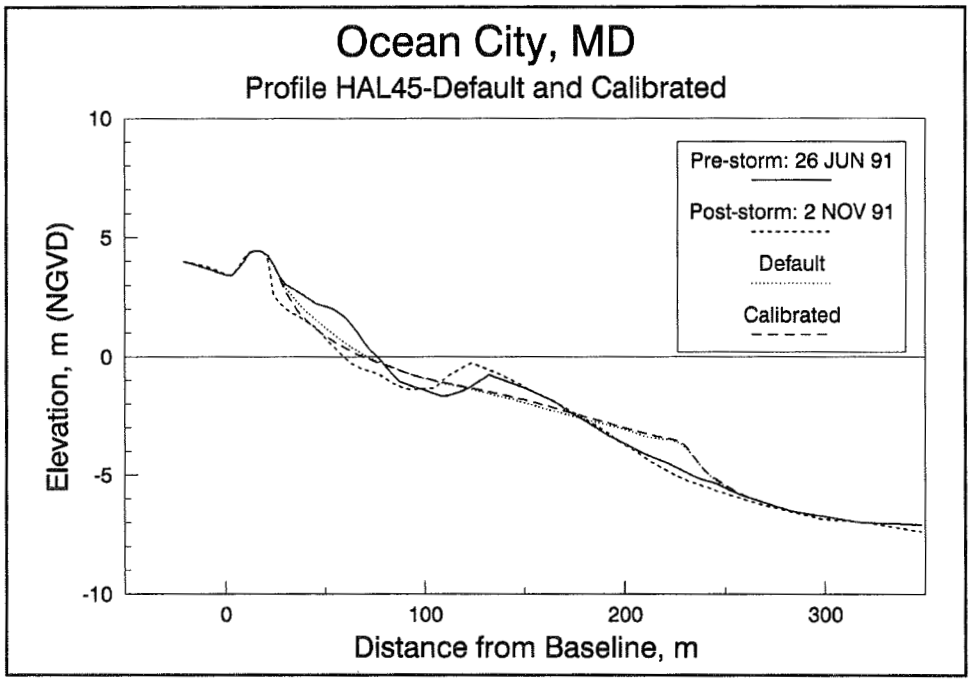

Figure 49. Results of default and calibrated simulations of the Halloween storm for profile 45, Ocean City, MD

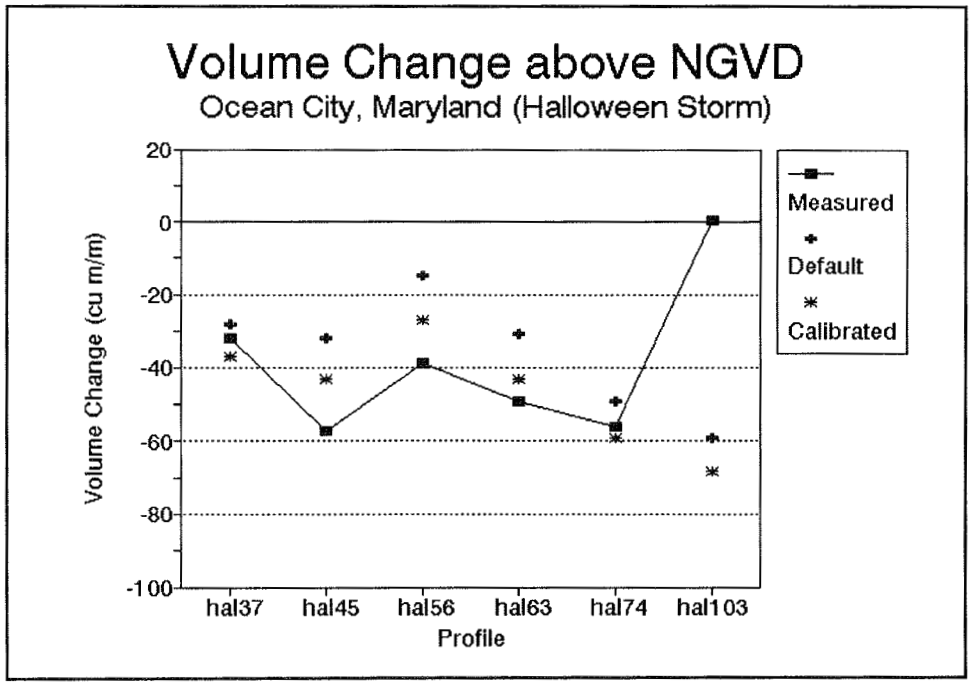

Figure 50. Comparison of measured and simulated volume change above NGVD for the Halloween storm, Ocean City, MD

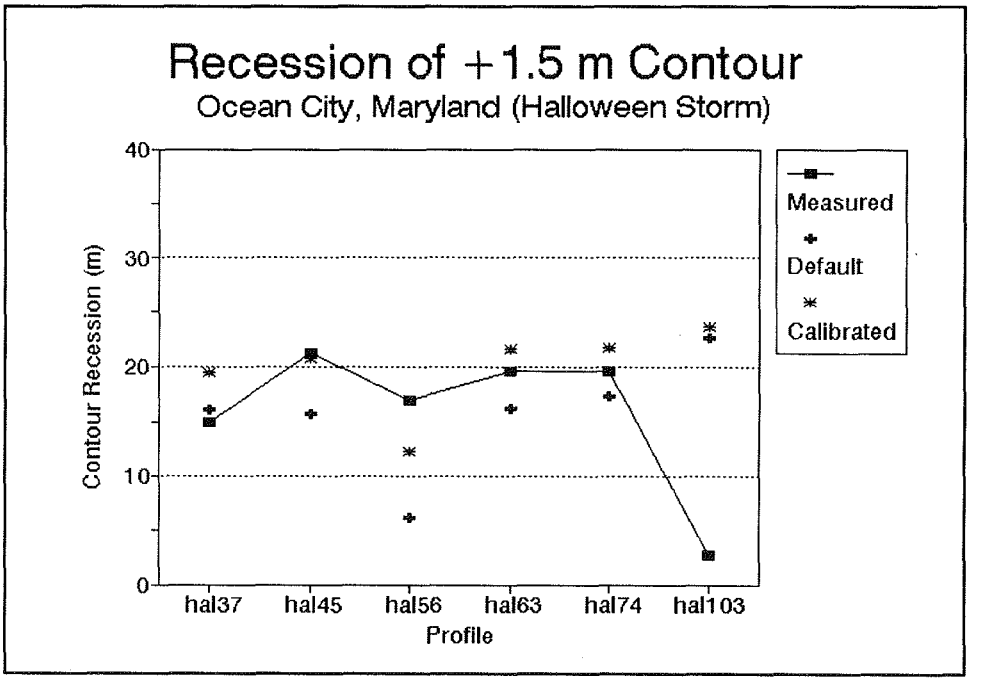

Figure 51. Comparison of measured and simulated recession of the 1.5-m contour for the Halloween storm, Ocean City, MD

recession of the 1.5-m contour for all cases. In general, the default simulations underestimated contour recession, while the calibrated runs provided better agreement with the data. Figure 52 displays the calculated and measured storm intrusion of the 0.3-m depth of erosion. Both the default and calibrated results are close to the measured values, with better agreement achieved with the calibrated results.

November-January storms. Application of the calibrated model to the NJ storm set provided improved agreement over the default runs for profiles 63, 74, and 103. Slightly less accurate results were obtained for profiles 37, 45, and 56, although in these cases the calibrated model still produced reasonable agreement. Figure 53 displays the measured and calculated beach response for profile 74, where simulation of dune erosion and overwash was improved with the calibrated model. Figure 54 shows results for profile 45 where the calibrated model slightly overestimated erosion of the subaerial beach in comparison to the default simulation. To quantify differences between the default and calibrated simulations, the three measures of performance at the foreshore were calculated for the NJ storm set. As shown in Figure 55, volume change above NGVD is modeled fairly well in each case except for profile 37 which gained a substantial amount of total volume between surveys and profile 103 which exhibited a recovery berm at the shoreline. Overall, the default calculations provided somewhat better results than the calibration runs based on this measure of performance. In calculating contour recession, the

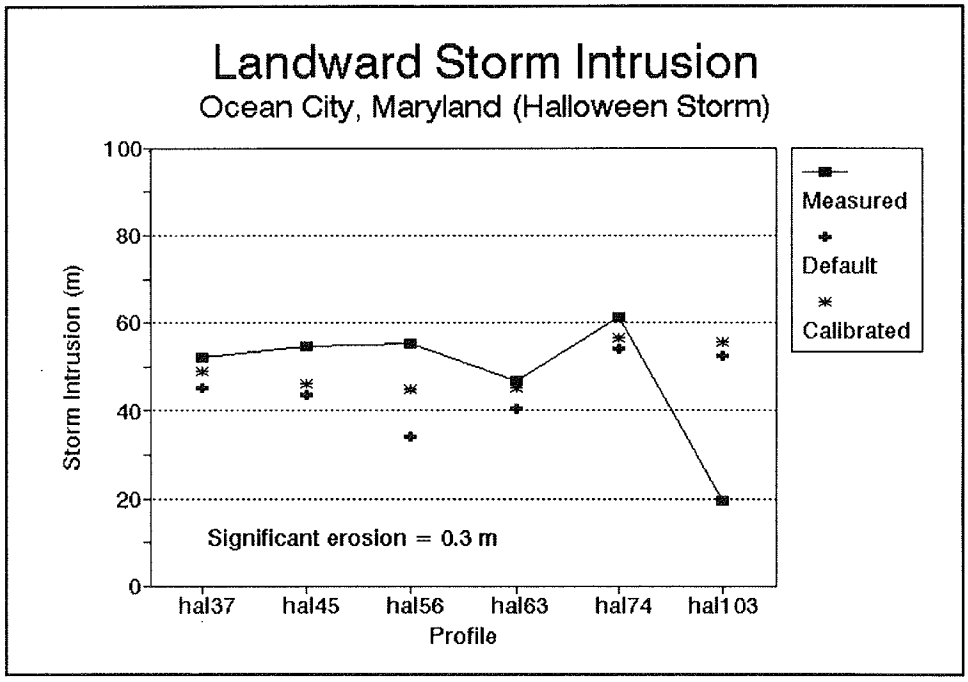

Figure 52. Comparison of measured and simulated storm intrusion for the Halloween storm, Ocean City, MD

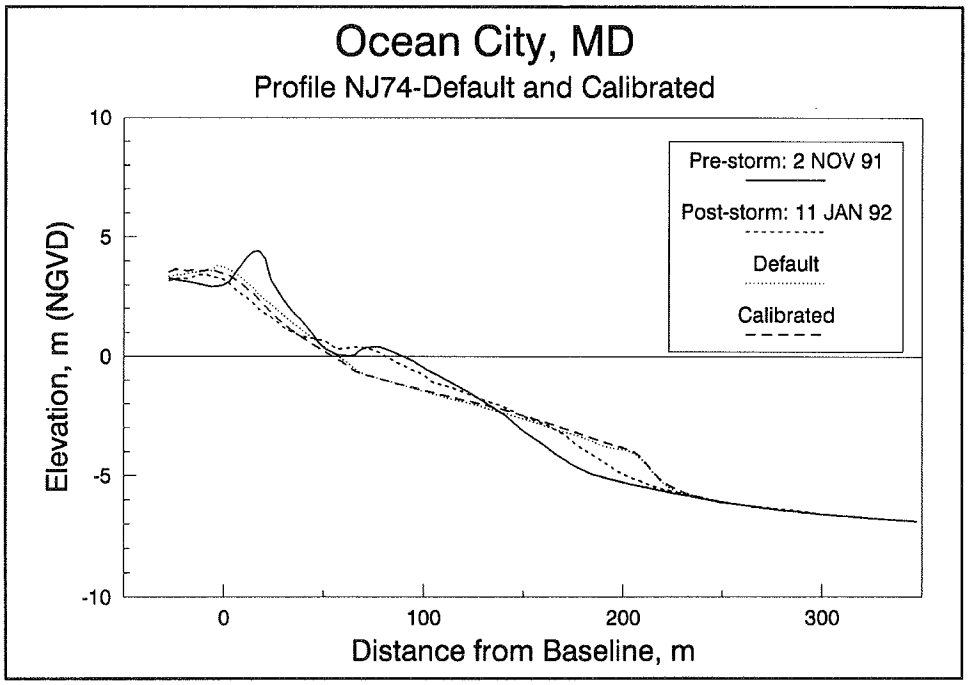

Figure 53. Results of default and calibrated simulations of the NJ storm series for profile 74, Ocean City, MD

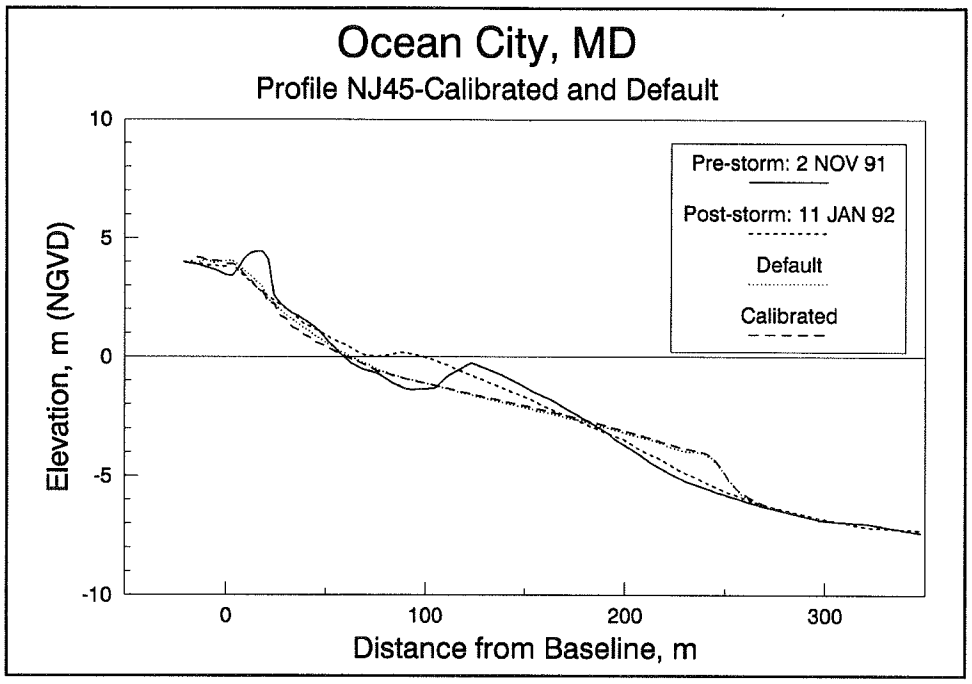

Figure 54. Results of default and calibrated simulations of the NJ storm series for profile 45, Ocean City, MD

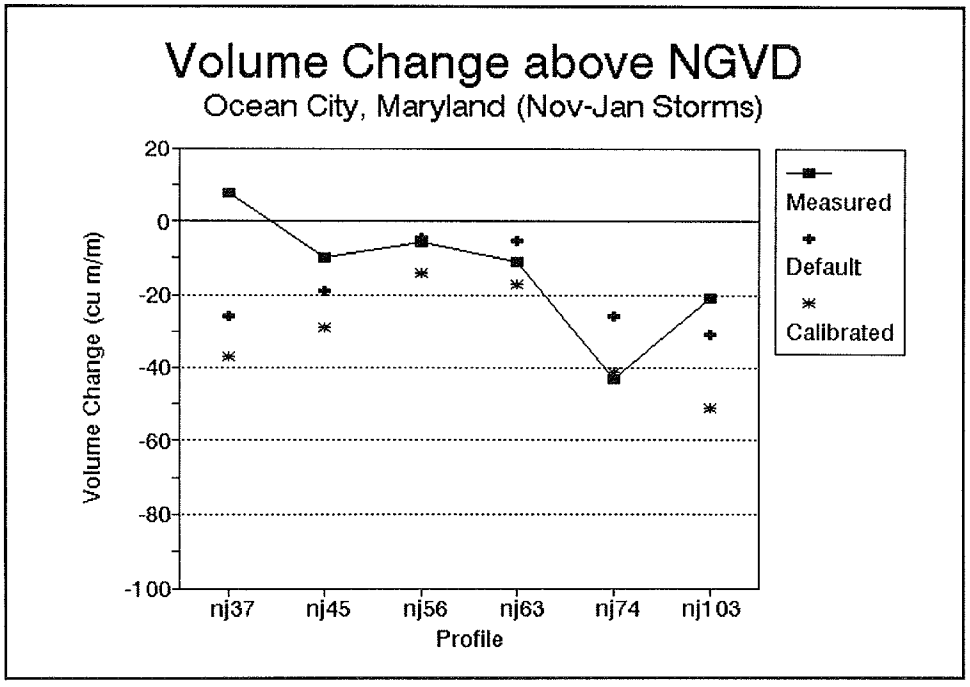

Figure 55. Comparison of measured and simulated volume change above NGVD for the NJ storm series, Ocean City, MD

2.5-m contour was selected as a representative value for the NJ set. Figure 56 displays contour recession calculated from the measured and simulated profile response. The default simulations provided better agreement for profiles 37, 45, and 56; while the calibrated model produced improved results for profiles 63, 74, and 103. Contour recession was underpredicted for profiles 63 and 74 which are located in the area of the erosional hotspot. Figure 57 shows landward storm intrusion for the NJ storm set. The calibrated model accurately simulated landward storm intrusion of the 0.3-m erosion depth for all cases except profile 37, where measured vertical erosion was less than 0.3 m across the entire subaerial profile.

October-January storms. The calibration parameters selected for profile 81 were applied to the remaining three profiles in the OJ storm set. For these cases, the calibrated model generally overestimated erosion at the dune and foreshore as illustrated in Figure 58 which shows the measured, default, and calibrated profile response for profile 52. Figures 59-61 display the measures of performance at the foreshore for the OJ storm cases. Loss of volume above NGVD was overestimated by the model although it is noted that profiles 81 and 86 included recovery berm features and profile 92 exhibited poor conservation of total volume between surveys. Recession of the 2.5-m contour (Figure 60) was reproduced fairly well in the default simulations, whereas the calibrated model overestimated recession for all cases except profile 81. As shown in Figure 61, landward storm intrusion was accurately modeled in both

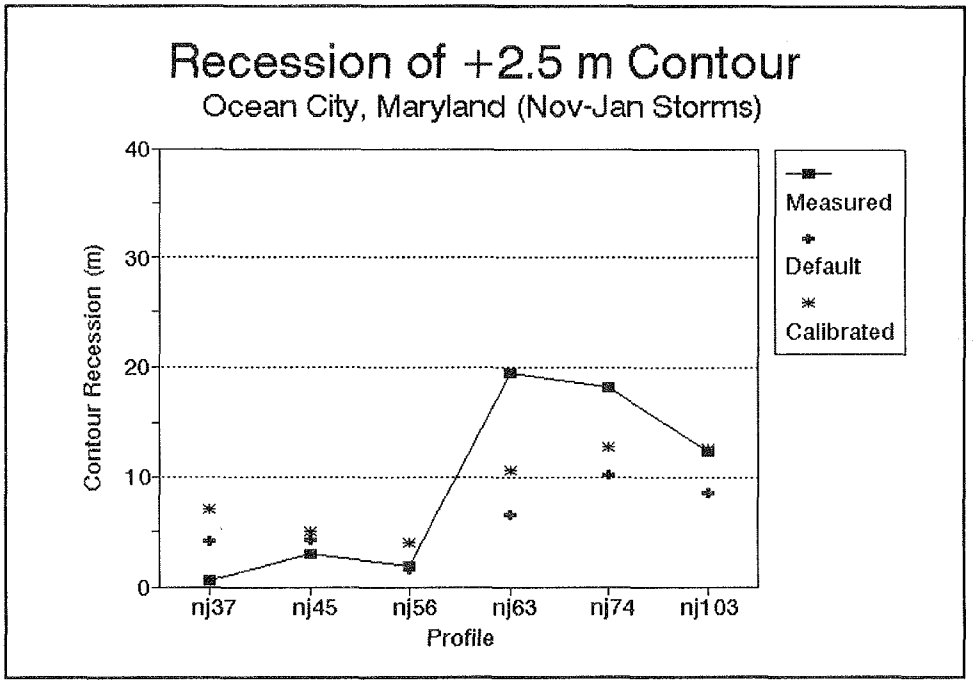

Figure 56. Comparison of measured and simulated recession of the 2.5-m contour for the NJ storm series, Ocean City, MD

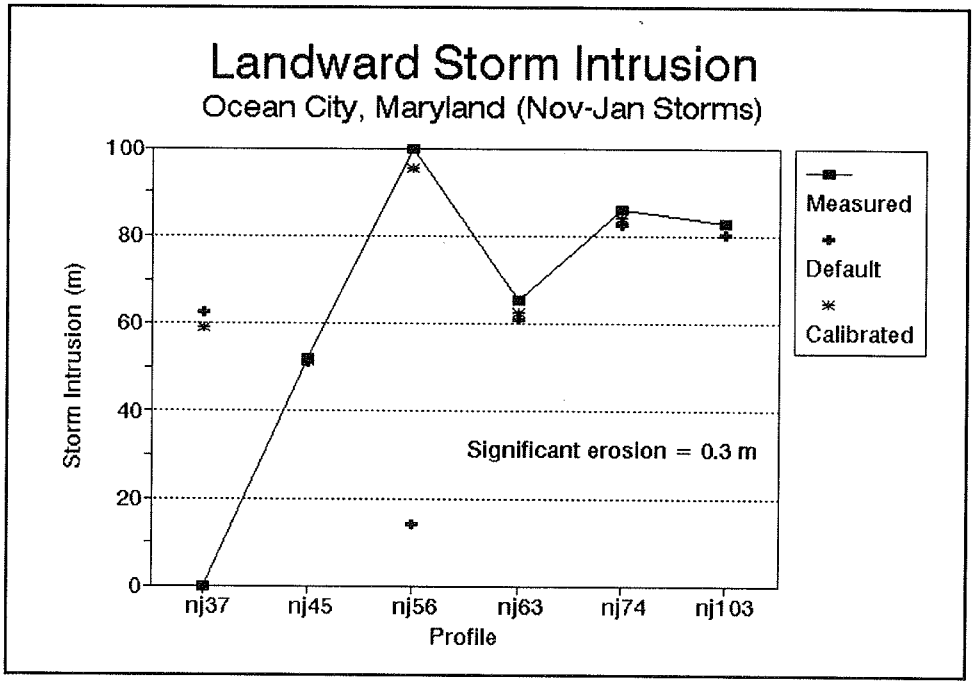

Figure 57. Comparison of measured and simulated storm intrusion for the NJ storm series, Ocean City, MD

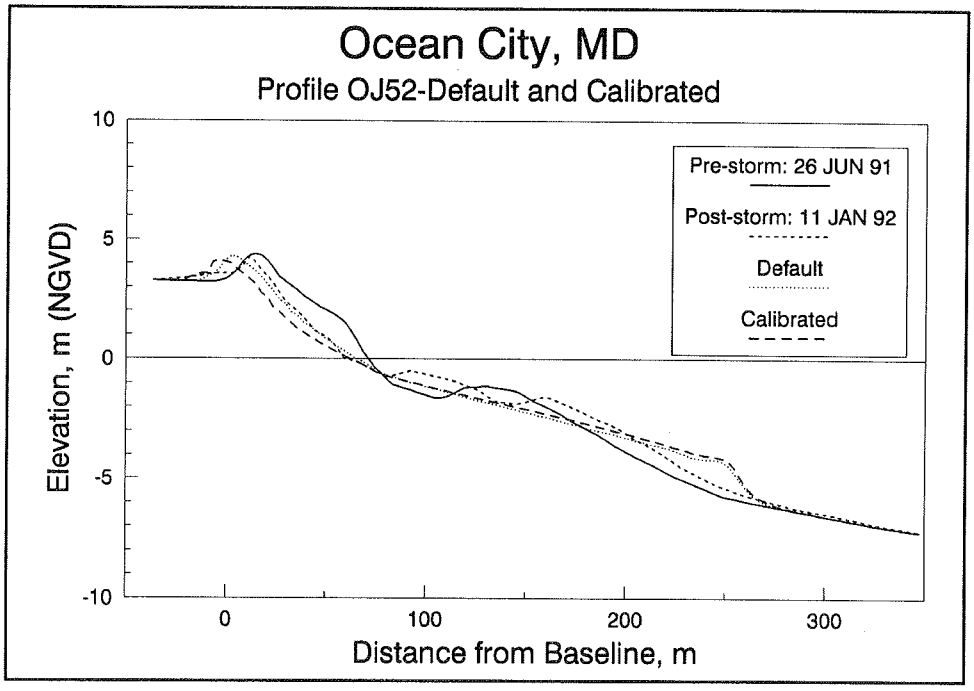

Figure 58. Results of default and calibrated simulations of the OJ storm series for profile 52, Ocean City, MD

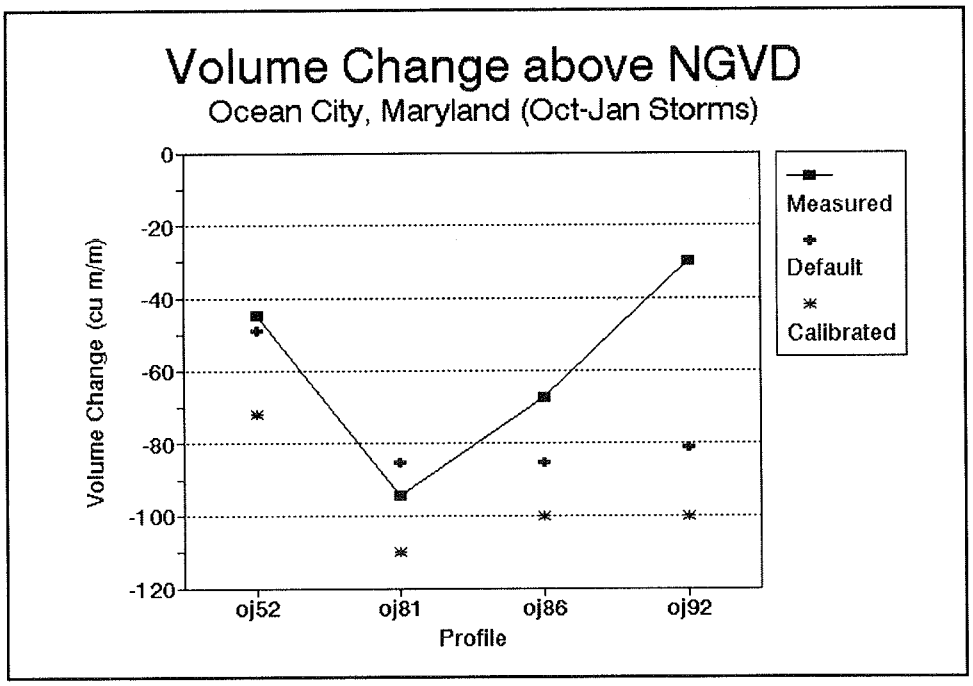

Figure 59. Comparison of measured and simulated volume change above NGVD for the OJ storm series, Ocean City, MD

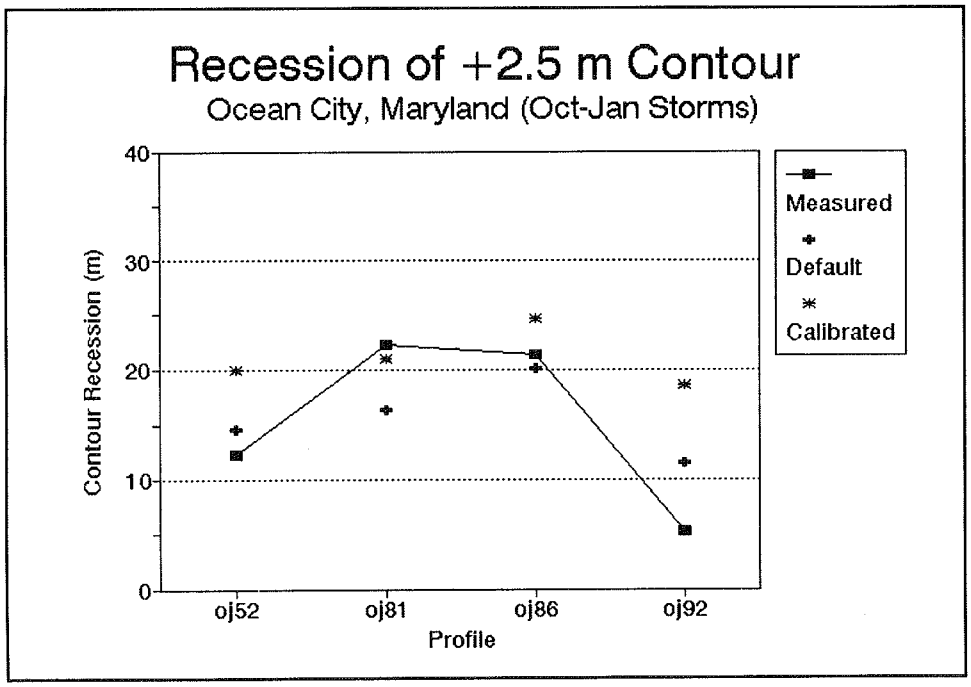

Figure 60. Comparison of measured and simulated recession of the 2.5-m contour for the OJ storm series, Ocean City, MD

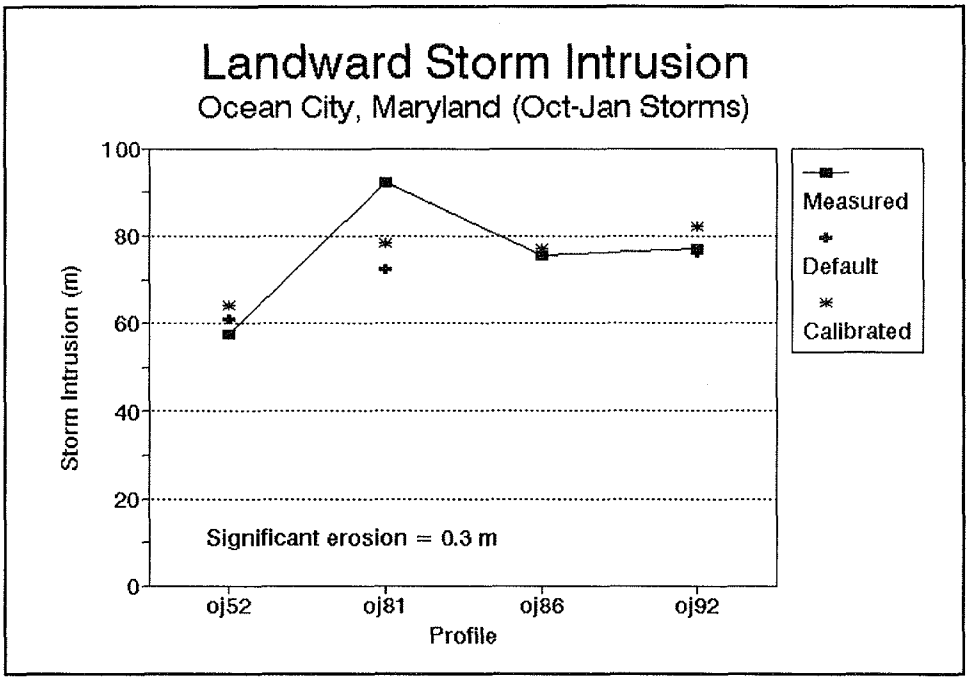

Figure 61. Comparison of measured and simulated storm intrusion for the OJ storm series, Ocean City, MD

the default and calibrated simulations except at profile 81, where erosion was underpredicted.

Summary

Overall, the model performed well in reproducing measured response to multiple storms at Ocean City, MD. The default simulations produced reasonable agreement in most cases. With calibration to a single profile, model results were improved in some cases, but were slightly less accurate than the default simulations in other cases. The largest discrepancies between calculations and data were associated with profiles for which the conservation of mass assumption was poorly satisfied between surveys. Also, the model tended to underestimate erosion in the hotspot region. The measures of performance at the foreshore demonstrated that the model provided valid estimates of foreshore and dune response in most cases.

Manasquan and Point Pleasant Beach, NJ

Point Pleasant Beach and Manasquan are adjacent beaches separated by the stabilized Manasquan Inlet on the Atlantic Coast of New Jersey. Manasquan is a relatively narrow beach with short groins spaced at 200 to 300-m intervals,

whereas Point Pleasant Beach is wide and includes no littoral traps other than the jetty at Manasquan Inlet (Larson, Kraus, and Byrnes 1990).

A northeaster impacted these two beaches between the dates of 28 and 30 March 1984 causing severe erosion. The effects of this storm were captured by profile surveys conducted by the U.S. Army Engineer District (USAED), Philadelphia, as part of the Corps of Engineers Monitoring Completed Coastal Projects (MCCP) Program. Subaerial profile surveys at the two beaches were taken approximately 1 to 2 days before the storm and again 3 to 4 days after the storm. Subaqueous profile surveys were taken approximately 3 months before and 2 weeks after the storm. The subaerial and subaqueous profiles were combined to obtain an approximation of the profile before the storm. Wave data for the northeaster were provided by a waverider buoy located at a depth of 15.2 m operated as another element of the MCCP Program. Water level data were obtained through a National Oceanographic Service (NOS) maintained tide gauge located near the shoreward side of Manasquan Inlet. The time-histories of the wave and water level data are shown in Figure 62. The storm duration was approximately 2 days with a peak significant wave height of about 7 m and a peak water level of about 2 m above NGVD. Additional information on the storm and data collection at Point Pleasant Beach and Manasquan, NJ, is presented by Larson, Kraus, and Byrnes (1990) and Gebert and Hemsley (1991).

Sediment grain size was found to vary substantially across the beach profile at Manasquan and Point Pleasant Beach. A characteristic grain size at the foreshore and dune was estimated to be approximately 0.50 mm based on sediment analyses (Larson, Kraus, and Byrnes 1990). The median grain size on the subaqueous profile was in the range of 0.20 mm. Because SBEACH requires a single grain size as input, a representative value of 0.40 mm was chosen for the present simulations. This value falls between that of the dune and subaqueous profile but is weighted closer to the grain size of the dune, which is the area of focus in the modeling.

Larson, Kraus, and Byrnes (1990) applied an earlier version of the SBEACH model to the Manasquan/Point Pleasant Beach data set using a single averaged profile for each site. In the present study, model simulations are performed on an individual profile basis for nine profiles at Manasquan and eight profiles at Point Pleasant Beach.

Default simulations

Manasquan. The beach at Manasquan is located on the north side of Manasquan Inlet. Total volume change per unit width of beach for each of the nine profile lines surveyed during the data collection is shown in Figure 63. Profile M1 was located closest to the inlet jetty and profiles M2 to M9 were located to the north along the beach. As shown in Figure 63, mass

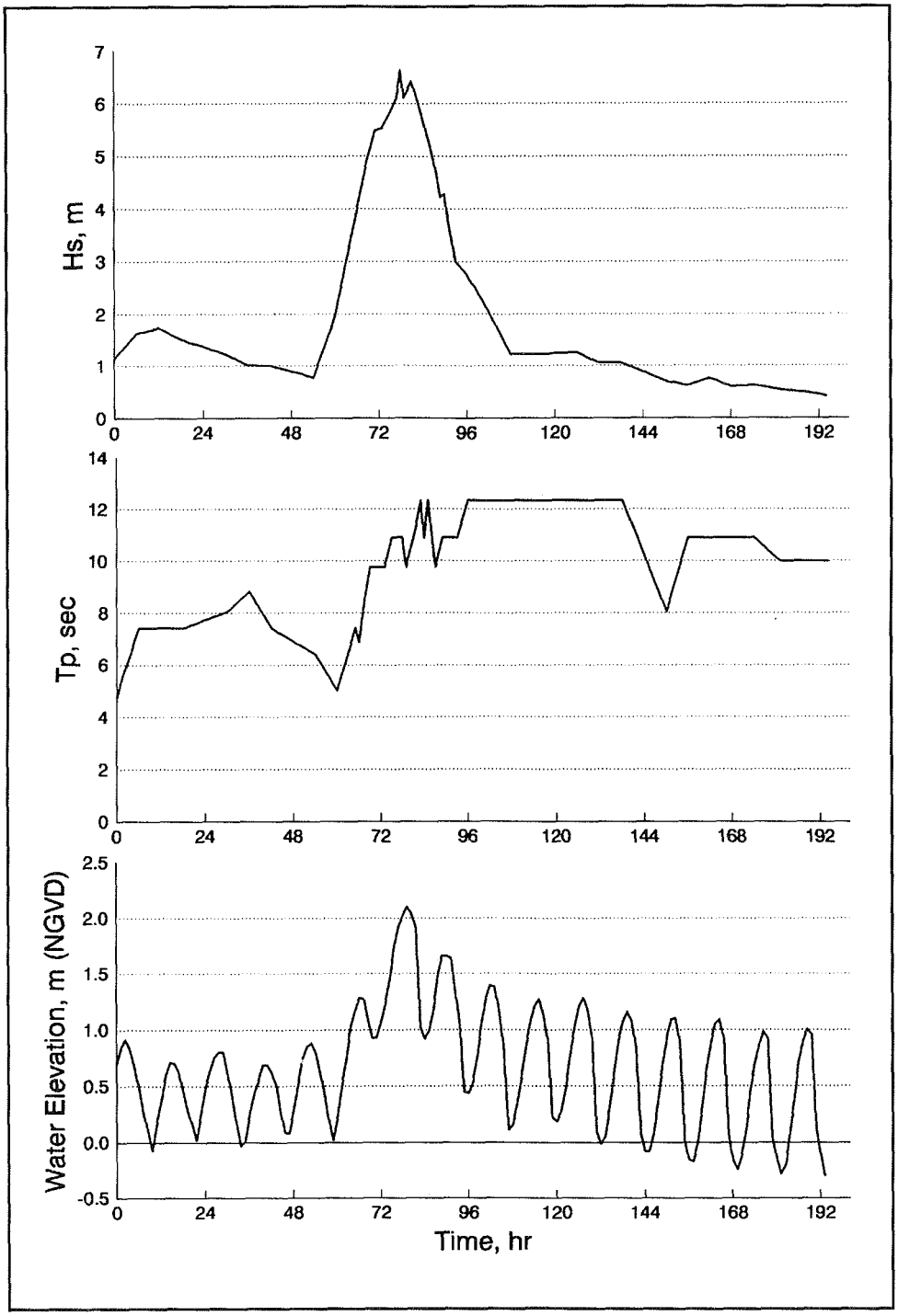

Figure 62. Wave height, wave period, and water elevation time-histories for the March 1984 storm, Manasquan/Point Pleasant Beach, NJ

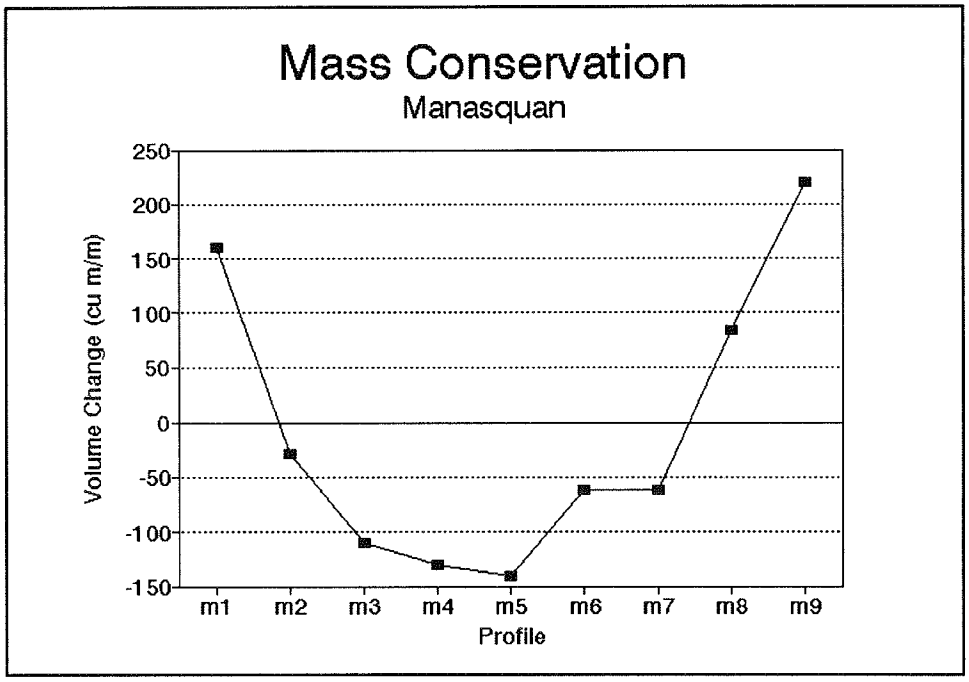

Figure 63. Conservation of mass between beach profile surveys for the March 1984 storm, Manasquan, NJ

conservation across the profiles was relatively poor with five of the nine profiles exhibiting a gain or loss of more than 100 m^3/m. The large changes in volume may be attributed to the relatively long time interval between subaqueous profile surveys, longshore effects produced by the inlet and structures, or possible survey error in the offshore. Despite the lack of volume conservation on the profiles, the default simulations produced reasonably good agreement with the measured response on the upper beach profile. Figure 64 shows the measured and modeled beach change for profile M3. The measured recession of the dune is well matched by the calculations. The model produced overwash at the dune crest which was not observed in the measurements. Such overwash was predicted in varying degrees by the model for the different profiles at Manasquan. Figure 65 displays default simulation results for profile M4. In this case, the predicted overwash better matches the measured response. Recession of the shoreline at the profile datum is not simulated by the model and may have resulted in part from longshore processes which produced a net loss of sediment from this profile.

Point Pleasant Beach. Eight profiles were surveyed at Point Pleasant Beach located south of Manasquan Inlet. Profile P1 was closest to the inlet jetty and profiles P2 to P8 were spaced to the south along the beach. Figure 66 displays the total volume change between surveys for each profile. A net loss of volume occurred for seven of the eight profiles surveyed. However, the magnitude of changes are less than those observed at Manasquan

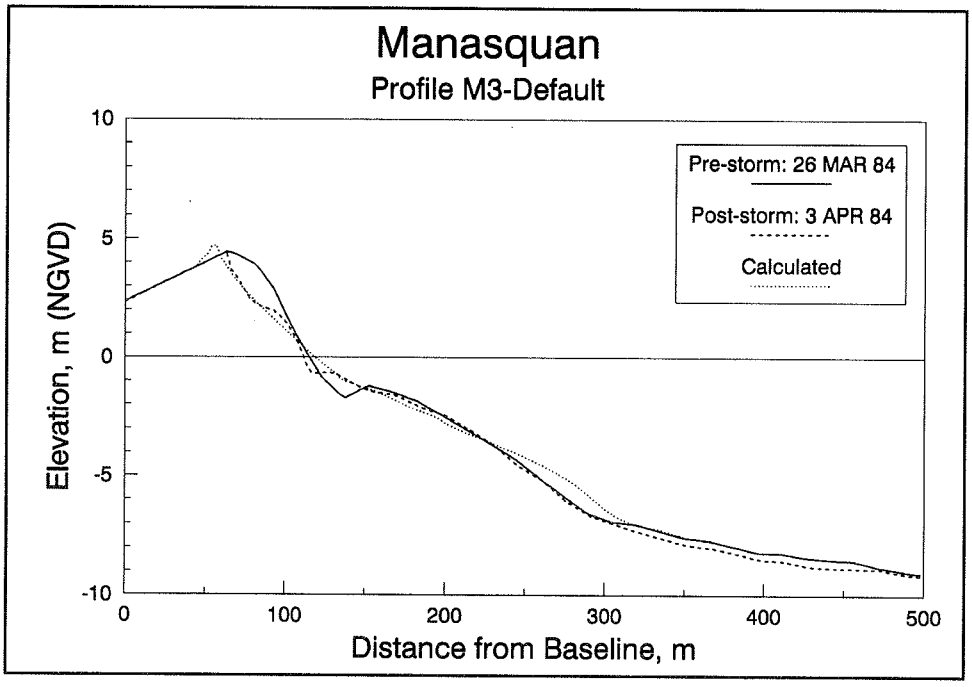

Figure 64. Result of default simulation of the March 1984 storm for profile M3, Manasquan, NJ

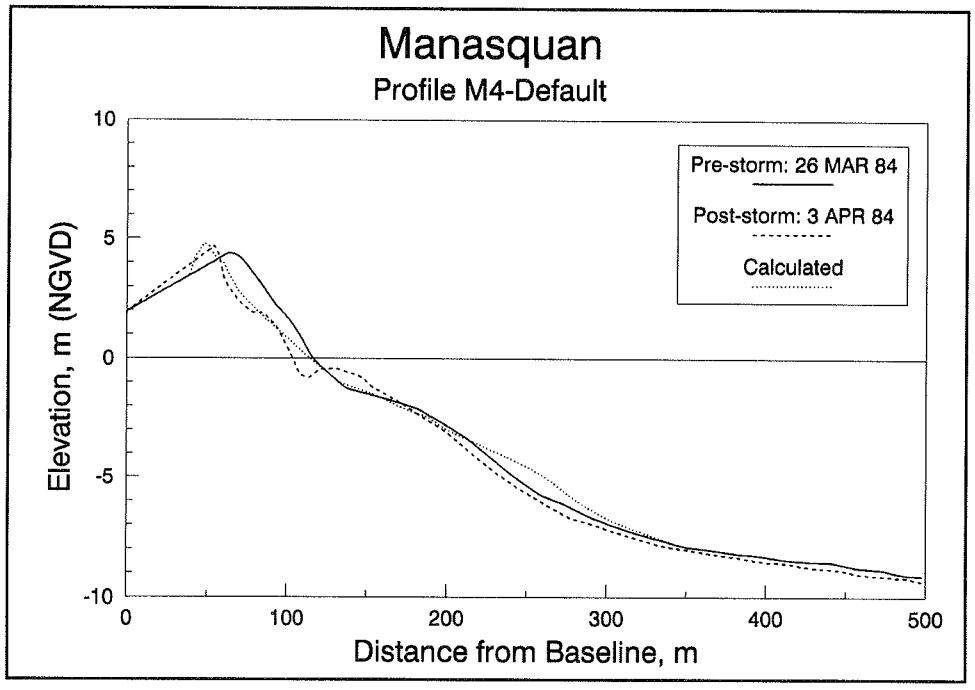

Figure 65. Result of default simulation of the March 1984 storm for profile M4, Manasquan, NJ

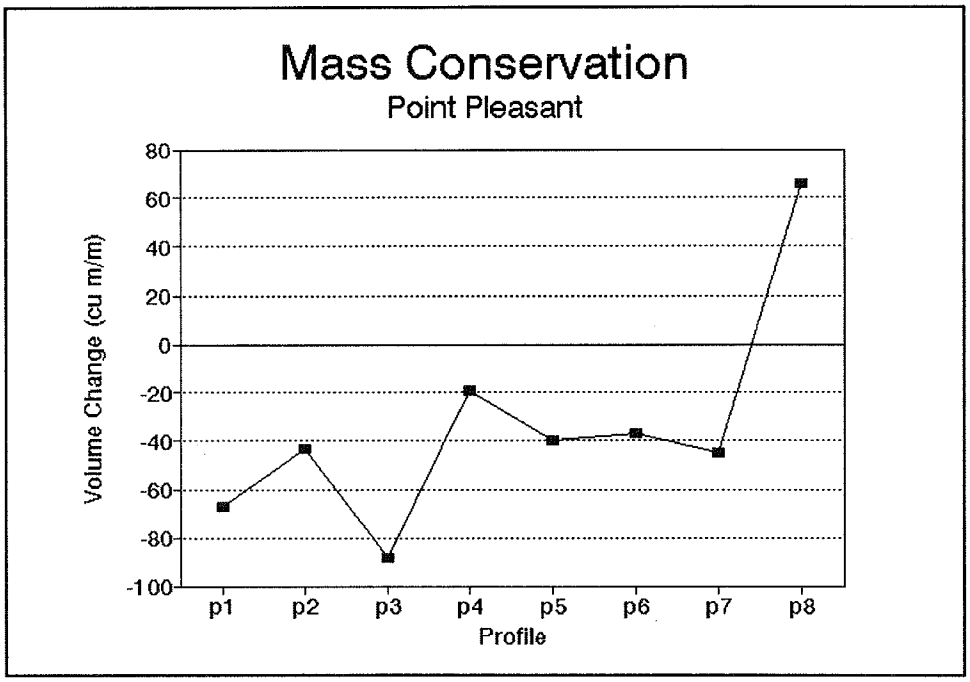

Figure 66. Conservation of mass between beach profile surveys for the March 1984 storm, Point Pleasant Beach, NJ

indicating better conservation of mass. In comparison to the beach response at Manasquan, Point Pleasant Beach experienced more erosion and recession of the upper profile. A prominent ridge was observed at the shoreline on nearly all of the post-storm measured profiles at Point Pleasant Beach. This feature is assumed to be a recovery berm formed by accretionary waves after the storm. Figure 67 displays default simulation results for profile P2. In this case, the model reproduced the measured erosion fairly well. The slope of the measured profile is closely matched by the model both in the offshore and on the beach face, except in the region where a recovery berm appears to have formed between approximately 0 and 2 m NGVD. Some overwash was evident in the measured response, but the model overestimated the magnitude of material transport landward on the dune. Figure 68 displays results for profile P5. For this case, the model underpredicted erosion of the upper profile. A prominent berm is present on the post-storm measured profile up to the 2.5-m contour. This berm, apparently produced by post-storm recovery, returned the shoreline nearly to its pre-storm location. Some overwash is evident on the measured profile, but none was predicted by the model. Another example of simulation results is shown in Figure 69. The measured response of profile P7 is similar to that of profile P5, but the model better reproduced the erosion in this case. As in the other cases, much of the eroded material deposited in the offshore during the storm presumably returned to the beach prior to the post-storm surveys.

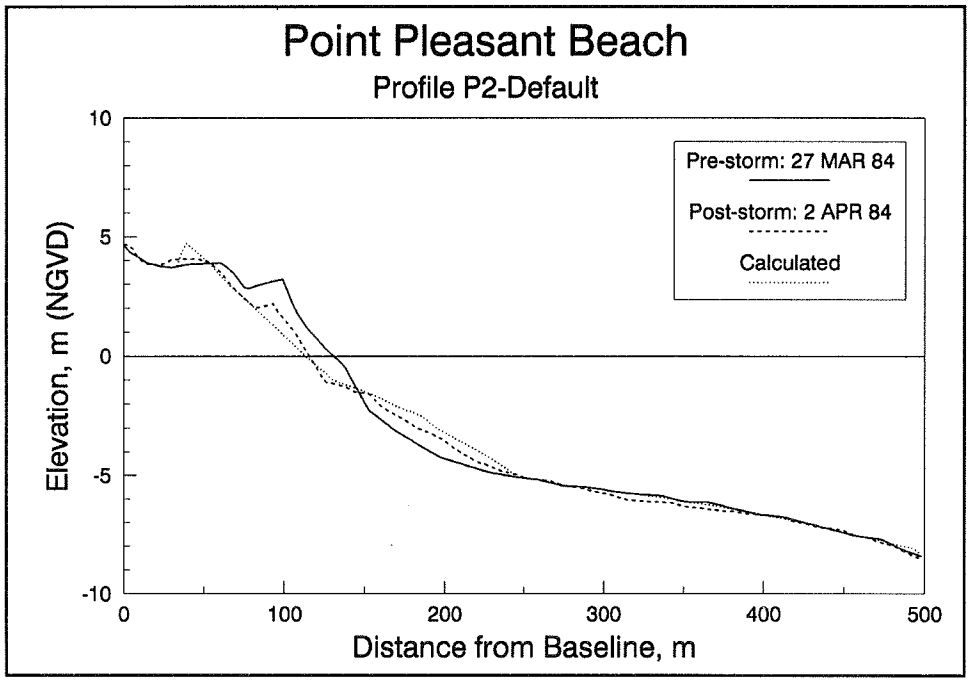

Figure 67. Result of default simulation of the March 1984 storm for profile P2, Point Pleasant Beach, NJ

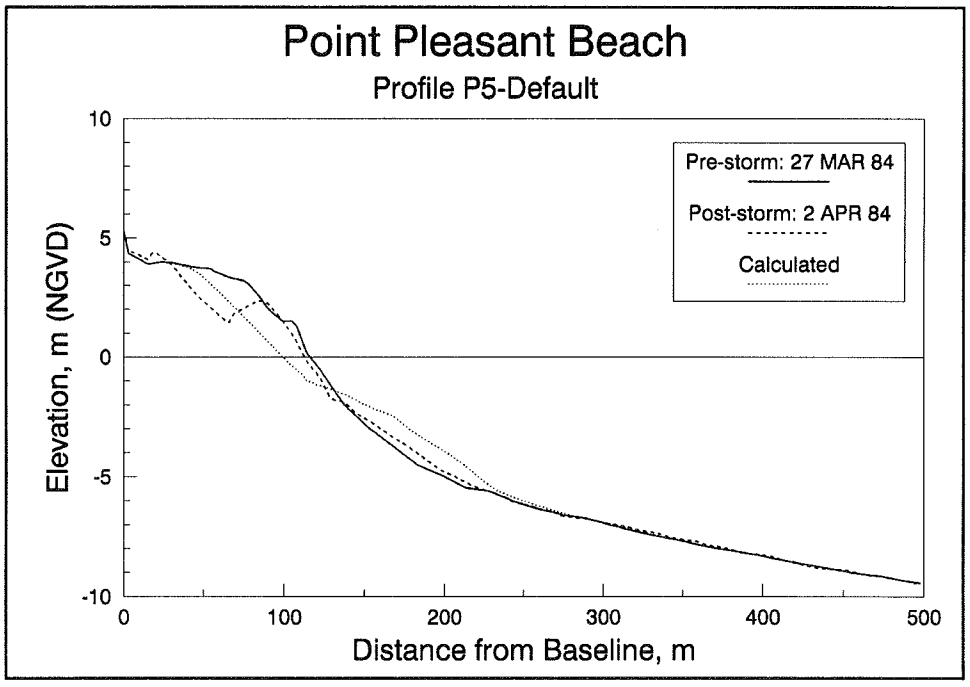

Figure 68. Result of default simulation of the March 1984 storm for profile P5, Point Pleasant Beach, NJ

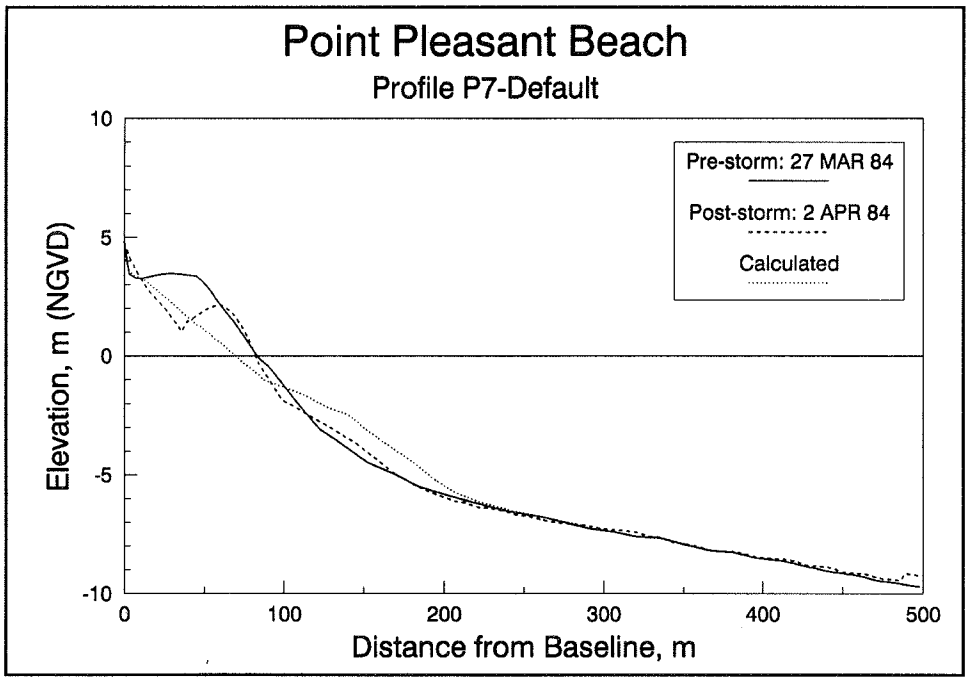

Figure 69. Result of default simulation of the March 1984 storm for profile P7, Point Pleasant Beach, NJ

Model calibration

Profile M5 at Manasquan was selected as the calibration profile for this data set. This profile was not situated near the inlet and did not exhibit a significant recovery feature at the foreshore evident on many of the other profiles. In the process of calibration, the best fit, as defined by minimum rms difference between calculated and measured profiles, was obtained with the values of $K = 1.80 \times 10^{-6}$ m^4/N, $\epsilon = 0.002$ m^2/s, $DFS = 0.30$ m. Random variation of the input wave height within ± 15 percent was employed. The selected calibration parameter values are very close to the default values and only minor changes were observed between default and calibrated simulation results. Comparison of the default and calibrated results is provided in Figure 70.

Calibrated simulations

Manasquan. The above calibration parameters were applied to the remaining profiles in the Manasquan data set. As with the calculation for profile M5, only minor differences were observed between default and calibrated runs for these cases. Figures 71-73 show the measures of performance at the foreshore calculated for the default and calibrated runs. In

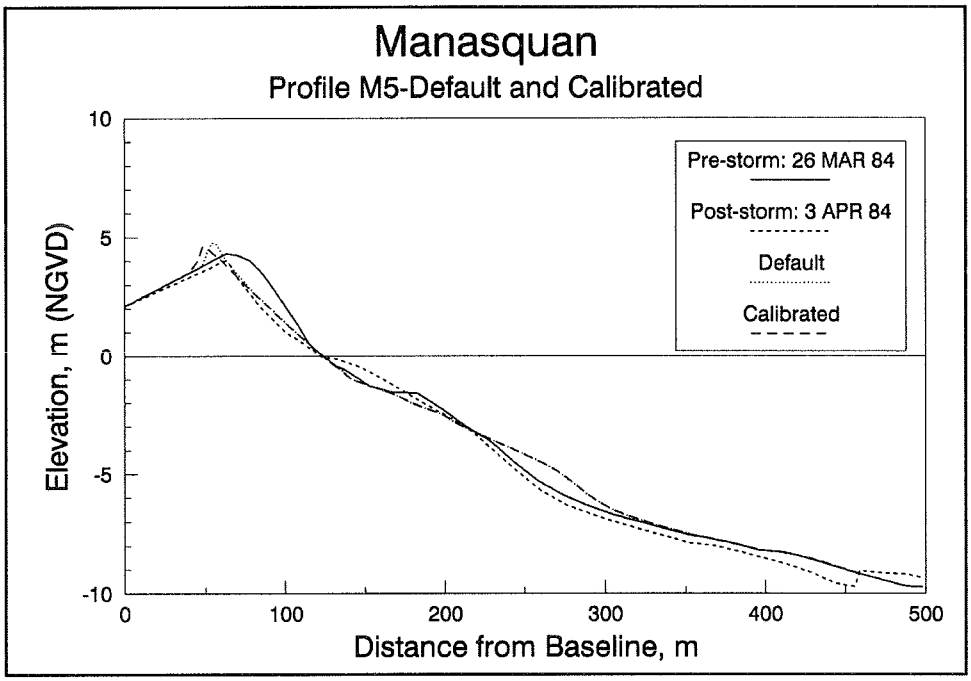

Figure 70. Results of default and calibrated simulations of the March 1984 storm for profile M5, Manasquan, NJ

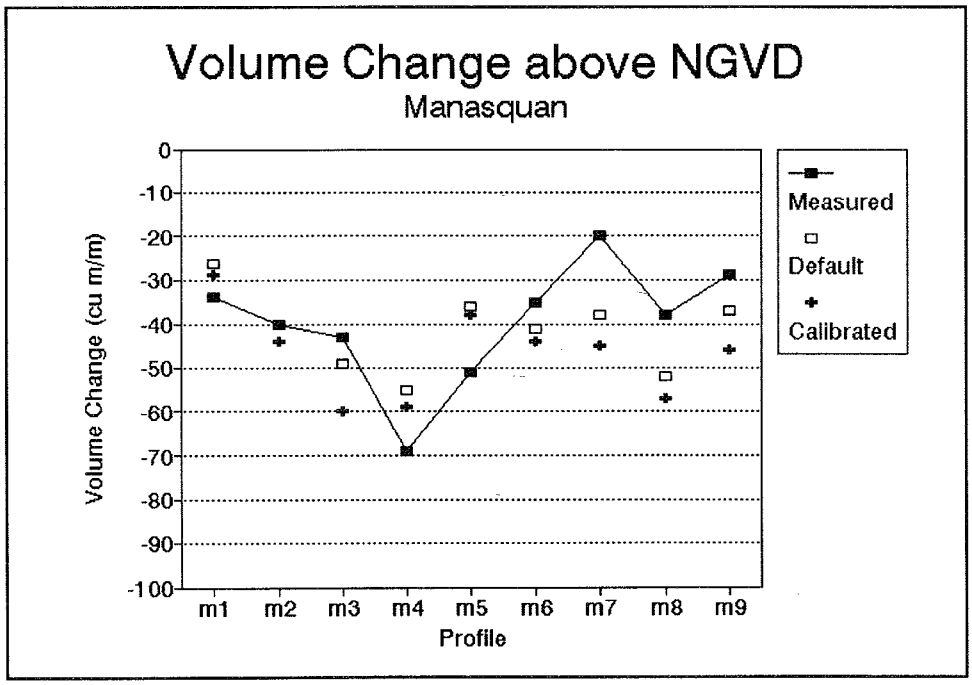

Figure 71. Comparison of measured and simulated volume change above NGVD for the March 1984 storm, Manasquan, NJ

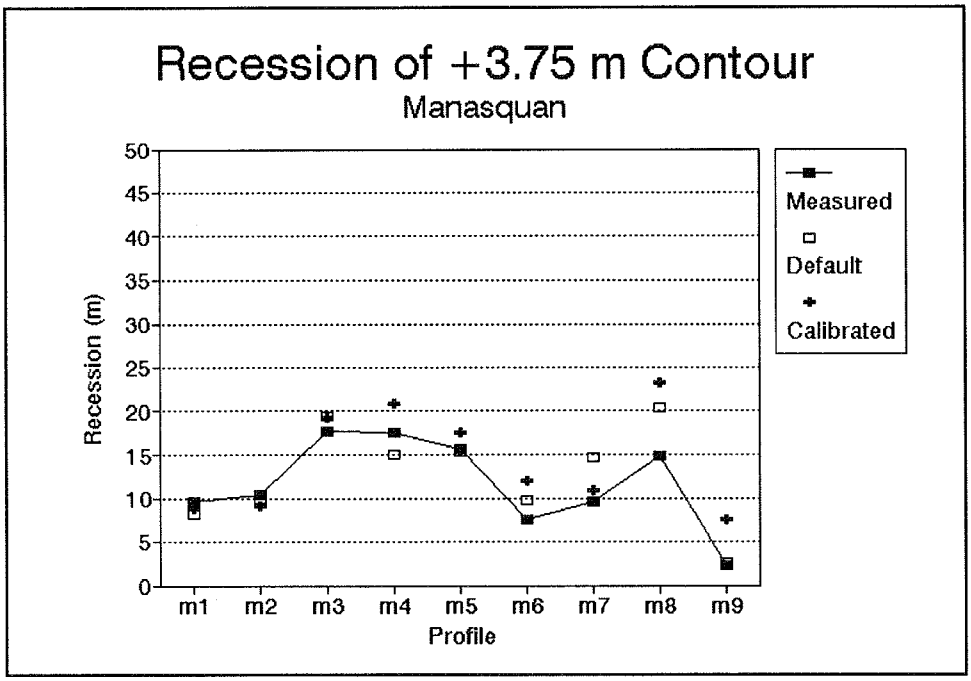

Figure 72. Comparison of measured and simulated recession of the 3.75-m contour for the March 1984 storm, Manasquan, NJ

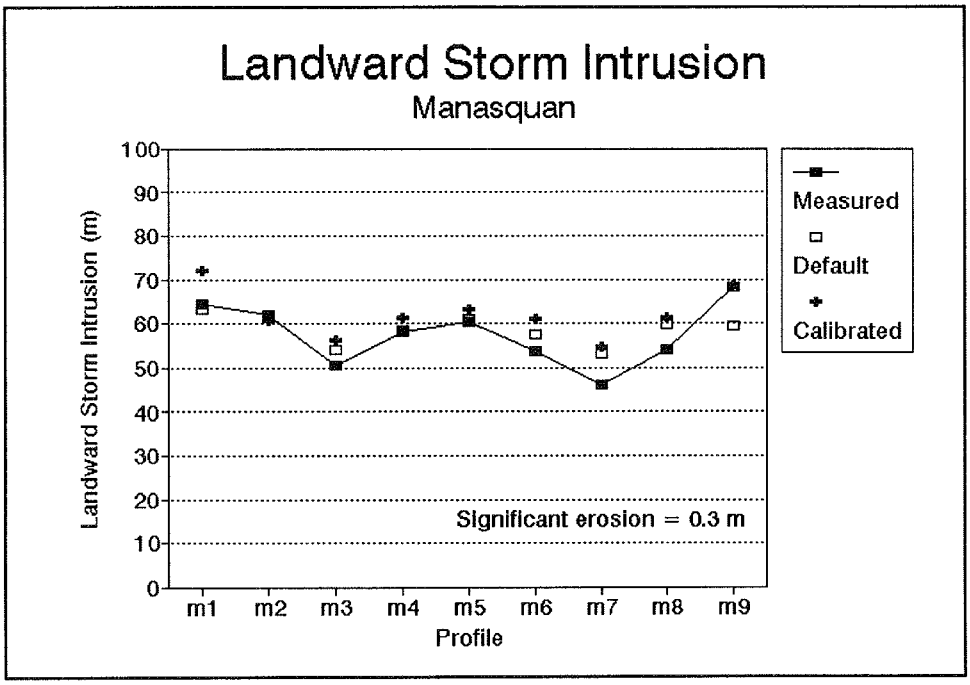

Figure 73. Comparison of measured and simulated storm intrusion for the March 1984 storm, Manasquan, NJ

general, the model tended to overpredict volume loss above NGVD, which may be accounted for in part by the presence of recovery berms on the post-storm measured profiles. Figure 72 shows comparison of contour recession calculations. The 3.75-m contour was selected for analysis to represent the response of the upper dune. For most of the profiles, recession was modeled to within a few meters of the measured values, with the default simulations producing slightly better agreement overall. As shown in Figure 73, the landward extent of erosion was predicted within 5 to 10 m for all profiles.

Point Pleasant Beach. As with the Manasquan simulations, only minor differences were observed between the default and calibrated runs for most of the Point Pleasant Beach cases. Figure 74 shows default and calibrated simulation results for profile P3, where somewhat larger differences were observed in comparison with the other cases. The calibrated run produced overwash, whereas no overwash was predicted in the default run. Also, measured beach recession was slightly better matched with the calibrated run for this case. Figure 75 displays the simulated and measured volume change above NGVD for all Point Pleasant Beach cases. Although predicted volume changes are relatively close to measured changes for profiles P3-P5, it is noted that the post-storm measured profiles include effects of profile recovery. Actual volume losses above NGVD immediately after the storm were likely greater than indicated in the measurements, and the simulated results for profiles P3-P5 probably represent an underprediction of eroded volume.

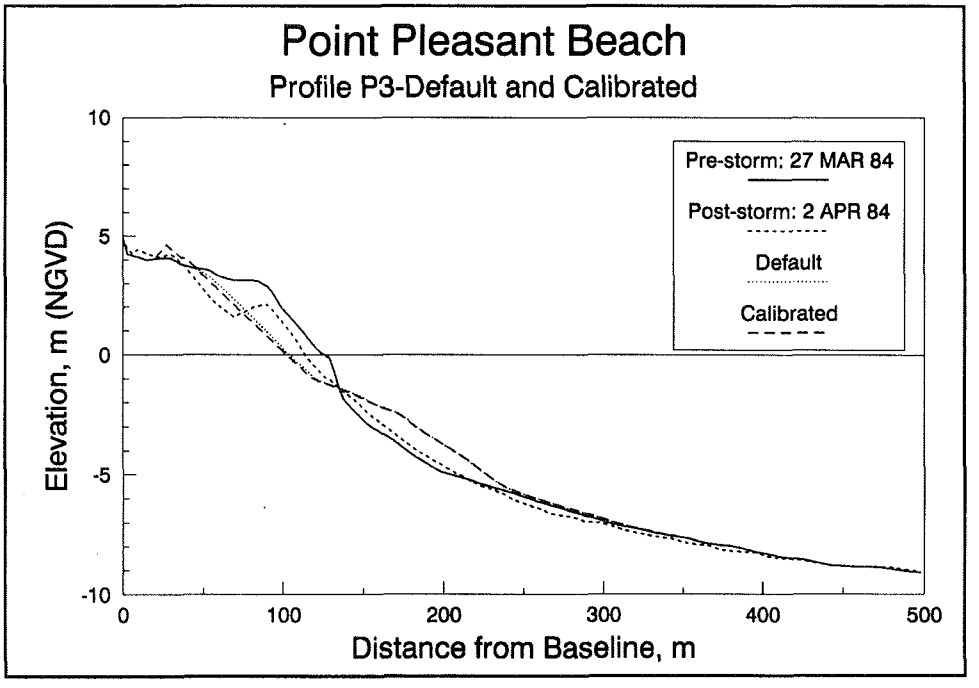

Figure 74. Results of default and calibrated simulations of the March 1984 storm for profile P3, Point Pleasant Beach, NJ

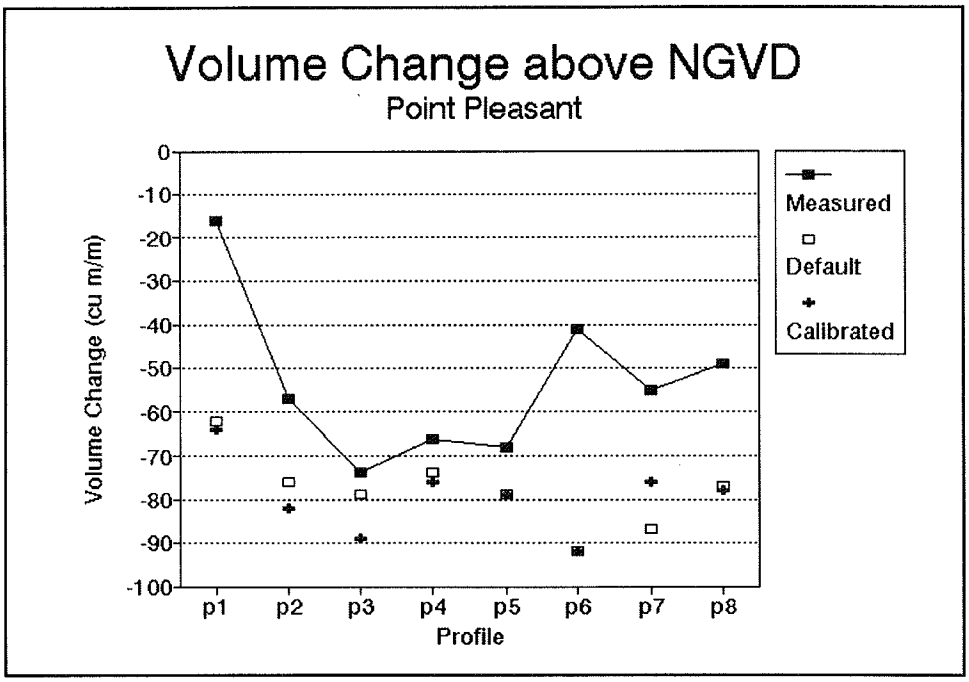

Figure 75. Comparison of measured and simulated volume change above NGVD for the March 1984 storm, Point Pleasant Beach, NJ

Contour recession was calculated at an elevation of +2.75 m NGVD, above the crest of the post-storm recovery berm. Figure 76 shows that the model significantly underpredicted recession for profiles P3-P5, while relatively good agreement was obtained for profiles P2 and P6-P8. No consistent improvements were observed for the calibrated versus default simulations. Figure 77 displays a comparison of measured and simulated landward storm intrusion. The measured extent of erosion was predicted to within 15 m for most cases. Poorest agreement was exhibited for profile P1 which was located closest to the inlet jetty.

Summary

The default simulations provided reasonable agreement with measurements for most of the Manasquan cases. Erosion was significantly underpredicted for three of the Point Pleasant Beach cases (P3-P5), while acceptable results were obtained for the remaining cases. Measured dune overwash was simulated with varying success in both the Manasquan and Point Pleasant Beach cases. Some of the differences which were observed between measured and modeled profile response may be related to several factors including the presence of post-storm recovery berms at the beach face, the substantial variation in sediment grain size across the profile, a lack of mass conservation on the profile produced by longshore processes, and proximity to and influence of the

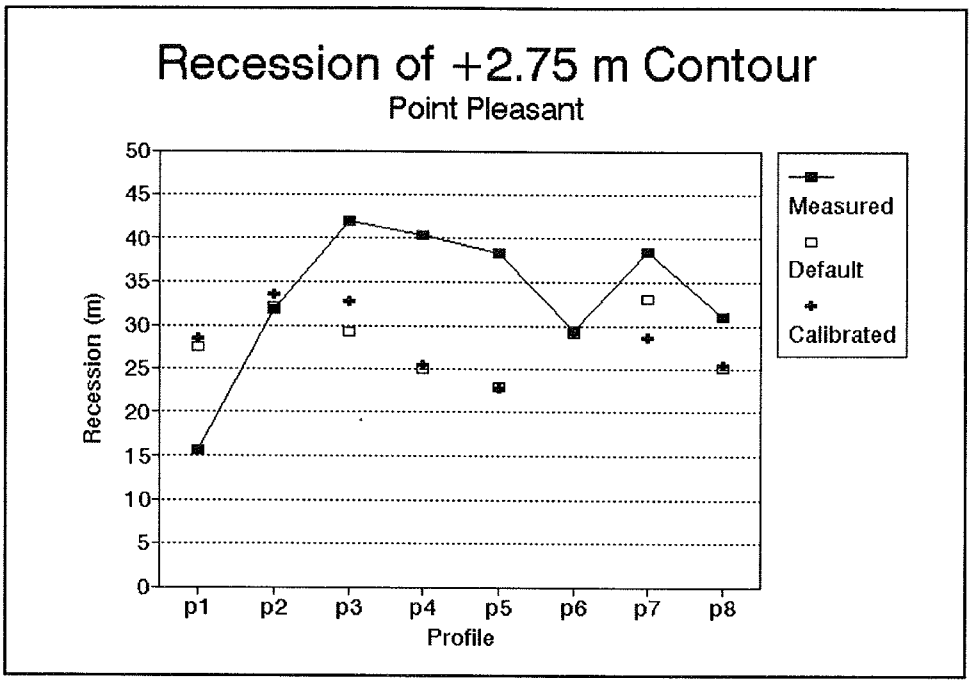

Figure 76. Comparison of measured and simulated recession of the 2.75-m contour for the March 1984 storm, Point Pleasant Beach, NJ

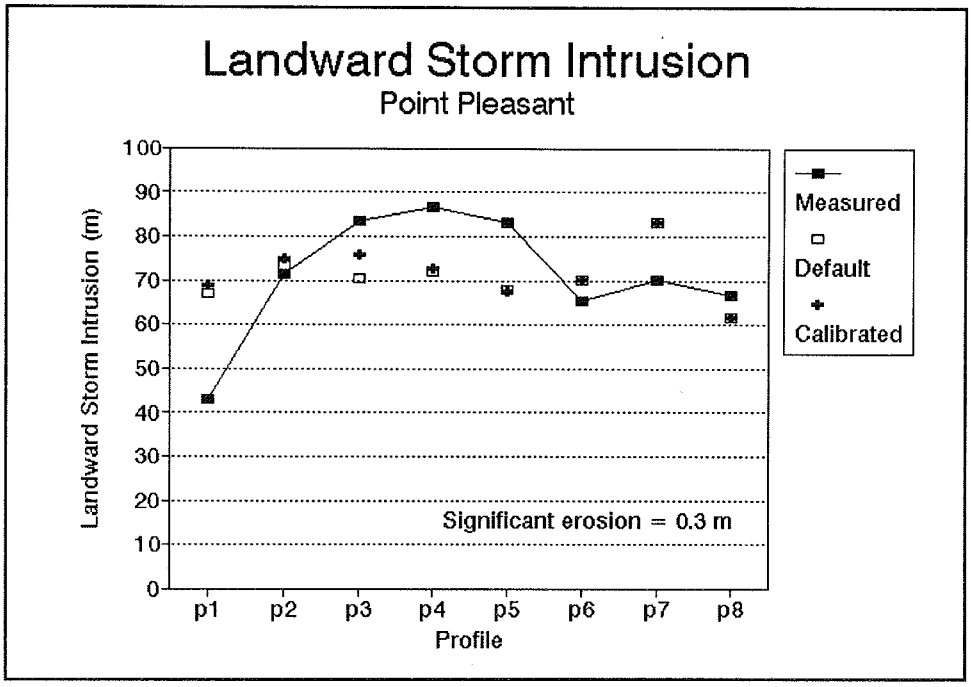

Figure 77. Comparison of measured and simulated storm intrusion for the March 1984 storm, Point Pleasant Beach, NJ

inlet and structures. Model calibration to profile M5 of the Manasquan data set was performed with only minor modification of the default calibration parameter values. The calibrated simulations produced no net improvements over the default runs, indicating that default values of the calibration parameters were near optimum for these data.

Dewey Beach and Rehoboth Beach, DE

On 10 December 1992, a northeaster attacked the adjacent beaches of Dewey Beach and Rehoboth Beach on the east coast of Delaware. The response of the beaches to the storm was captured by profile surveys collected by the USAED, Philadelphia, as part of a project feasibility study. Pre-storm profiles were measured on 29 October 1992 and post-storm surveys were performed shortly after the storm on 18 December 1992. Wave conditions during the storm were recorded by a wave gauge located at a depth of approximately 9 m off the coast of Dewey Beach. Tide information was available from a nearby tide gauge located at Lewes, DE. Figure 78 displays time-histories of the wave and water level information for the storm. The storm had a peak significant wave height of 4 m, a peak water level of approximately 2 m NGVD, and a duration of 4 days. A sediment grain size of 0.33 mm was used in the model simulations based on beach sediment analyses performed as part of the project feasibility study. Additional information on the data collection and beach response at Dewey and Rehoboth Beaches is presented by USAED, Philadelphia (1995).

Default simulations

Dewey Beach. Pre- and post-storm measurements were available for seven profile lines at Dewey Beach. Figure 79 displays volume change between surveys for each profile. All profiles experienced some loss of volume. Profile 140 maintained the best mass conservation, while profile 240 showed the greatest change in volume with a loss of 120 m^3/m. The default simulations provided close agreement with measured beach changes above NGVD for all seven profiles. Figures 80-82 provide examples of default simulation results for three cases with different initial beach profile configurations. As shown in Figure 80, the pre-storm beach at profile 100 had a relatively flat berm at 2 m NGVD backed by a small dune. Both the post-storm measured and calculated profiles showed extensive erosion of the berm and dune with material deposited offshore. The calculation produced more erosion of the nearshore profile below NGVD than observed in the measurements; however, some eroded material deposited in the bar may have returned to the nearshore prior to the post-storm survey. No recovery of the beach above NGVD was evident. Figure 81 shows simulation results for profile 140. In this case, the pre-storm beach had a peaked berm that was backed by a higher dune with a crest at 5 m NGVD. The storm produced extensive erosion of the berm and

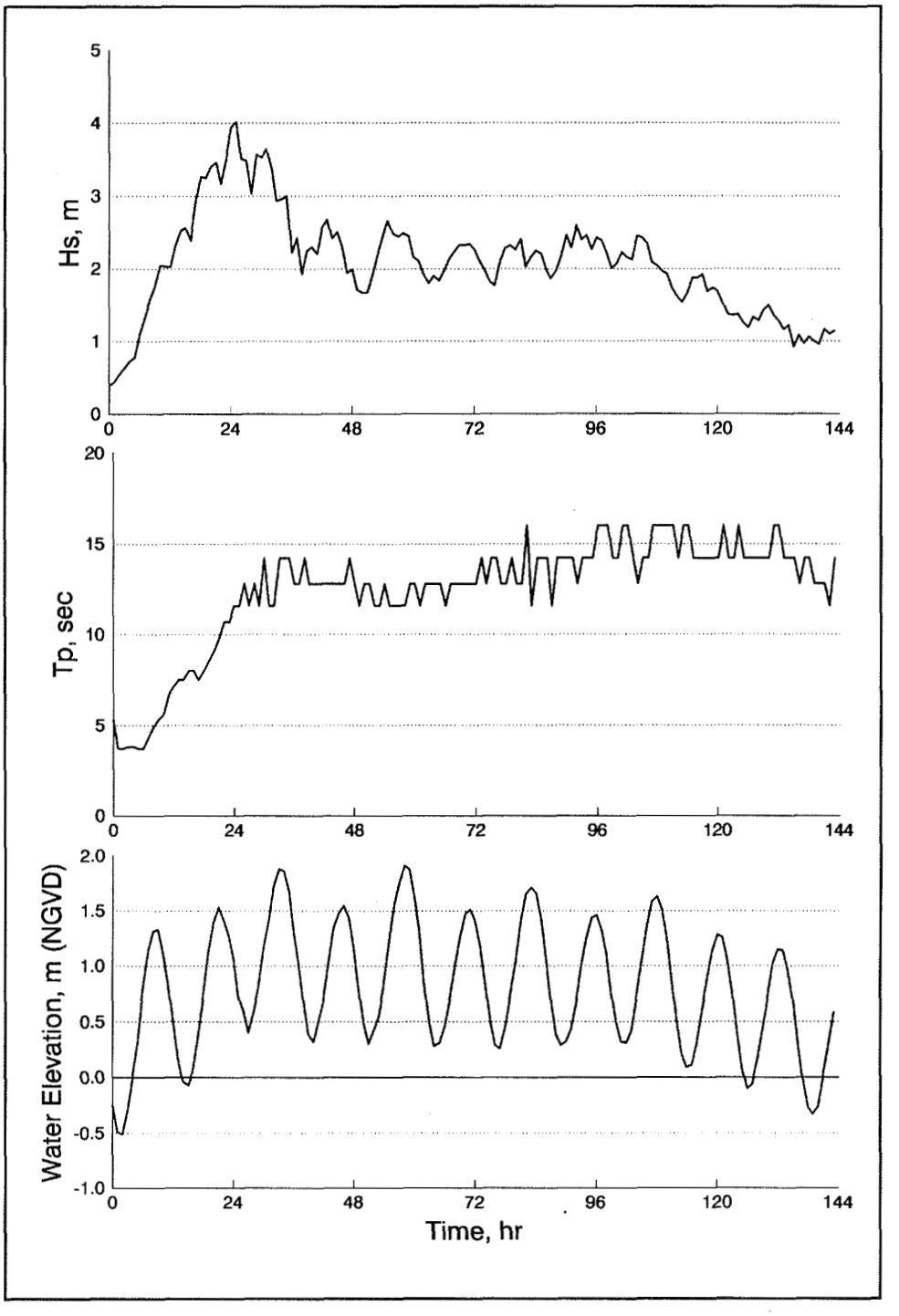

Figure 78. Wave height, wave period, and water elevation time-histories for the December 1992 storm, Dewey Beach/Rehoboth Beach, DE

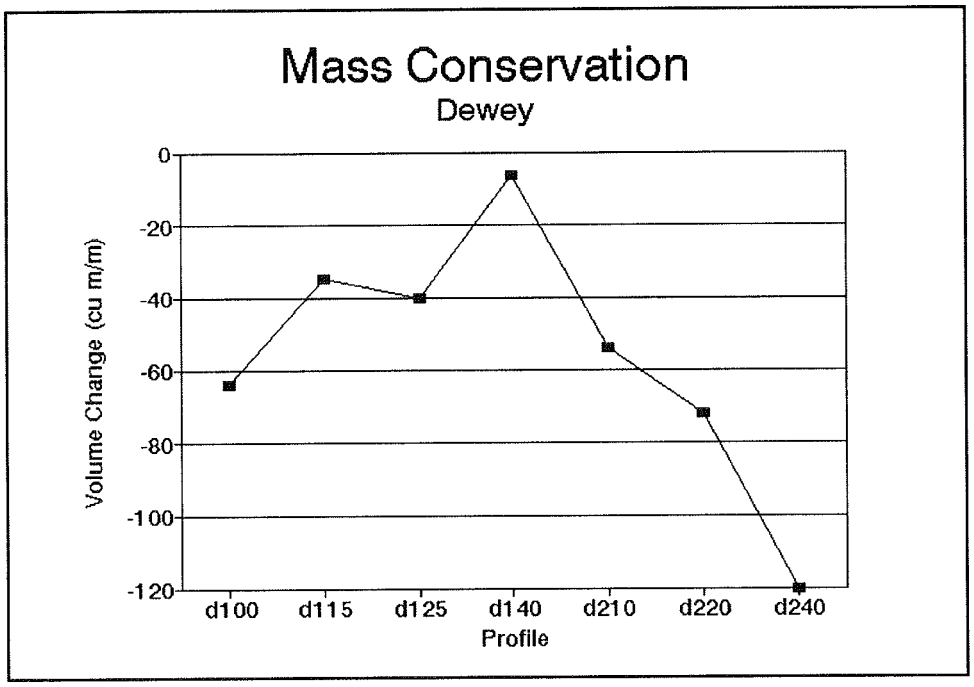

Figure 79. Conservation of mass between beach profile surveys for the December 1992 storm, Dewey Beach, DE

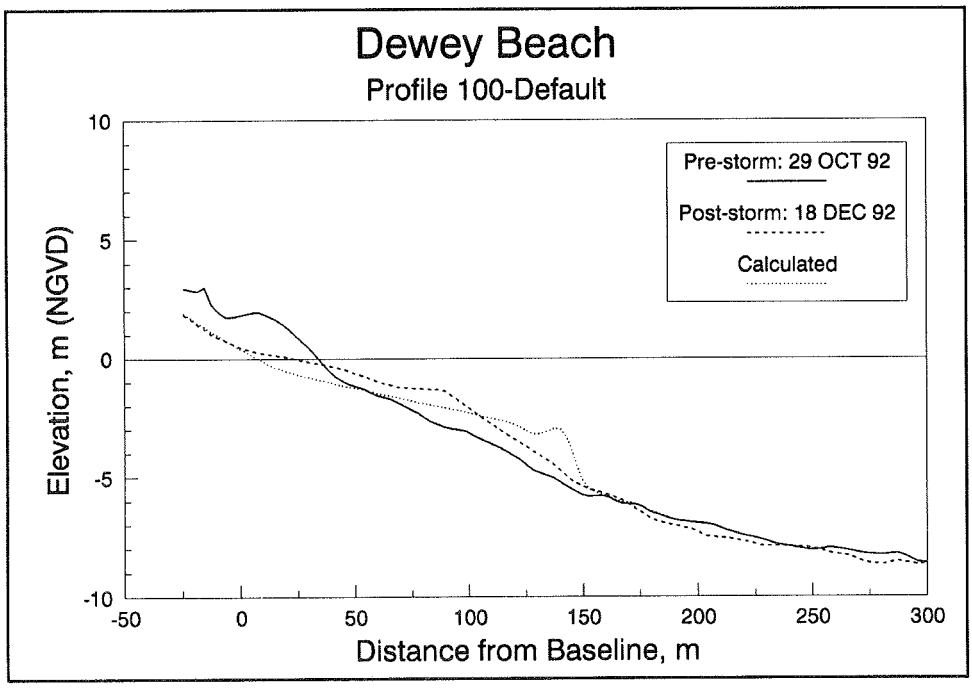

Figure 80. Result of default simulation of the December 1992 storm for profile 100, Dewey Beach, DE

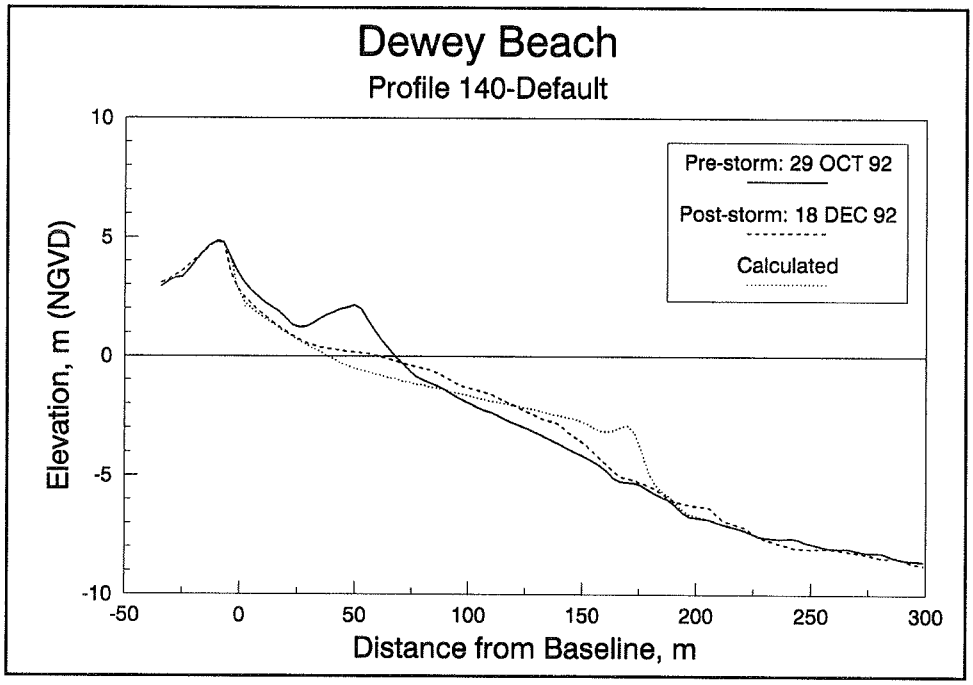

Figure 81. Result of default simulation of the December 1992 storm for profile 140, Dewey Beach, DE

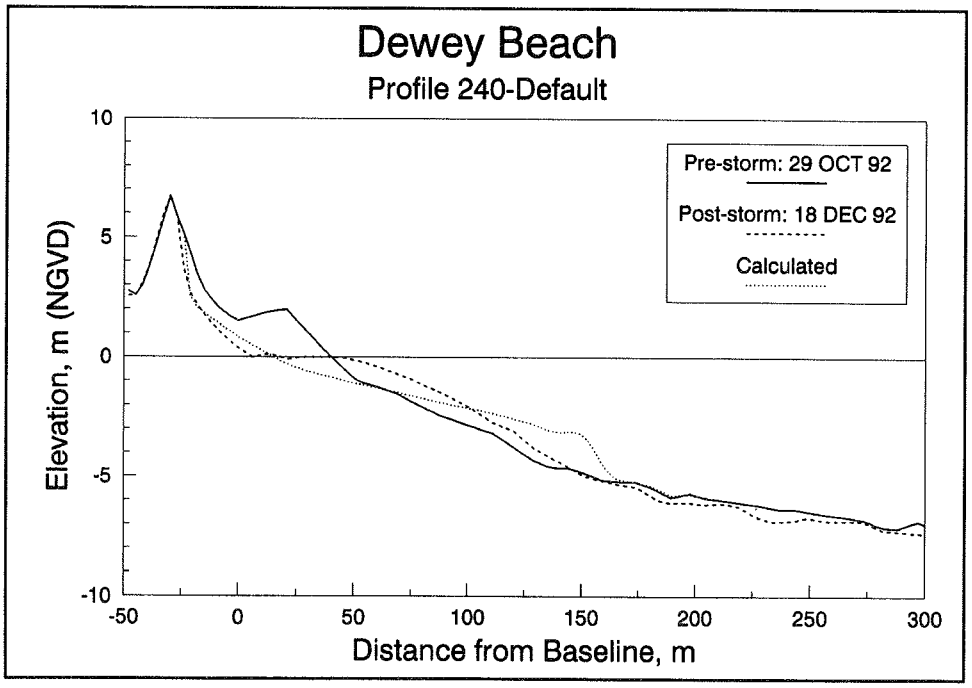

Figure 82. Result of default simulation of the December 1992 storm for profile 240, Dewey Beach, DE

relatively minor erosion of the dune. The measured response of the berm and dune was accurately simulated by the model, including magnitude and landward extent of erosion. As with profile 100, the model produced more erosion at the nearshore profile below NGVD than observed in the measurements. Calculation results for profile 240 are displayed in Figure 82. In this case, the elevation of the dune crest was approximately 7 m NGVD. The model slightly underestimated measured recession at certain elevations on the berm and dune, but overall erosion above NGVD was well simulated.

Rehoboth Beach. Rehoboth Beach is located to the north of Dewey Beach along the Delaware Coast. Survey data for eight profile lines at Rehoboth Beach were available to model beach response to the December 1992 storm. Figure 83 displays the volume changes between pre- and post-storm surveys for each profile line. Mass conservation was satisfied fairly well on four of the profiles, while the remaining profiles exhibited a loss of volume of between approximately 40 and 60 m^3/m. An example of default simulation results is shown in Figure 84 for profile 131. The pre-storm beach had a berm near the shoreline which was backed by a higher dune. The model predicted complete erosion of the berm and partial erosion of the dune. The measurements showed similar erosion of the berm and dune above the 1-m NGVD contour. Differences between measurements and calculations below the 1-m NGVD contour may be attributed to beach recovery which is indicated by the convex shape of the measured post-storm profile in the vicinity of the pre-storm berm. Profiles 117, 122, and 200 of the Rehoboth Beach data set

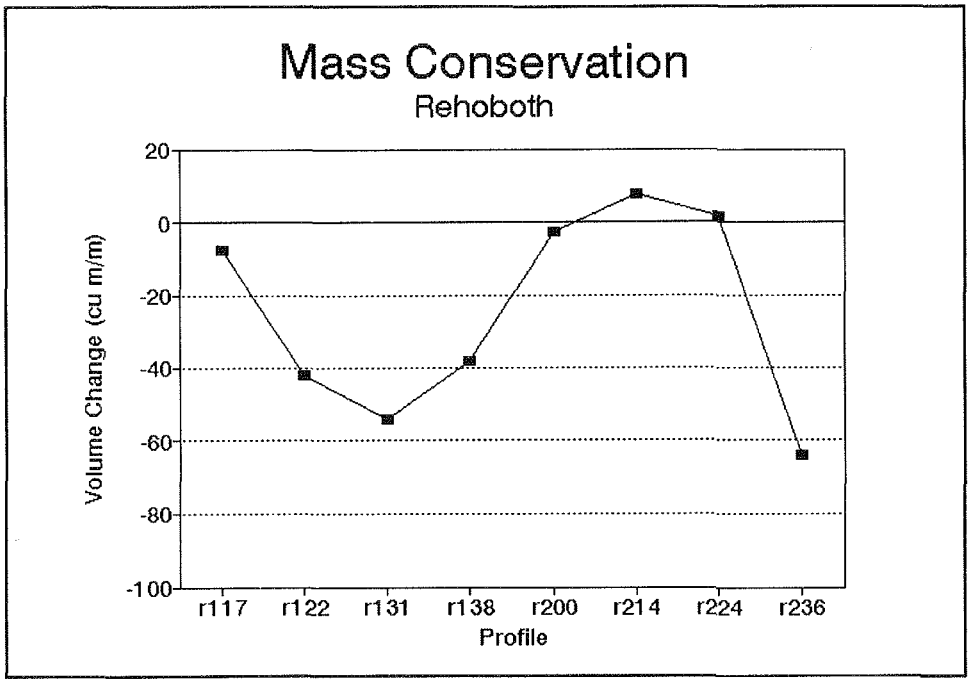

Figure 83. Conservation of mass between beach profile surveys for the December 1992 storm, Rehoboth Beach, DE

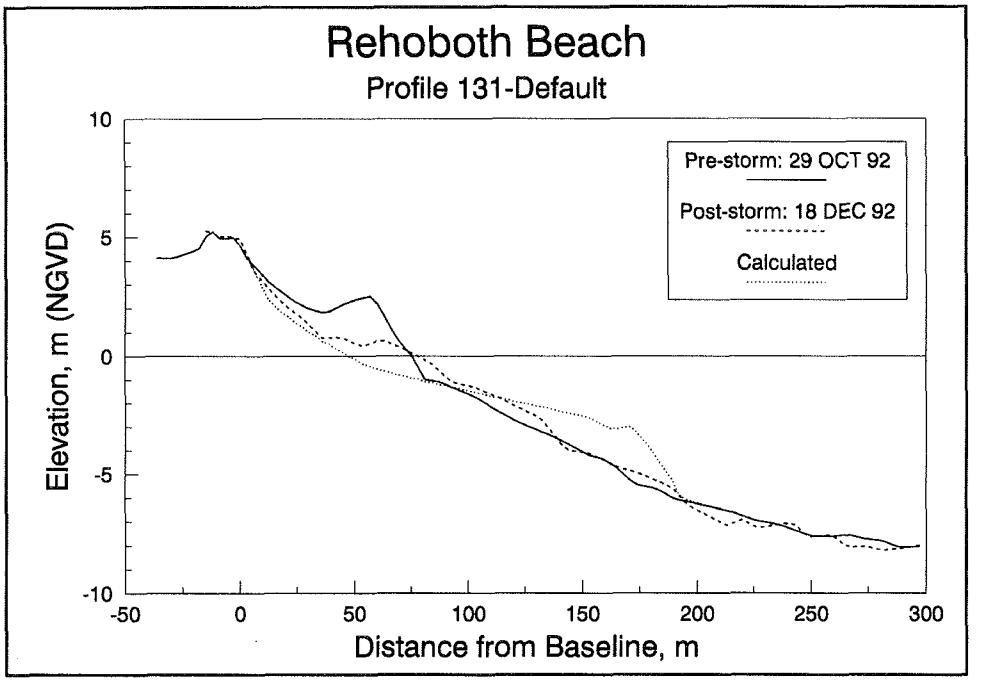

Figure 84. Result of default simulation of the December 1992 storm for profile 131, Rehoboth Beach, DE

included seawalls which influenced beach response during the storm. To simulate these cases, seawalls were implemented in SBEACH at the nearest calculation cell corresponding to the actual location of the seawall on the profile. An example of simulation results for a seawall case is shown in Figure 85 for profile 117. Erosion of the berm was modeled reasonably well, accounting for possible beach recovery in the measured profile. However, the model overpredicts the amount of erosion directly in front of the seawall (between approximately the 0 and 12 m distance from the baseline). Similar overprediction of erosion was observed in the other seawall cases, as well. A final example of default simulations is shown in Figure 86 for profile 236. In this case, erosion of the berm was well modeled, but dune erosion was underestimated. Unlike the other Rehoboth Beach cases, the post-storm measured profile for this case showed no evidence of recovery above NGVD. The lesser amount of beach recovery apparent on profile 236 may be related to the fact that this profile exhibited the largest net loss of volume between surveys (Figure 83).

Model calibration

Although default model predictions of beach and dune erosion were generally very close to the measurements, calibration of the model was performed to determine if improvements could be made to the simulations.

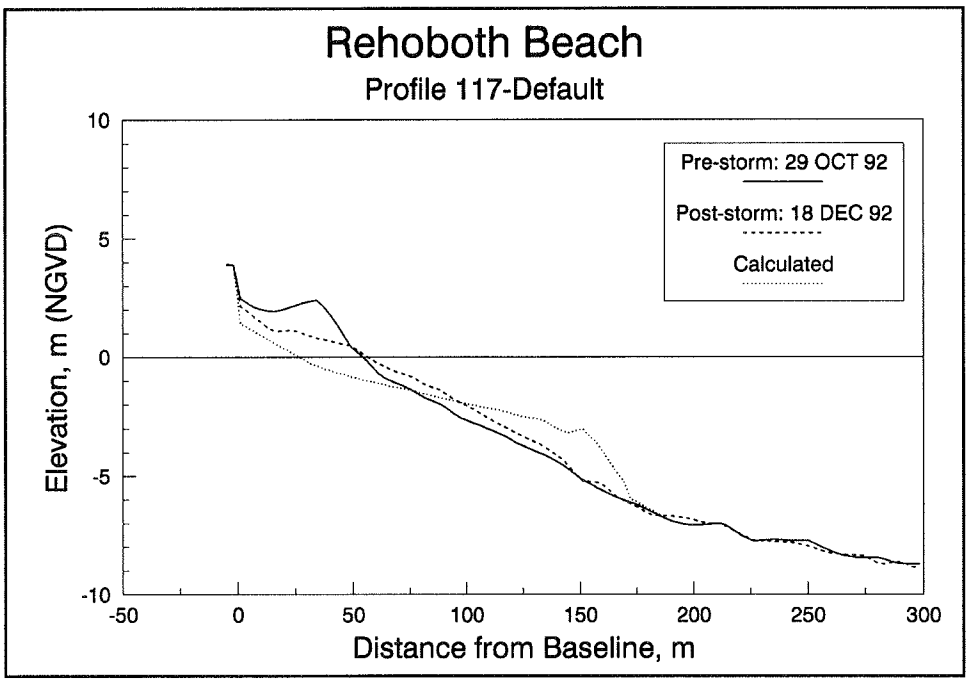

Figure 85. Result of default simulation of the December 1992 storm for profile 117, Rehoboth Beach, DE

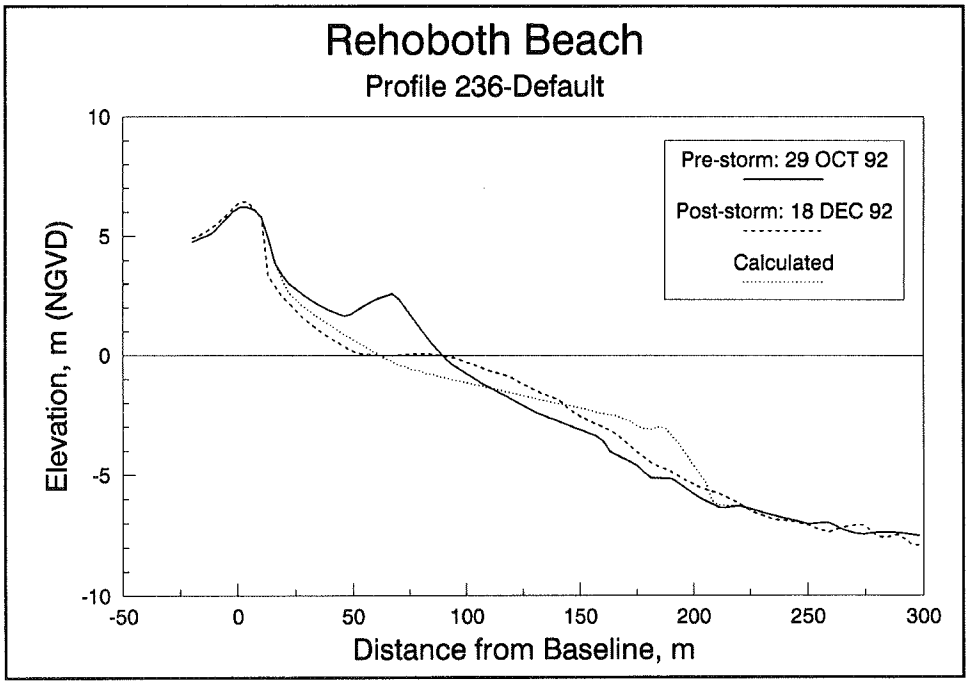

Figure 86. Result of default simulation of the December 1992 storm for profile 236, Rehoboth Beach, DE

Profile 140 of the Dewey Beach set was chosen for calibration due to the relatively small loss of volume over the entire profile and representative shape of the berm and dune. Best numerical fit was achieved with the following values of the calibration parameters: $K = 1.90 \times 10^{-6}$ m^4/N, $\epsilon = 0.001$ m^2/s, and $DFS = 0.20$ m. Variation of the input wave height within ± 10 percent was employed. Figure 87 shows a comparison of the default and calibrated results for profile 140. Only minor differences are observed between the two calculated profiles. The calibrated run produced a slightly better match of the measured profile across the beach face. In the offshore, the calibrated run produced a more defined bar and trough as a result of the higher value of K and lower value of ϵ.

Calibrated simulations

Dewey Beach. The calibration of the model to profile D140 resulted in only minor changes from the default simulations producing slightly better agreement in some cases and slightly poorer agreement in others. Plots comparing the measures of model performance for the default and calibrated simulations are given in Figures 88-90. In Figure 88, the overprediction of volume loss for profiles 115 and 140 may be attributed to profile recovery which occurred above NGVD. Underprediction of volume loss for profiles 220 and 240 resulted from incomplete simulation of measured dune erosion. Volume changes for the remaining profiles were modeled within 5 m^3/m.

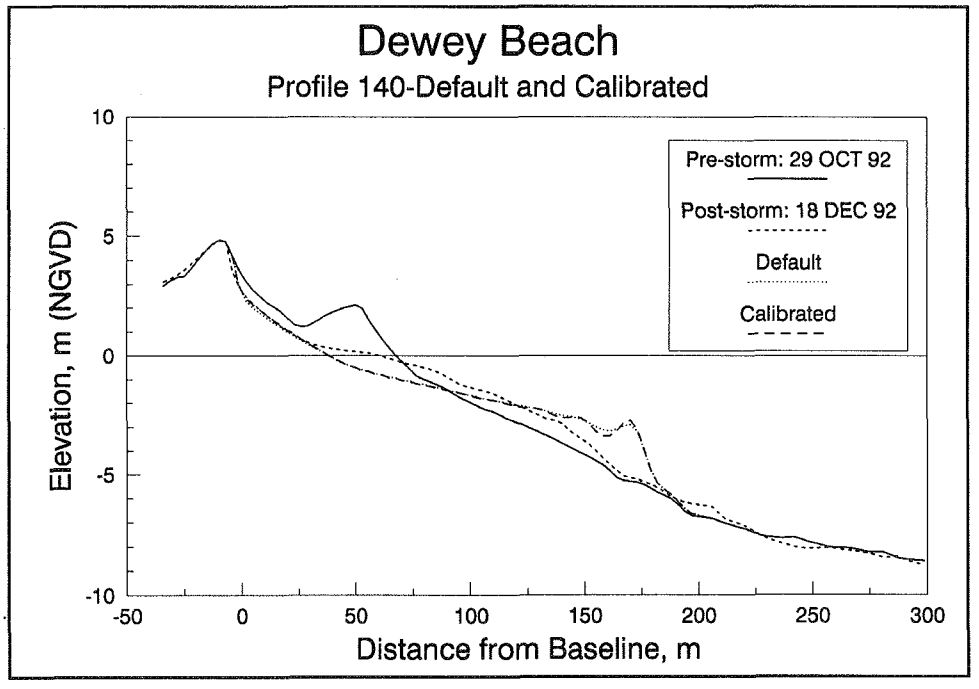

Figure 87. Results of default and calibrated simulations of the December 1992 storm for profile 140, Dewey Beach, DE

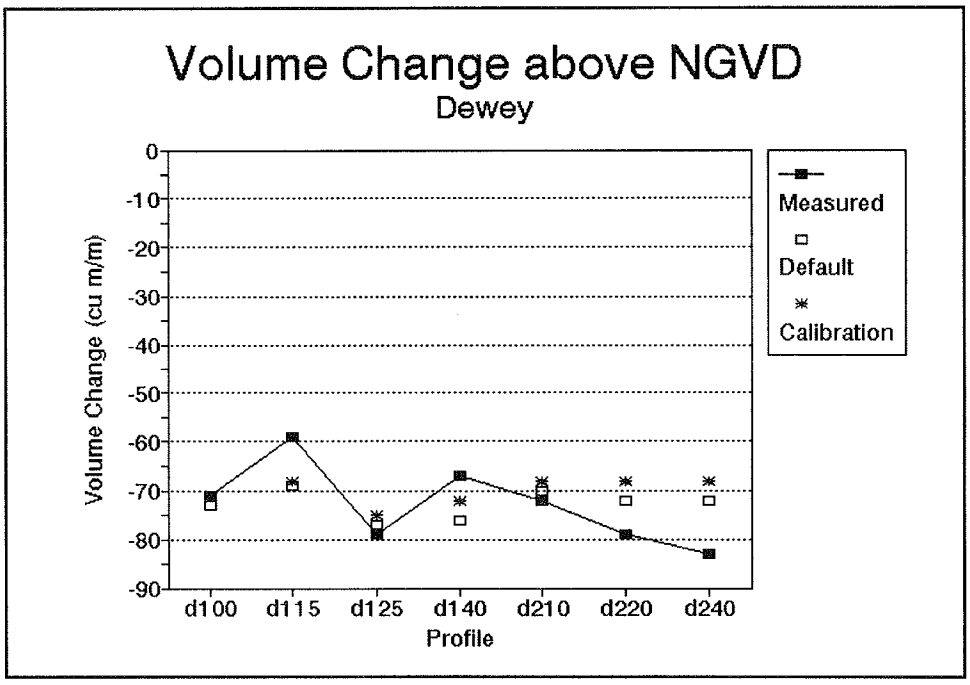

Figure 88. Comparison of measured and simulated volume change above NGVD for the December 1992 storm, Dewey Beach, DE

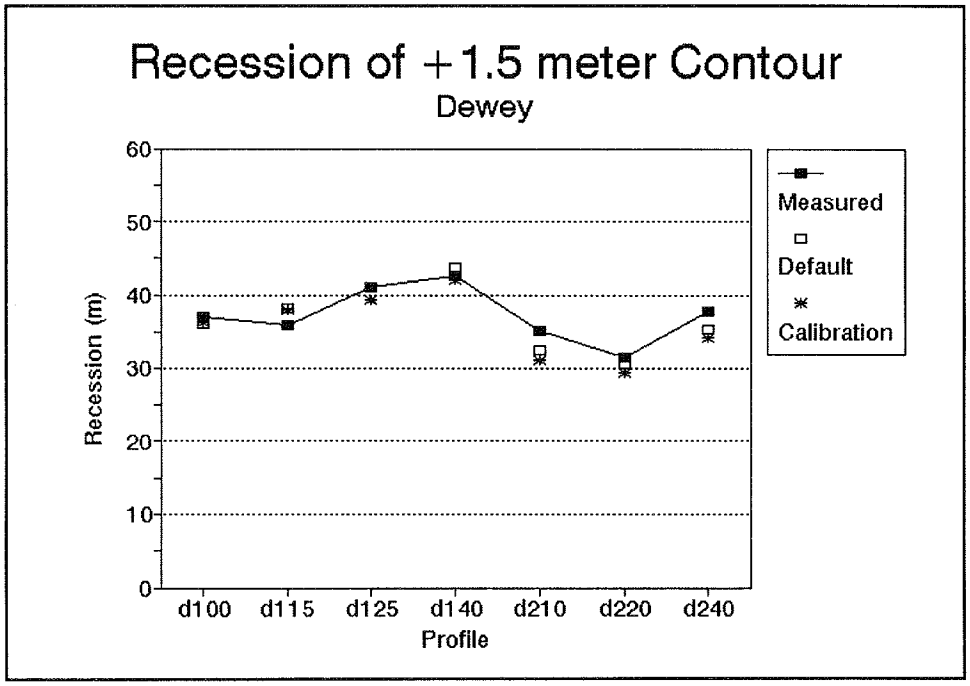

Figure 89. Comparison of measured and simulated recession of the 1.5-m contour for the December 1992 storm, Dewey Beach, DE

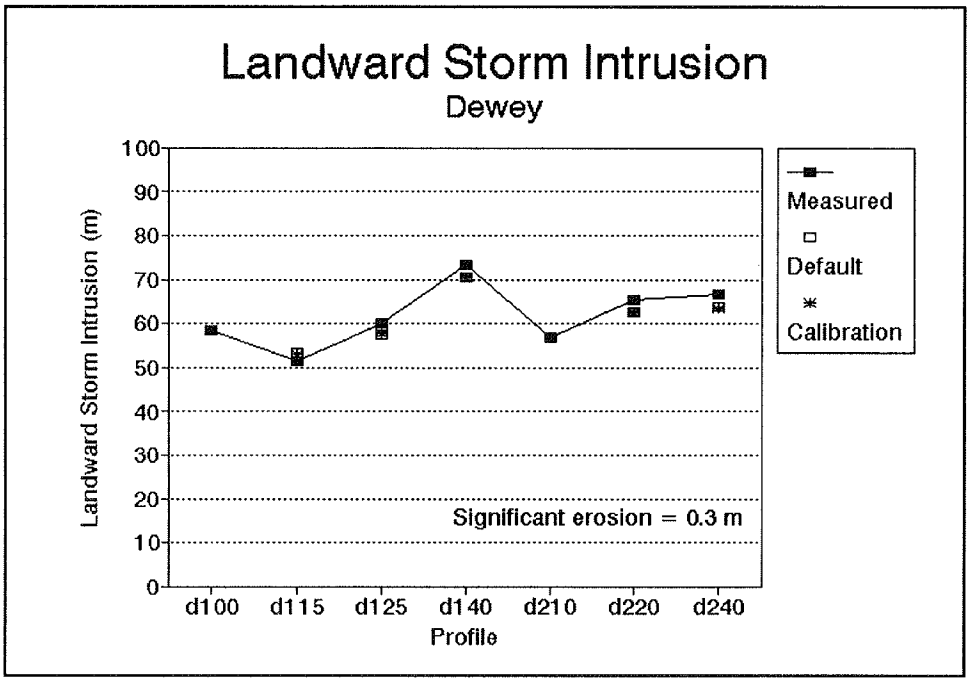

Figure 90. Comparison of measured and simulated storm intrusion for the December 1992 storm, Dewey Beach, DE

Figure 89 displays measured and simulated recession of the 1.5-m NGVD contour corresponding to the elevation of upper berm on the pre-storm profiles. Figure 90 shows the measured and simulated storm intrusion. Both contour recession and the landward extent of erosion were well predicted by the model for all profiles. No distinct trends were observed regarding differences between default and calibrated results.

Rehoboth Beach. As with the Dewey Beach cases, no significant improvements over the default simulations were gained from applying the calibrated model to the Rehoboth Beach data set. Plots of the measures of performance at the foreshore are given in Figures 91-93 for the Rehoboth Beach cases. Figure 91 displays volume change above NGVD. The model overestimated the measured loss of volume in all cases except for profile 236. However, with the exception of profile 236, the modeled results closely follow the trends in the measurements, further indicating that the differences may be related to beach recovery which occurred prior to the post-storm surveys. Figure 92 compares simulated and measured recession of the 2-m NGVD contour selected to represent the elevation of the upper berm. Figure 93 displays calculations of the landward extent of storm erosion. Measures of profile recession and landward storm intrusion both indicate good agreement between the simulated and measured beach response for most cases.

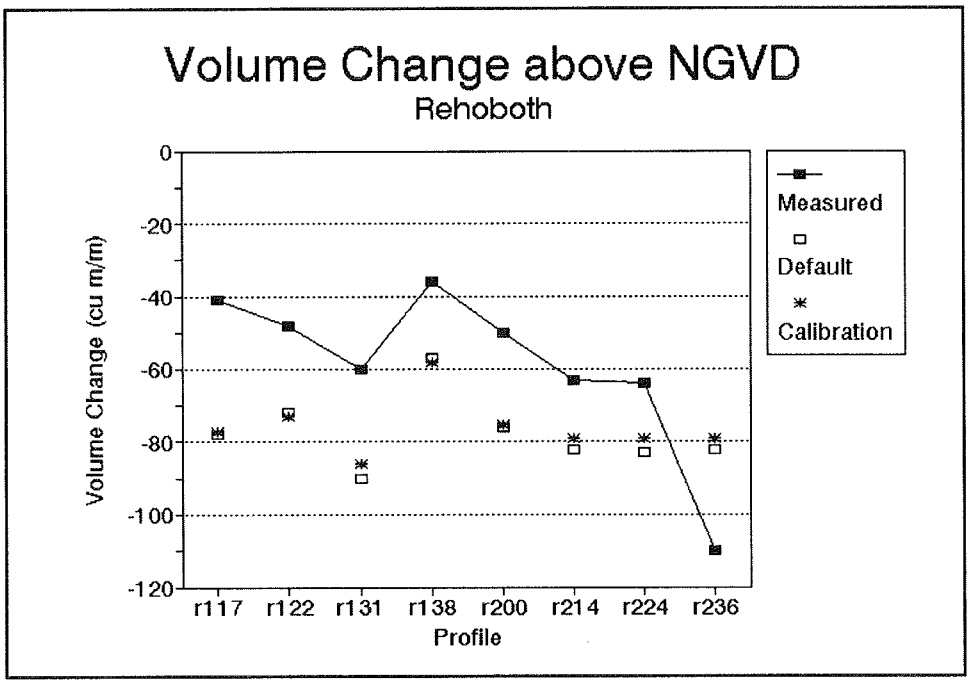

Figure 91. Comparison of measured and simulated volume change above NGVD for the December 1992 storm, Rehoboth Beach, DE

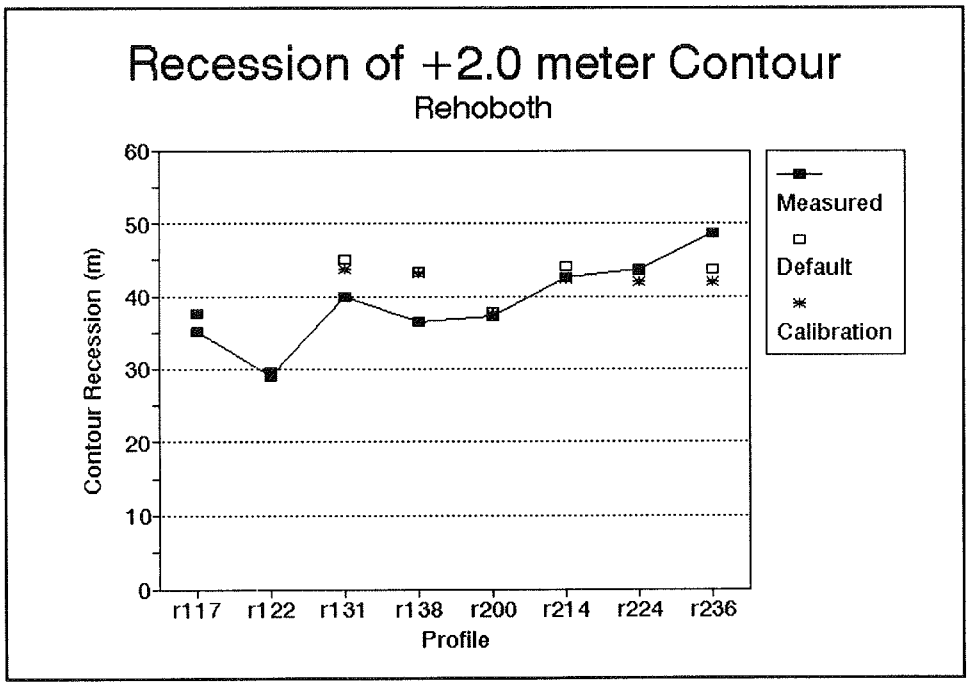

Figure 92. Comparison of measured and simulated recession of the 2.0-m contour for the December 1992 storm, Rehoboth Beach, DE

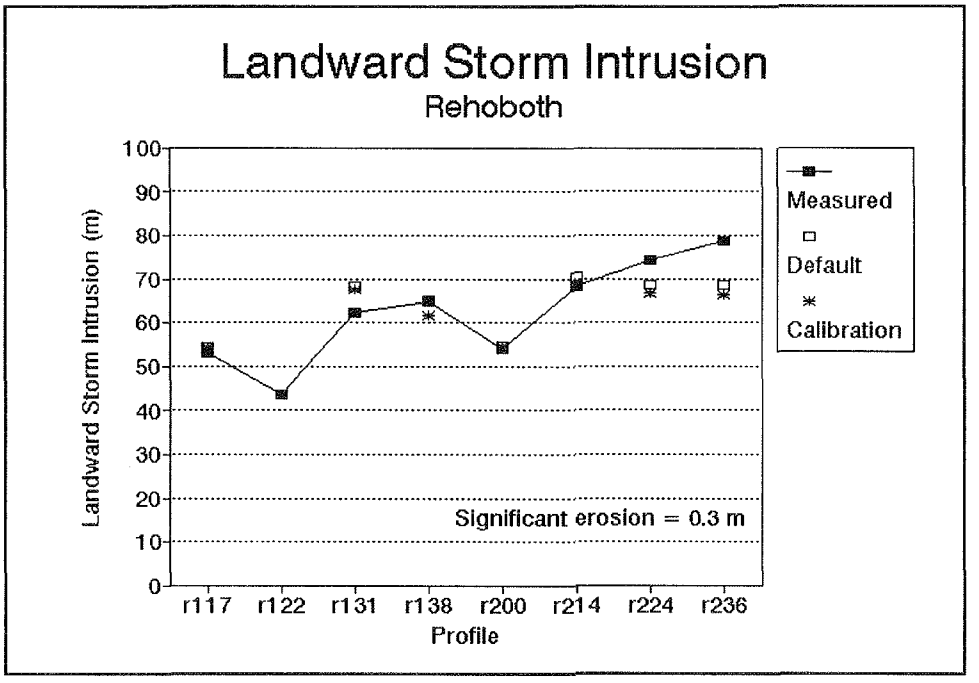

Figure 93. Comparison of measured and simulated storm intrusion for the December 1992 storm, Rehoboth Beach, DE

Summary

SBEACH performed well in reproducing the response of the upper beach and dune for nearly all cases in the Dewey Beach and Rehoboth Beach data sets. The greatest deviations between the measured and modeled profiles were found below NGVD and appeared to be related to potential beach recovery occurring prior to the collection of post-storm profile surveys. For the cases at Rehoboth Beach which included seawalls, the model tended to overpredict the amount of erosion at the base of the seawall. Measures of performance at the foreshore showed that application of the model using default calibration parameter values provided as good agreement as application of the model when calibrated to a single profile. This indicates that the default values were near optimum for the data at Dewey Beach and Rehoboth Beach.

Debidue Beach and Myrtle Beach, SC

On 22 September 1989, Hurricane Hugo made landfall near Charleston, SC. Beaches along the coast of South Carolina to the north of the eye of the hurricane were exposed to strong onshore winds and high waves and water levels. The severe erosional effects of Hurricane Hugo were captured by beach surveys performed by Coastal Science and Engineering, Inc. and the U.S. Army Corps of Engineers, Waterways Experiment Station, Coastal

Engineering Research Center (Stauble et al. 1990). Beach profile data collected at Debidue Beach and Myrtle Beach in June 1989 provided pre-storm profiles for use in modeling beach response to Hurricane Hugo. Post-storm profile surveys were collected within a week of the passing of the hurricane. A single profile line at each site was available for use in the present study. A median grain size of 0.20 mm was employed in the simulations as a representative value for both beaches (Glover and Hales 1991). Additional information on profile data collection and impacts of Hurricane Hugo on the coast of South Carolina is presented in a special issue of the journal *Shore and Beach* (Vol. 58 No. 4, 1990).

Water surface elevations during Hurricane Hugo were recorded by a tide gauge located in Winyah Bay, approximately 10 miles (16 km) south of Debidue Beach and 40 miles (64 km) south of Myrtle Beach (Garcia, Jarvinen, and Schuck-Kolben 1990). These tide gauge data represented the best available estimates of water level variations produced by the hurricane at both beaches. Actual storm surge (not counting wave setup and runup) at the study sites was probably somewhat lower than the measurements since the beaches were located farther north away from the center of the storm. Due to lack of wave gauge measurements, wave hindcast information was used as input to SBEACH. As part of a previous study of Hurricane Hugo, wave hindcast information was generated at several locations along the coast (Glover and Hales 1991). To account for spatial variation in wave conditions, wave information from different hindcast stations was used for the two beaches. Figures 94 and 95 display hindcast wave height and period and measured water level time histories for Debidue Beach and Myrtle Beach, respectively. According to the wave hindcast, the peak significant wave height was approximately 6 m at Debidue Beach and 4 m at Myrtle Beach. The differences in hindcast wave conditions at the two sites were related primarily to distance from the center of the hurricane. As shown in Figures 94 and 95, the maximum water elevation measured at the Winyah Bay tide gauge was just under 2.5 m NGVD.

Default simulations

The SBEACH model was applied to each site using default values of the calibration parameters. Results of the default simulation at Debidue Beach are presented in Figure 96. Based on the pre- and post-storm beach surveys, the profile at Debidue Beach gained approximately 4 m^3/m of material. As shown in Figure 96, the model reproduced measured erosion of the small berm on the beach face, but underpredicted erosion of the wide foredune. Also, the model predicted more overwash of material at the foredune than was measured. Both the measured and calculated profiles displayed no erosion of the higher dune backing the foredune. Below NGVD, model results showed deposition of eroded material farther offshore than observed on the post-storm profile. Figure 97 shows default simulation results for the Myrtle Beach case, where the profile lost approximately 25 m^3/m between surveys. The shape of the

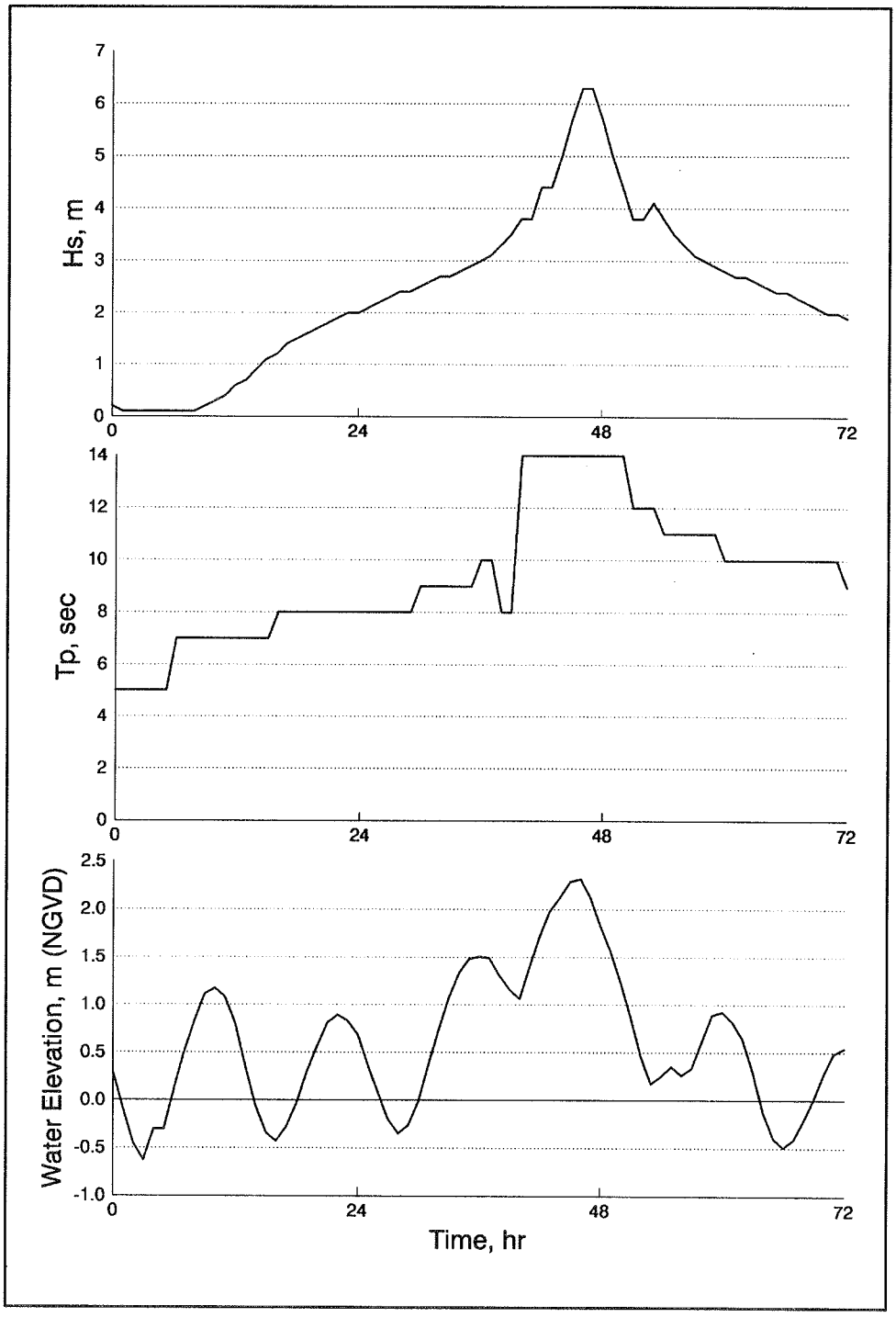

Figure 94. Wave height, wave period, and water elevation time-histories for Hurricane Hugo, Debidue Beach, SC

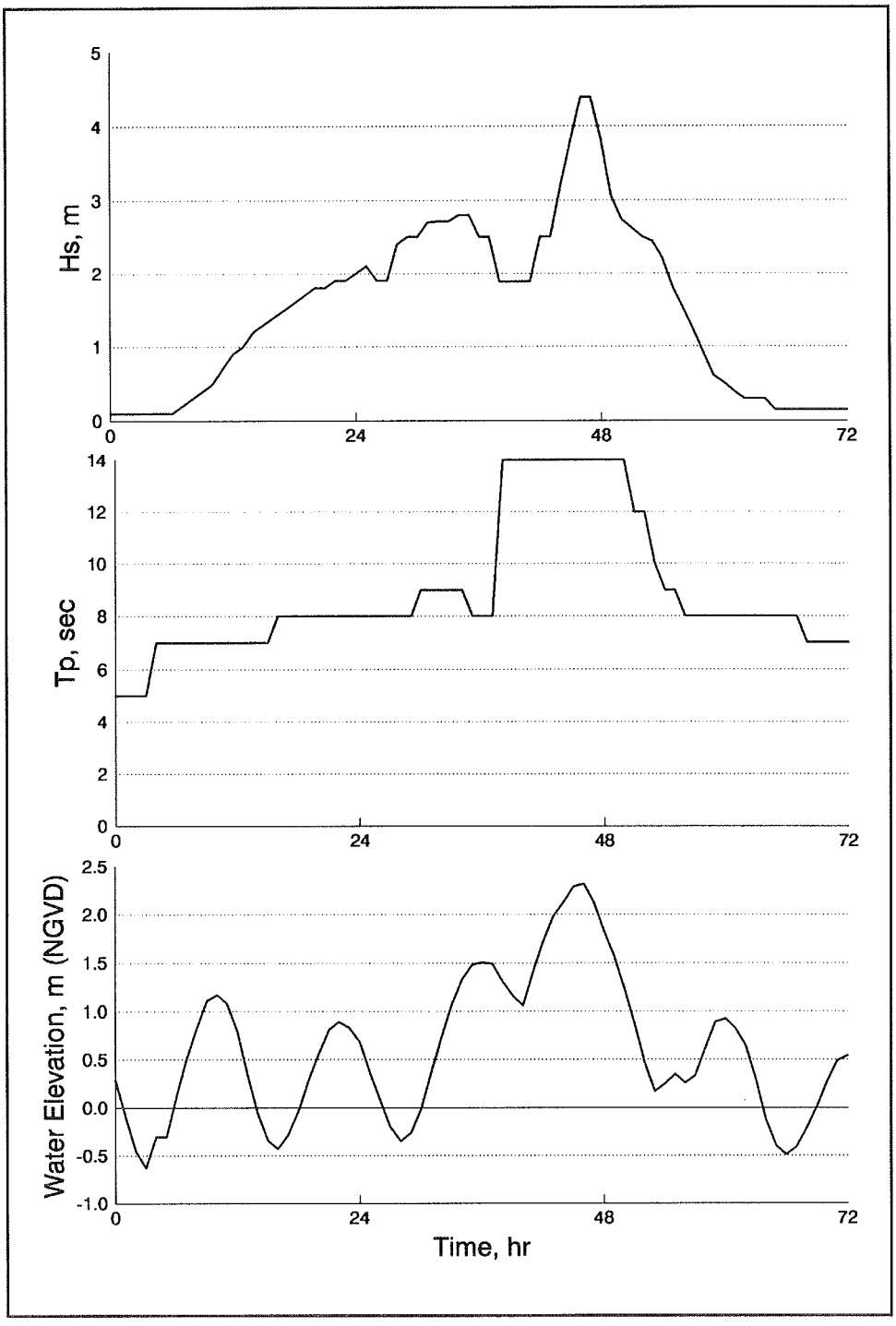

Figure 95. Wave height, wave period, and water elevation time-histories for Hurricane Hugo, Myrtle Beach, SC

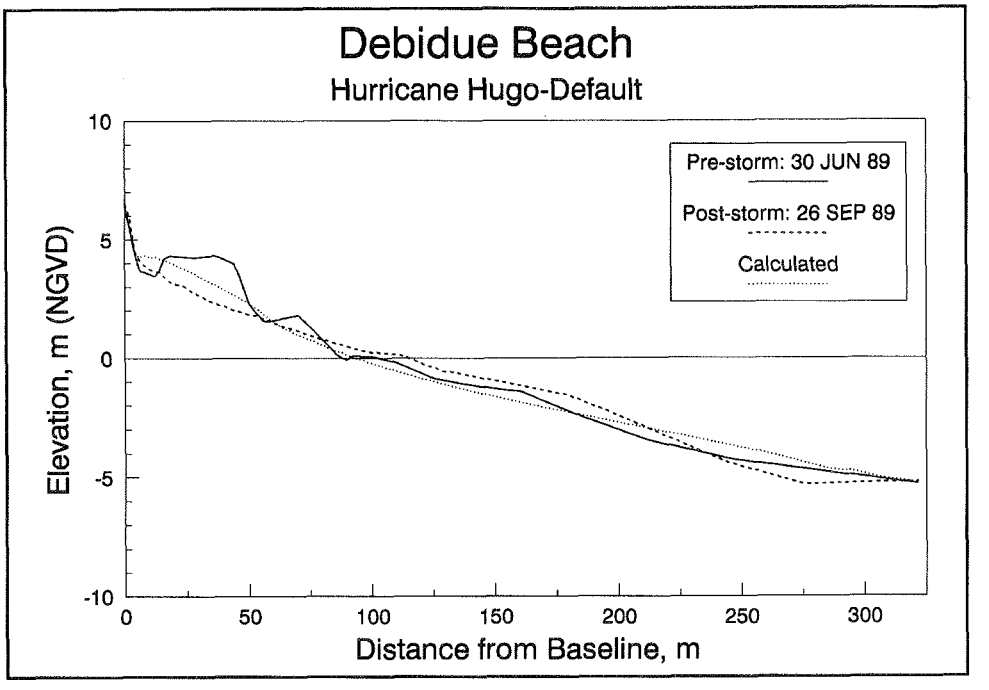

Figure 96. Result of default simulation of Hurricane Hugo, Debidue Beach, SC

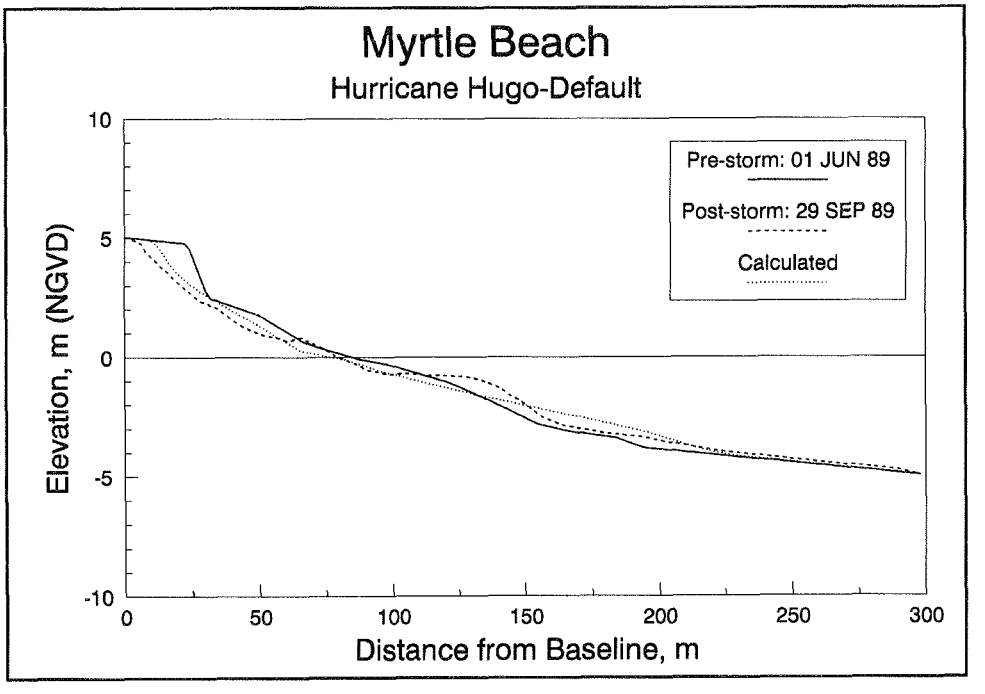

Figure 97. Result of default simulation of Hurricane Hugo, Myrtle Beach, SC

measured post-storm beach profile is matched fairly well by the calculations, but the model underpredicts the magnitude of erosion at the dune and foreshore.

Model calibration and calibrated simulations

The profile at Debidue Beach was selected for calibration based on better conservation of mass on the profile, and relative proximity of Debidue Beach to the tide gauge at Winyah Bay. Calibration of the model resulted in the following values: $K = 2.50 \times 10^{-6}$ m^4/N, $\epsilon = 0.005$ m^2/s, $DFS = 0.30$ m. Figure 98 shows results of the calibrated model for the Debidue Beach case. Although improvements were achieved over the default simulation, the calibrated model still underpredicted erosion of the foredune, despite selection of maximum values of K and ϵ within the recommended ranges. Predicted erosion at the berm and overwash of material over the foredune were greater than measured. The discrepancies in modeling dune erosion and overwash for this case could be related to the relatively wide and flat shape of the foredune in contrast to the narrower, more-peaked dunes which were studied in development of the overwash algorithm. Figure 99 displays results of the calibrated simulation for the Myrtle Beach profile. In this case, the calibrated model produced good agreement with measured erosion across the entire beach face except at the upper limit of the dune where erosion was underpredicted. The measures of model performance for the Debidue Beach and Myrtle Beach simulations are summarized in Table 3. Although volume change above NGVD was well modeled in the calibrated runs, the distribution of eroded volume did not match the post-storm measurements, as discussed above. Recession of the 3.5-m contour (corresponding to the elevation at the upper foredune) was underpredicted at Debidue Beach, but was accurately simulated at Myrtle Beach. Landward storm intrusion, defined by 0.3 m of vertical erosion, was predicted within 5 m by the calibrated model in both cases.

Summary

Application of SBEACH with limited data of beach response to Hurricane Hugo showed that the model underpredicted the measured erosion using default values of the calibration parameters. Agreement was improved through calibration by selecting the maximum recommended values of the calibration parameters K and ϵ. However, in the case of Debidue Beach, the calibrated model still produced incomplete erosion of the foredune. Underprediction of erosion by the model may be related to deficiencies in simulating foreshore transport and overwash for certain beach configurations. Discrepancies between measurements and modeled results could also be related to inadequate representation of local storm conditions at the field sites by the wave hindcast and tide gauge information.

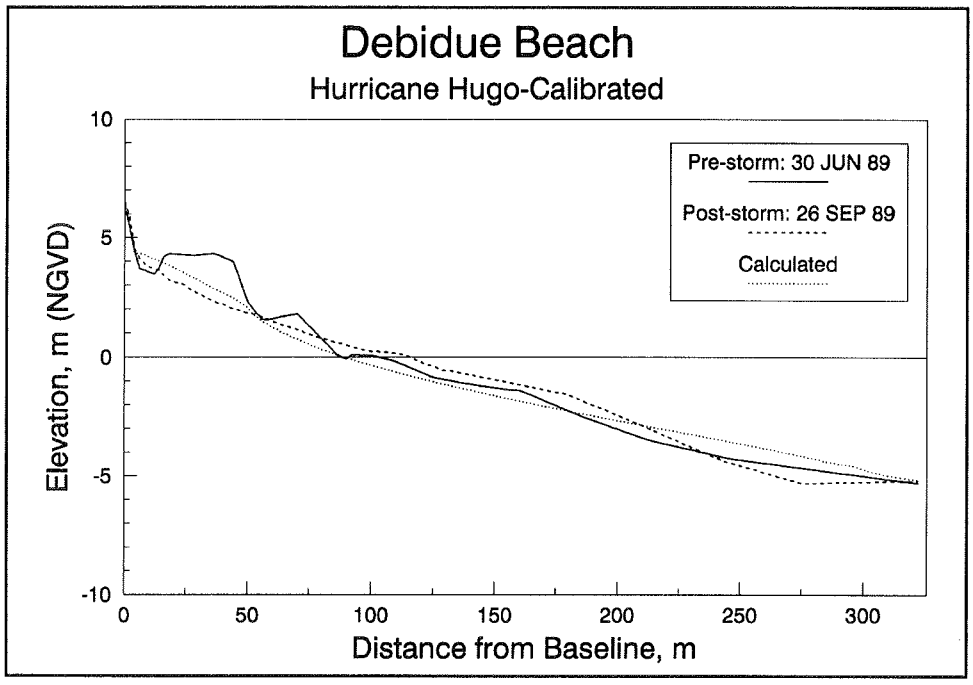

Figure 98. Result of calibrated simulation of Hurricane Hugo, Debidue Beach, SC

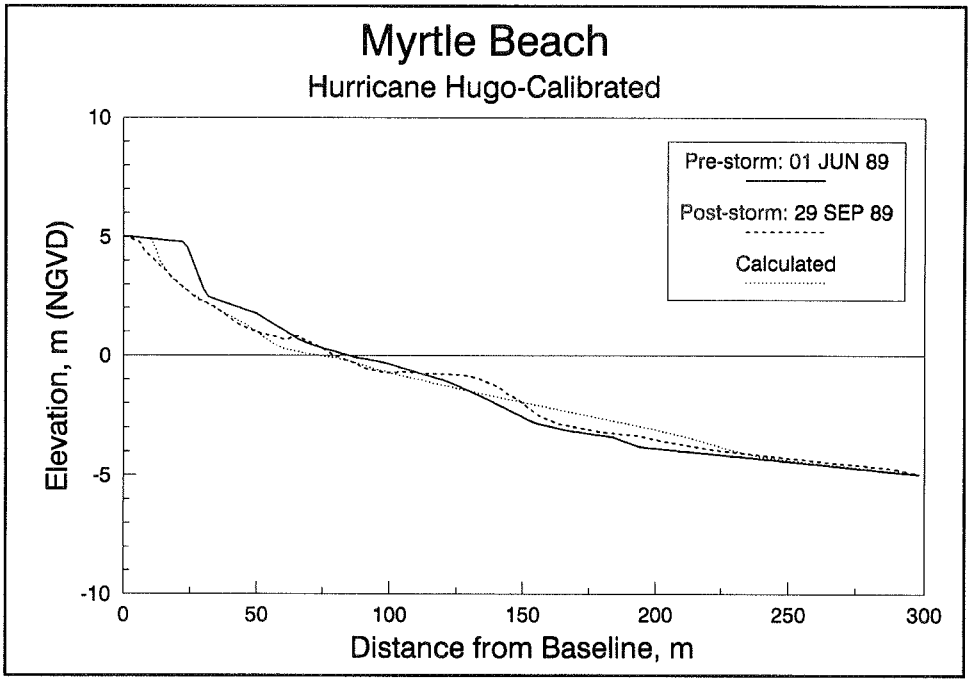

Figure 99. Result of calibrated simulation of Hurricane Hugo, Myrtle Beach, SC

Table 3
Measures of Model Performance at the Foreshore for Hurricane Hugo Simulations

Measure of Performance	Debidue Beach			Myrtle Beach		
	Default	Calibrated	Measured	Default	Calibrated	Measured
Volume change above NGVD (m^3/m)	-30	-49	-49	-33	-52	-47
Recession of 3.5-m contour (m)	17	22	31	8	11	11
Landward storm intrusion (m)	84	86	88	72	73	78

6 Summary and Conclusions

The SBEACH numerical simulation model was developed for engineering use in predicting storm-induced beach change produced by breaking waves and varying water levels. Original formulation of the model involved study of LWT data describing beach profile change under monochromatic waves, and included model tests with field data as discussed in previous reports (Larson and Kraus 1989a, Larson, Kraus, and Byrnes 1990). In the present report, a random wave model and modified sediment transport relationships were developed for SBEACH to improve calculation of beach response to random waves. The modified version of SBEACH was validated with profile change data from the SUPERTANK project and with several high-quality data sets describing storm-induced erosion in the field. Overall, the model performed well in simulating measured erosion in the laboratory and field case studies.

The monochromatic wave model previously included in SBEACH was modified to account for variation in wave heights of a random wave field. The random wave model was developed under the assumption that transformation of random waves across the profile can be described by superimposing the effects of a large number of individual waves representing the random wave field. The model was formulated such that transformation of only one representative wave height is required for a given incident random wave condition. A Rayleigh distribution was employed in the model to characterize random waves outside the surf zone where wave breaking is negligible. Inside the surf zone, the wave model computes transformation of random wave properties across the profile, including the effects of wave re-formation. Calculations from the random wave model were validated with laboratory and field data.

Sediment transport relationships for calculating profile change under random waves were developed based on transport relationships previously derived from monochromatic wave tests. Separate relationships were formulated to calculate the transport rate under broken and nonbroken waves. The transport rate under broken waves was expressed as a function of wave energy dissipation in excess of an equilibrium energy dissipation. Transport under nonbroken waves was represented by an exponential decay with distance seaward from the breakpoint. The net transport rate under random waves is

calculated in the model by superimposing transport rates of individual broken and nonbroken waves across the beach profile. A refined relationship for calculating the transport rate in the swash zone was derived based on a schematic description of sediment transport processes across the foreshore. An algorithm for simulating beach change produced by dune overwash was also developed.

The SUPERTANK laboratory project provided an extensive collection of data describing cross-shore beach change under various wave conditions for different profile configurations. Model validation was performed for 23 SUPERTANK cases, involving both random and monochromatic waves. In general, simulation of the SUPERTANK cases with default calibration parameters resulted in overprediction of erosion. Through a single model calibration, good agreement between calculations and measurements was achieved for the random wave cases. A separate calibration was required to obtain satisfactory results for the monochromatic wave cases. Model performance was measured through calculation of statistical fit parameters across the entire profile and at the foreshore and bar. The model was also validated using data from a laboratory test conducted at the University of Hannover, Germany.

SBEACH was evaluated in field case studies using high-quality data describing severe beach erosion at seven different sites for six storms. Assessment of model performance focused on the capability of the model to predict erosion of the berm and dune. Model performance was quantified by comparing measured and calculated volume change, profile recession, and landward extent of erosion. The model was applied to all field data sets using default calibration parameter values. The model was then calibrated to a single case from each data set and applied to the remaining cases. Overall, the model satisfactorily reproduced measured beach erosion for various initial beach profile shapes and storm conditions. In case studies of storm-induced erosion at Ocean City, MD; Manasquan and Point Pleasant Beach, NJ; and Dewey Beach and Rehoboth Beach, DE; application of the model with default values of the calibration parameters produced good overall agreement with measurements. Model calibration for these case studies improved agreement for some individual profiles; but, in general, default parameter values were found to be near optimum for these data sets. In simulating the beach response to Hurricane Hugo at Debidue Beach and Myrtle Beach, SC, erosion was underpredicted with the default parameters, while model calibration produced better agreement with the data.

Evaluation of SBEACH with laboratory and field data demonstrated model effectiveness in simulating beach erosion, but also identified several areas requiring further research and model refinement. Recent model enhancements presented in this report included refined calculation of swash zone transport and simulation of dune overwash. While these algorithms provided good agreement with many of the laboratory and field cases, an improved

description of foreshore sediment transport processes and dune overwash is required to more accurately model the details of beach and dune response over a wide range of conditions. For example, the dune overwash algorithm included in SBEACH was developed and validated with field data describing overwash of relatively narrow and peaked dunes. In the present study, model predictions of overwash were less successful for cases involving broad-crested dunes. A better understanding of swash zone processes will enable more accurate and robust modeling of foreshore and dune response through development of formulations that are less site- or condition-specific.

Another important area for further research is the description of onshore sand transport and berm development. The present version of SBEACH does not have the capability to accurately model accretionary processes observed in the field. The post-storm recovery phase must be reproduced to accurately model measured profile response across the entire profile, since post-storm field surveys are typically performed after some beach recovery has already occurred. Accurate modeling of onshore transport and beach recovery is important for longer term (seasonal) assessment of beach fill performance and maintenance volume requirements. Calculation of accretion is also important to predicting response of mounds placed in the offshore. Evaluation of SBEACH with SUPERTANK data showed that the model was less successful in modeling profile response for cases involving offshore mounds. The influence of mounds on beach change at the shoreline as well as onshore movement of material placed in mounds requires further study. Present specification in SBEACH of a single representative grain size for the entire profile limits model applicability in some cases. For example, material placed in an offshore mound or beach fill may have a significantly different median grain size than the native beach. The inclusion of a variable grain size across the beach profile in SBEACH will improve simulation of profile response in such cases.

Many coastal regions are characterized by beaches not comprised entirely of sand. Estimation of storm-induced erosion is difficult in these environments where features such as reefs, bedrock, or clay substrate influence the response of the beach profile. SBEACH has been developed for use with completely sandy profiles, and cannot presently treat nonerodible hard bottoms. Study of beach response in hard-bottom environments and subsequent modification of SBEACH are required to provide such a capability. A related area of study is the influence of seawalls on beach response. In application of SBEACH in the present study to cases involving seawalls, the model qualitatively reproduced measured response but tended to overestimate the magnitude of erosion in front of the seawall. Also, the present model does not calculate erosion on the landward side of a seawall which may occur during extreme events when the seawall is overtopped. Improved simulation of sediment transport and beach response over non-erodible boundaries and at structures such as a seawalls will enable more versatile application of the model.

Field data of beach erosion collected immediately before, during, and after storms provide information essential to evaluating model reliability and improving individual algorithms within the model. Field case studies presented in this report included the best available data suited for evaluating model predictions of beach and dune erosion. Broader collection and publication of high-quality data of storm-induced beach response in various physical environments and geographic regions will enable further model validation and will provide greater confidence in model predictions over a range of applications.

References

Battjes, J. A., and Janssen, J. P. F. M. (1978). "Energy loss and setup due to breaking of random waves." *Proceedings 16th Coastal Engineering Conference*. American Society of Civil Engineers, 569-87.

Dally, W. R. (1990). "Random breaking waves: A closed-form solution for planar beaches," *Journal of Coastal Engineering* 14, 233-63.

_____. (1992). "Random breaking waves: Field verification of a wave-by-wave algorithm for engineering application," *Journal of Coastal Engineering* 16, 369-97.

Dally, W. R., Dean, R. G., and Dalrymple, R. A. (1985). "Wave height variation across beaches of arbitrary profile," *Journal of Geophysical Research* 90(C6), 11,917-27.

Dean, R. G. (1973). "Heuristic models of sand transport in the surf zone." *Proceedings Conference on Engineering Dynamics in the Surf Zone.* Sydney, Australia, 208-14.

_____. (1977). "Equilibrium beach profiles: U.S. Atlantic and the Gulf Coasts," Department of Civil Engineering, Ocean Engineering Report No. 12, University of Delaware, Newark, DE.

Dette, H. H., and Uliczka, K. (1986). "Prototype and model evolution of beach profile," *Symposium on Scale Effects in Modelling Sediment Transport,* International Association of Hydraulic Research, 35-48.

Ebersole, B. A. (1987). "Measurement and prediction of wave height decay in the surf zone." *Proceedings Coastal Hydrodynamics '87.* American Society of Civil Engineers, 1-16.

Garcia, A. W., Jarvinen, B. R., and Schuck-Kolben, R. E. (1990). "Storm surge observations and model hindcast comparison for Hurricane Hugo," *Shore and Beach: Journal of the American Shore and Beach Preservation Association* 58(4), 15-21.

Gebert, J. A., and Hemsley, J. M. (1991). "Monitoring of jetty rehabilitation at Manasquan Inlet, New Jersey," Miscellaneous Paper CERC-91-8, Coastal Engineering Research Center, U.S. Army Engineer Waterways Experiment Station, Vicksburg, MS.

Glover, L. B., and Hales, L. Z. (1991). "Numerical simulation of beach profile response to Hurricane Hugo." *Proceedings Coastal Sediments '91.* Specialty Conference on Quantitative Approaches to Coastal Sediment Processes, 1712-26.

Grosskopf, W. G., and Stauble, D. K. (1993). "Atlantic Coast of Maryland (Ocean City) shoreline-protection project," *Shore and Beach: Journal of the American Shore and Beach Preservation Association* 61(1), 3-7.

Holland, K. T., Holman, R. A., and Sallenger, A. H. (1991). "Estimation of overwash bore velocities using video techniques." *Proceedings Coastal Sediments '91.* American Society of Civil Engineers, 489-97.

Iwagaki, Y., and Noda, H. (1962). "Laboratory studies of scale effects in two-dimensional beach processes." *Proceedings 8th Coastal Engineering Conference.* American Society of Civil Engineers, 194-210.

Kraus, N. C., and Smith, J. M. (1994). "SUPERTANK laboratory data collection project, Volume I: Main Text," Technical Report CERC-94-3, Coastal Engineering Research Center, U.S. Army Engineer Waterways Experiment Station, Vicksburg, MS.

Kraus, N. C., and Wise, R. A. (1993). "Simulation of January 4, 1992 storm erosion at Ocean City, Maryland," *Shore and Beach* (61)1, 34-41.

Kraus, N. C., Larson, M., and Kriebel, D. L. (1991). "Evaluation of beach erosion and accretion predictors." *Proceedings Coastal Sediments '91.* American Society of Civil Engineers, 572-87.

Kraus, N. C., Smith, J. M., and Sollitt, C. K. (1992). "SUPERTANK laboratory data collection project." *Proceedings 23rd Coastal Engineering Conference.* American Society of Civil Engineers, 2191-2204.

Kriebel, D. L. (1986). "Verification study of a dune erosion model," *Shore and Beach* 54(3), 13-21.

Kriebel, D. L., and Dean, R. G. (1985). "Numerical simulation of time-dependent beach and dune erosion," *Coastal Engineering* 9, 221-45.

Larson, M. (1994). "Prediction of beach profile change at mesoscale under random waves." *Proceedings of the 24th International Coastal Engineering Conference.* American Society of Civil Engineers, 2252-66.

Larson, M. (1995). "Model for decay of random waves in the surf zone," *Journal of Waterways, Port, Coastal, and Ocean Engineering* 121(1), 1-12.

_____. (1996). "A model of beach profile change under random waves." *Journal of Waterways, Port, Harbor, and Coastal Engineering*. To be published.

Larson, M., and Kraus, N. C. (1989a). "SBEACH: Numerical model for simulating storm-induced beach change; Report 1, Empirical foundation and model development," Technical Report CERC-89-9, Coastal Engineering Research Center, U.S. Army Engineer Waterways Experiment Station, Vicksburg, MS.

_____. (1989b). "Prediction of beach fill response to varying waves and water level." *Proceedings Coastal Zone '89*. American Society of Civil Engineers, 607-21.

_____. (1991). "Mathematical modeling of the fate of beach fill," *Artificial Beach Nourishments*, Special Issue of *Coastal Engineering* 16, D. Niemayer, J. van Overeem, and J. van de Graaff, ed., 83-114.

_____. (1992). "Numerical model of longshore current for bar and trough beaches," *Journal of Waterways, Port, Coastal, and Ocean Engineering* 117(4), 326-47.

_____. (1994). "Cross-shore sand transport under random waves at SUPERTANK examined at mesoscale." *Proceedings of Coastal Dynamics '94*. American Society of Civil Engineers, 204-19.

_____. (1995). "Prediction of cross-shore sediment transport at different spatial and temporal scales." *Marine Geology*. In press.

Larson, M., Kraus, N. C., and Byrnes, M. R. (1990). "SBEACH: Numerical model for simulating storm-induced beach change; Report 2, Numerical formulation and model tests," Technical Report CERC-89-9, Coastal Engineering Research Center, U.S. Army Engineer Waterways Experiment Station, Vicksburg, MS.

Le Méhauté, B. (1976). *An introduction to water waves*. Springer-Verlag, New York, NY, 315 pp.

Longuet-Higgins, M. S. (1952). "On the statistical distribution of the heights of sea waves," *Journal of Marine Research* 11, 245-66.

Madsen, O. S. (1991). "Mechanics of cohesionless sediment transport in coastal waters." *Proceedings Coastal Sediments '91*. American Society of Civil Engineers, 15-27.

Madsen, O. S. (1993). "Sediment transport on the shelf," *Sediment Transport Workshop DRP TA1*, 8-9 June, Coastal Engineering Research Center, Vicksburg MS.

Miller, R. L. (1976). "Role of vortices in surf zone prediction: Sedimentation and wave forces." *Beach and Nearshore Sedimentation*, R. A. Davis and R. I. Ethington, ed., Society of Economic Paleontologists and Mineralogists, Special Publication No. 24, 92-114.

Rector, R. L. (1954). "Laboratory study of equilibrium profiles of beaches," Technical Memorandum No. 41, Beach Erosion Board, Coastal Engineering Research Center, U.S. Army Engineer Waterways Experiment Station, Vicksburg, MS.

Rosati, J. D., Wise, R. A., Kraus, N. C., and Larson, M. (1993). "SBEACH: Numerical model for simulating storm-induced beach change; Report 3, User's manual," Instruction Report CERC-93-2, Coastal Engineering Research Center, U.S. Army Engineer Waterways Experiment Station, Vicksburg, MS.

Shen, M. C., and Meyer, R. E. (1962). "Climb of bore on a beach, Part 3: Run-up," *Journal of Fluid Mechanics* 16, 113-25.

Shore and beach. (1990). 58(4), American Shore and Beach Preservation Society.

Shore and beach. (1993). 61(1), American Shore and Beach Preservation Society.

Skjelbreia, J. E. (1987). "Observations of breaking waves on sloping bottoms by use of laser doppler velocimetry," Report No. KH-R-48, Division of Engineering and Applied Science, California Institute of Technology, Pasadena, CA.

Smith, J. M., and Kraus, N. C. (1995). "SUPERTANK laboratory data collection project; Volume II: Appendices A-I," Technical Report CERC-94-3, Coastal Engineering Research Center, U.S. Army Engineer Waterways Experiment Station, Vicksburg, MS.

Smith, J. M., Larson, M., and Kraus, N. C. (1993). "Longshore current on a barred beach: Field measurements and calculation," *Journal of Geophysical Research*, (under revision).

Stauble, D. K., and Kraus, N. C. (1993). "Project performance: Ocean City, Maryland, beach nourishment." *Proceedings Coastal Zone '93*. Beach Nourishment Engineering and Management Considerations, Coastlines of the World, American Society of Civil Engineers, 1-15.

Stauble, D. K., Eiser, W. C., Birkemeier, W. A., Hales, L. Z., and Seabergh, W. C. (1990). "Erosion characteristics of Hurricane Hugo on the beaches of South Carolina," *Shore and Beach: Journal of the American Shore and Beach Preservation Society* 58(4), 23-36.

Stauble, D. K., Garcia, A. W., Kraus, N. C., Grosskopf, W. G., and Bass, G. P. (1993). "Beach nourishment project response and design evaluation, Ocean City, Maryland; Report 1, 1988-1992," Technical Report CERC-93-13, Coastal Engineering Research Center, U.S. Army Engineer Waterways Experiment Station, Vicksburg, MS.

Sunamura, T., and Horikawa, K. (1974). "Two-dimensional beach transformation due to waves." *Proceedings 14th Coastal Engineering Conference*. American Society of Civil Engineers, 920-38.

Svendsen, I. A. (1984). "Wave heights and set-up in a surf zone," *Coastal Engineering* 8, 303-29.

Svendsen, I. A., Madsen, P. A., and Buhr Hansen, J. (1978). "Wave characteristics in the surf zone." *Proceedings 16th Coastal Engineering Conference*. American Society of Civil Engineers, 520-39.

U.S. Army Engineer District, Philadelphia. (1995). "Delaware Coast from Cape Henlopen to Fenwick Island," Rehoboth Beach/Dewey Beach Interim Feasibility Study, Draft Feasibility Report and Draft Environmental Impact Statement, April.

The WAMDI Group. (1988). "The WAM model - a third generation ocean wave prediction model," *Journal of Physical Oceanography*, 1775-1810.

Thornton, E. B., and Guza, R. T. (1983). "Transformation of wave height distribution," *Journal of Geophysical Research* 88(C10), 5925-38.

Waddell, E. (1973). "A field investigation of swash characteristics," *Coastal Engineering in Japan* 16, 61-71.

Watanabe, A. (1982). "Numerical models of nearshore currents and beach deformation," *Coastal Engineering in Japan* 25, 147-61.

_____. (1985). "Three-dimensional predictive model of beach evolution around a structure." *Proceedings International Symposium on Water Wave Research*. University of Hannover, 121-42.

Waters, C. H. (1939). "Equilibrium slopes of sea beaches," unpublished M.S. thesis, University of California, Berkeley, CA.

Wise, R. A., and Kraus, N. C. (1993). "Simulation of beach fill response to multiple storms, Ocean City, MD." *Proceedings Coastal Zone '93*, Beach Nourishment Engineering and Management Considerations, Coastlines of the World. American Society of Civil Engineers, 133-47.

Zheng, J., and Dean, R. G. (1995). "Evaluation study and comparison of erosion models and effects of seawalls for coastal construction control line; Task 1d: Compare models with results from Hurricane Eloise and other data," UFL/COEL-95/006, Coastal and Oceanographic Engineering Department, University of Florida, Gainesville, FL.

Appendix A
Simulation Results for SUPERTANK Case Studies

Table A1
Test Conditions for SUPERTANK Case Studies

Case	Wave Type	H_s (m)	T (sec)	Duration (min)	SUPERTANK Run IDs	Comments
Equilibrium Erosion						
P1A	RANDOM	0.8	3.0	270	A0509A A0510A A0512A A0515A A0517A	
P1D	RANDOM	0.8	4.5	274	A0709A A0710A A0711A A0713A A0715A A0715A	
P1E1	RANDOM	0.8	4.5	170	A0808A A0809A A0812A A0814A A0815A	
P1E2	MONOCHROMATIC	0.8	4.5	40	A0816A A0817A	
P1F	RANDOM	0.8	6.0	40	A0908A	
	RANDOM	0.5	5.0	40	A0910A	
	RANDOM	0.7	3.0	40	A0911A	
	RANDOM	0.9	3.0	40	A0912A	
	RANDOM	0.9	4.5	40	A0914A	
	RANDOM	0.7	5.0	40	A0915A	
P2B7	RANDOM	0.8	3.0	40	A1315A	
PGA	MONOCHROMATIC	0.8	3.0	210	S0414A S0415A S0416A S0417A S0418A	

(Sheet 1 of 4)

Table A1 (Continued)

Case	Wave Type	H_s (m)	T (sec)	Duration (min)	SUPERTANK Run IDs	Comments
Dune Erosion						
P5A	RANDOM	0.8	3.0	30	A2208A A2209A	Water level increase of 0.3 m at t = 90 min
	RANDOM	0.8	4.5	30	A2209B	
	RANDOM	0.8	6.0	30	A2210A	
	RANDOM	0.8	3.0	30	A2213B	
	RANDOM	0.7	4.5	30	A2214A	
	RANDOM	0.7	6.0	30	A2215A	
P6A	RANDOM	0.7	3.0	60	A2308A A2308B A2309A	Water level increase of 0.15 m at t = 120 min
	RANDOM	0.7	4.5	60	A2310A A2311A A2311B	
	RANDOM	0.5	6.0	60	A2313B A2315A A2316A	
Foredune Erosion						
PAA	RANDOM	0.7	3.0	10	A2816B	
Berm Flooding						
P9A	RANDOM	0.7	3.0	50	A2809B A2810A A2811A	
PDA1	RANDOM	0.7	3.0	60	S0309A S0310A S0311A	
Seawall						
P7A	RANDOM	0.7	4.5	70	A2609A A2610A A2610B	
P7B	RANDOM	0.7	4.5	30	A2612B A2613A A2614A A2615A	
	RANDOM	1.0	4.5	60		

(Sheet 2 of 4)

Table A1 (Continued)

Case	Wave Type	H_s (m)	T (sec)	Duration (min)	SUPERTANK Run IDs	Comments
P7C	RANDOM	0.8	4.5	10	A2617B	
	RANDOM	0.7	4.5	40	A2618A A2618B	
P7D	RANDOM	varied	4.5	210	A2609A A2610A A2610B A2612B A2613A A2614A A2615A A2617B A2618A A2618B	Combined simulation of cases P7A-P7C including water level increase of 0.15 m at t = 70 min and additional increase of 0.3 m at t = 160 min
P8A1	RANDOM	0.7	4.5	100	A2708A A2708B A2709A	
P8A2	MONOCHROMATIC	0.7	4.5	60	A2710A A2711A	
PCA	RANDOM	0.8	3.0	120	S0210A S0211A S0214A S0214B	Water level increase of 0.3 m at t = 60 min
	RANDOM	0.4	3.0	40	S0216A	
	RANDOM	0.4	8.0	40	S0217A	
Narrow-Crested Mound						
PJA	RANDOM	0.7	3.0	150	S0913A S0914A S0915A S0916A	
PJC	MONOCHROMATIC	0.7	3.0	190	S1014A S1015A S1015B S1016A S1018A	

(Sheet 3 of 4)

Table A1 (Concluded)

Case	Wave Type	H_s (m)	T (sec)	Duration (min)	SUPERTANK Run IDs	Comments
Broad-Crested Mound						
PKA	RANDOM	0.7	3.0	220	S1208B S1209A S1209B S1210A S1212A	
PKC	MONOCHROMATIC	0.7	3.0	190	S1307B S1308A S1309A S1310A S1311A	

(Sheet 4 of 4)

Table A2
Statistical Fit Parameters for SUPERTANK Case Studies

Case	Profile Range	Default		Calibrated	
		RMS	Residual	RMS	Residual
Equilibrium Erosion					
P1A	TOTAL	0.14	1.14	0.06	0.18
	FORESHORE	0.17	0.74	0.04	0.04
	BAR	0.20	1.14	0.11	0.36
P1D	TOTAL	0.17	5.00	0.09	1.42
	FORESHORE	0.23	7.37	0.09	1.20
	BAR	0.18	2.54	0.14	1.56
P1E1	TOTAL	0.13	2.63	0.10	1.46
	FORESHORE	0.15	1.04	0.14	0.90
	BAR	0.19	13.88	0.13	6.38
P1E2	TOTAL	0.08	1.64	0.09	1.85
	FORESHORE	0.04	1.95	0.07	6.13
	BAR	0.15	1.66	0.15	1.65
P1F	TOTAL	0.14	4.03	0.08	1.56
	FORESHORE	0.12	4.24	0.07	1.24
	BAR	0.22	3.91	0.14	1.67
P2B7	TOTAL	0.05	1.09	0.03	0.33
	FORESHORE	0.03	6.11	0.02	3.44
	BAR	0.10	0.99	0.05	0.26
PGA	TOTAL	0.11	1.07	0.13	1.35
	FORESHORE	0.12	0.66	0.23	2.47
	BAR	0.16	1.15	0.15	1.07
Dune Erosion					
P5A	TOTAL	0.11	0.63	0.08	0.31
	FORESHORE	0.10	0.14	0.12	0.20
	BAR	0.16	4.06	0.09	1.34

(Sheet 1 of 3)

Table A2 (Continued)

Case	Profile Range	Default		Calibrated	
		RMS	Residual	RMS	Residual
Dune Erosion (continued)					
P6A	TOTAL	0.12	0.70	0.06	0.18
	FORESHORE	0.15	0.40	0.07	0.08
	BAR	0.17	102.26	0.10	2.82
Foredune Erosion					
PAA	TOTAL	0.03	0.13	0.03	0.14
	FORESHORE	0.06	0.12	0.07	0.13
Berm Flooding					
P9A	TOTAL	0.05	0.45	0.02	0.07
	FORESHORE	0.11	0.34	0.07	0.14
	BAR	0.10	0.46	0.02	0.03
PDA1	TOTAL	0.06	1.10	0.03	0.37
	ACTIVE	0.09	0.95	0.05	0.33
Seawall					
P7A	TOTAL	0.06	4.65	0.03	1.29
	FORESHORE	0.05	1.54	0.04	1.02
	BAR	0.12	8.52	0.05	1.60
P7B	TOTAL	0.08	2.53	0.04	0.71
	FORESHORE	0.06	1.58	0.04	0.89
	BAR	0.14	2.50	0.07	0.63
P7C	TOTAL	0.03	1.43	0.02	0.64
	FORESHORE	0.03	0.57	0.02	0.34
	BAR	0.06	5.34	0.03	1.83
P7D	TOTAL	0.11	3.63	0.06	0.94
	FORESHORE	0.07	1.87	0.05	0.80
	BAR	0.19	4.48	0.09	1.00

(Sheet 2 of 3)

Table A2 (Concluded)

Case	Profile Range	Default		Calibrated	
		RMS	Residual	RMS	Residual
Seawall (continued)					
P8A1	TOTAL	0.10	0.91	0.08	0.80
	FORESHORE	0.16	0.79	0.03	1.09
	BAR	0.11	1.14	0.10	0.93
P8A2	TOTAL	0.08	0.80	0.08	0.78
	FORESHORE	0.03	1.59	0.03	1.45
	BAR	0.14	0.78	0.14	0.76
PCA	TOTAL	0.06	1.70	0.03	0.57
	ACTIVE	0.08	1.72	0.05	0.57
Narrow-Crested Mound					
PJA	TOTAL	0.11	1.27	0.08	0.57
	FORESHORE	0.10	2.24	0.04	0.46
	MOUND	0.16	1.01	0.13	0.69
PJC	TOTAL	0.11	1.84	0.12	2.28
	FORESHORE	0.12	3.38	0.15	4.91
	MOUND	0.12	1.22	0.12	1.22
Broad-Crested Mound					
PKA	TOTAL	0.17	2.45	0.13	1.40
	FORESHORE	0.11	19.10	0.08	0.60
	MOUND	0.23	2.01	0.18	1.16
PKC	TOTAL	0.12	1.52	0.14	2.29
	FORESHORE	0.06	1.52	0.13	7.76
	MOUND	0.17	1.52	0.17	1.59

(Sheet 3 of 3)

Random Wave Cases

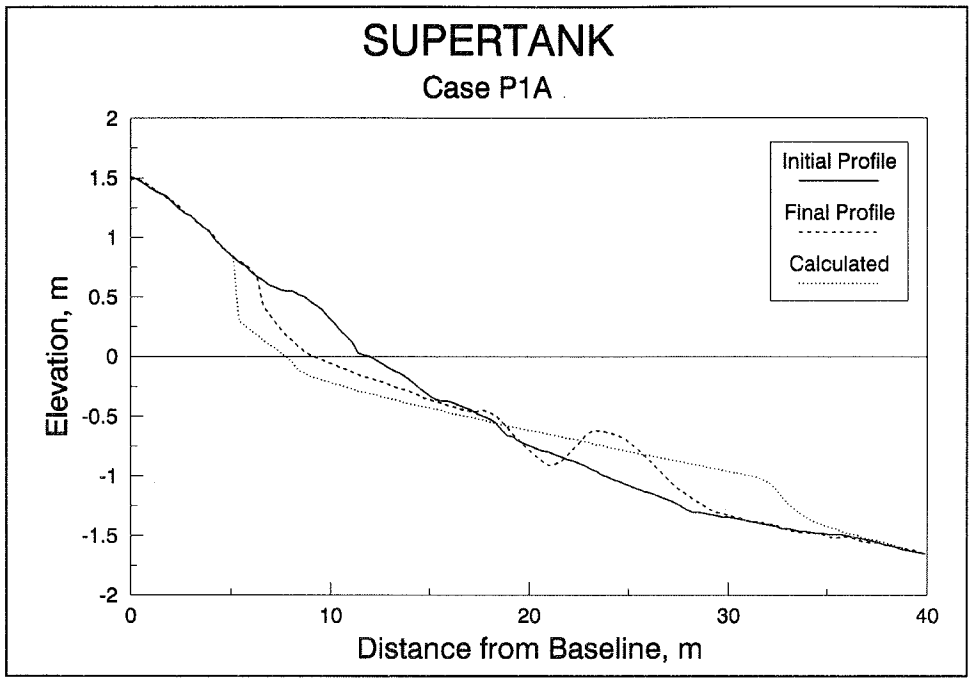

Figure A1. Result of default simulation, SUPERTANK case P1A

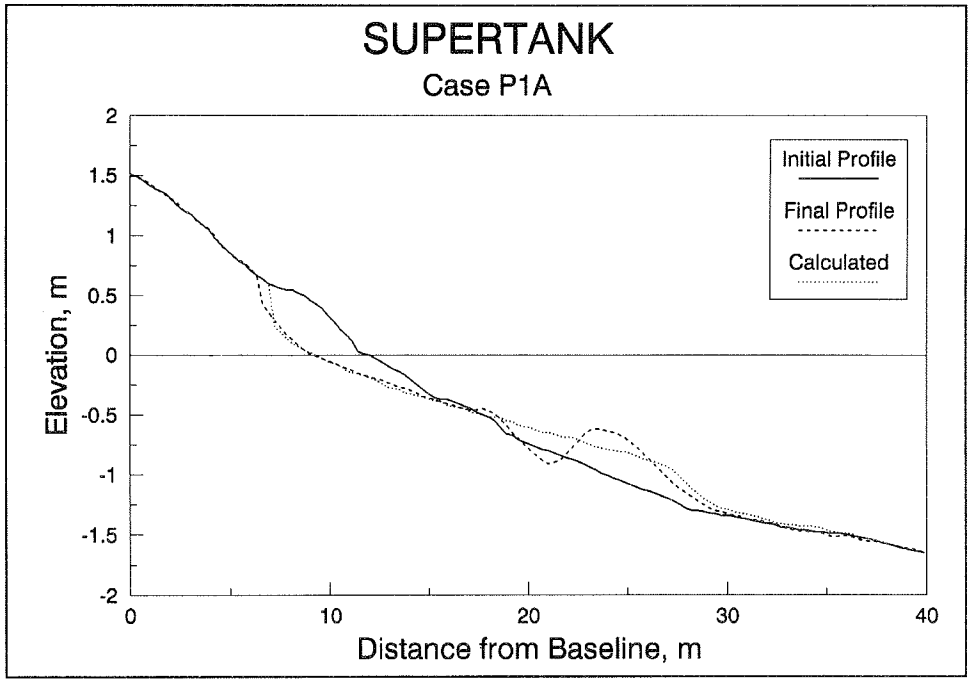

Figure A2. Result of calibrated simulation, SUPERTANK case P1A (model calibrated to case P5A)

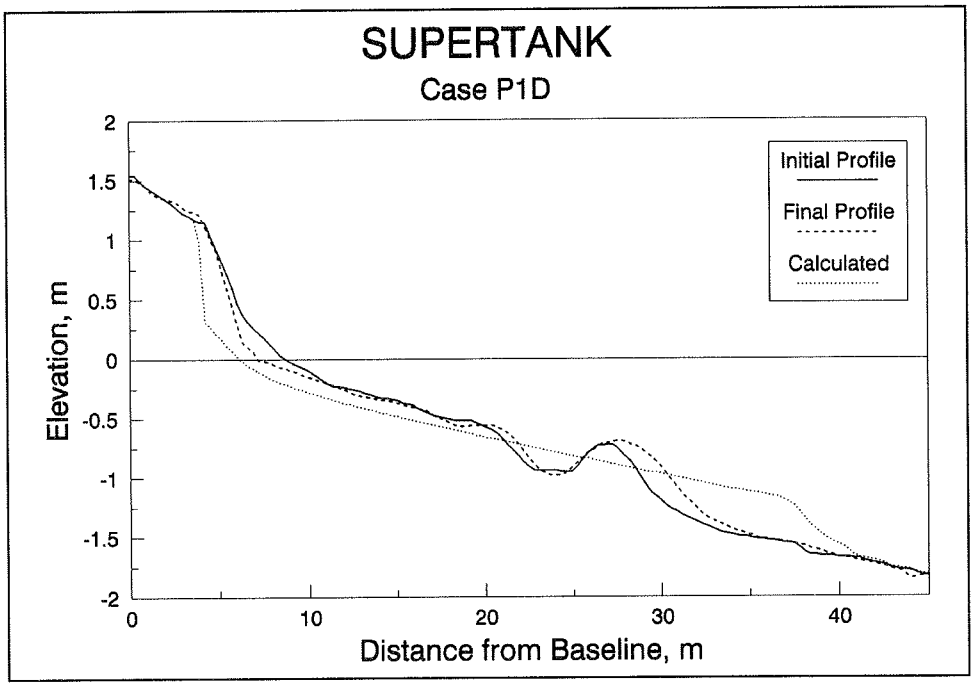

Figure A3. Result of default simulation, SUPERTANK case P1D

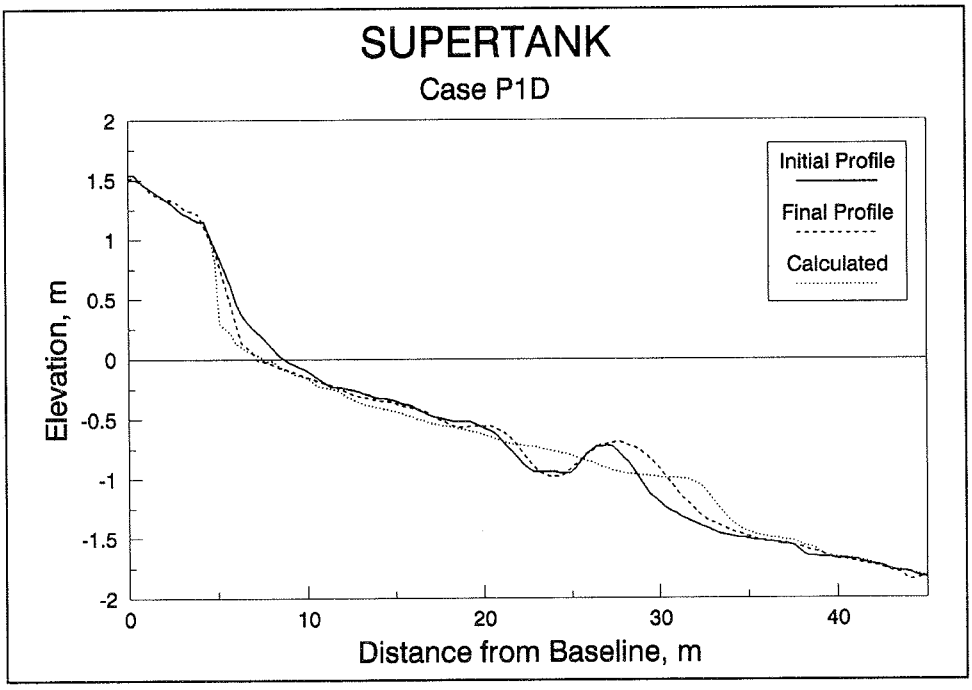

Figure A4. Result of calibrated simulation, SUPERTANK case P1D (model calibrated to case P5A)

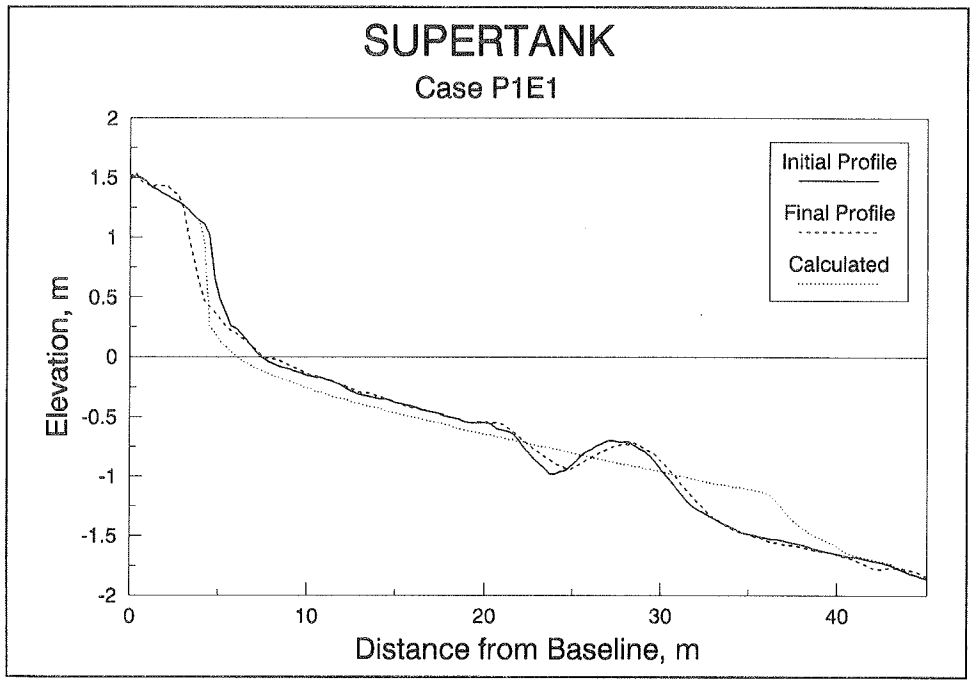

Figure A5. Result of default simulation, SUPERTANK case P1E1

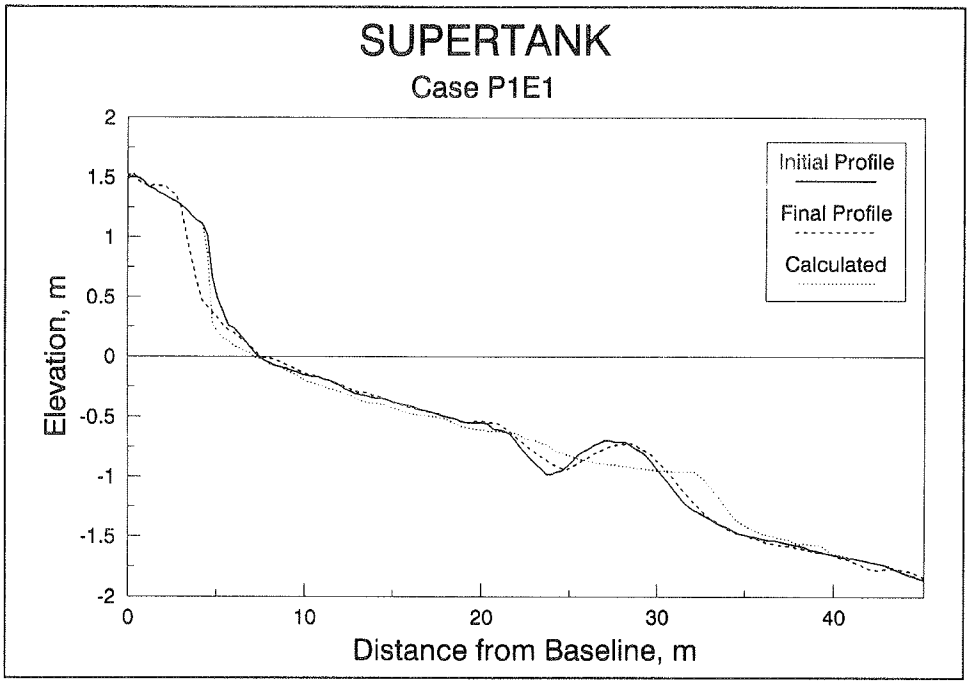

Figure A6. Result of calibrated simulation, SUPERTANK case P1E1 (model calibrated to case P5A)

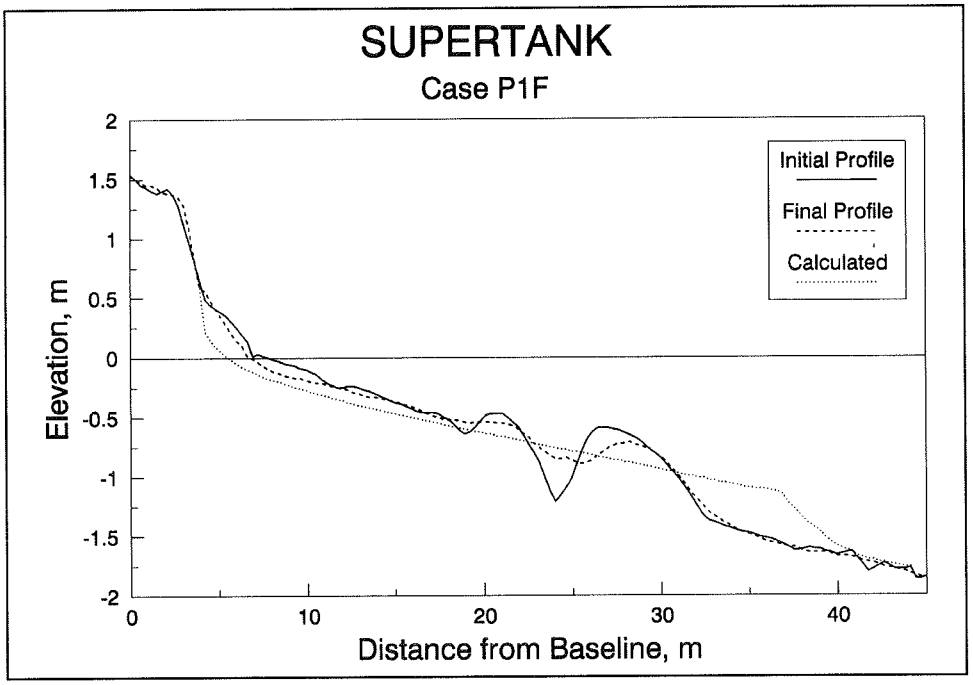

Figure A7. Result of default simulation, SUPERTANK case P1F

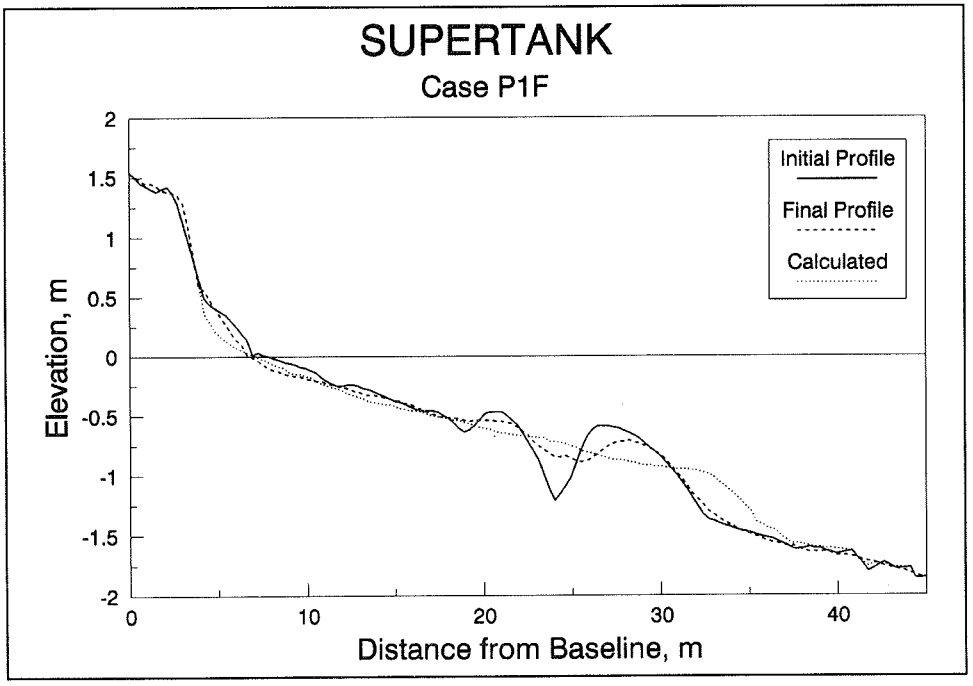

Figure A8. Result of calibrated simulation, SUPERTANK case P1F (model calibrated to case P5A)

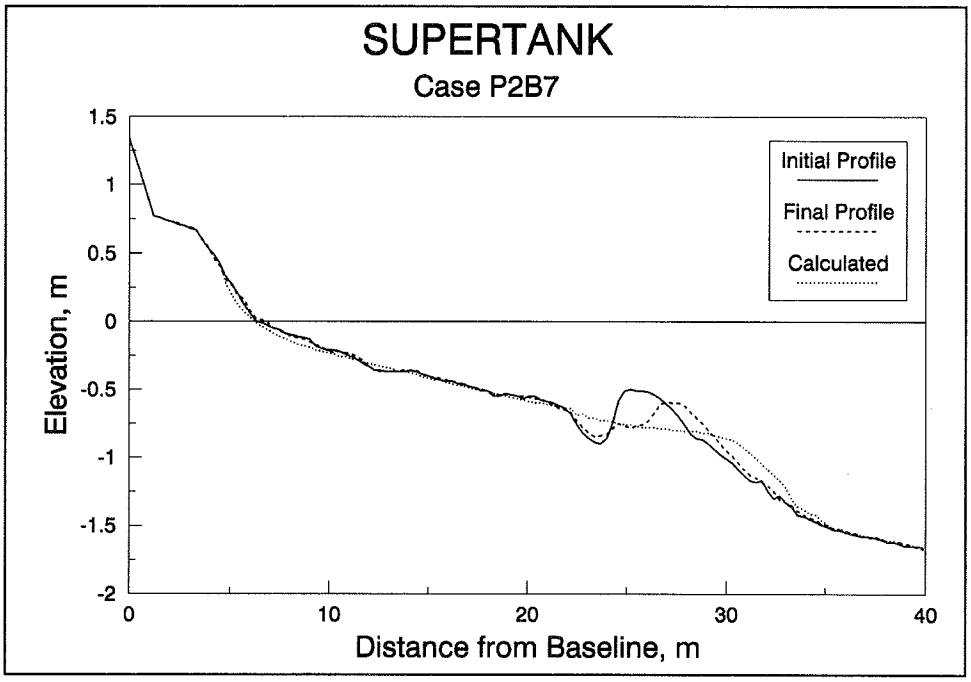

Figure A9. Result of default simulation, SUPERTANK case P2B7

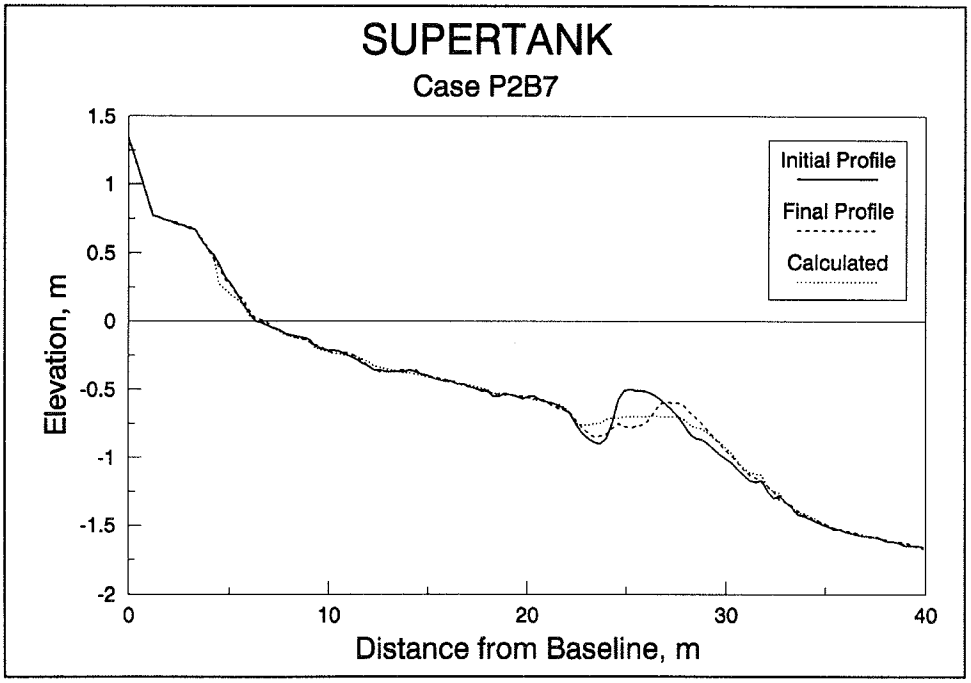

Figure A10. Result of calibrated simulation, SUPERTANK case P2B7 (model calibrated to case P5A)

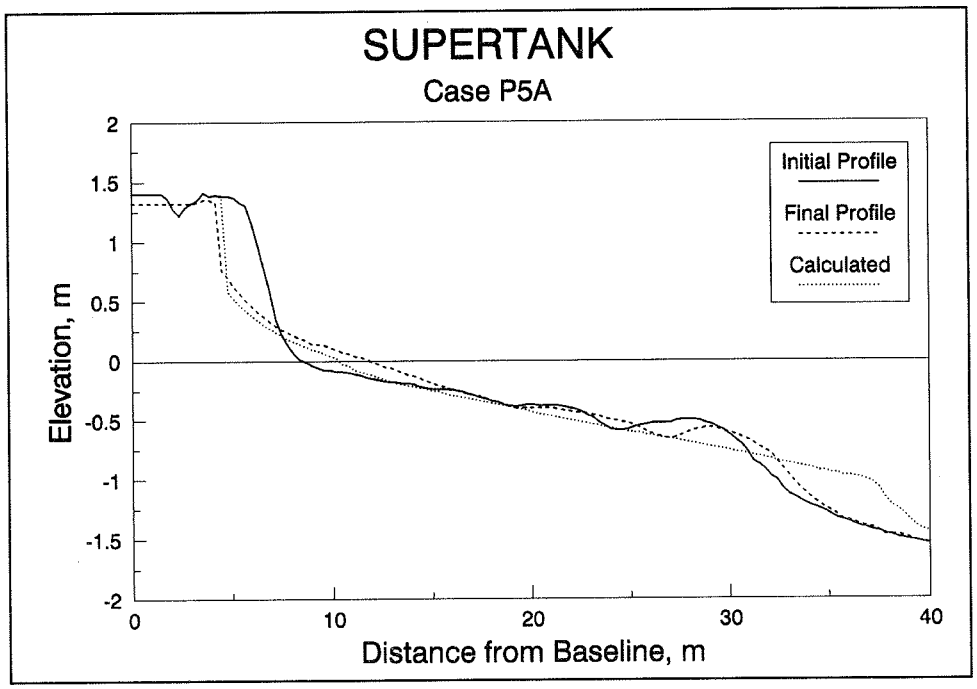

Figure A11. Result of default simulation, SUPERTANK case P5A

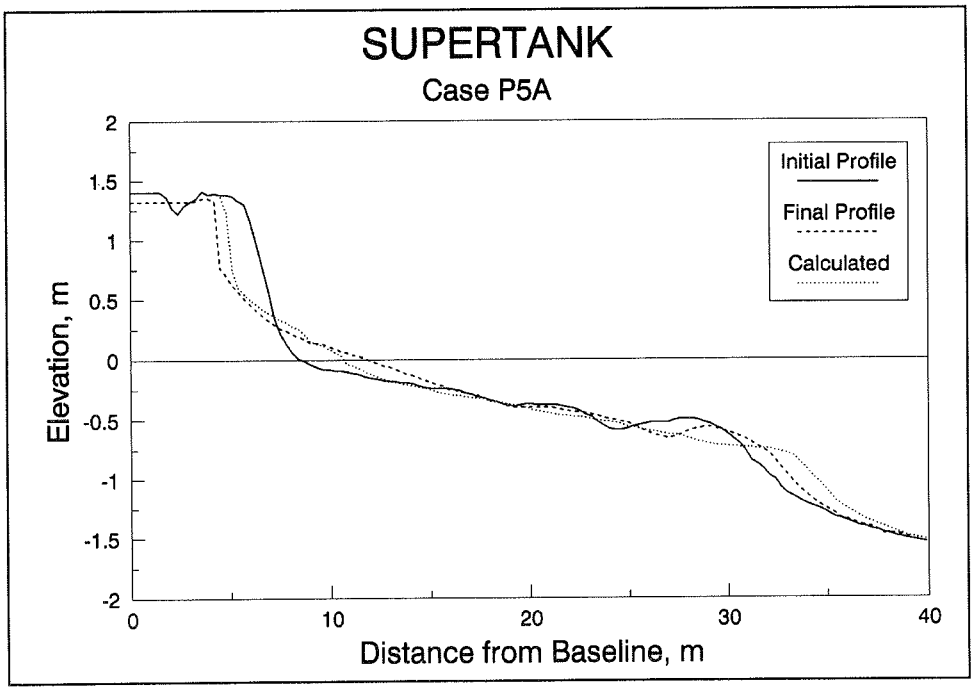

Figure A12. Result of calibrated simulation, SUPERTANK case P5A (model calibrated to case P5A)

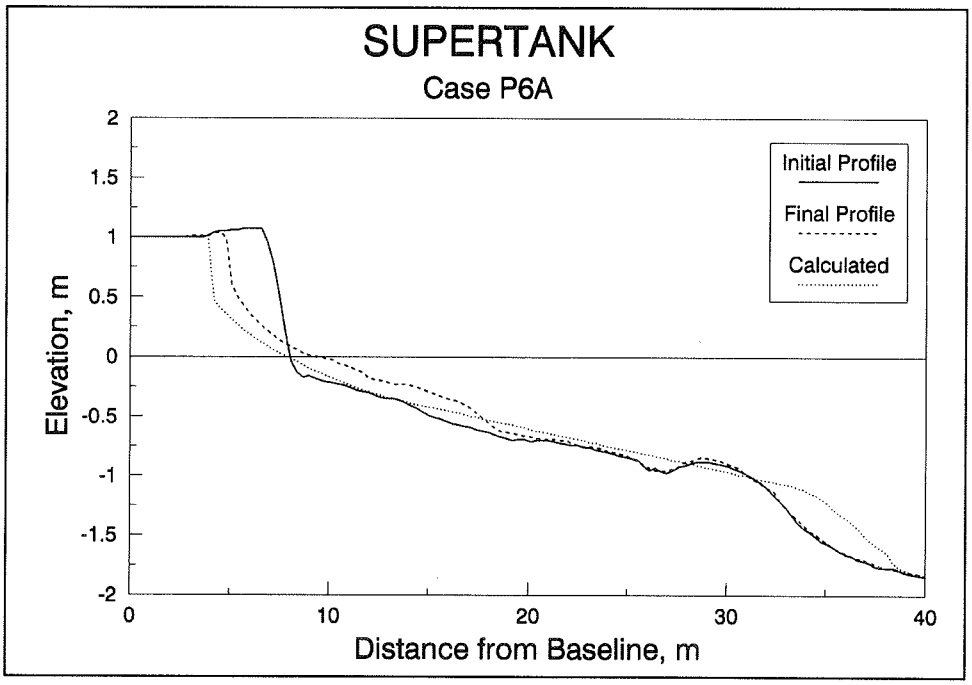

Figure A13. Result of default simulation, SUPERTANK case P6A

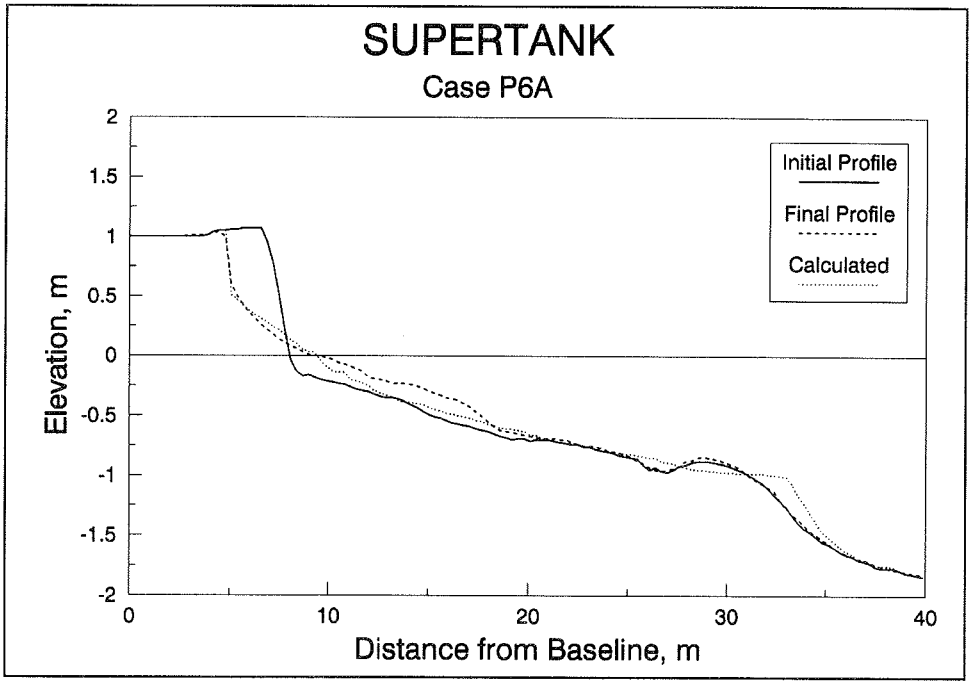

Figure A14. Result of calibrated simulation, SUPERTANK case P6A (model calibrated to case P5A)

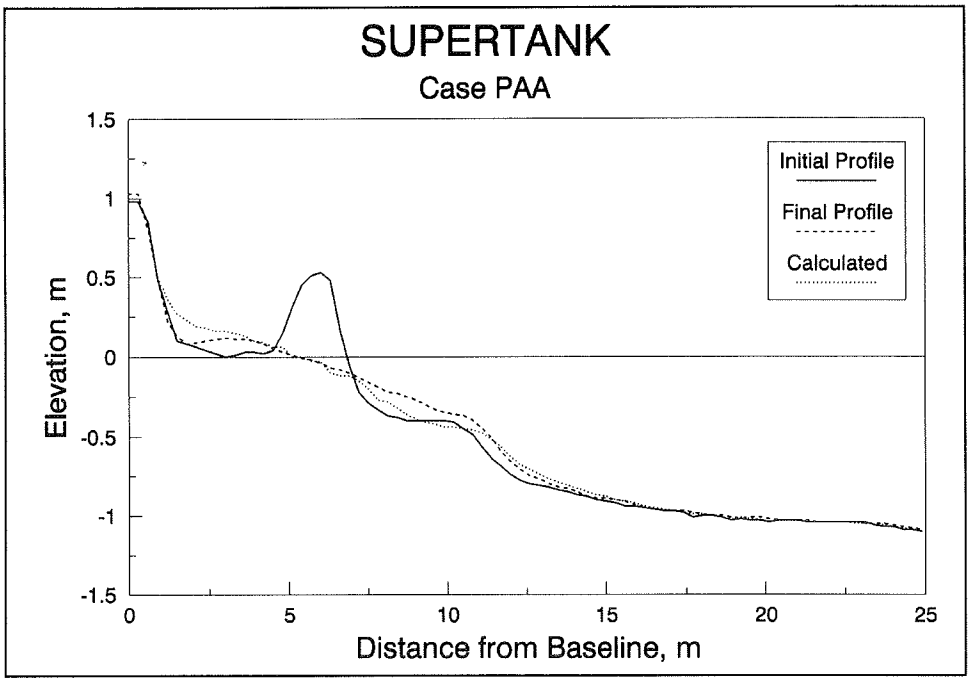

Figure A15. Result of default simulation, SUPERTANK case PAA

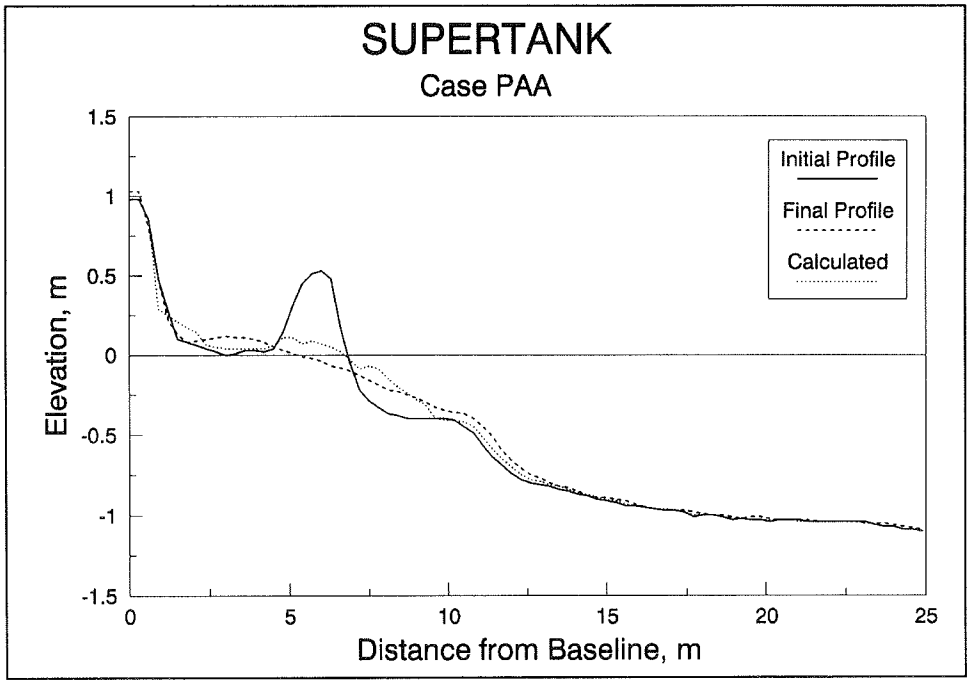

Figure A16. Result of calibrated simulation, SUPERTANK case PAA (model calibrated to case P5A)

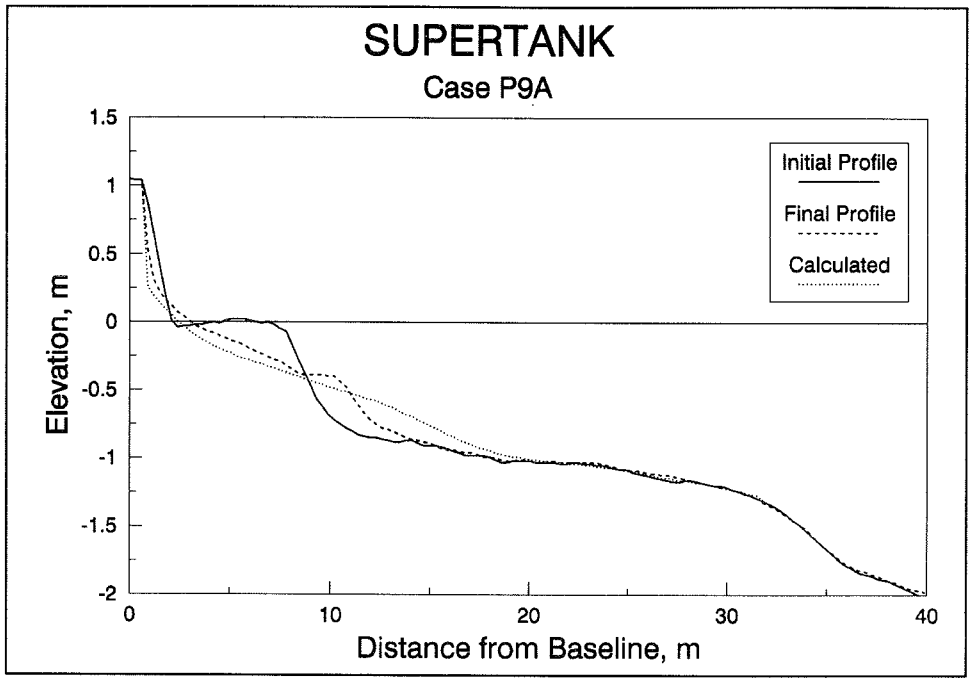

Figure A17. Result of default simulation, SUPERTANK case P9A

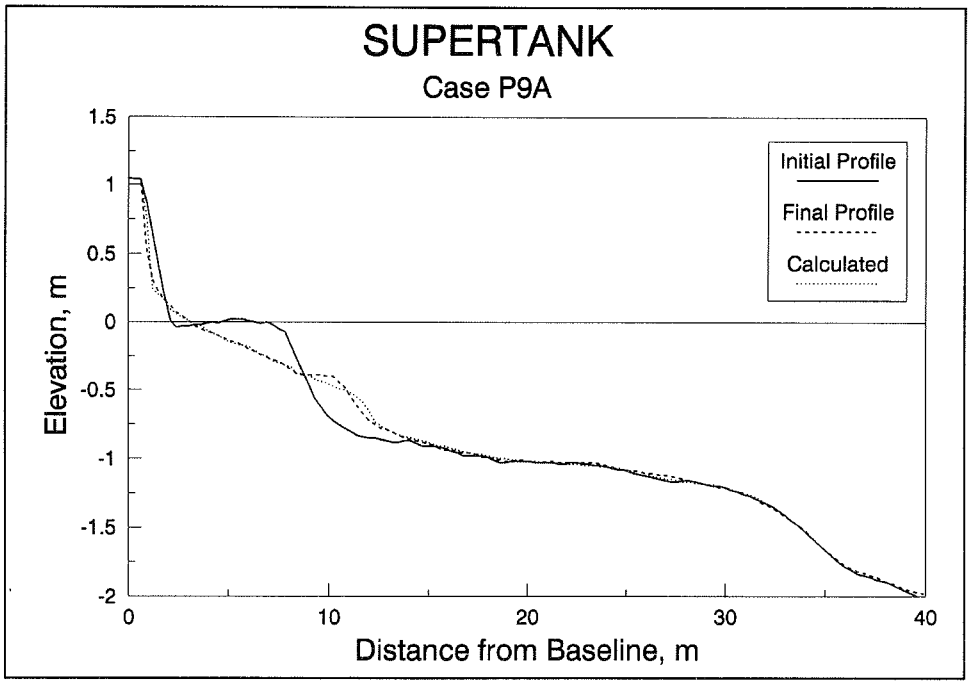

Figure A18. Result of calibrated simulation, SUPERTANK case P9A (model calibrated to case P5A)

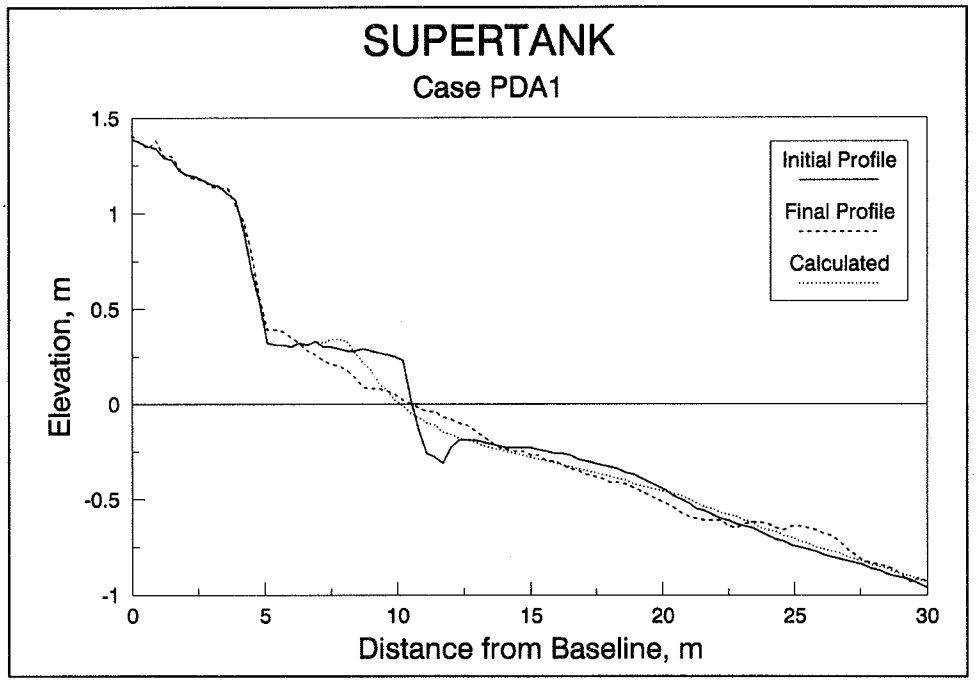

Figure A19. Result of default simulation, SUPERTANK case PDA1

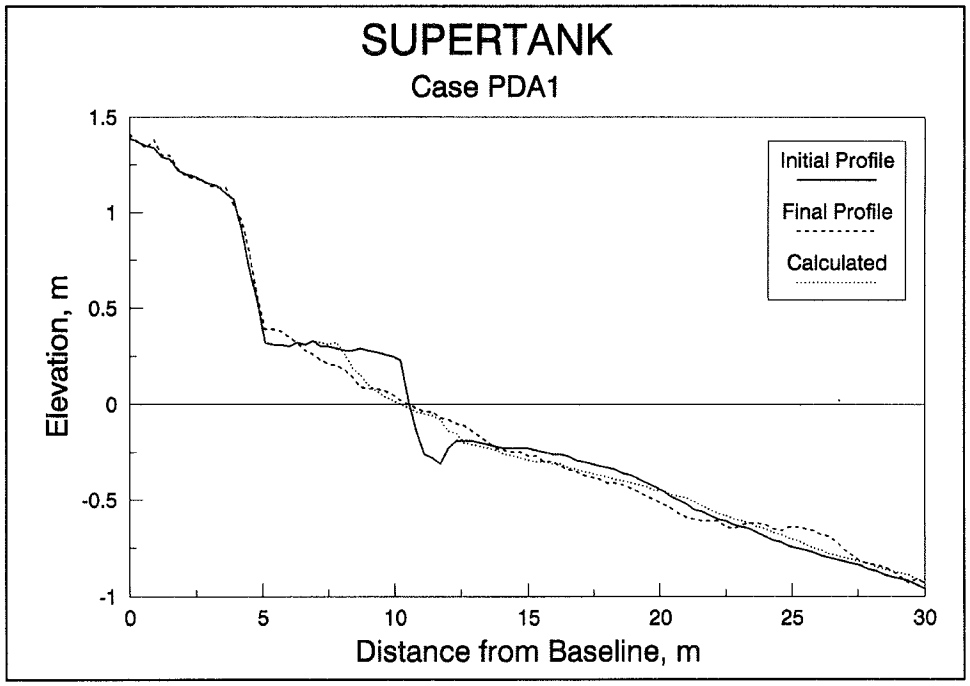

Figure A20. Result of calibrated simulation, SUPERTANK case PDA1 (model calibrated to case P5A)

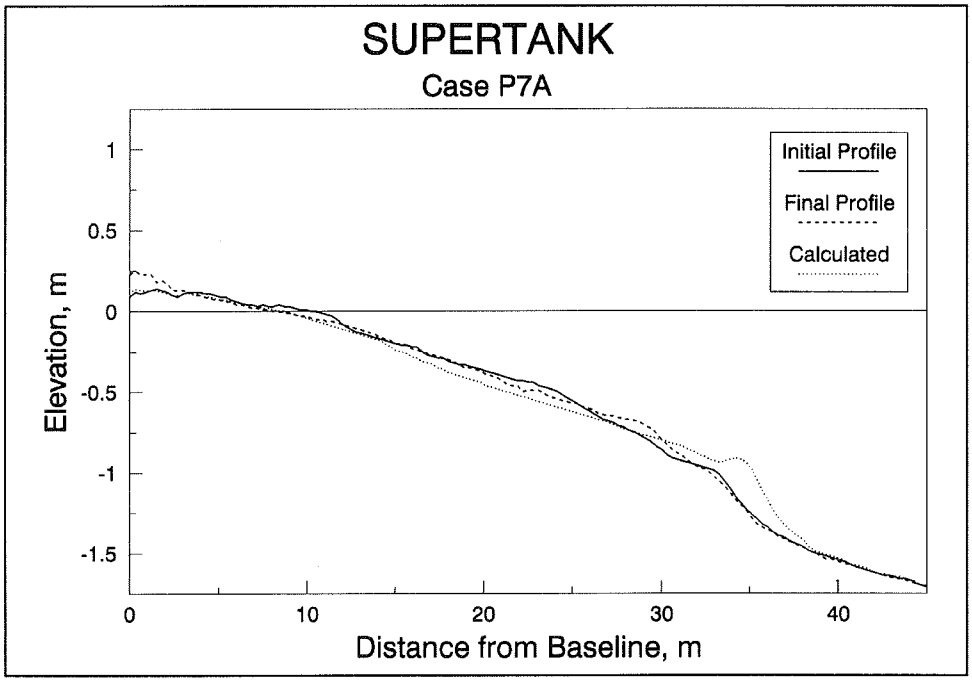

Figure A21. Result of default simulation, SUPERTANK case P7A

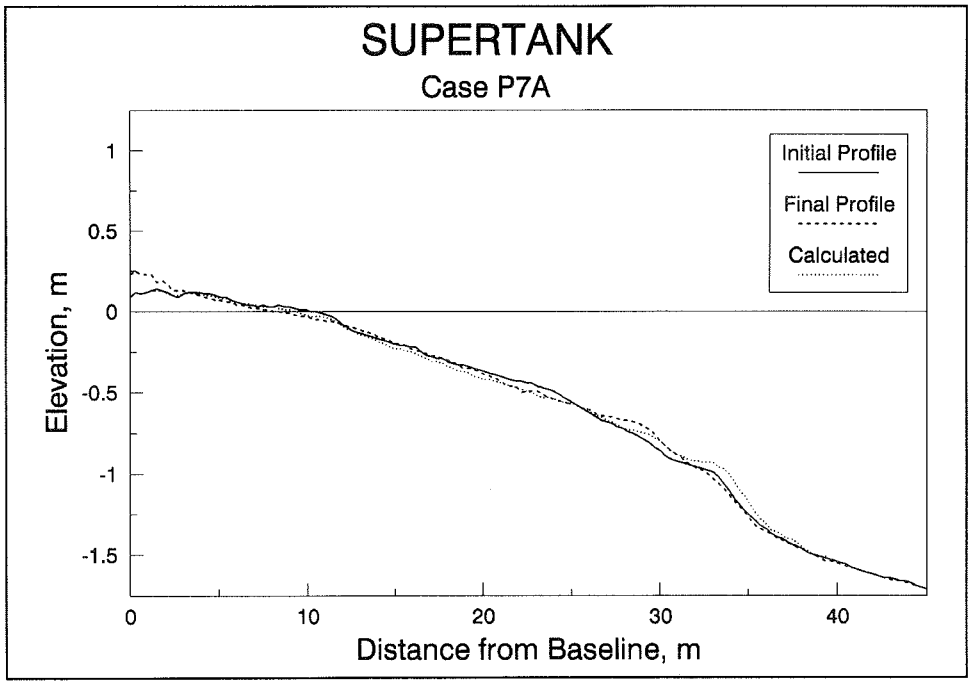

Figure A22. Result of calibrated simulation, SUPERTANK case P7A (model calibrated to case P5A)

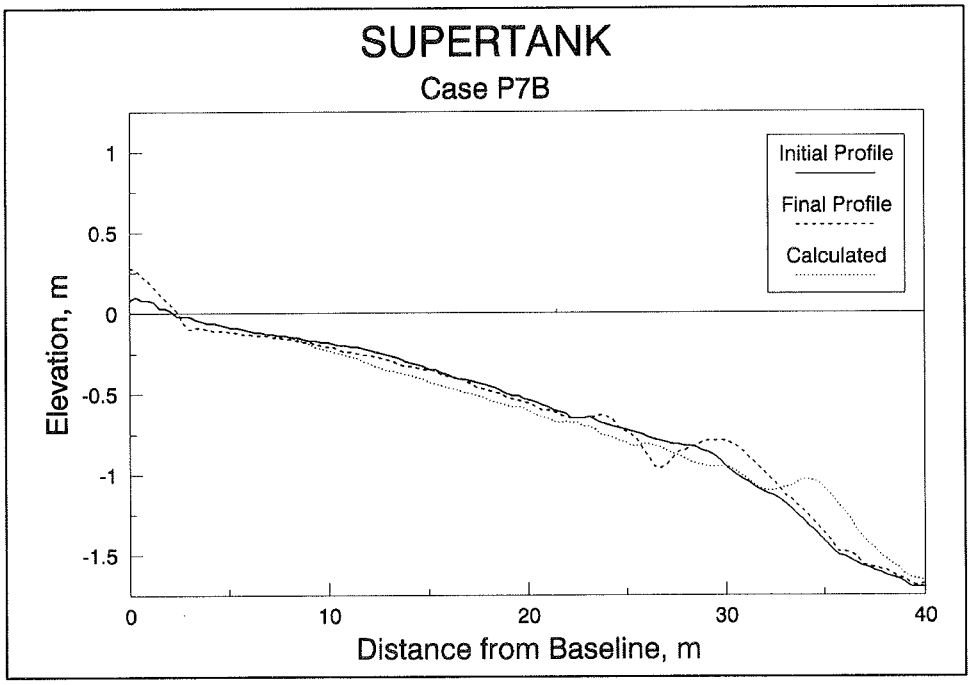

Figure A23. Result of default simulation, SUPERTANK case P7B

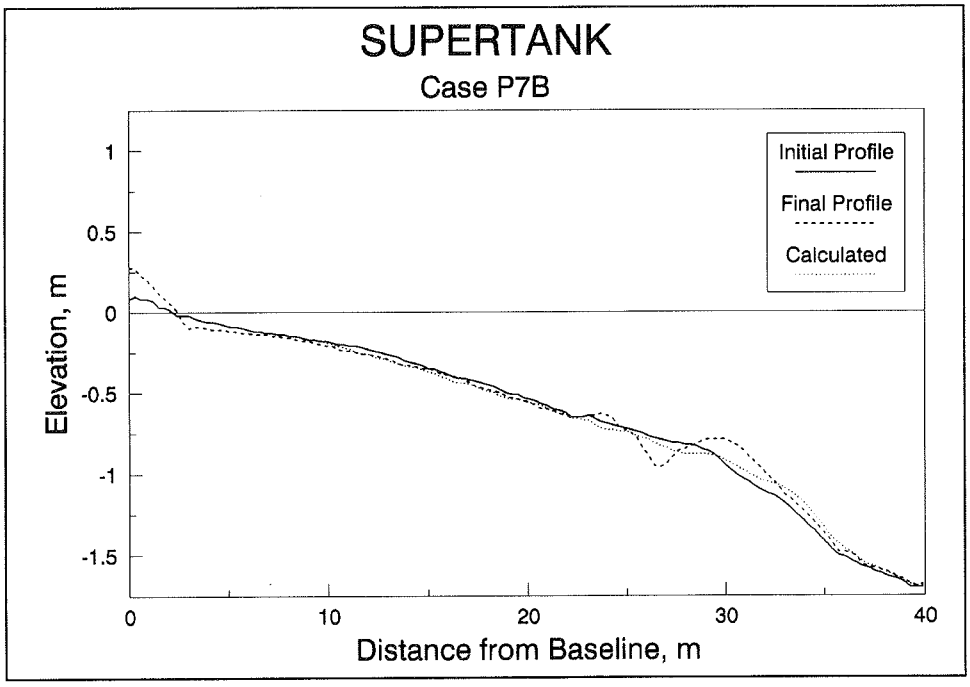

Figure A24. Result of calibrated simulation, SUPERTANK case P7B (model calibrated to case P5A)

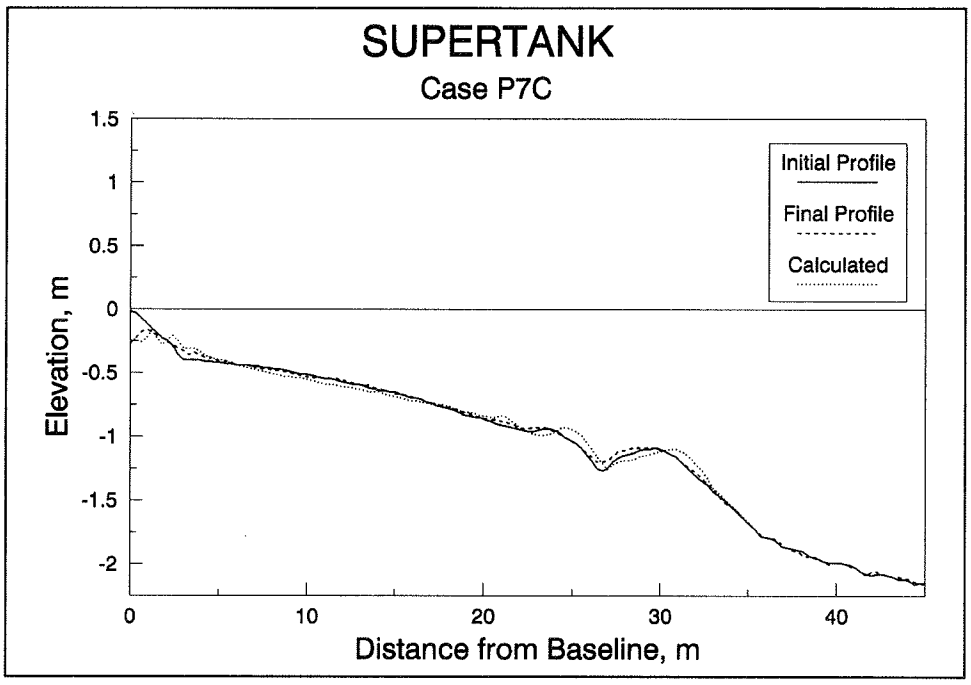

Figure A25. Result of default simulation, SUPERTANK case P7C

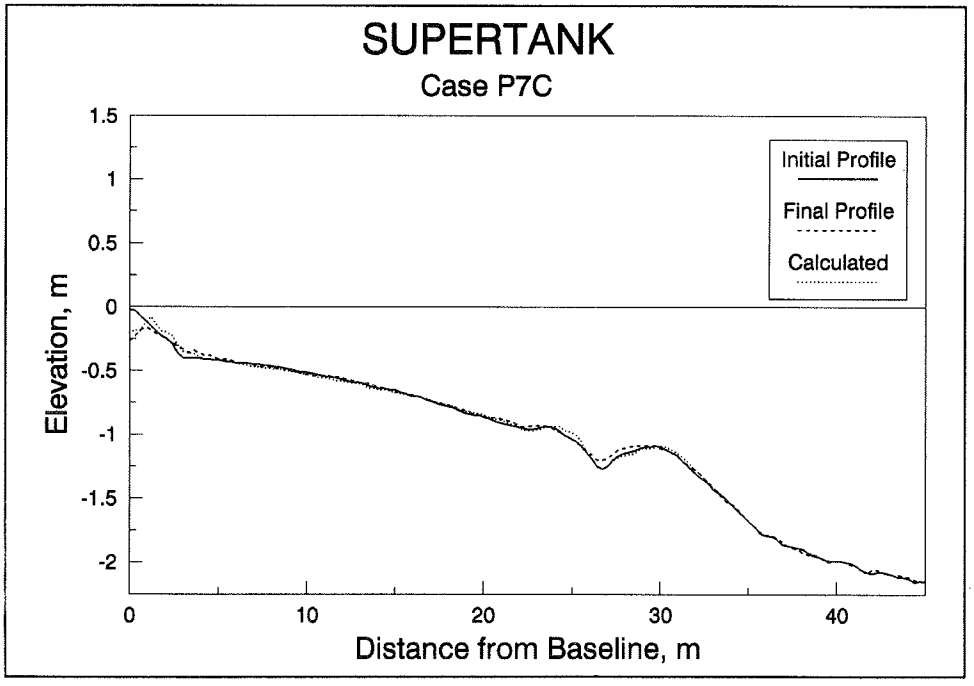

Figure A26. Result of calibrated simulation, SUPERTANK case P7C (model calibrated to case P5A)

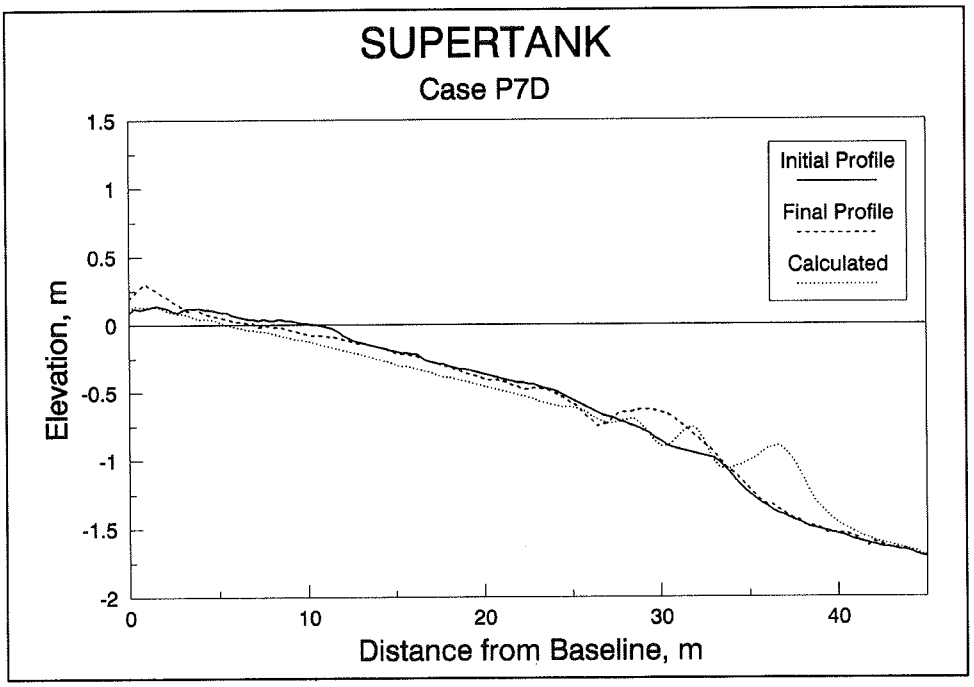

Figure A27. Result of default simulation, SUPERTANK case P7D

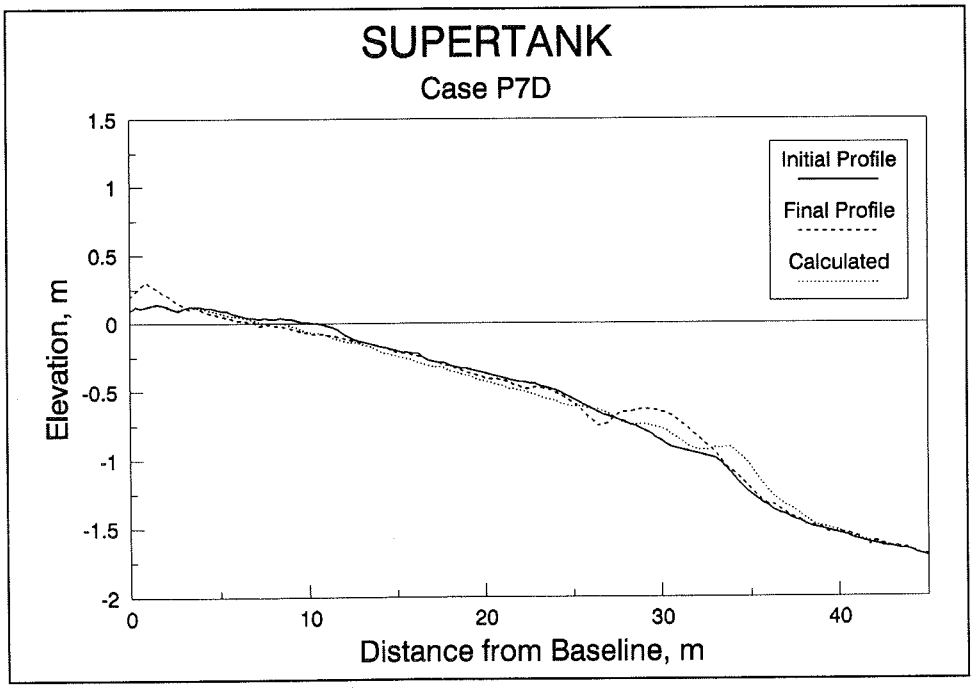

Figure A28. Result of calibrated simulation, SUPERTANK case P7D (model calibrated to case P5A)

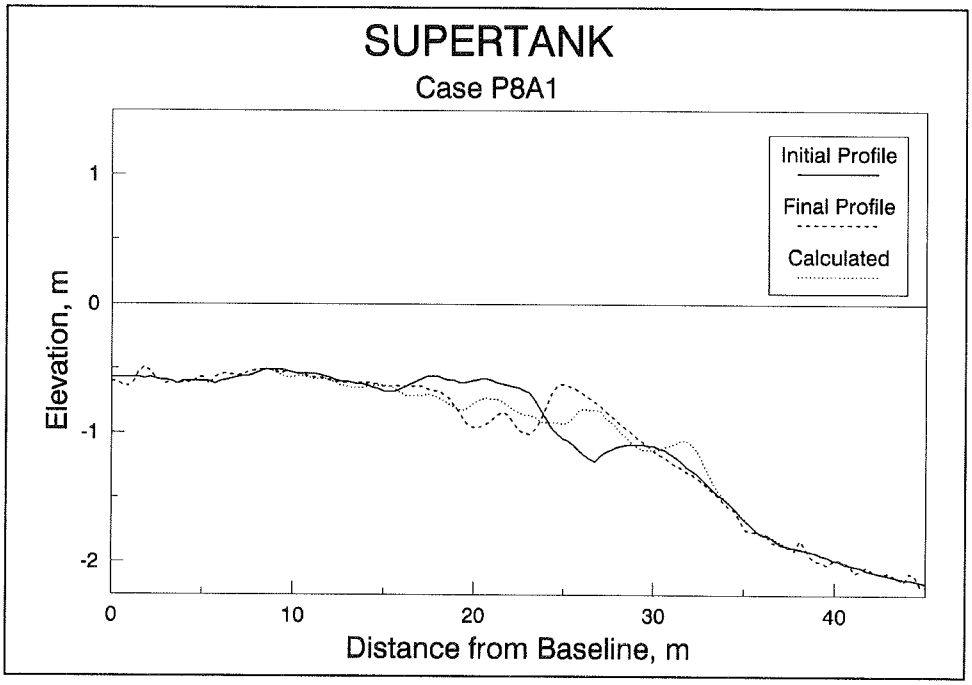

Figure A29. Result of default simulation, SUPERTANK case P8A1

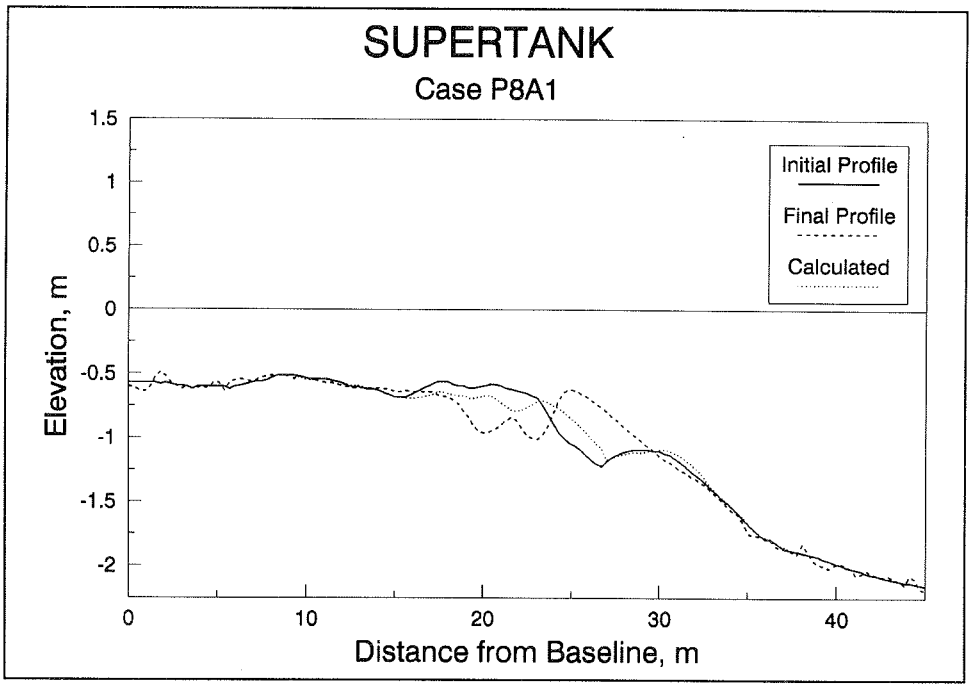

Figure A30. Result of calibrated simulation, SUPERTANK case P8A1 (model calibrated to case P5A)

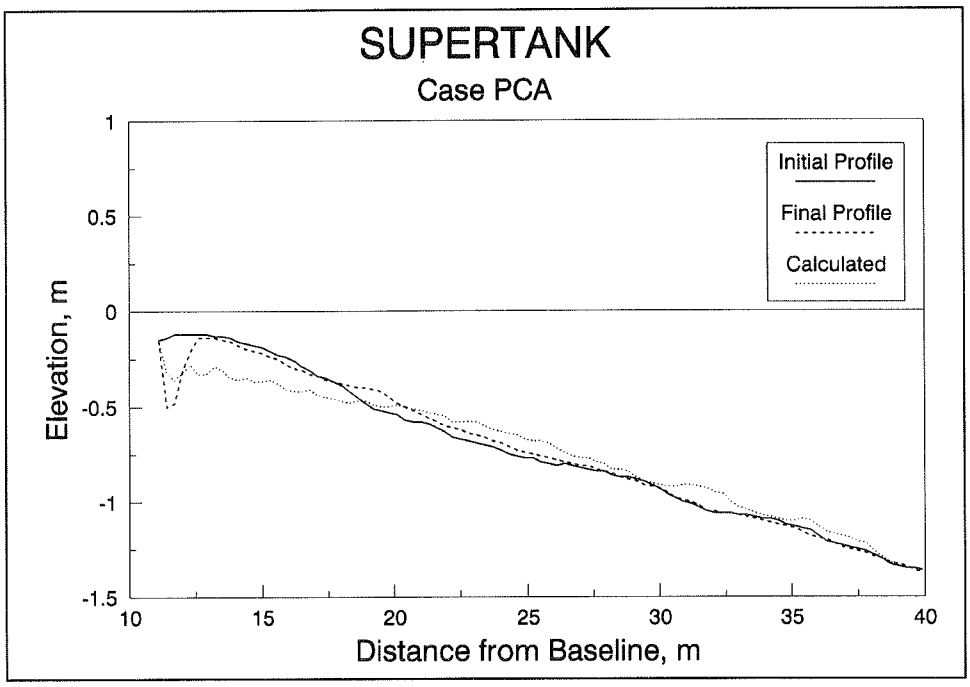

Figure A31. Result of default simulation, SUPERTANK case PCA

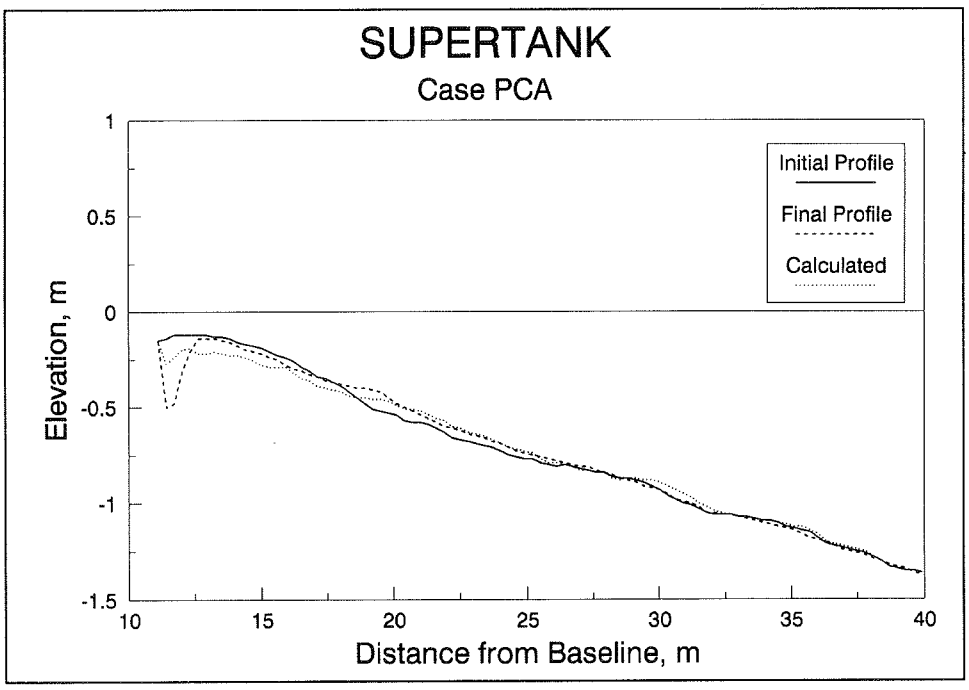

Figure A32. Result of calibrated simulation, SUPERTANK case PCA (model calibrated to case P5A)

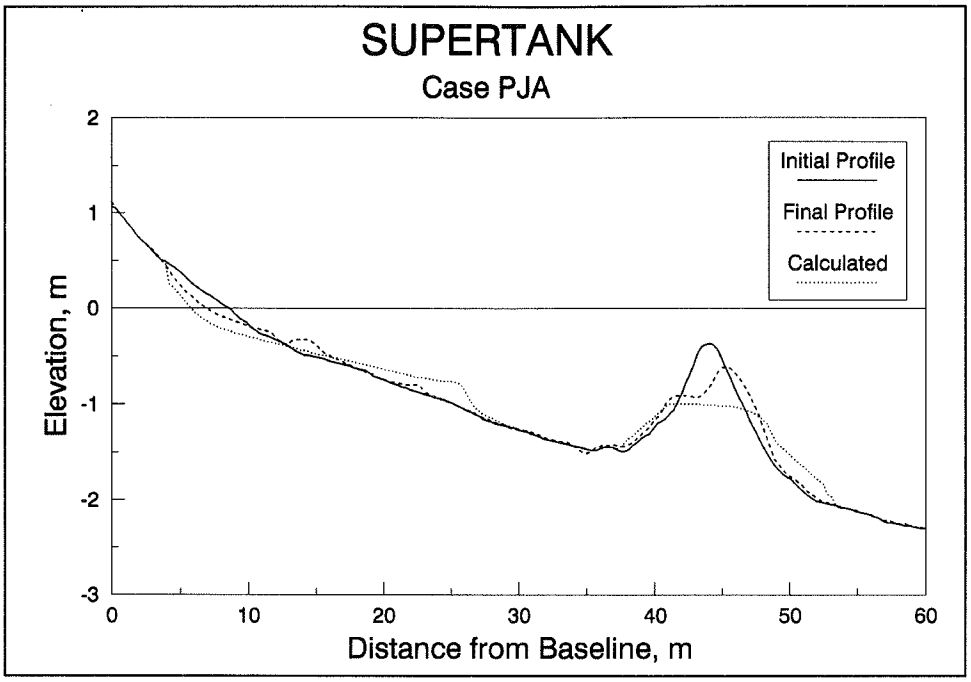

Figure A33. Result of default simulation, SUPERTANK case PJA

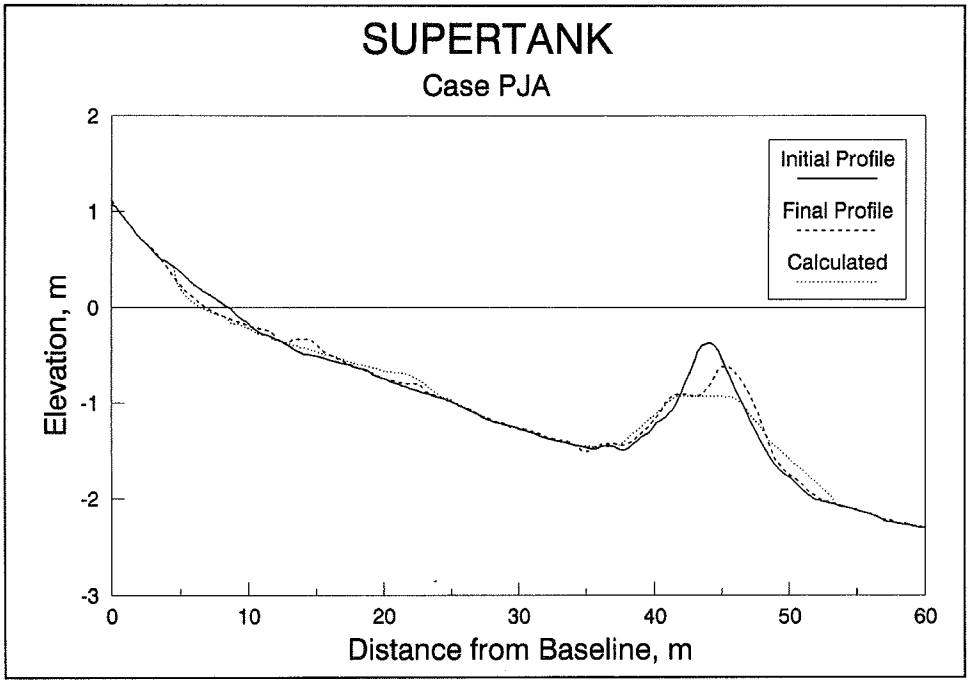

Figure A34. Result of calibrated simulation, SUPERTANK case PJA (model calibrated to case P5A)

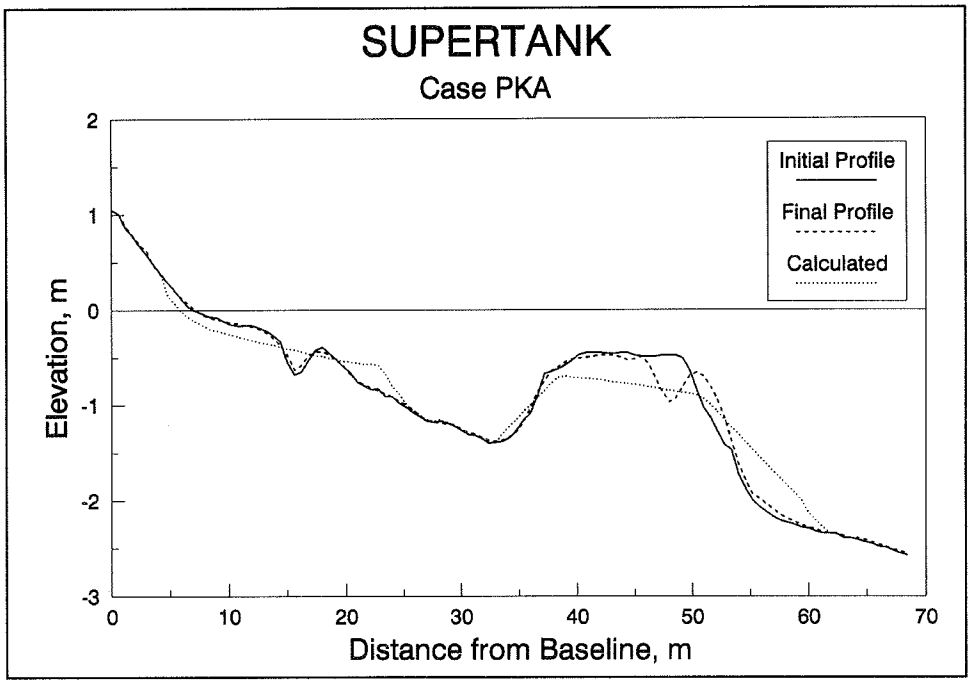

Figure A35. Result of default simulation, SUPERTANK case PKA

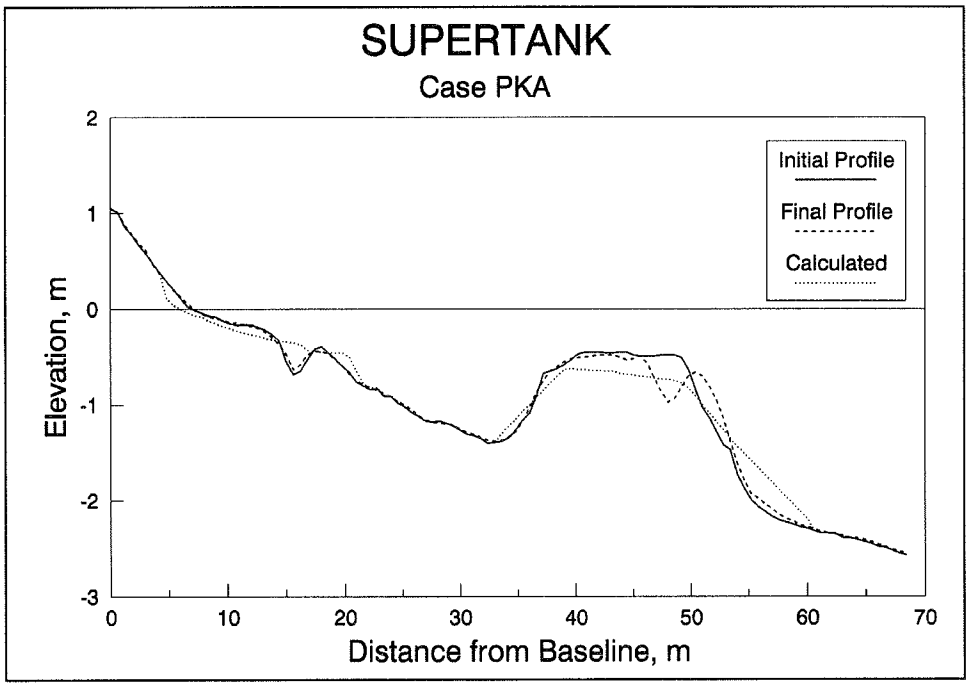

Figure A36. Result of calibrated simulation, SUPERTANK case PKA (model calibrated to case P5A)

Monochromatic Wave Cases

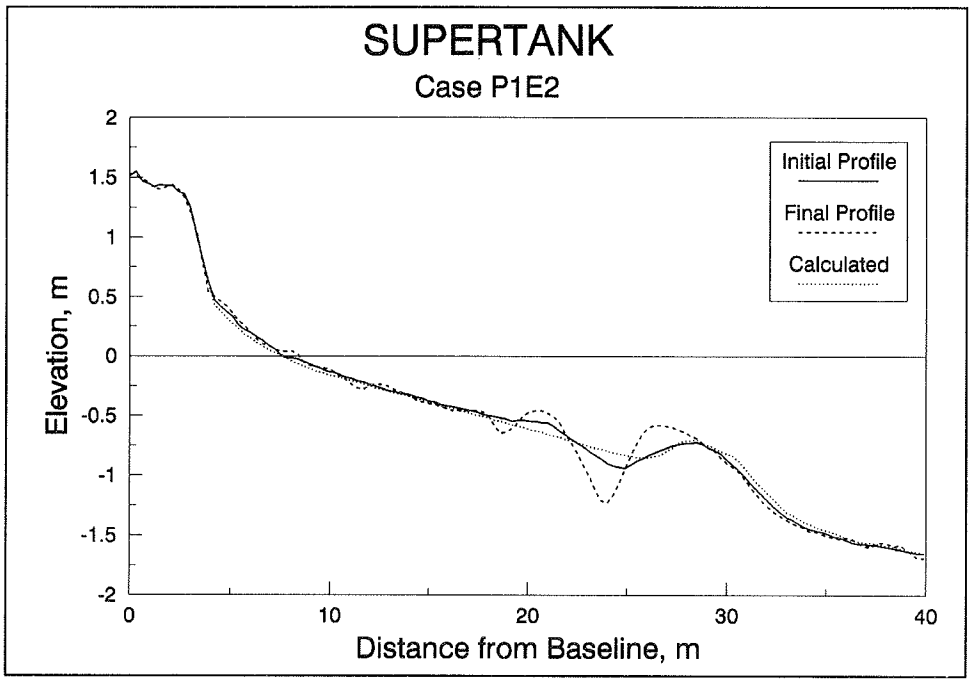

Figure A37. Result of default simulation, SUPERTANK case P1E2

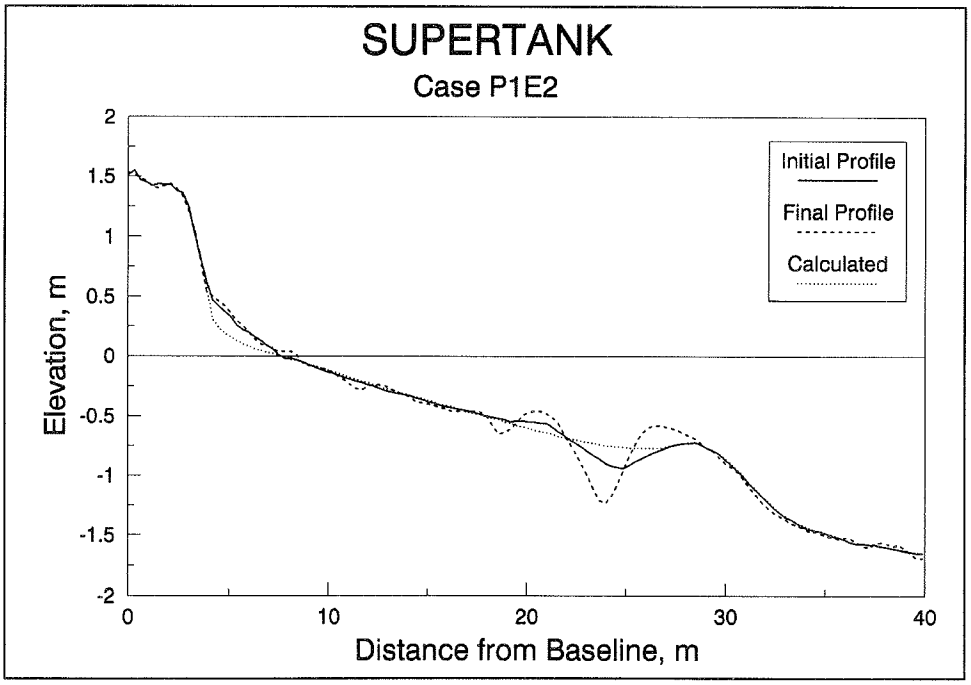

Figure A38. Result of calibrated simulation, SUPERTANK case P1E2 (model calibrated to case P5A)

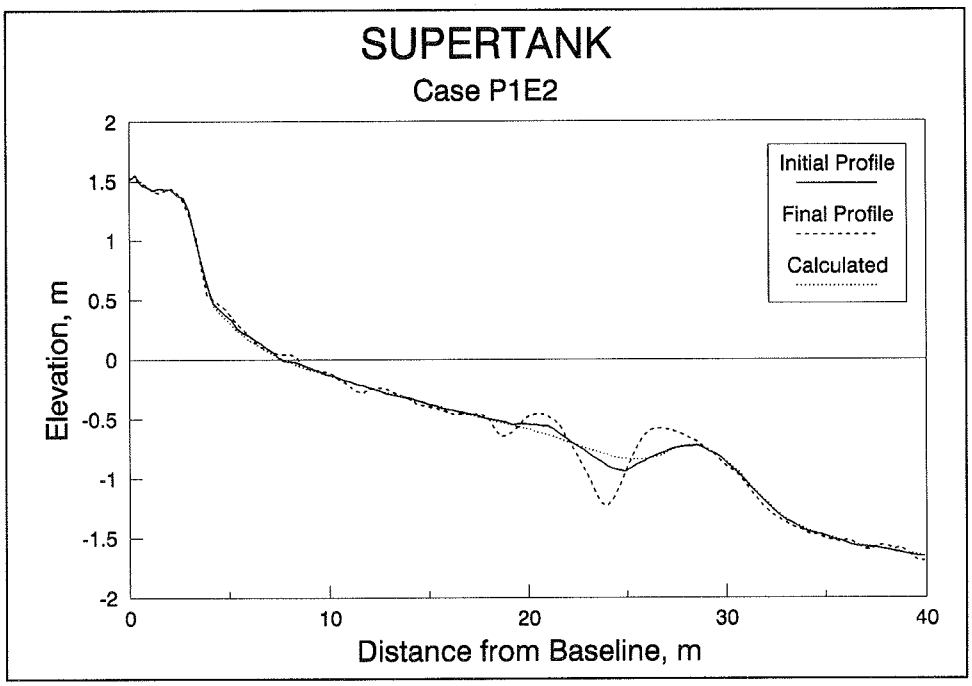

Figure A39. Result of calibrated simulation, SUPERTANK case P1E2 (model calibrated to case PGA)

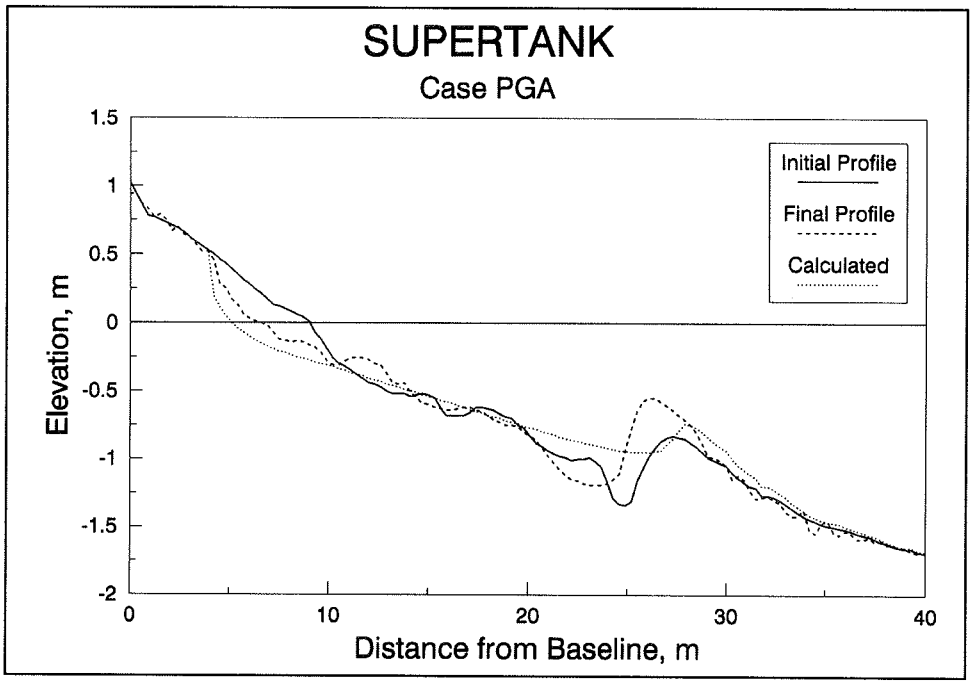

Figure A40. Result of default simulation, SUPERTANK case PGA

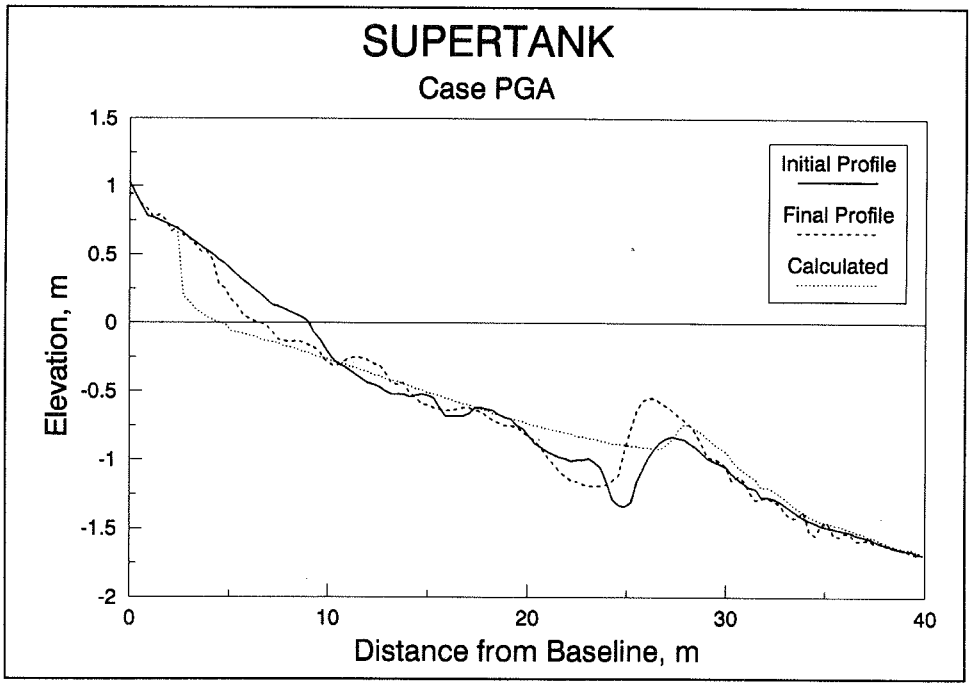

Figure A41. Result of calibrated simulation, SUPERTANK case PGA (model calibrated to case P5A)

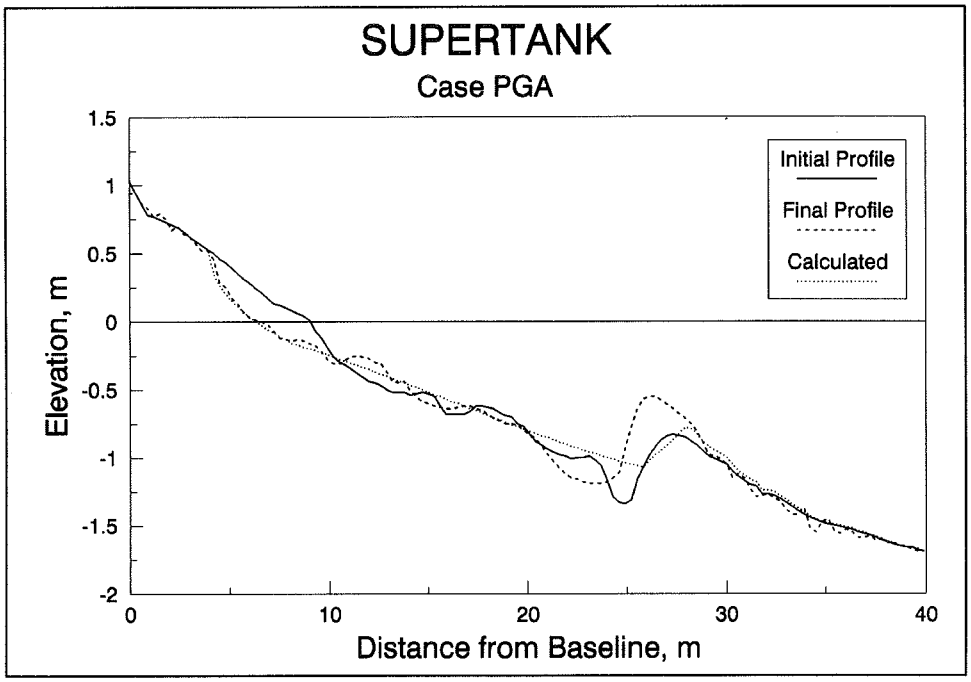

Figure A42. Result of calibrated simulation, SUPERTANK case PGA (model calibrated to case PGA)

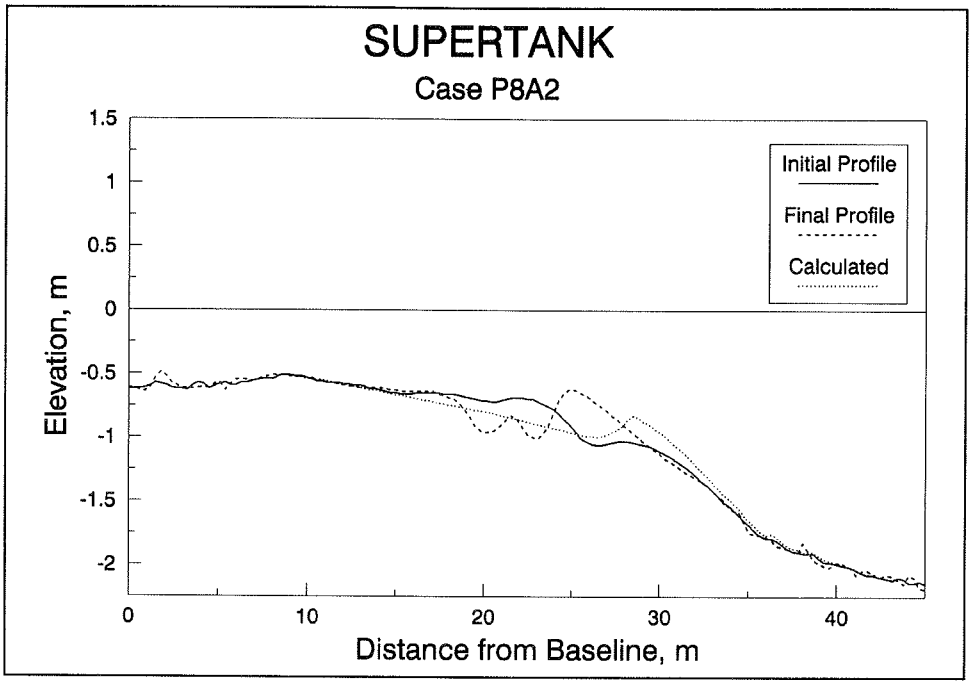

Figure A43. Result of default simulation, SUPERTANK case P8A2

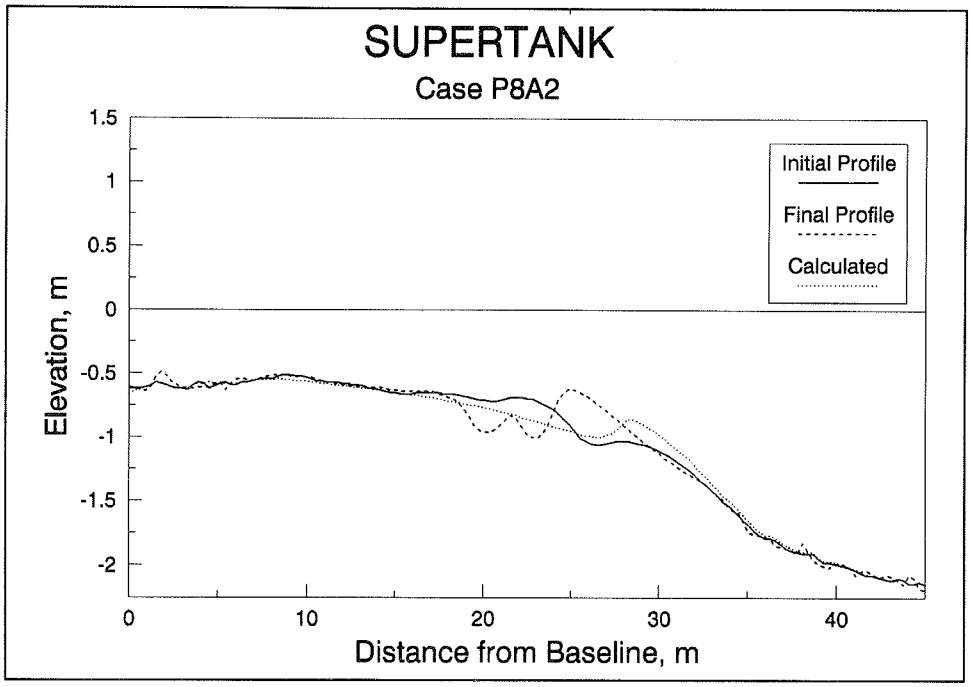

Figure A44. Result of calibrated simulation, SUPERTANK case P8A2 (model calibrated to case P5A)

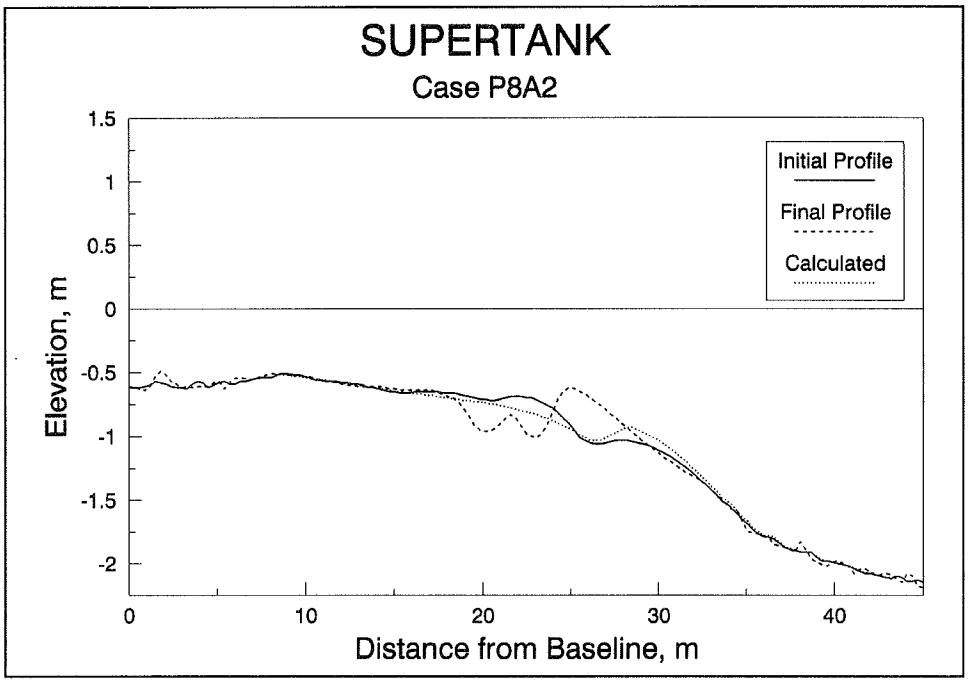

Figure A45. Result of calibrated simulation, SUPERTANK case P8A2 (model calibrated to case PGA)

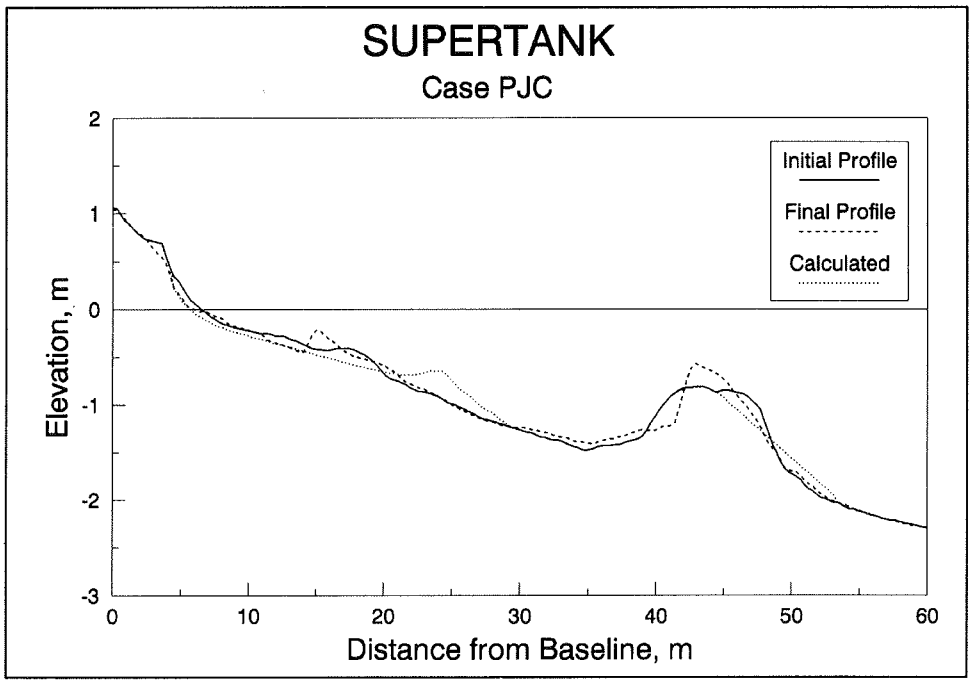

Figure A46. Result of default simulation, SUPERTANK case PJC

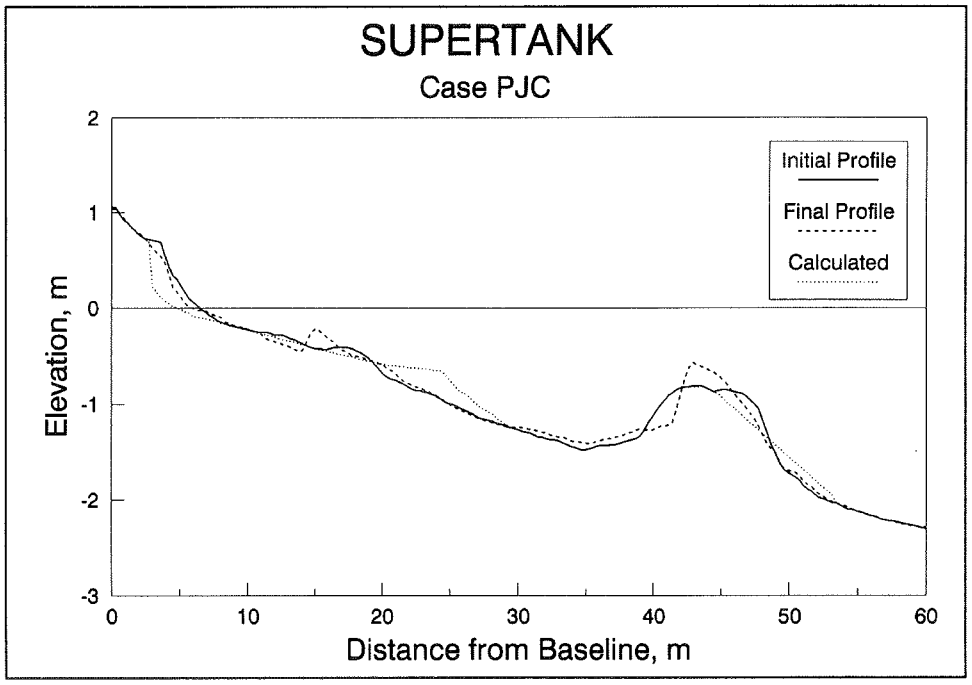

Figure A47. Result of calibrated simulation, SUPERTANK case PJC (model calibrated to case P5A)

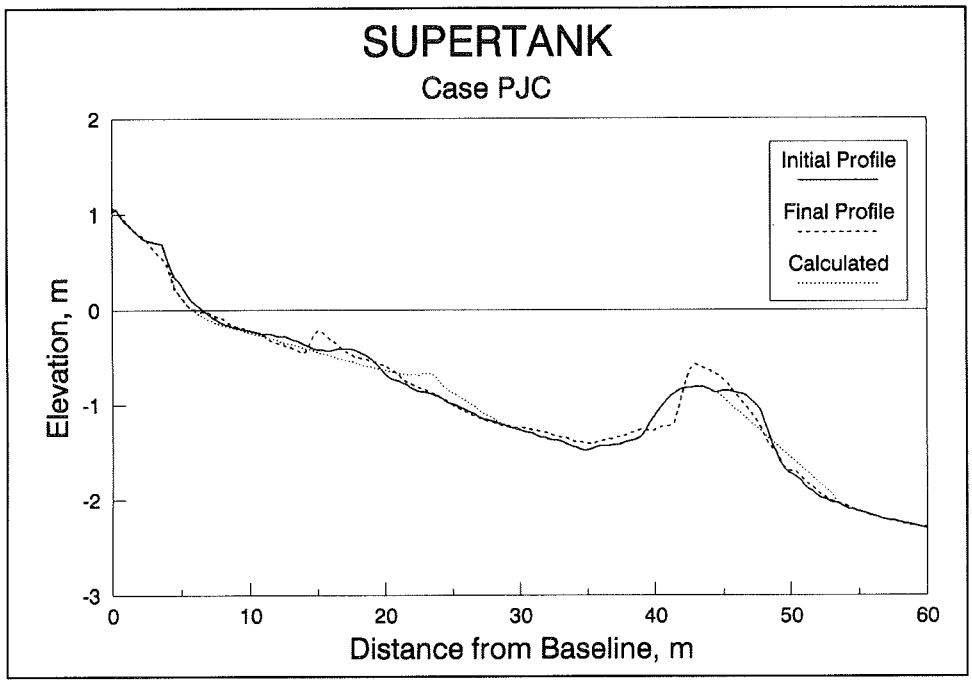

Figure A48. Result of calibrated simulation, SUPERTANK case PJC (model calibrated to case PGA)

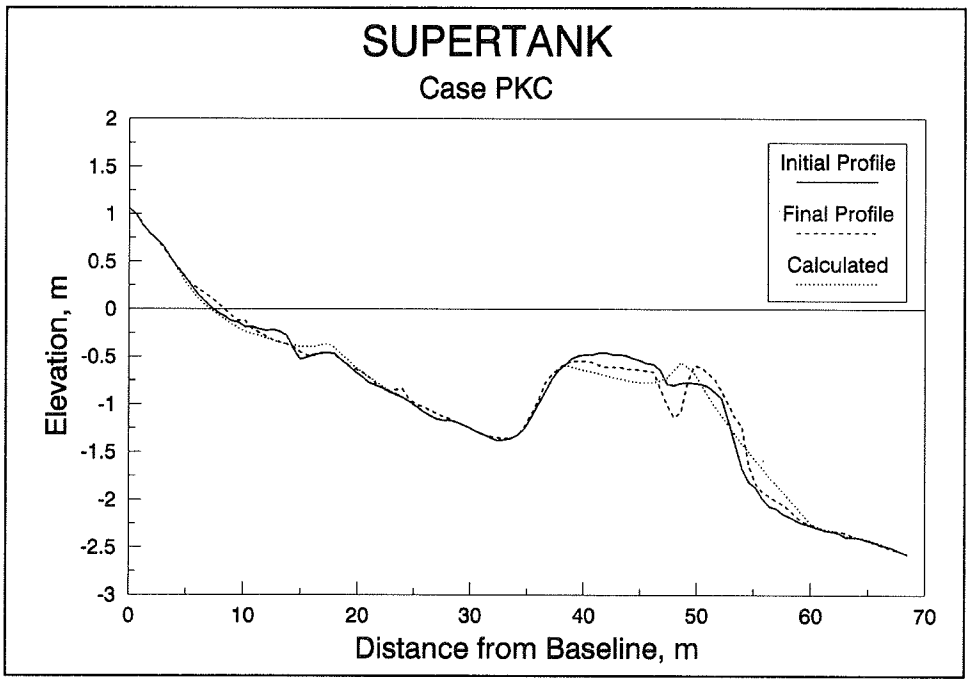

Figure A49. Result of default simulation, SUPERTANK case PKC

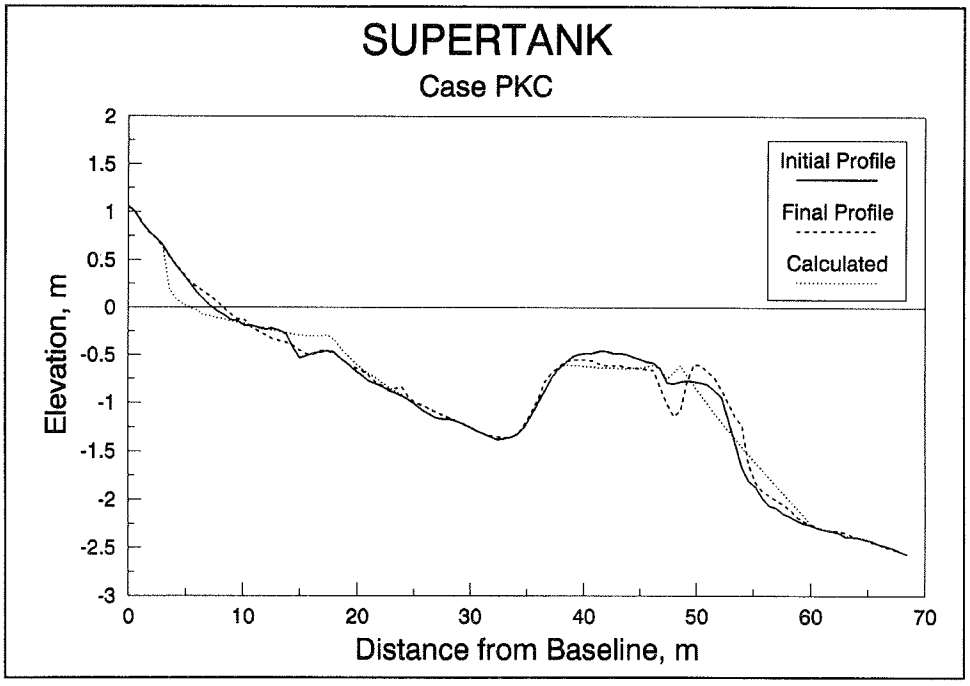

Figure A50. Result of calibrated simulation, SUPERTANK case PKC (model calibrated to case P5A)

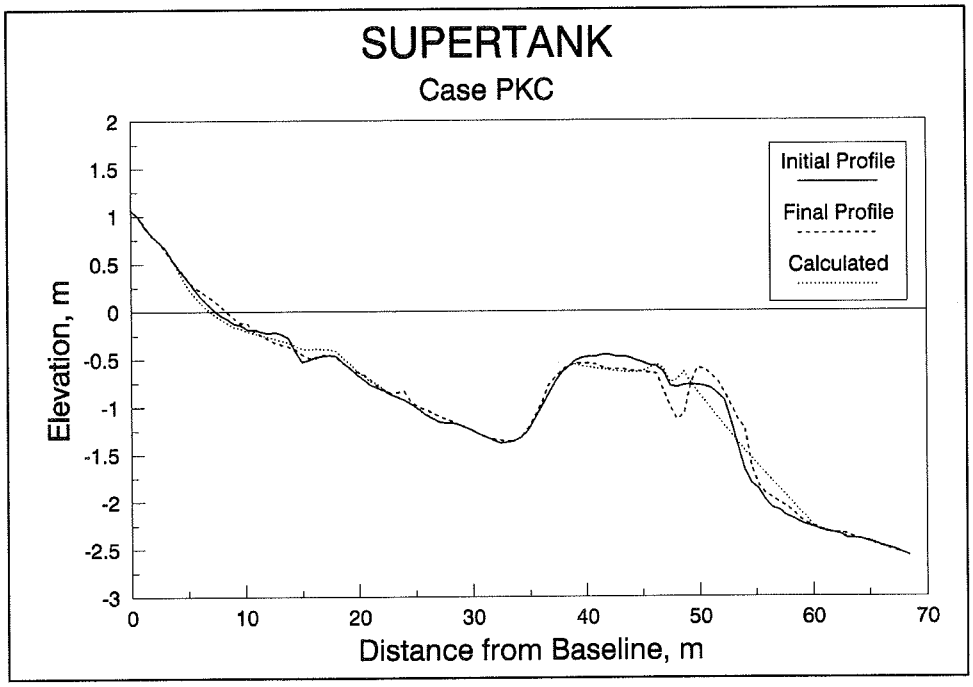

Figure A51. Result of calibrated simulation, SUPERTANK case PKC (model calibrated to case PGA)

Appendix B
Simulation Results for Field Case Studies

Ocean City, MD

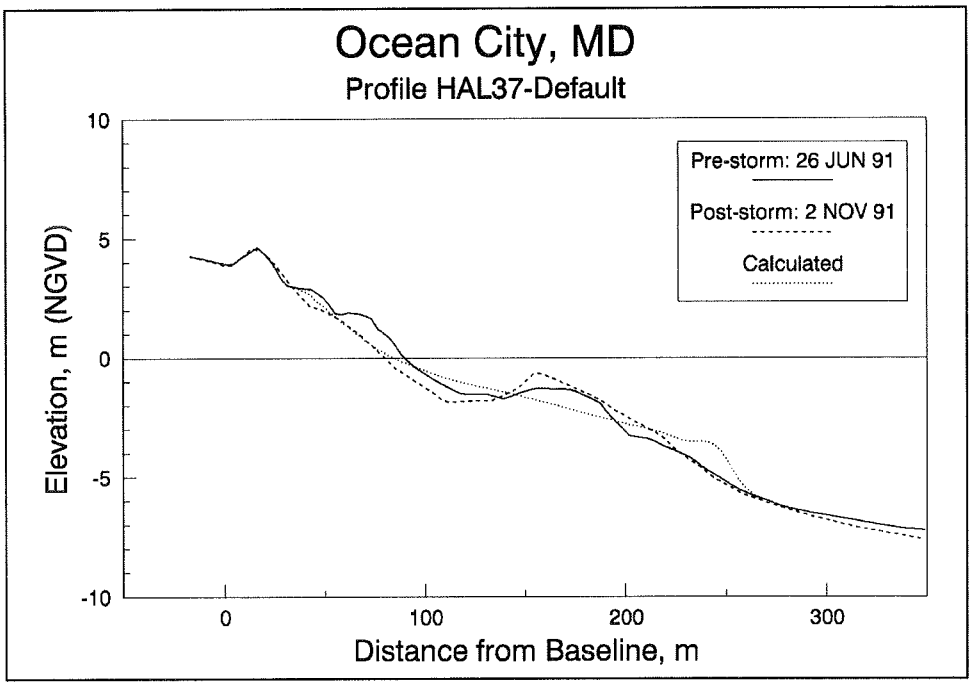

Figure B1. Result of default simulation of the Halloween storm for profile 37, Ocean City, MD

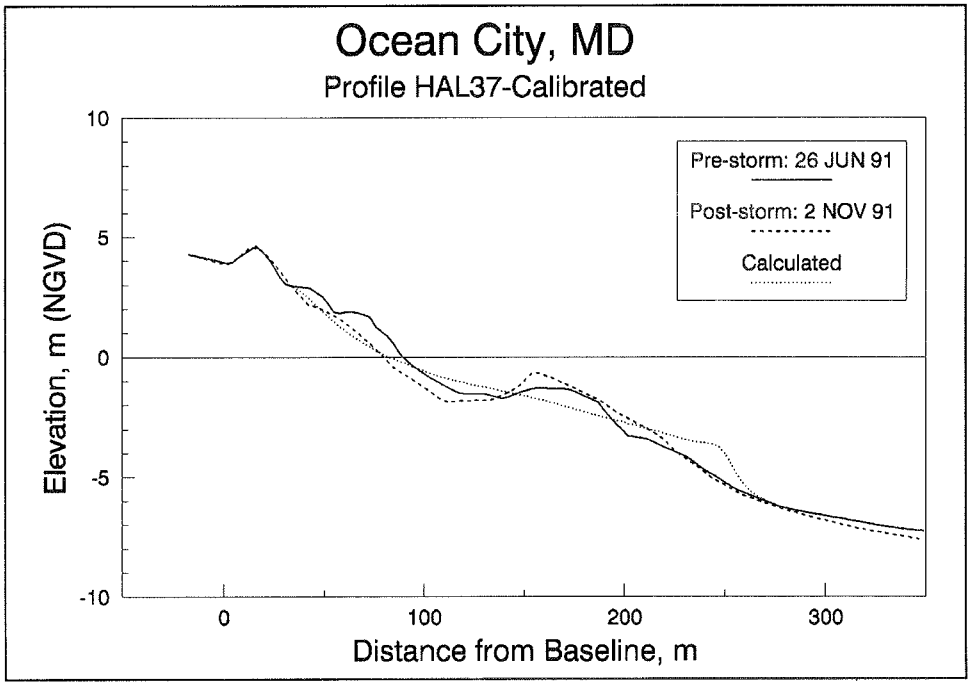

Figure B2. Result of calibrated simulation of the Halloween storm for profile 37, Ocean City, MD (model calibrated to case OJ81)

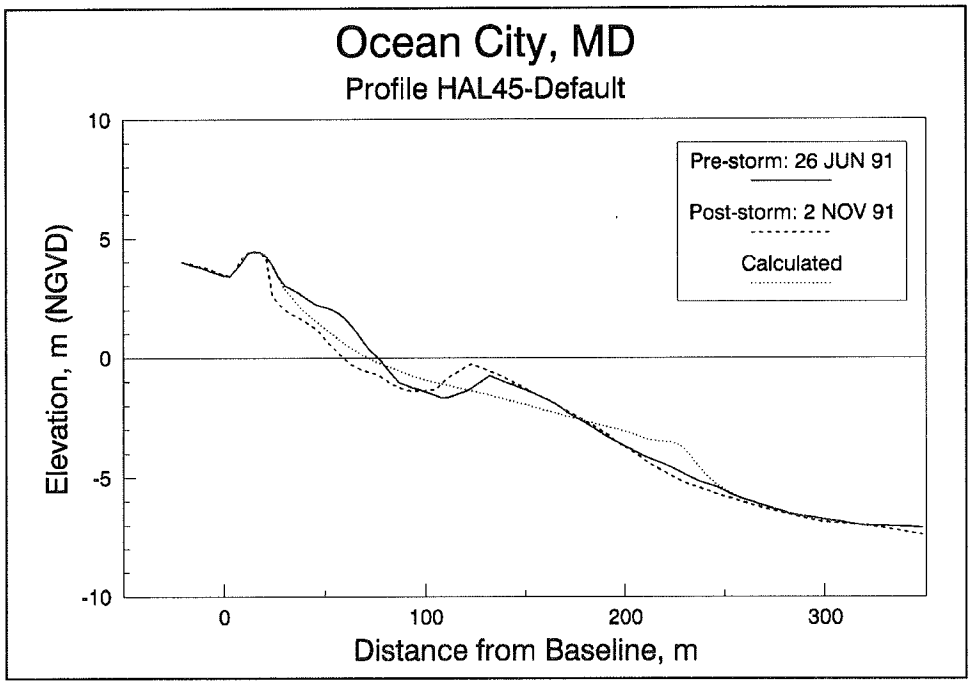

Figure B3. Result of default simulation of the Halloween storm for profile 45, Ocean City, MD

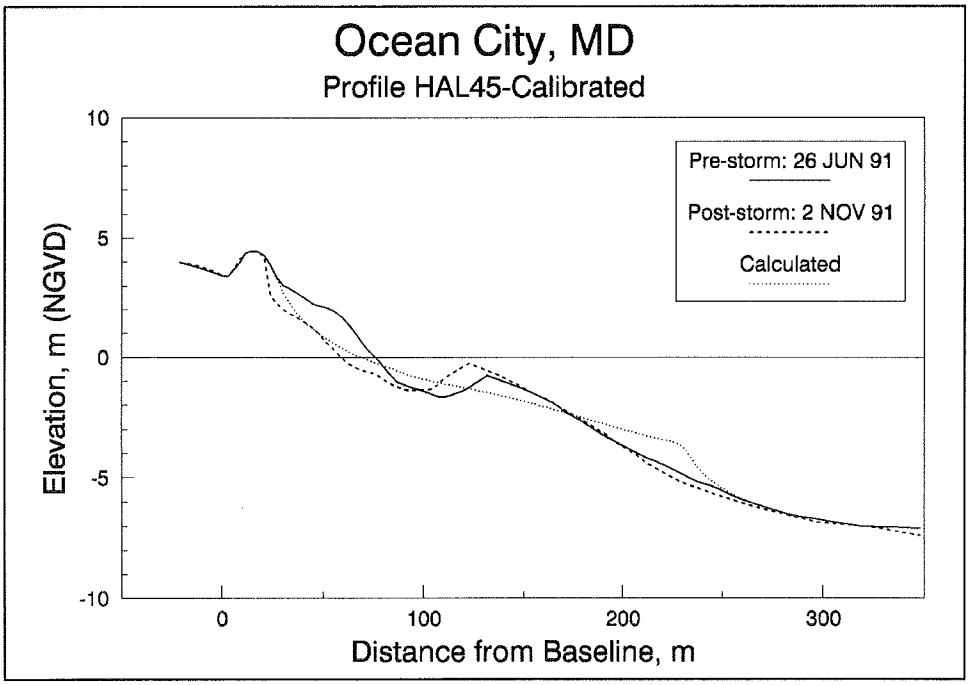

Figure B4. Result of calibrated simulation of the Halloween storm for profile 45, Ocean City, MD (model calibrated to case OJ81)

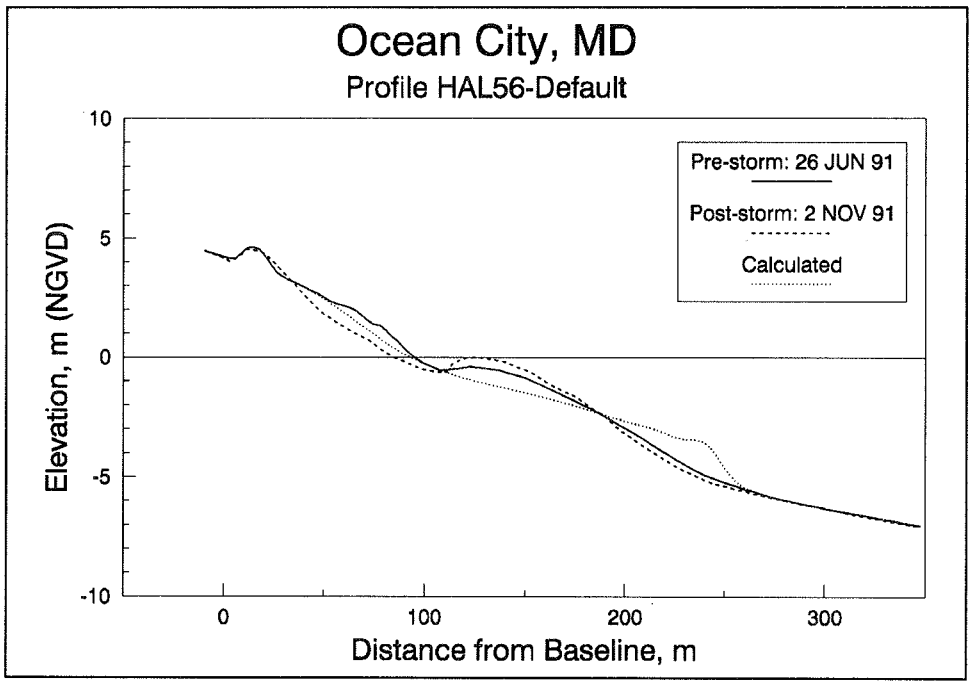

Figure B5. Result of default simulation of the Halloween storm for profile 56, Ocean City, MD

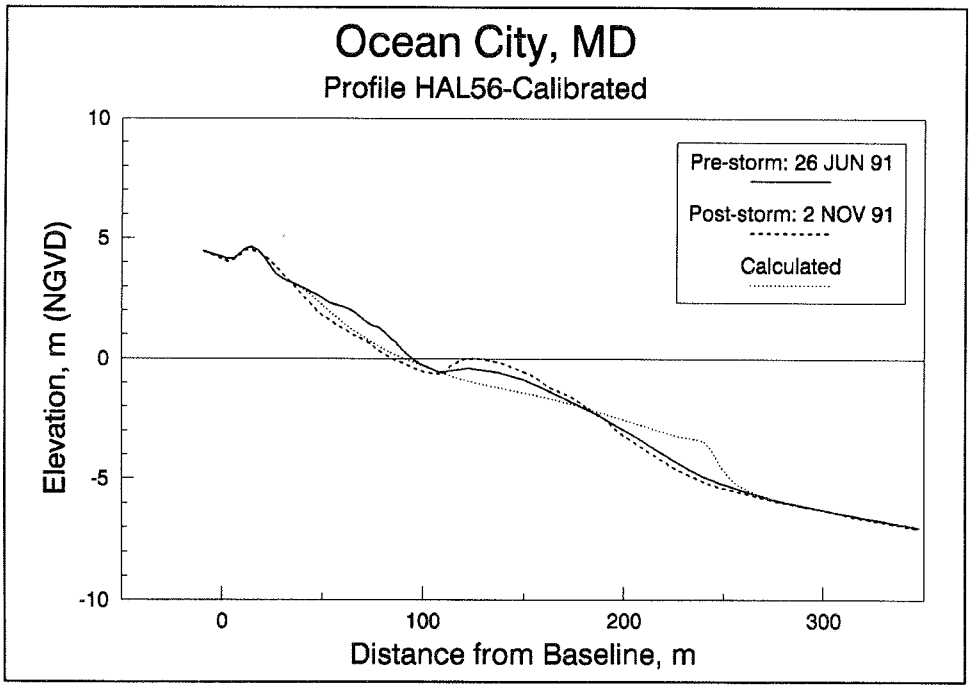

Figure B6. Result of calibrated simulation of the Halloween storm for profile 56, Ocean City, MD (model calibrated to case OJ81)

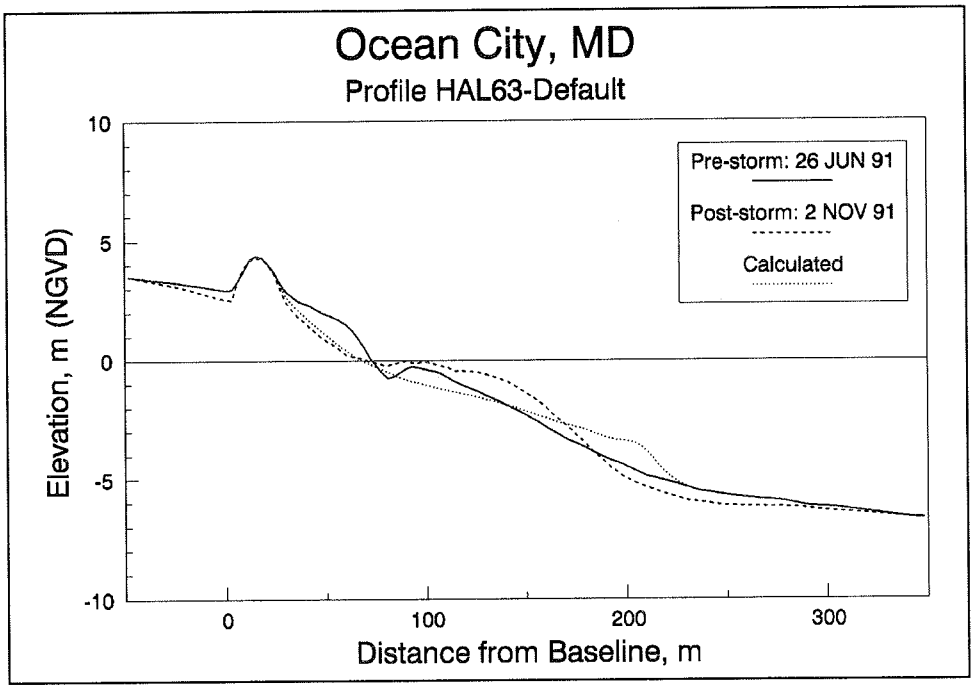

Figure B7. Result of default simulation of the Halloween storm for profile 63, Ocean City, MD

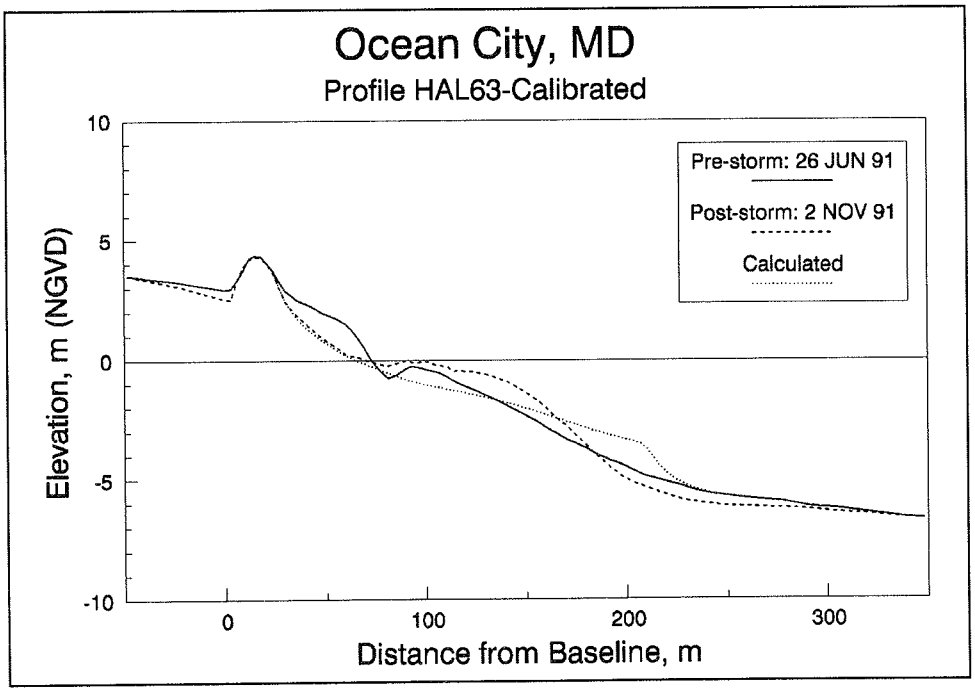

Figure B8. Result of calibrated simulation of the Halloween storm for profile 63, Ocean City, MD (model calibrated to case OJ81)

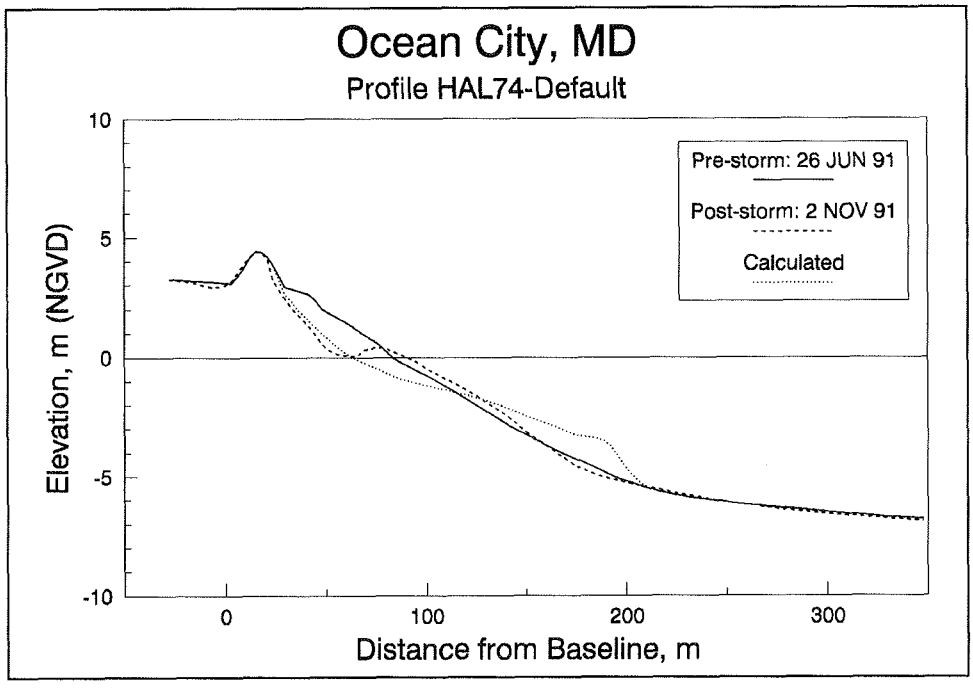

Figure B9. Result of default simulation of the Halloween storm for profile 74, Ocean City, MD

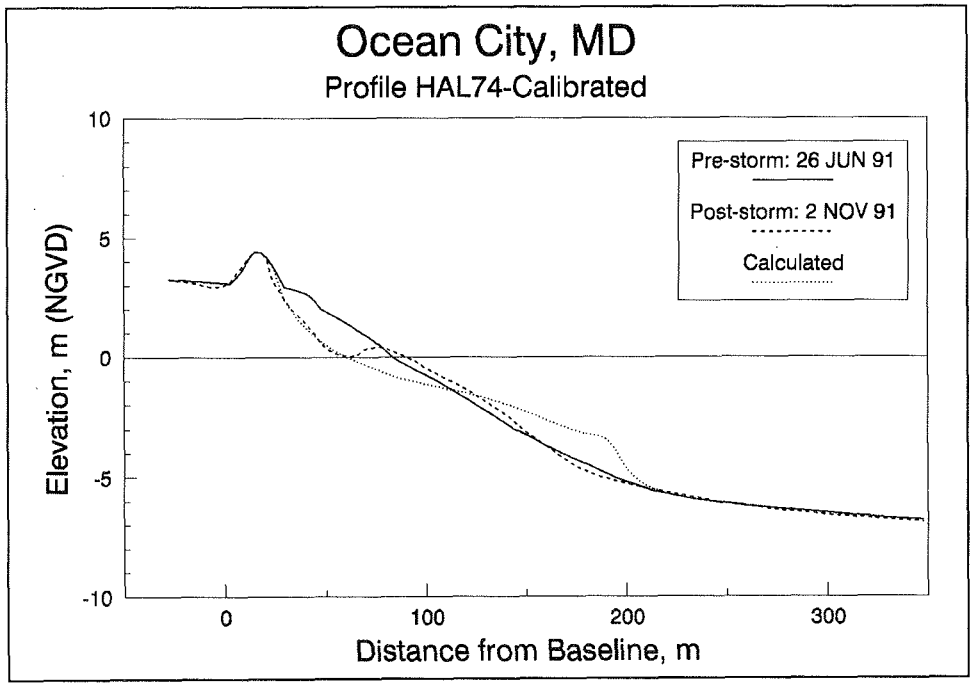

Figure B10. Result of calibrated simulation of the Halloween storm for profile 74, Ocean City, MD (model calibrated to case OJ81)

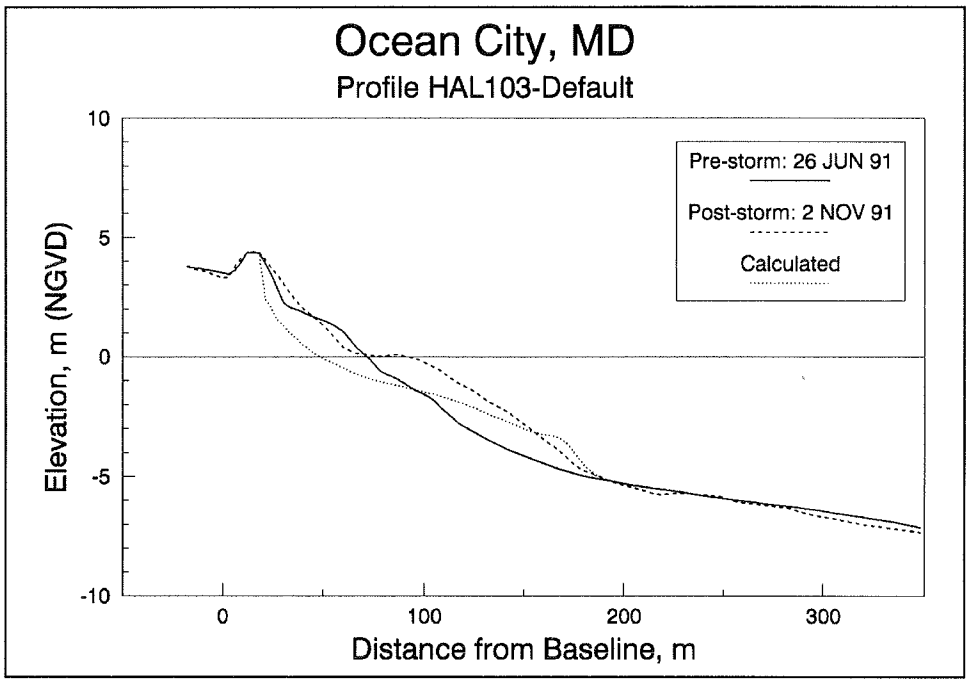

Figure B11. Result of default simulation of the Halloween storm for profile 103, Ocean City, MD

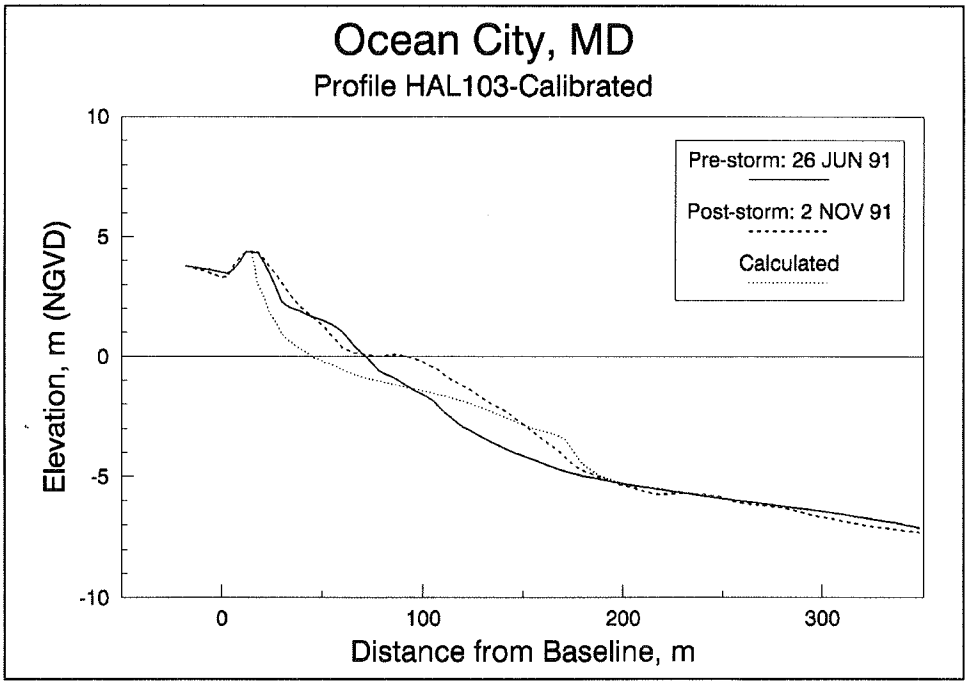

Figure B12. Result of calibrated simulation of the Halloween storm for profile 103, Ocean City, MD (model calibrated to case OJ81)

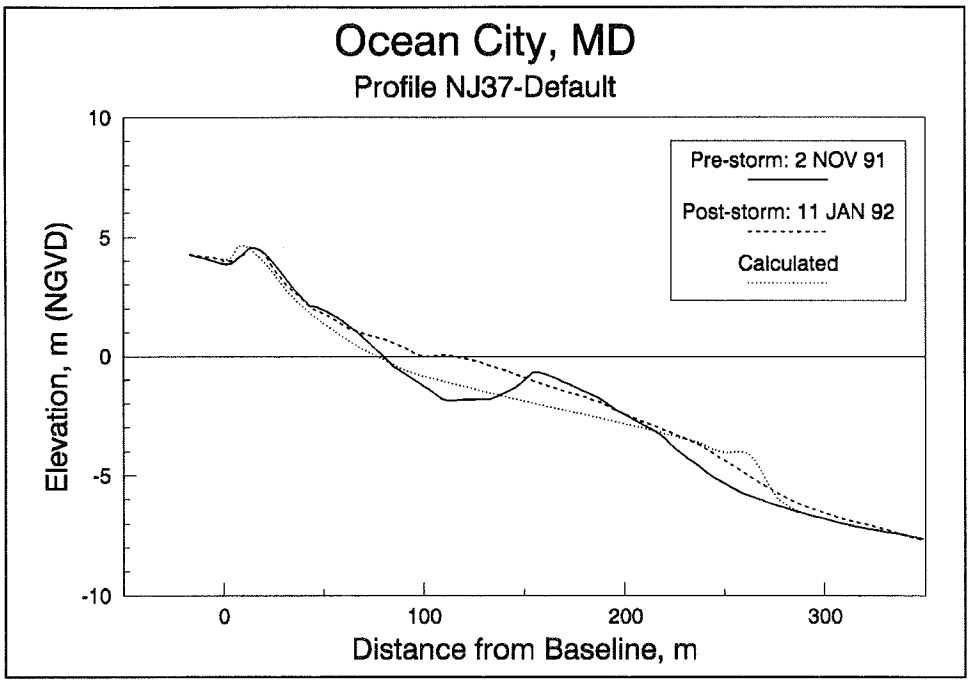

Figure B13. Result of default simulation of the NJ storm series for profile 37, Ocean City, MD

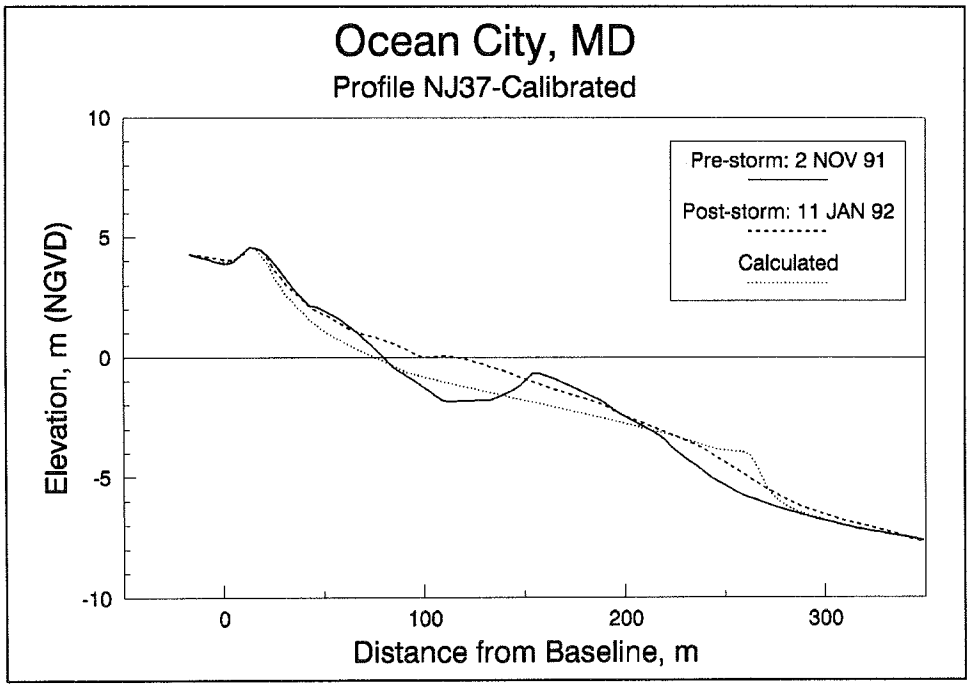

Figure B14. Result of calibrated simulation of the NJ storm series for profile 37, Ocean City, MD (model calibrated to case OJ81)

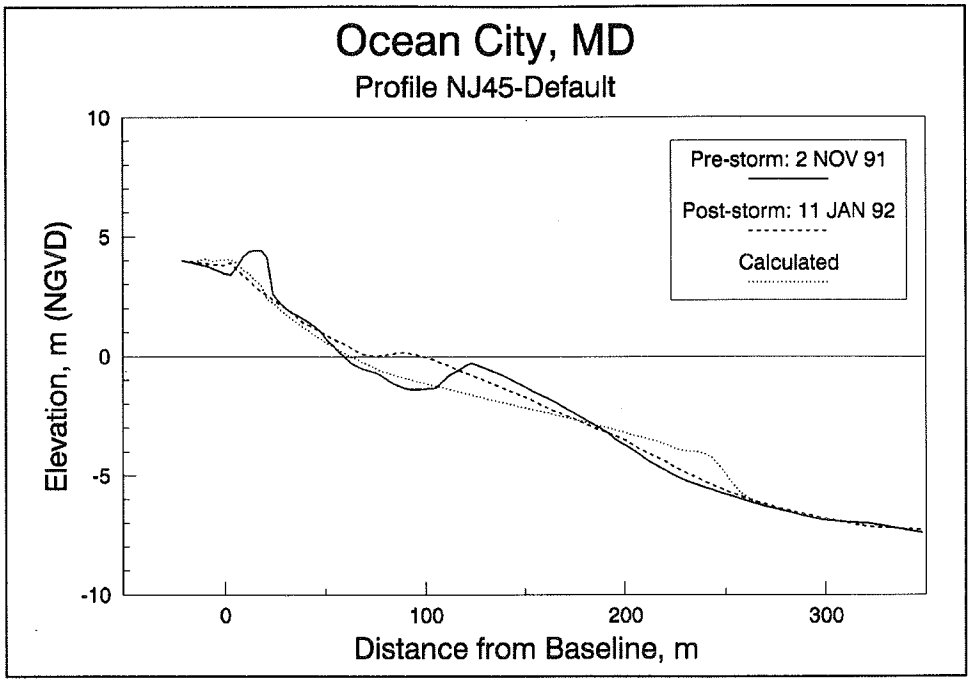

Figure B15. Result of default simulation of the NJ storm series for profile 45, Ocean City, MD

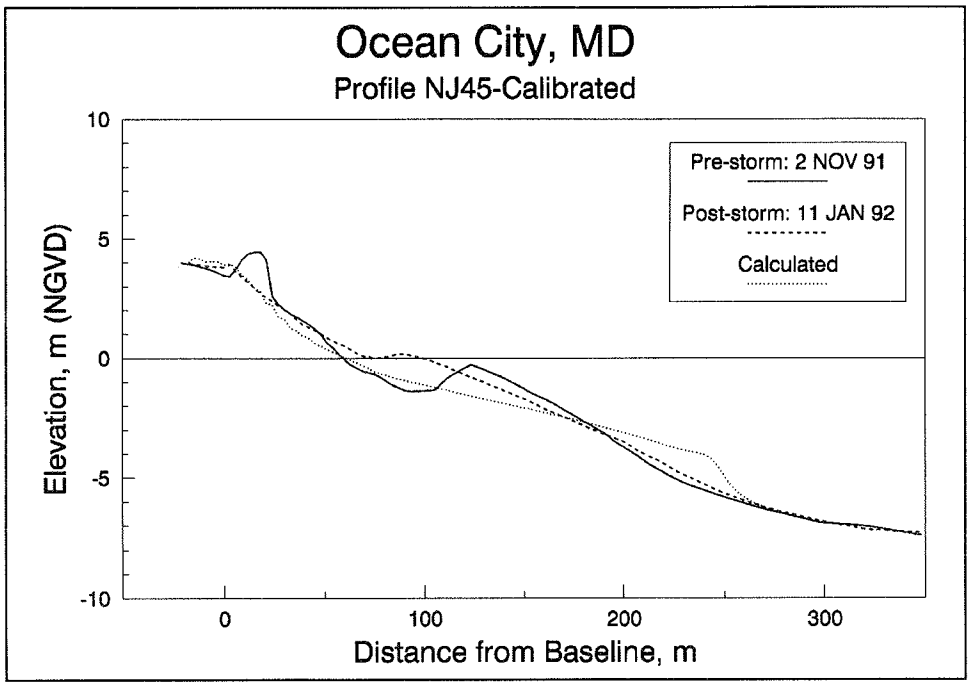

Figure B16. Result of calibrated simulation of the NJ storm series for profile 45, Ocean City, MD (model calibrated to case OJ81)

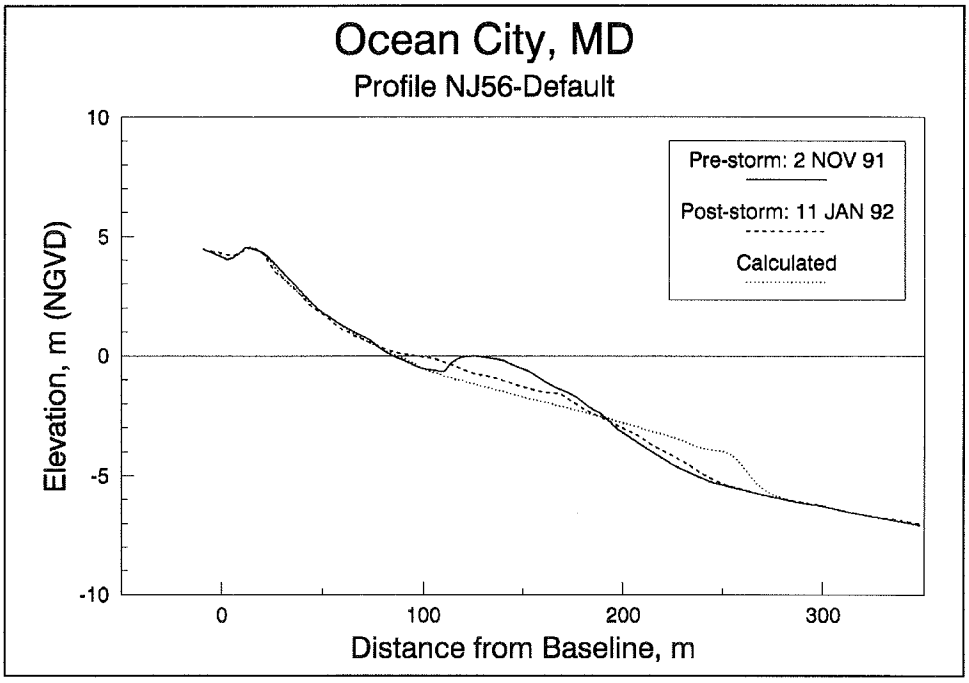

Figure B17. Result of default simulation of the NJ storm series for profile 56, Ocean City, MD

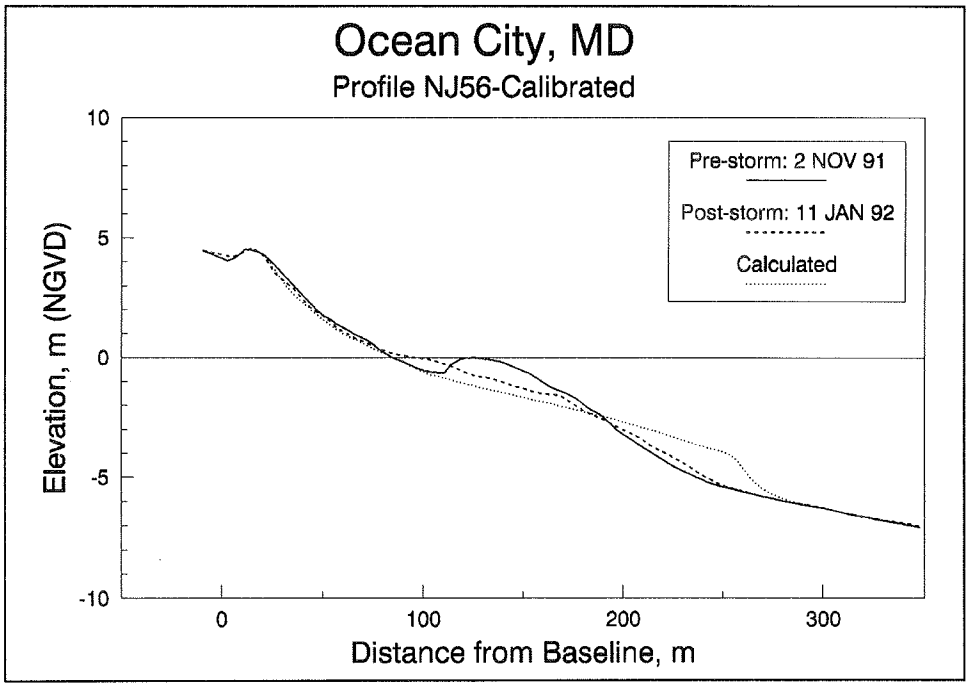

Figure B18. Result of calibrated simulation of the NJ storm series for profile 56, Ocean City, MD (model calibrated to case OJ81)

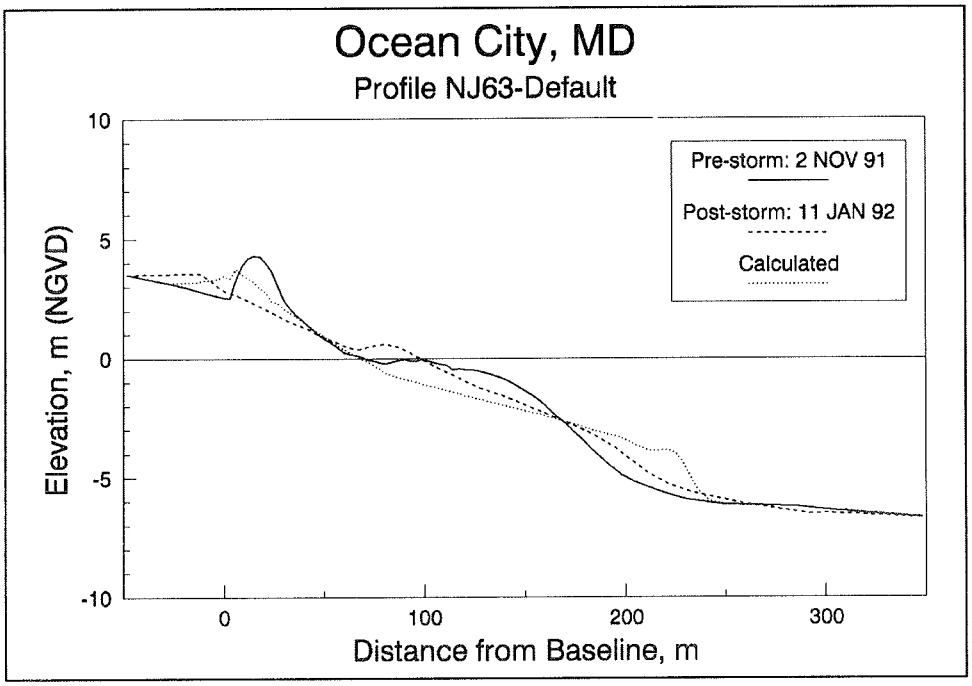

Figure B19. Result of default simulation of the NJ storm series for profile 63, Ocean City, MD

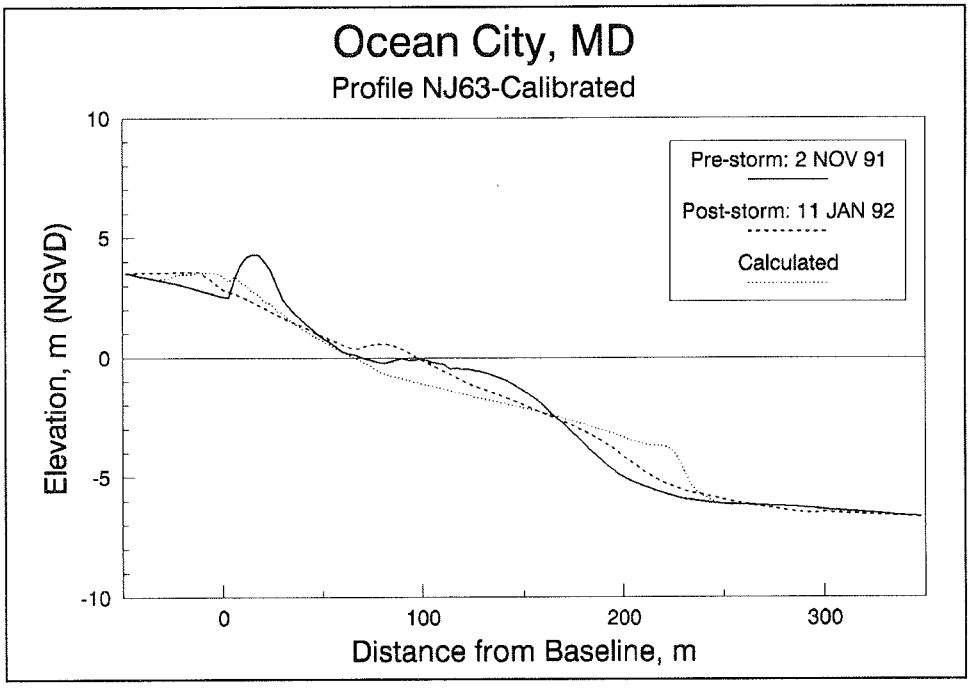

Figure B20. Result of calibrated simulation of the NJ storm series for profile 63, Ocean City, MD (model calibrated to case OJ81)

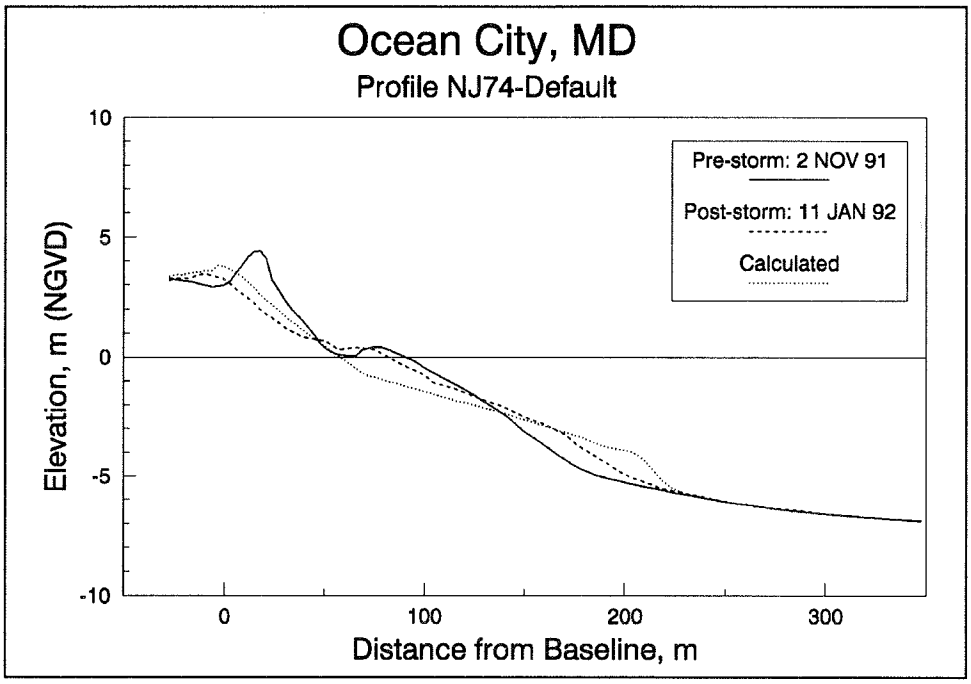

Figure B21. Result of default simulation of the NJ storm series for profile 74, Ocean City, MD

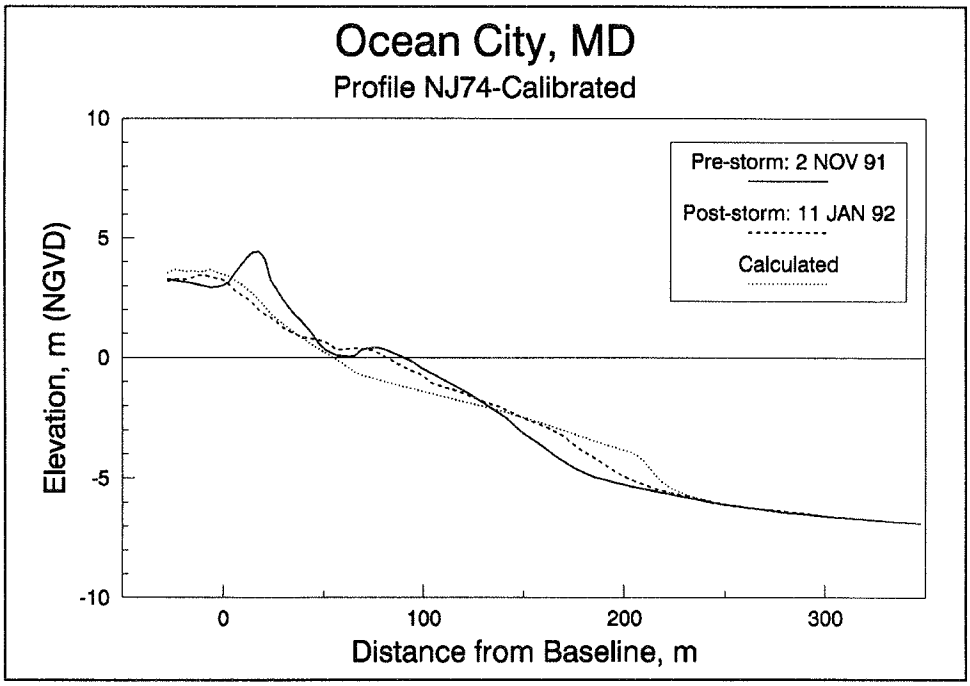

Figure B22. Result of calibrated simulation of the NJ storm series for profile 74, Ocean City, MD (model calibrated to case OJ81)

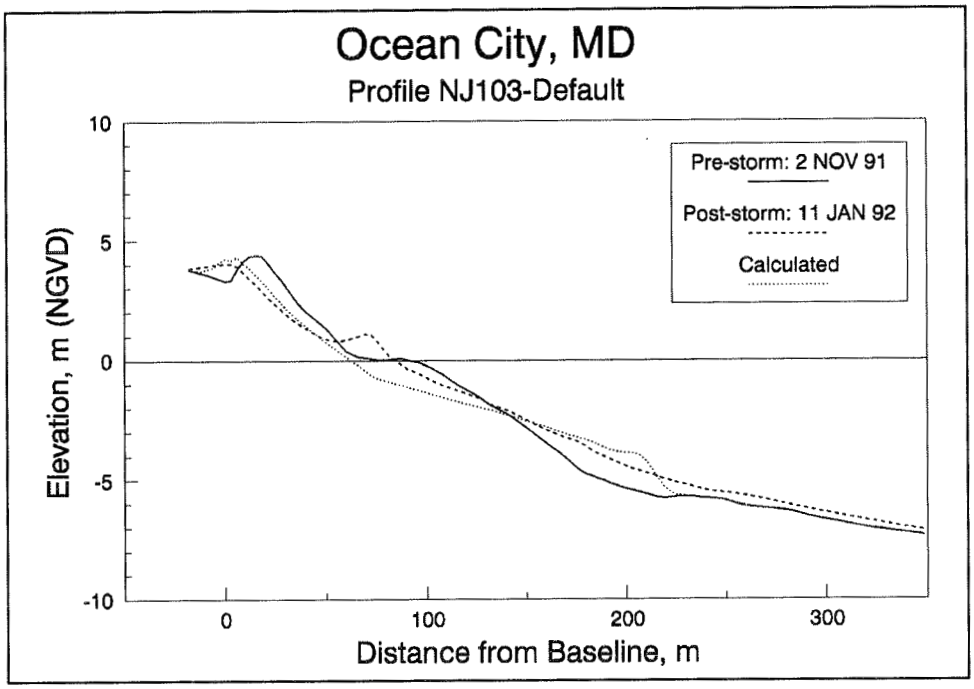

Figure B23. Result of default simulation of the NJ storm series for profile 103, Ocean City, MD

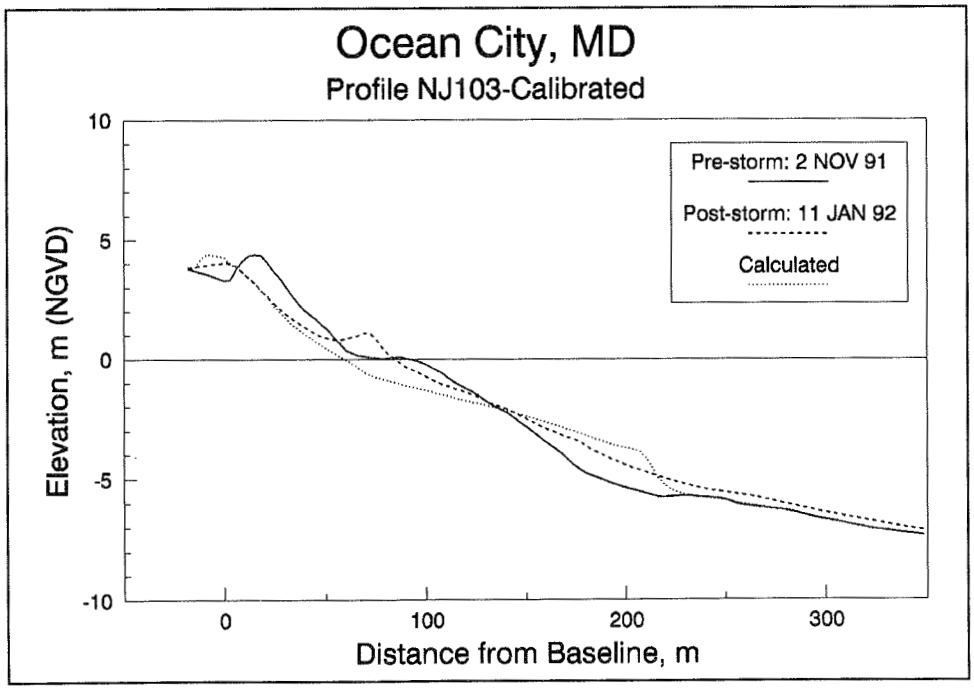

Figure B24. Result of calibrated simulation of the NJ storm series for profile 103, Ocean City, MD (model calibrated to case OJ81)

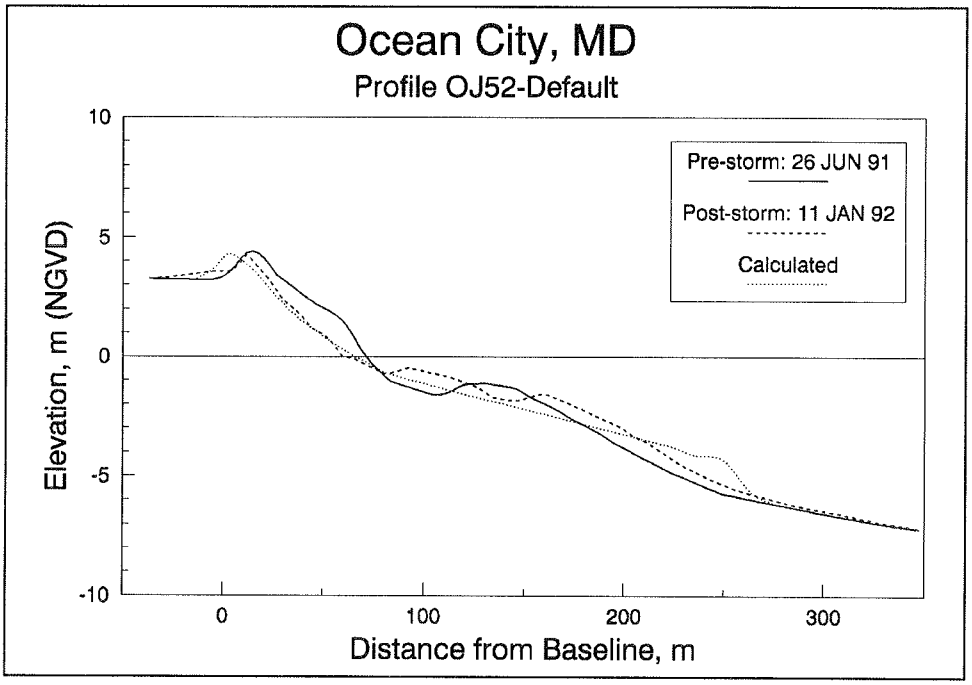

Figure B25. Result of default simulation of the OJ storm series for profile 52, Ocean City, MD

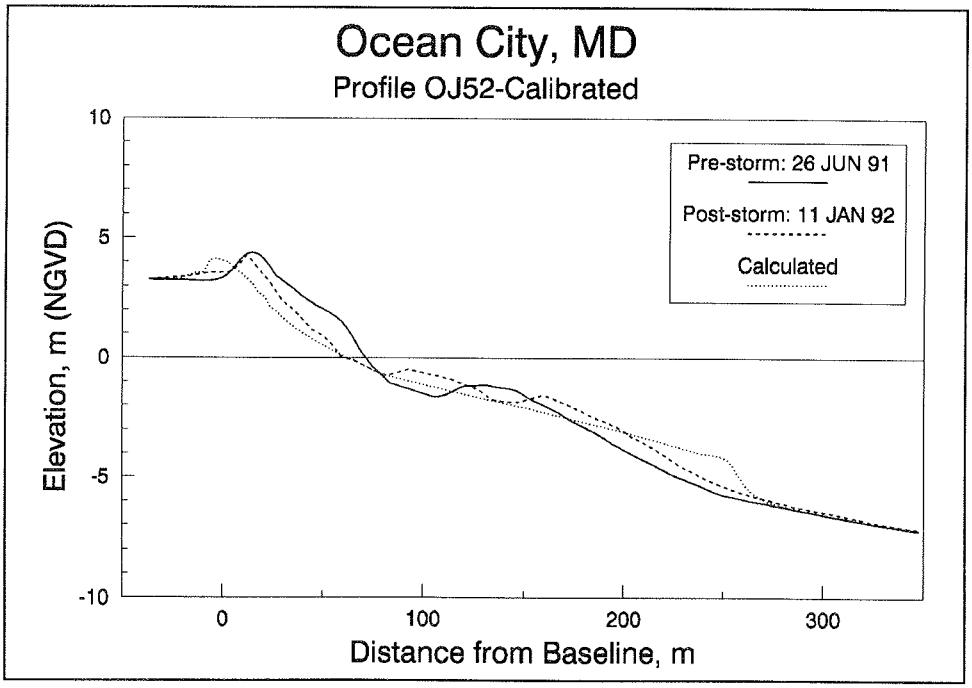

Figure B26. Result of calibrated simulation of the OJ storm series for profile 52, Ocean City, MD (model calibrated to case OJ81)

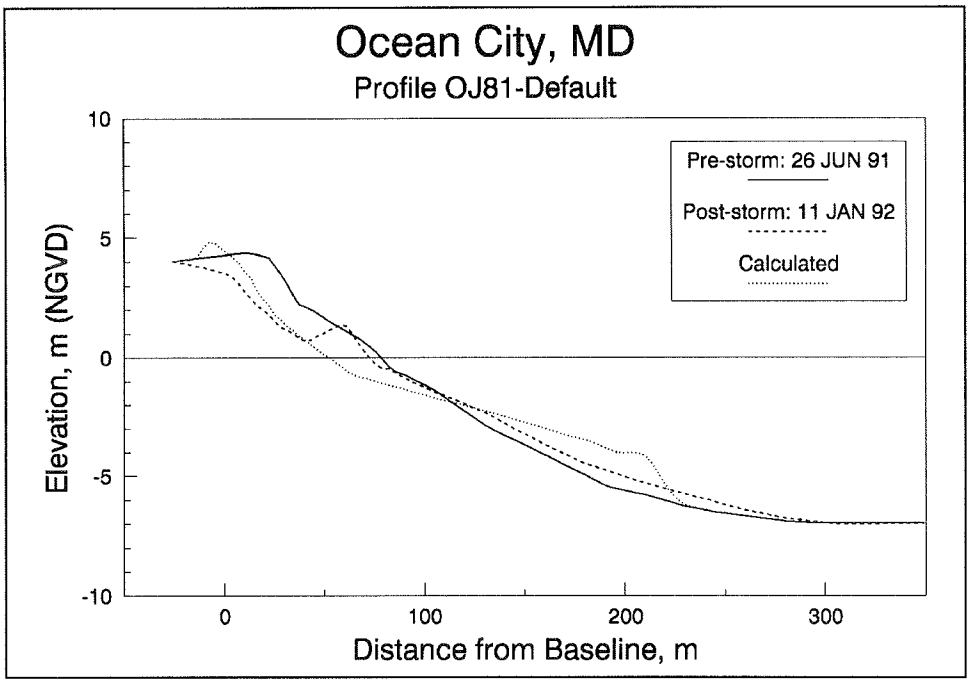

Figure B27. Result of default simulation of the OJ storm series for profile 81, Ocean City, MD

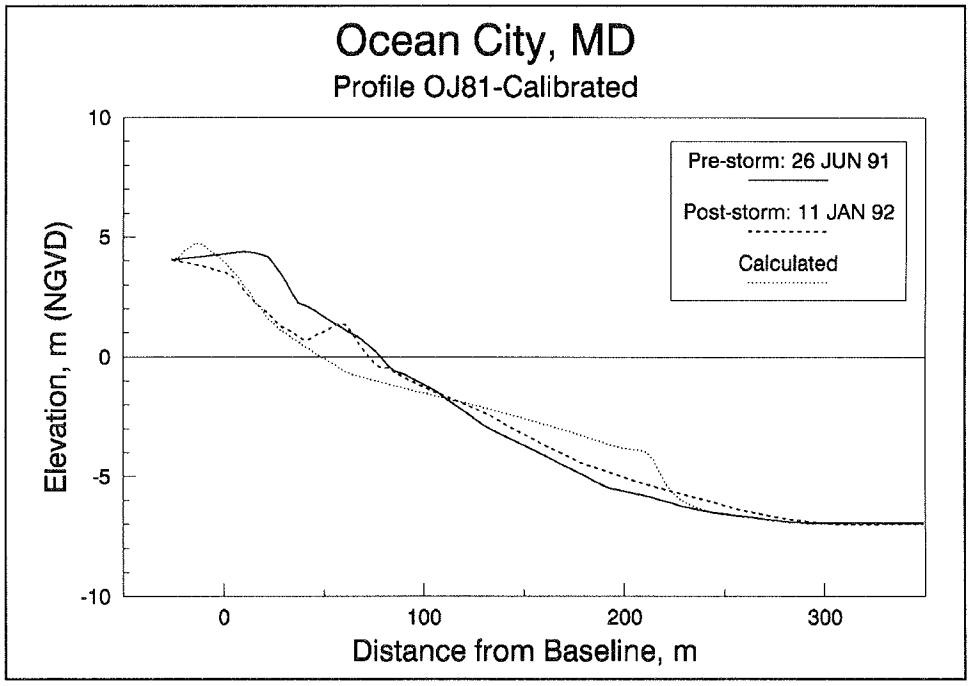

Figure B28. Result of calibrated simulation of the OJ storm series for profile 81, Ocean City, MD (model calibrated to case OJ81)

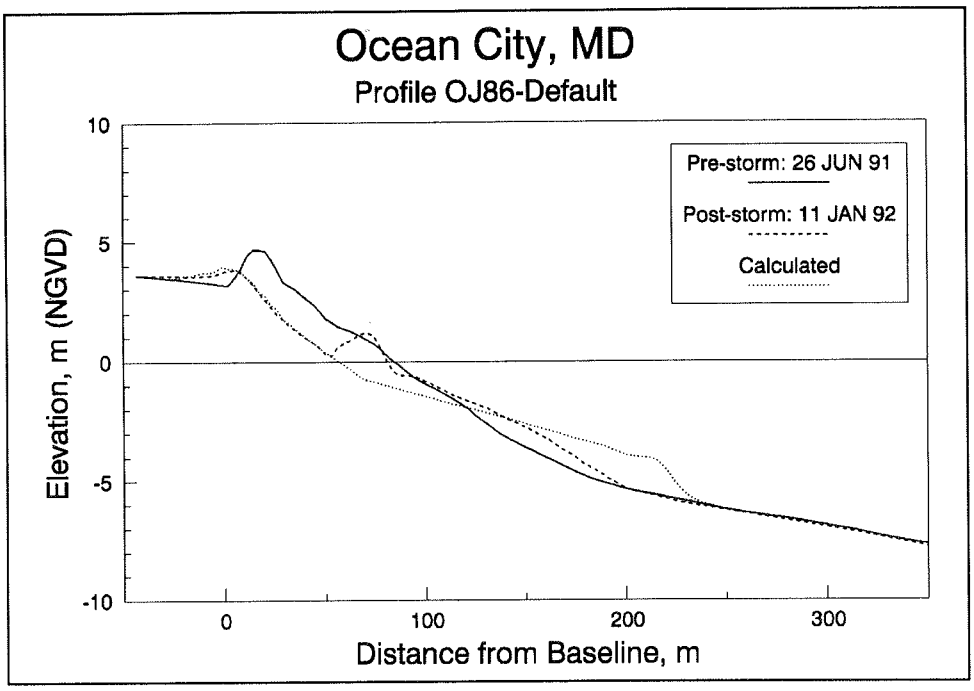

Figure B29. Result of default simulation of the OJ storm series for profile 86, Ocean City, MD

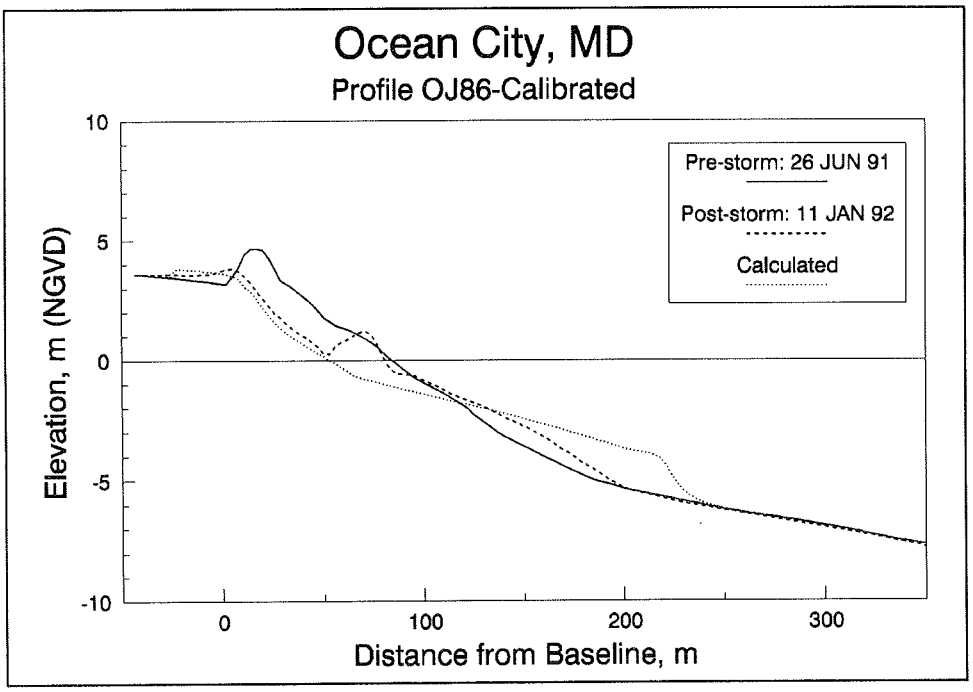

Figure B30. Result of calibrated simulation of the OJ storm series for profile 86, Ocean City, MD (model calibrated to case OJ81)

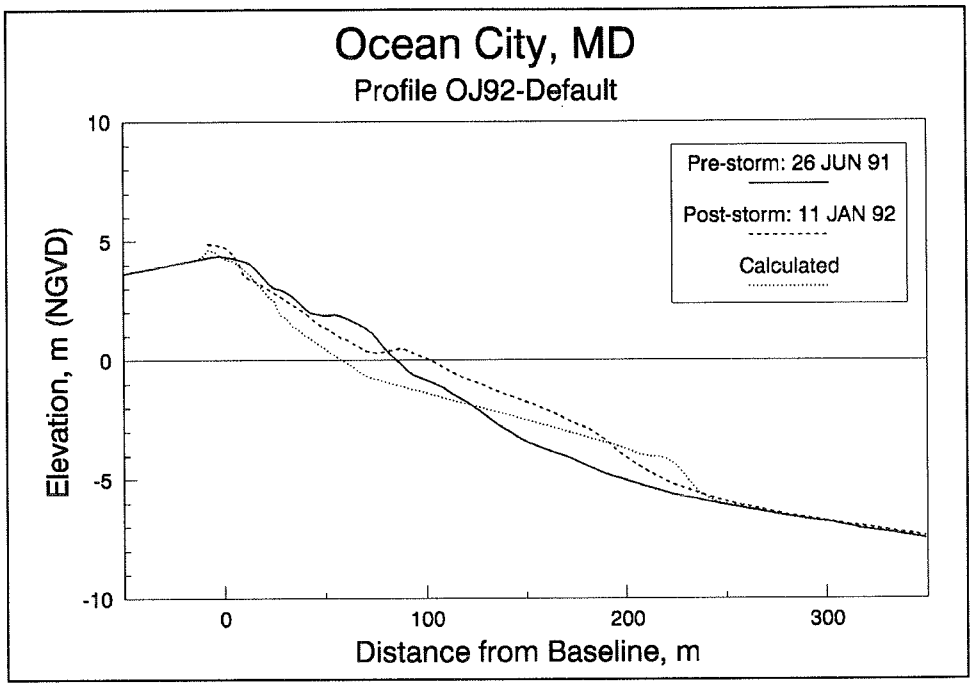

Figure B31. Result of default simulation of the OJ storm series for profile 92, Ocean City, MD

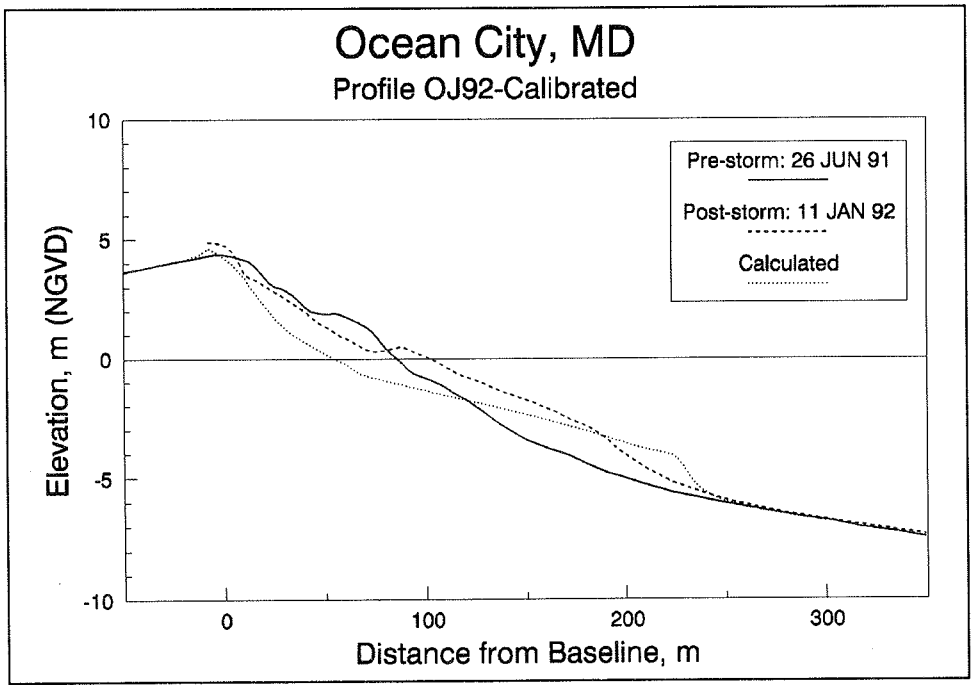

Figure B32. Result of calibrated simulation of the OJ storm series for profile 92, Ocean City, MD (model calibrated to case OJ81)

Manasquan and Point Pleasant Beach, NJ

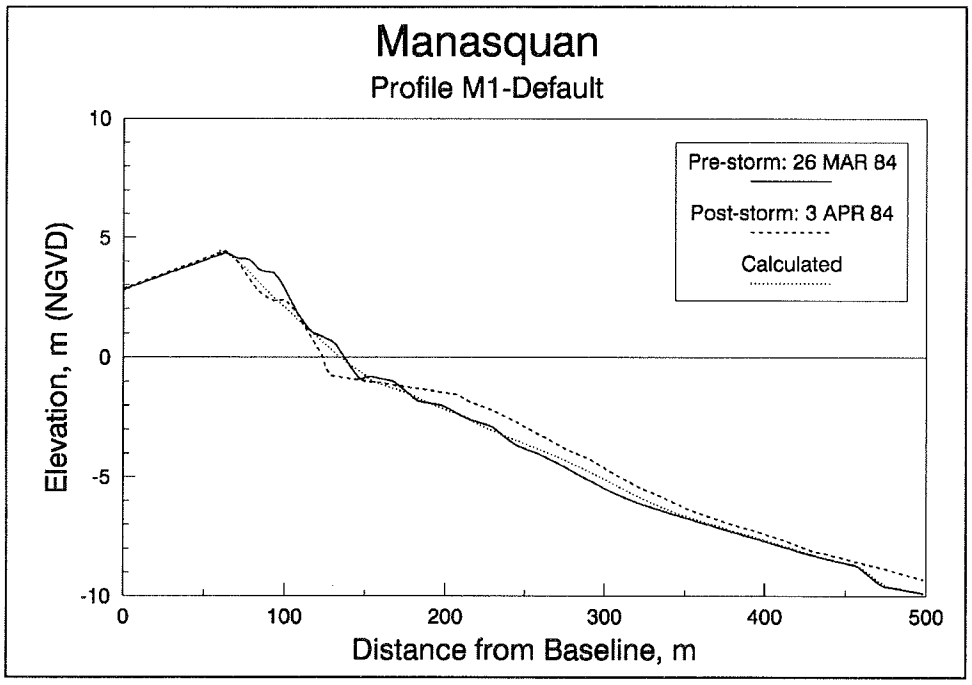

Figure B33. Result of default simulation of the March 1984 storm for profile M1, Manasquan, NJ

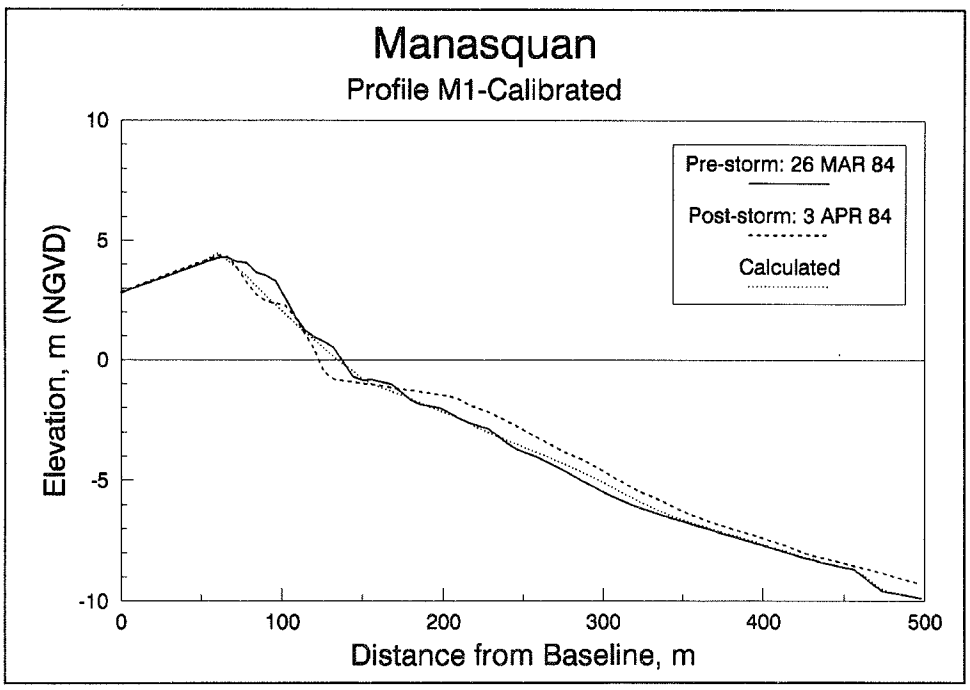

Figure B34. Result of calibrated simulation of the March 1984 storm for profile M1, Manasquan, NJ (model calibrated to case M5)

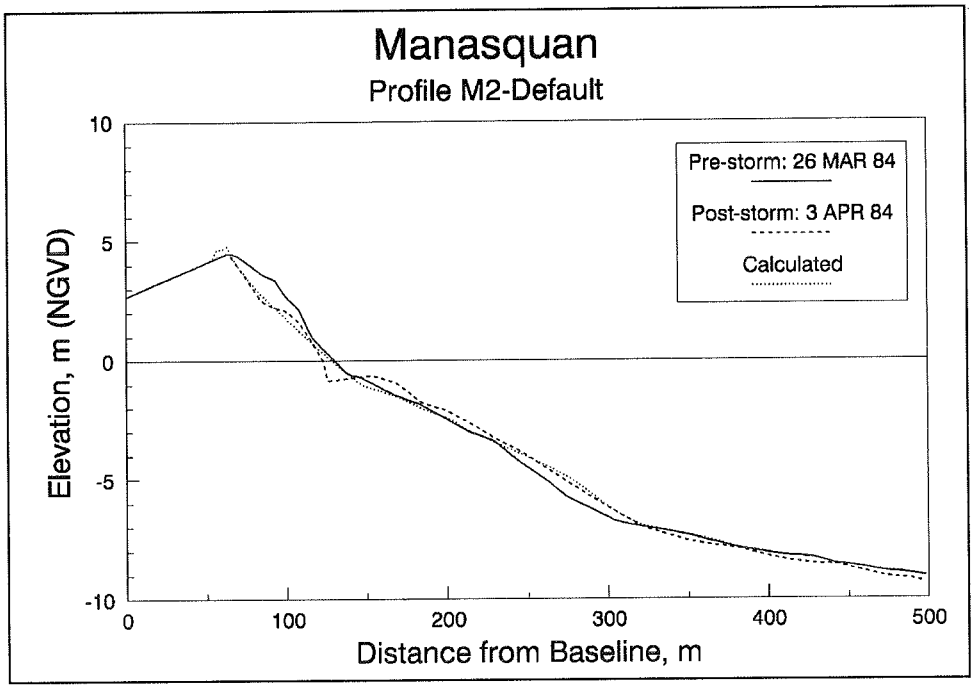

Figure B35. Result of default simulation of the March 1984 storm for profile M2, Manasquan, NJ

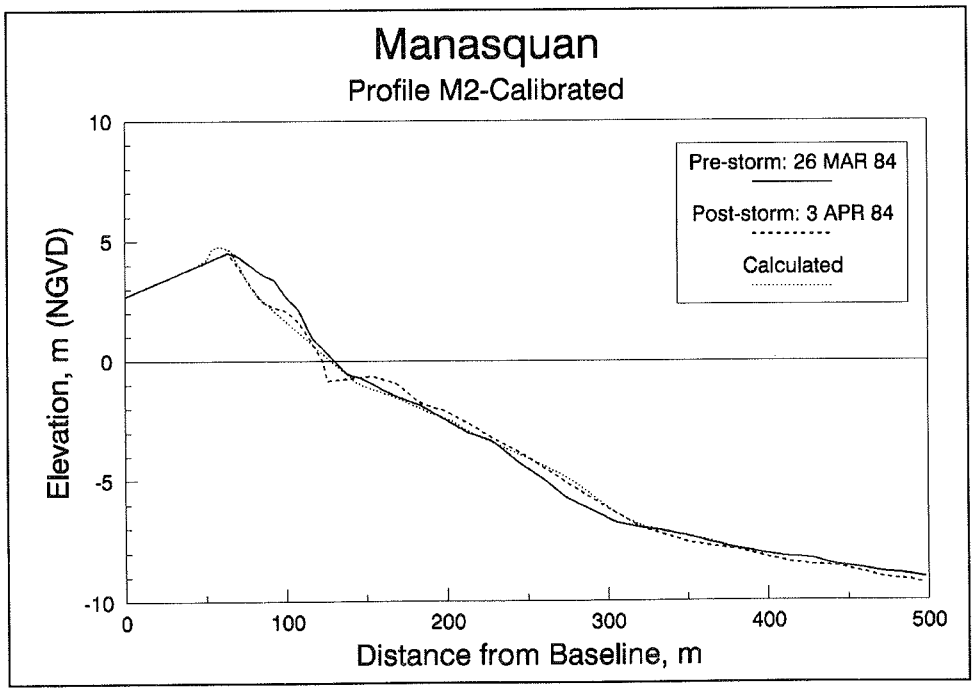

Figure B36. Result of calibrated simulation of the March 1984 storm for profile M2, Manasquan, NJ (model calibrated to case M5)

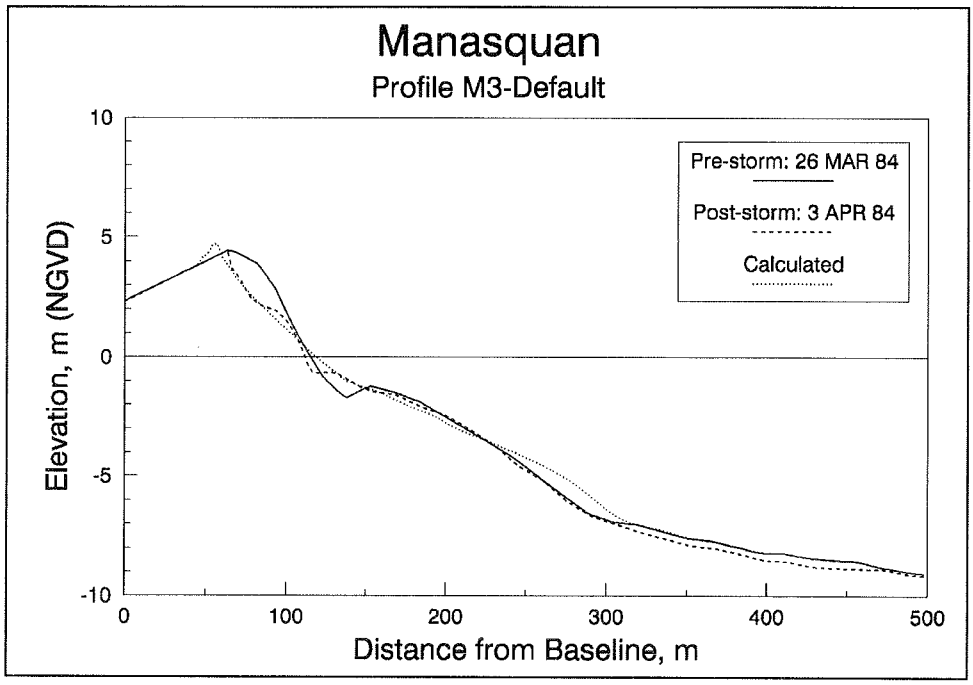

Figure B37. Result of default simulation of the March 1984 storm for profile M3, Manasquan, NJ

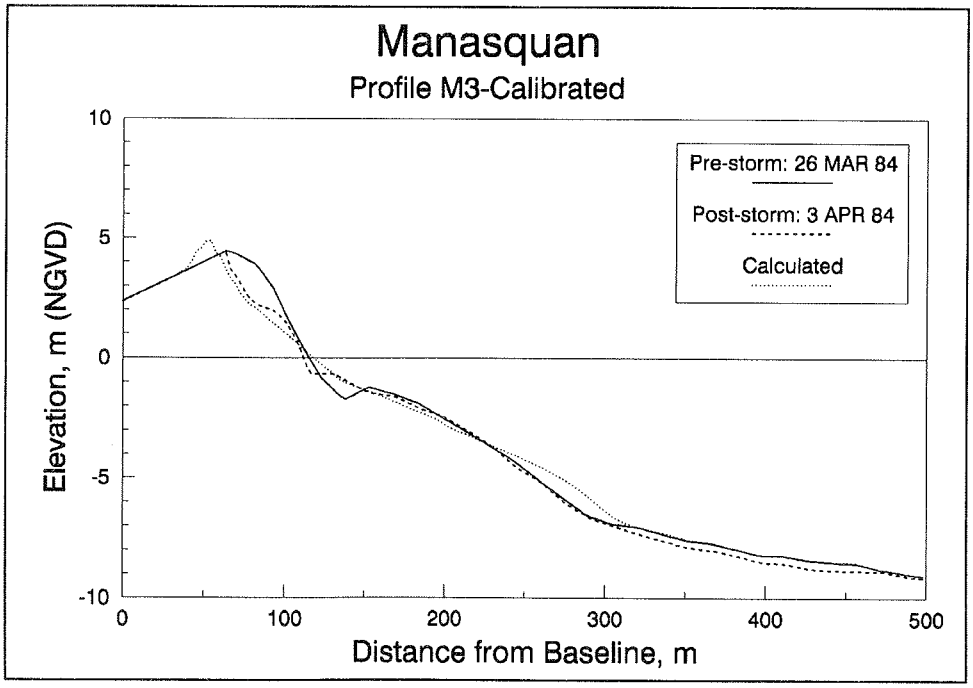

Figure B38. Result of calibrated simulation of the March 1984 storm for profile M3, Manasquan, NJ (model calibrated to case M5)

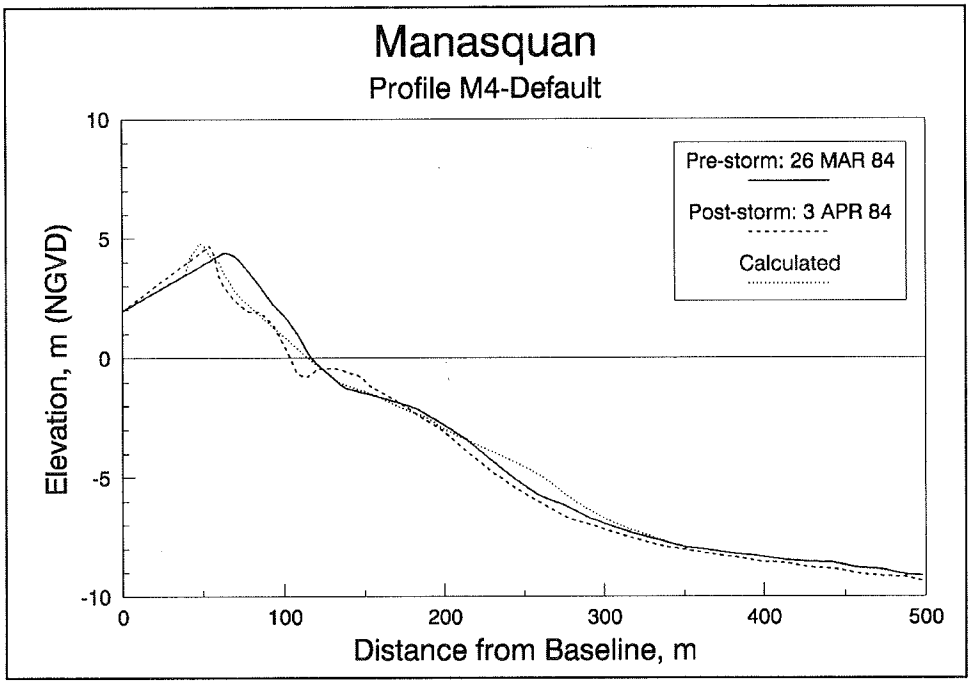

Figure B39. Result of default simulation of the March 1984 storm for profile M4, Manasquan, NJ

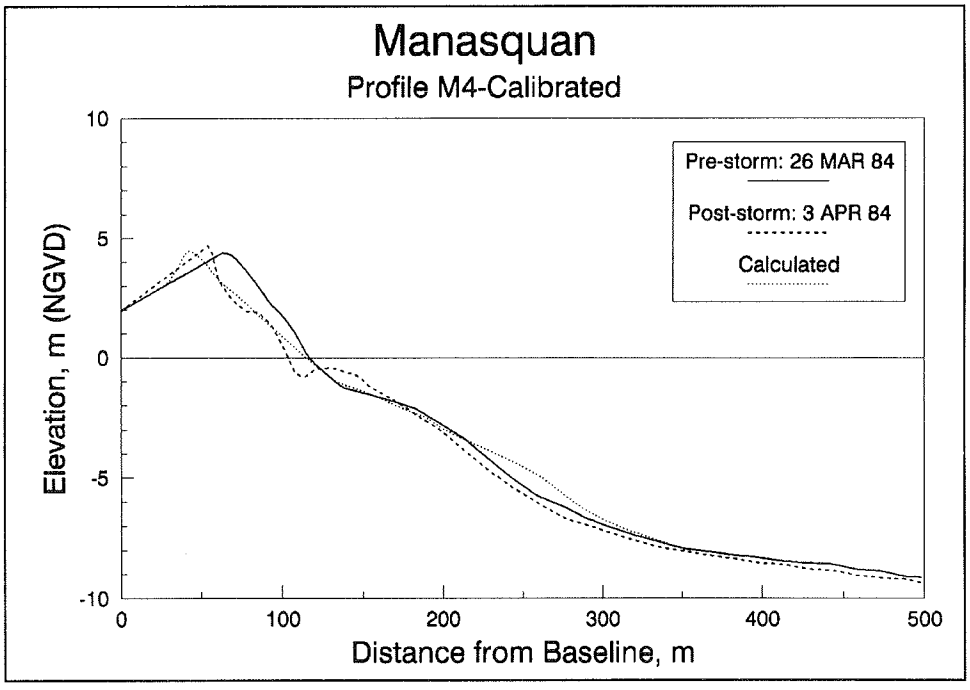

Figure B40. Result of calibrated simulation of the March 1984 storm for profile M4, Manasquan, NJ (model calibrated to case M5)

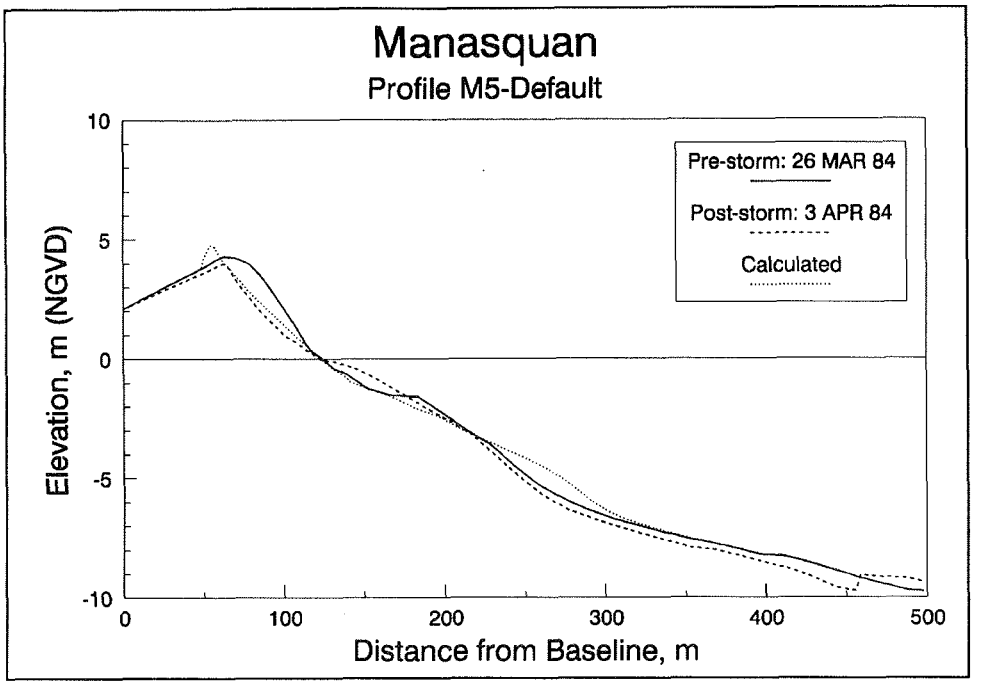

Figure B41. Result of default simulation of the March 1984 storm for profile M5, Manasquan, NJ

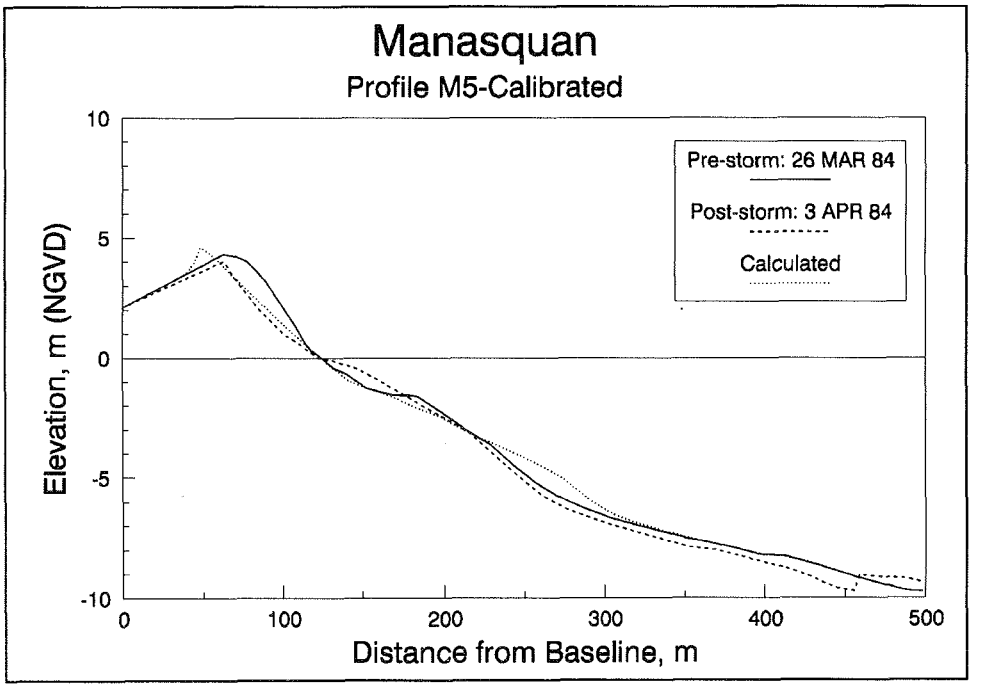

Figure B42. Result of calibrated simulation of the March 1984 storm for profile M5, Manasquan, NJ (model calibrated to case M5)

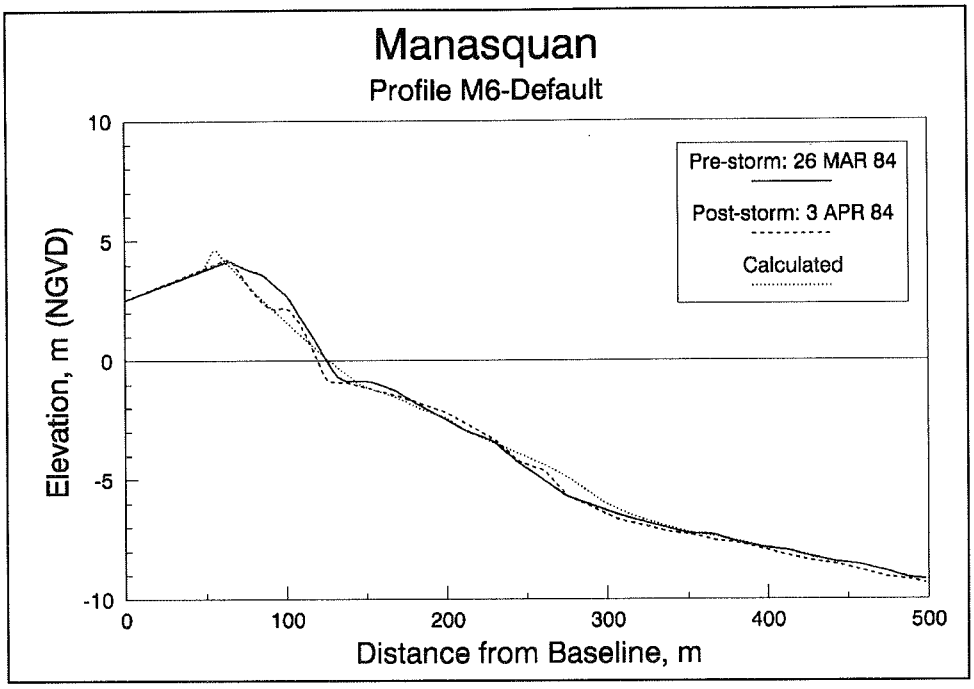

Figure B43. Result of default simulation of the March 1984 storm for profile M6, Manasquan, NJ

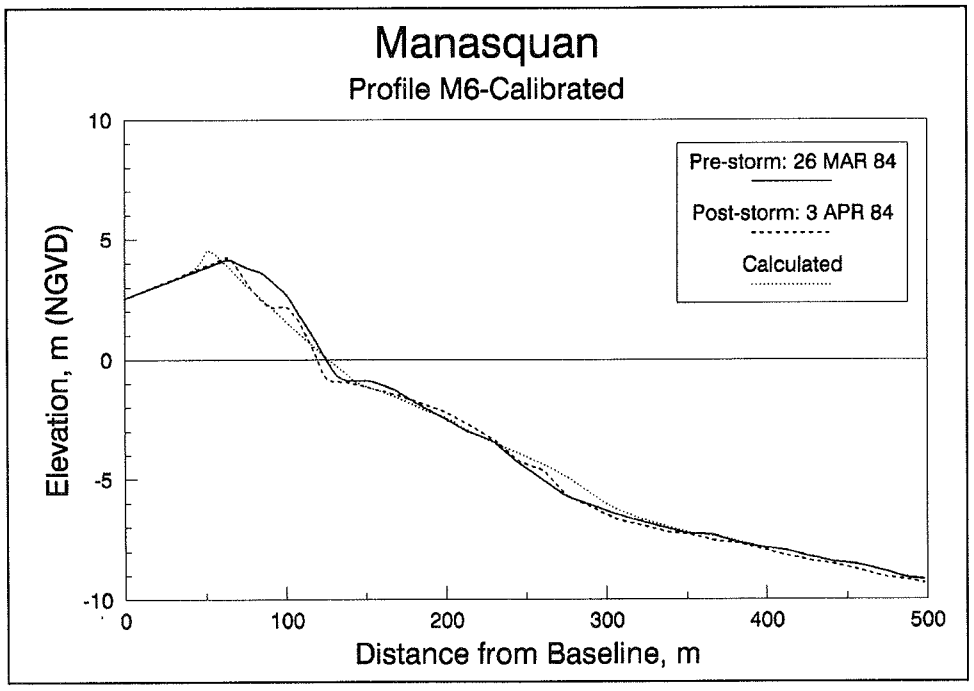

Figure B44. Result of calibrated simulation of the March 1984 storm for profile M6, Manasquan, NJ (model calibrated to case M5)

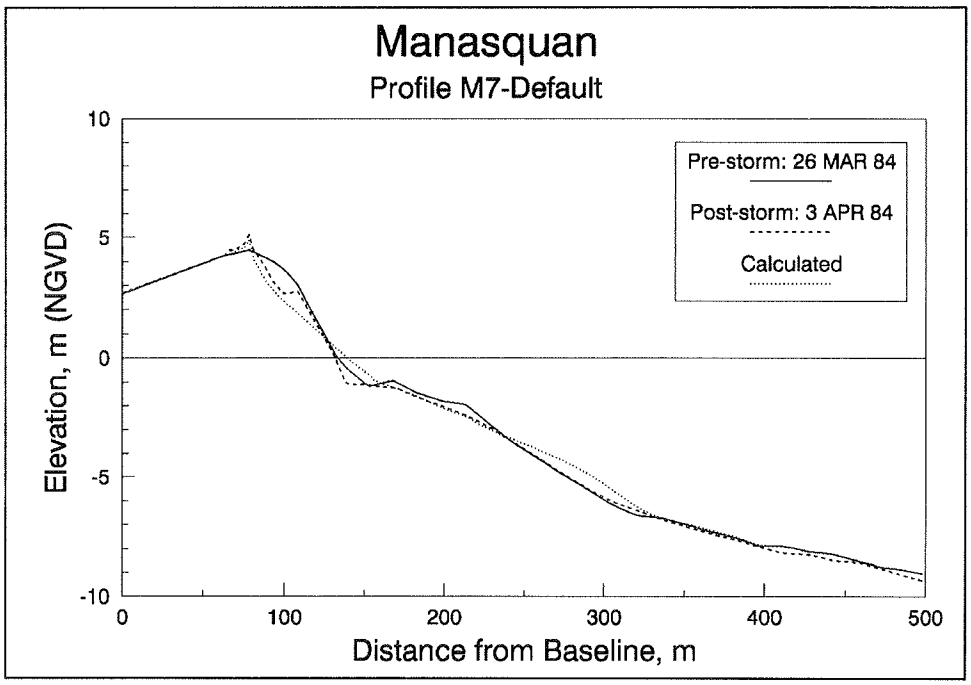

Figure B45. Result of default simulation of the March 1984 storm for profile M7, Manasquan, NJ

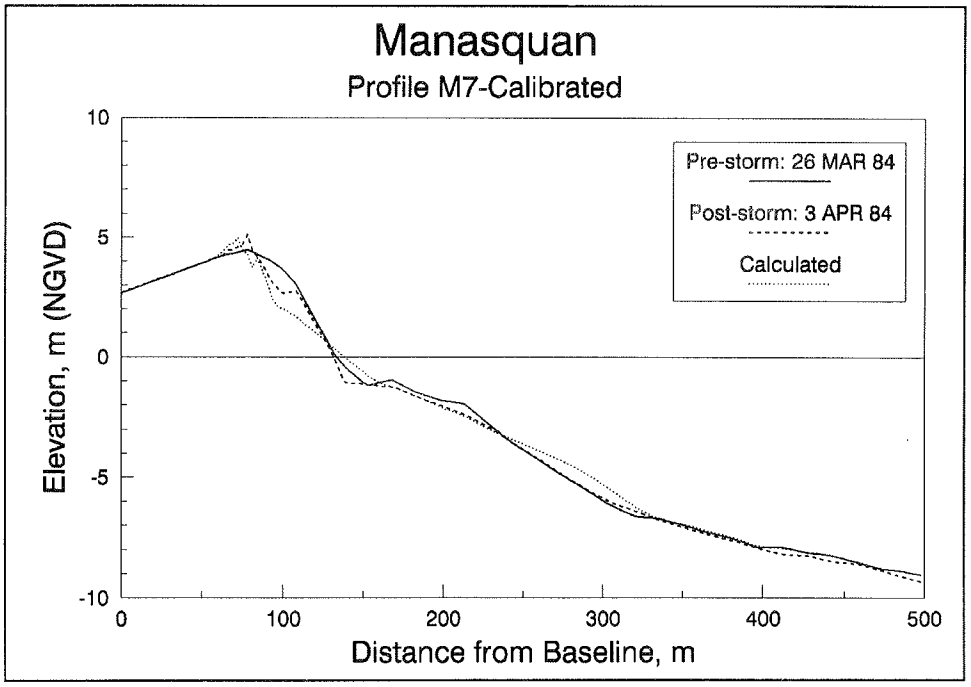

Figure B46. Result of calibrated simulation of the March 1984 storm for profile M7, Manasquan, NJ (model calibrated to case M5)

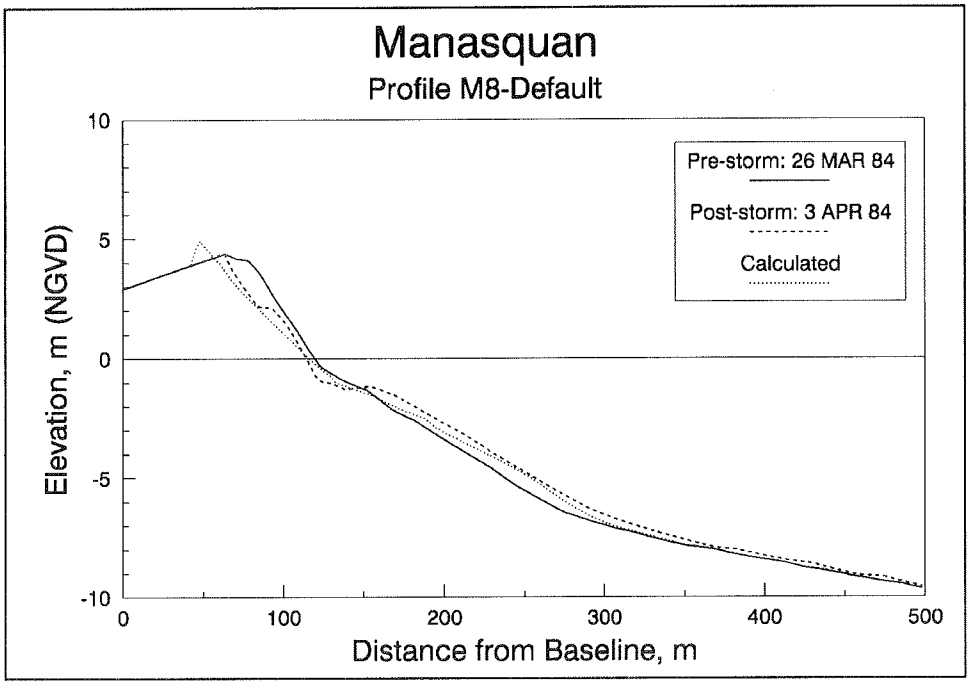

Figure B47. Result of default simulation of the March 1984 storm for profile M8, Manasquan, NJ

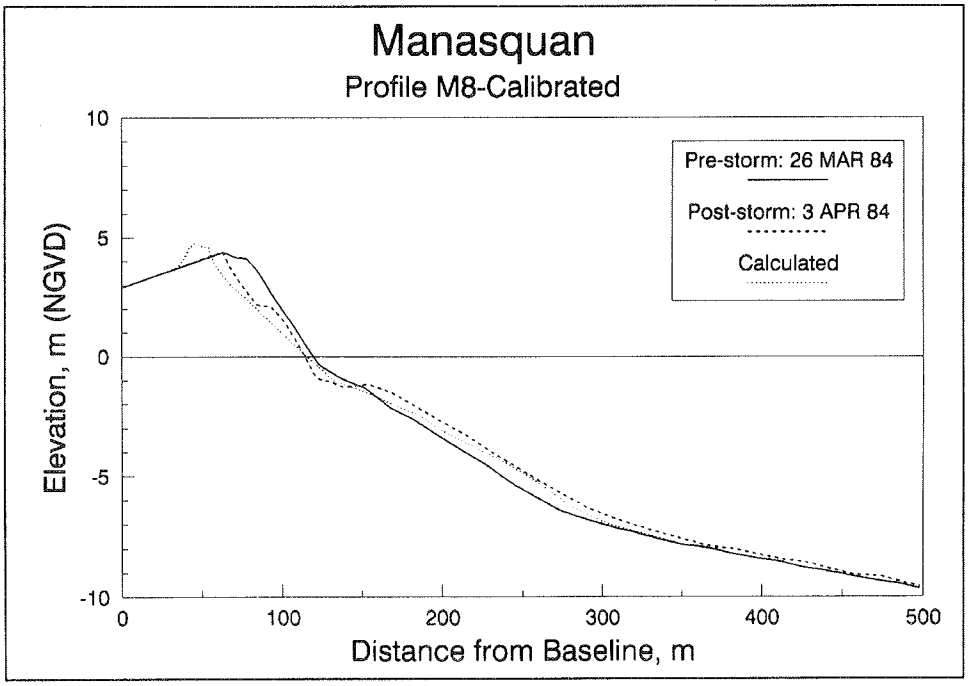

Figure B48. Result of calibrated simulation of the March 1984 storm for profile M8, Manasquan, NJ (model calibrated to case M5)

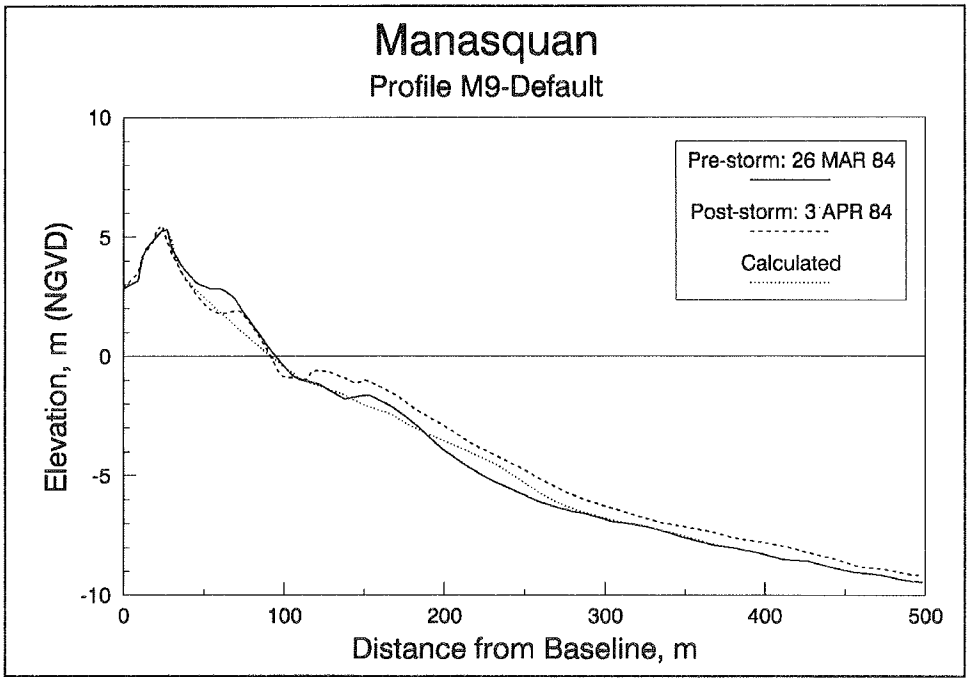

Figure B49. Result of default simulation of the March 1984 storm for profile M9, Manasquan, NJ

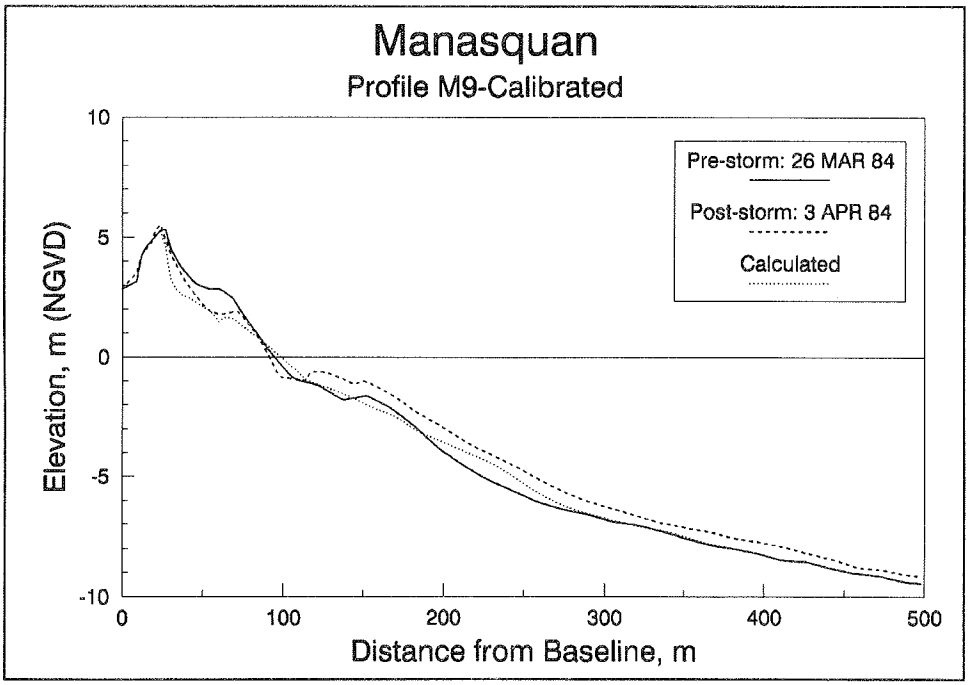

Figure B50. Result of calibrated simulation of the March 1984 storm for profile M9, Manasquan, NJ (model calibrated to case M5)

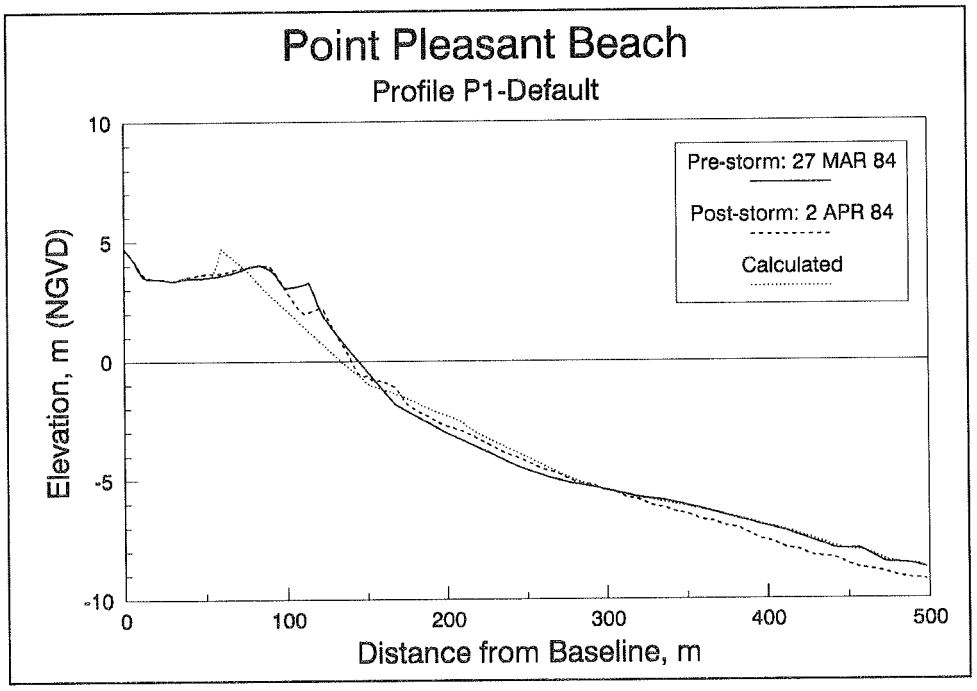

Figure B51. Result of default simulation of the March 1984 storm for profile P1, Point Pleasant Beach, NJ

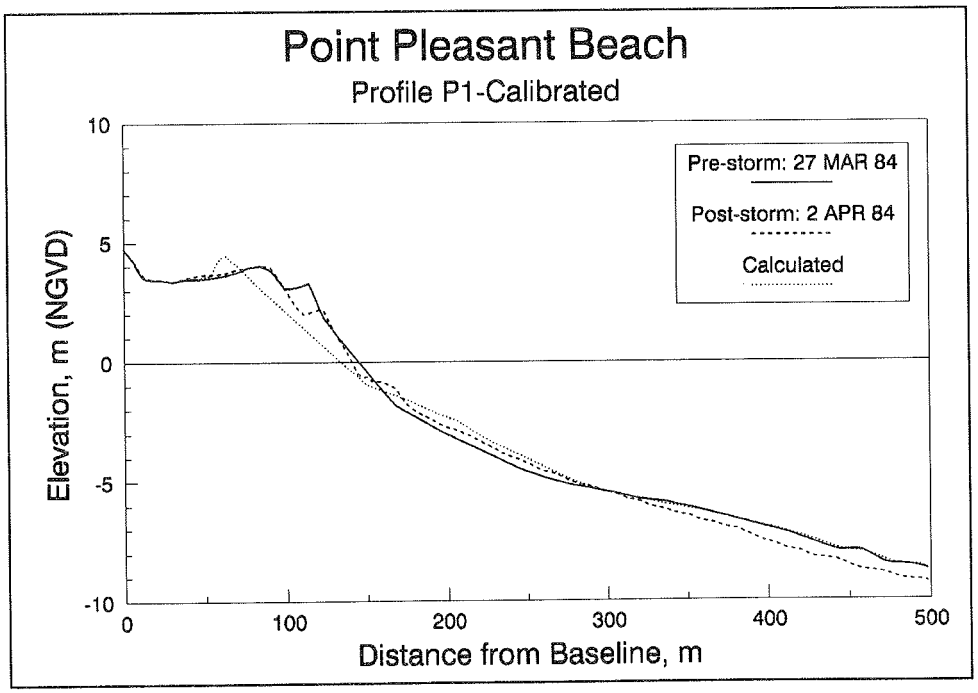

Figure B52. Result of calibrated simulation of the March 1984 storm for profile P1, Point Pleasant Beach, NJ (model calibrated to case M5)

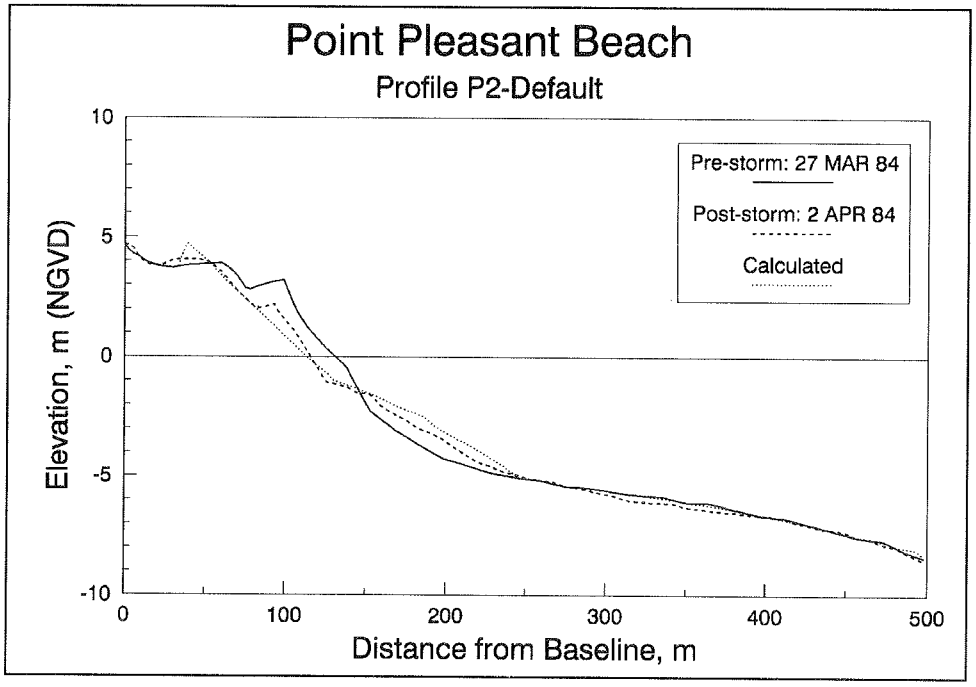

Figure B53. Result of default simulation of the March 1984 storm for profile P2, Point Pleasant Beach, NJ

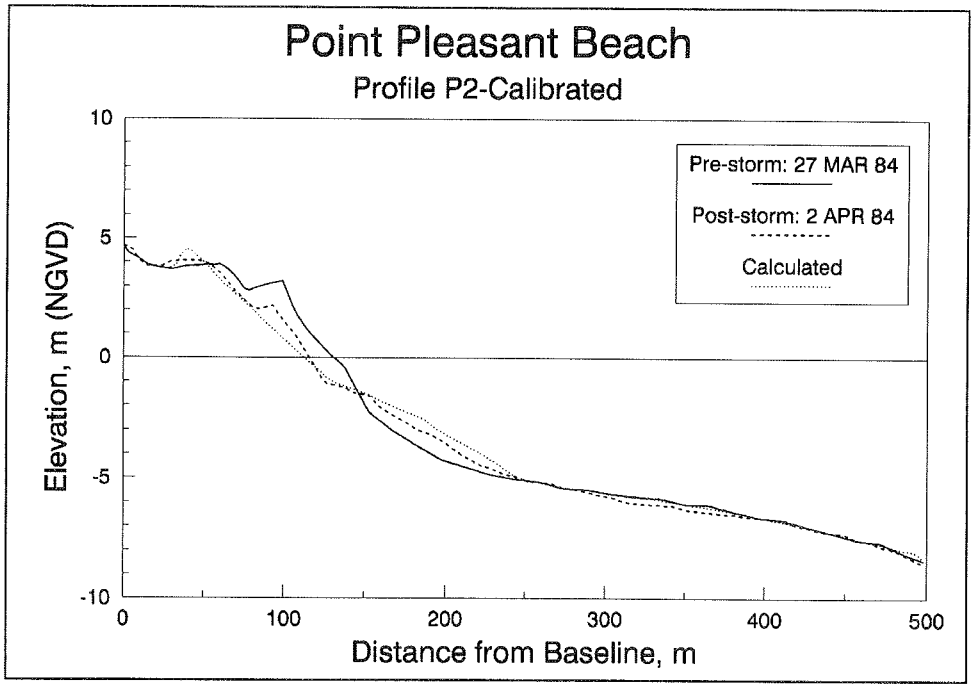

Figure B54. Result of calibrated simulation of the March 1984 storm for profile P2, Point Pleasant Beach, NJ (model calibrated to case M5)

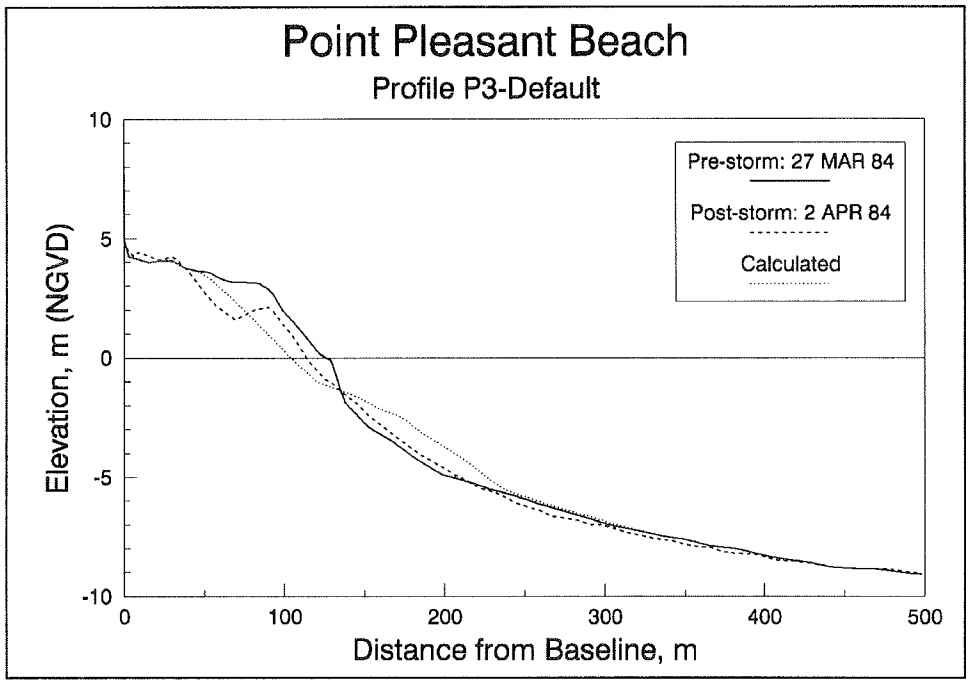

Figure B55. Result of default simulation of the March 1984 storm for profile P3, Point Pleasant Beach, NJ

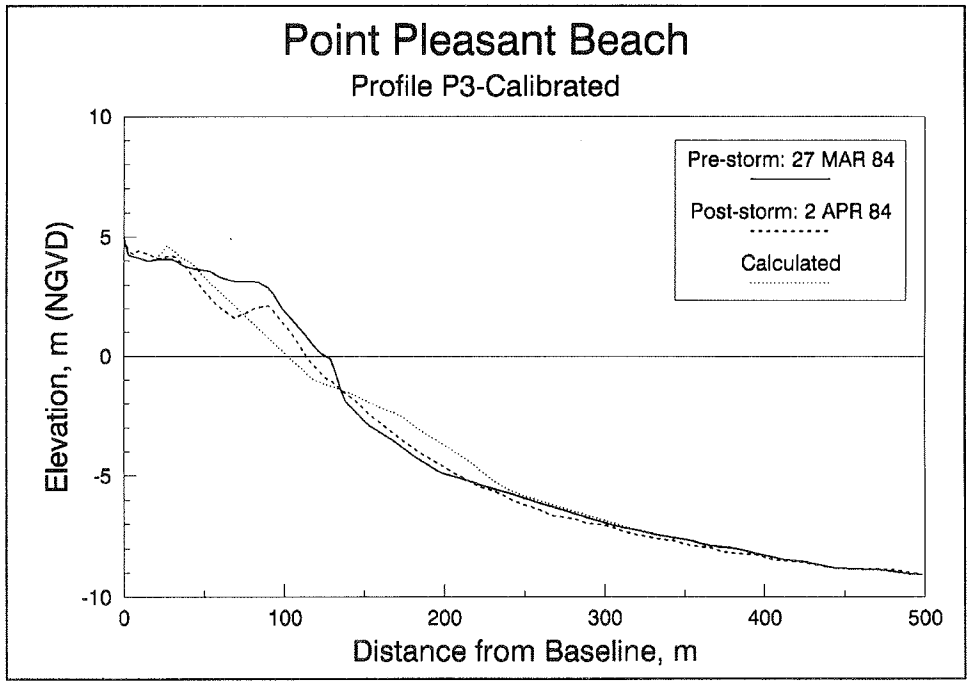

Figure B56. Result of calibrated simulation of the March 1984 storm for profile P3, Point Pleasant Beach, NJ (model calibrated to case M5)

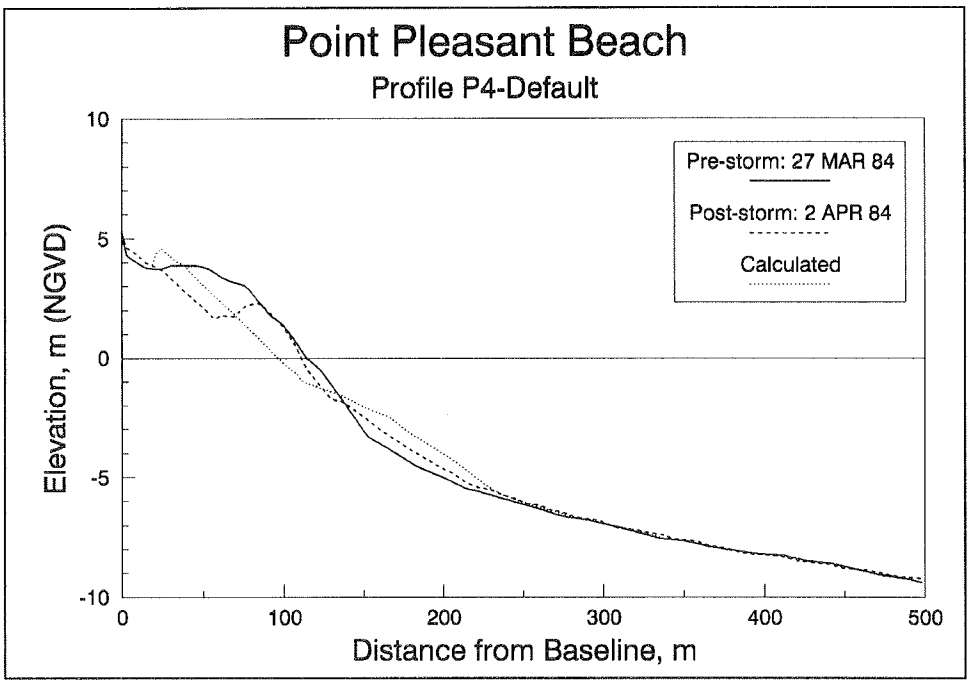

Figure B57. Result of default simulation of the March 1984 storm for profile P4, Point Pleasant Beach, NJ

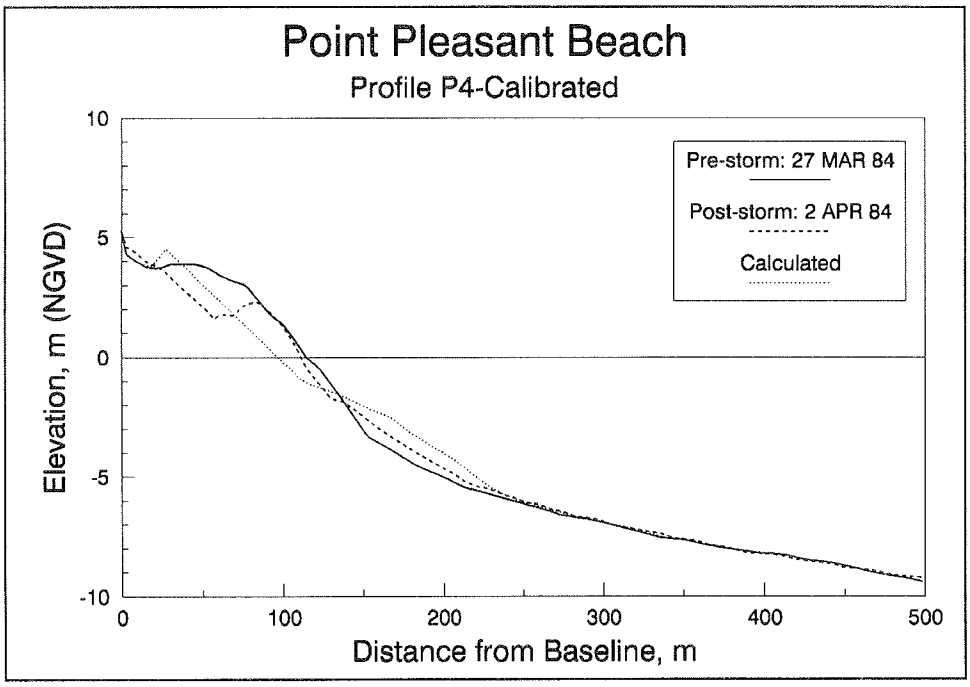

Figure B58. Result of calibrated simulation of the March 1984 storm for profile P4, Point Pleasant Beach, NJ (model calibrated to case M5)

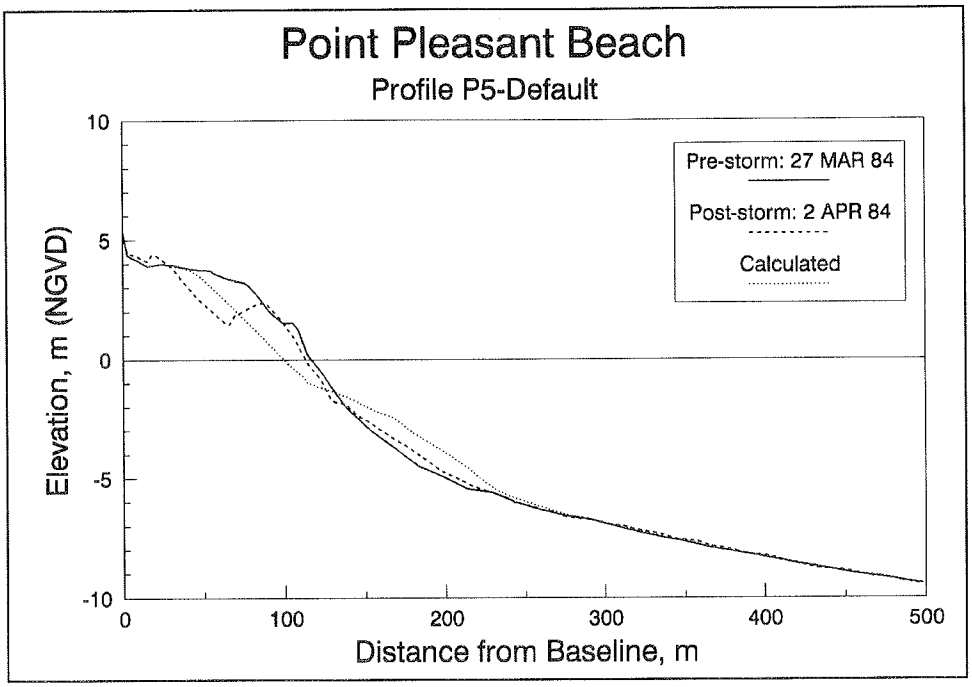

Figure B59. Result of default simulation of the March 1984 storm for profile P5, Point Pleasant Beach, NJ

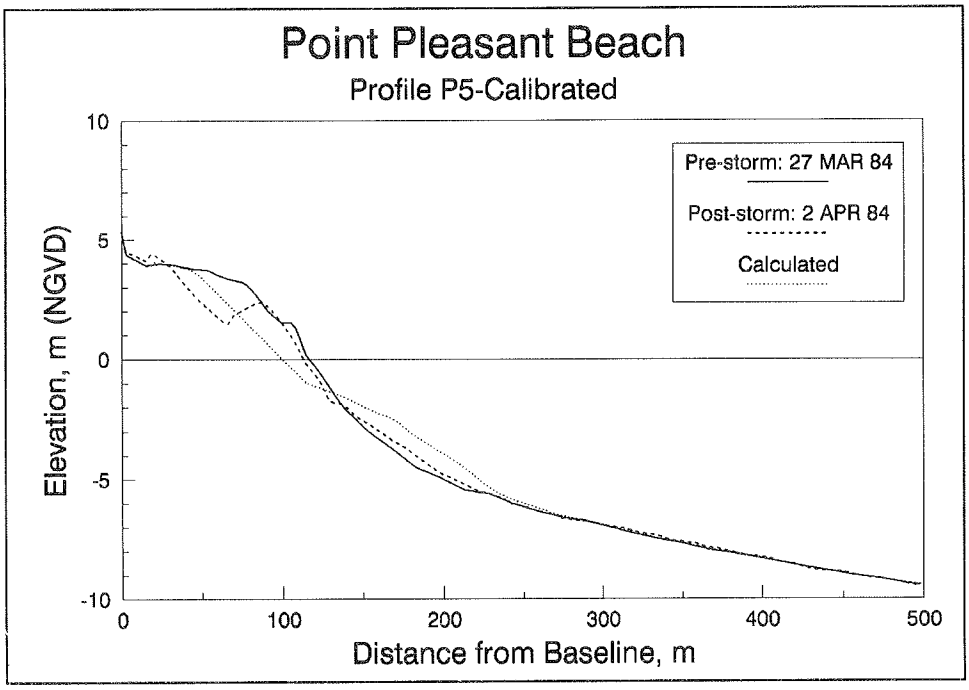

Figure B60. Result of calibrated simulation of the March 1984 storm for profile P5, Point Pleasant Beach, NJ (model calibrated to case M5)

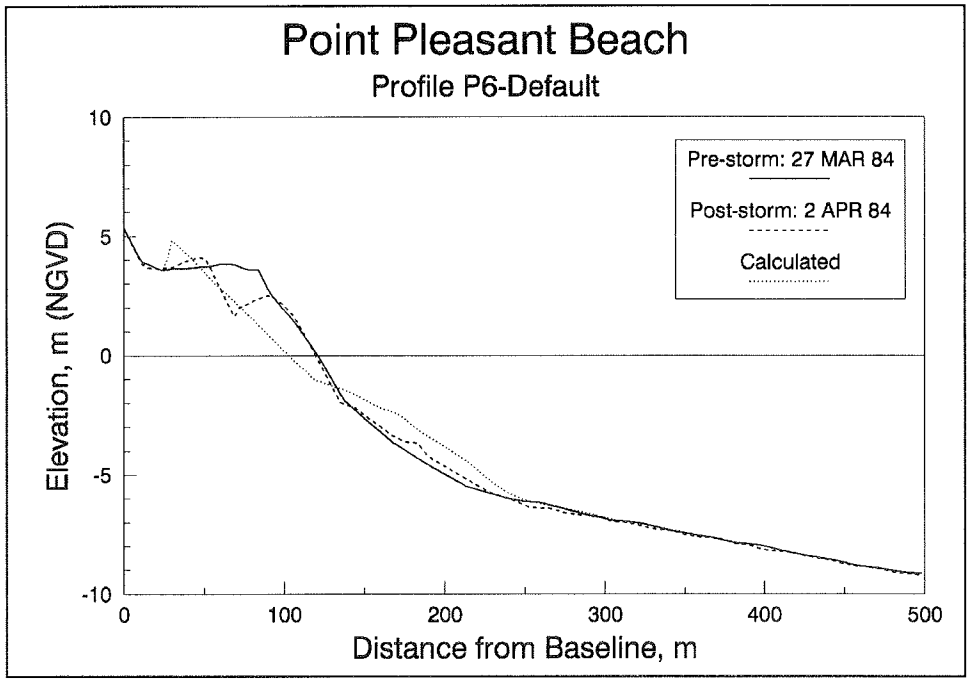

Figure B61. Result of default simulation of the March 1984 storm for profile P6, Point Pleasant Beach, NJ

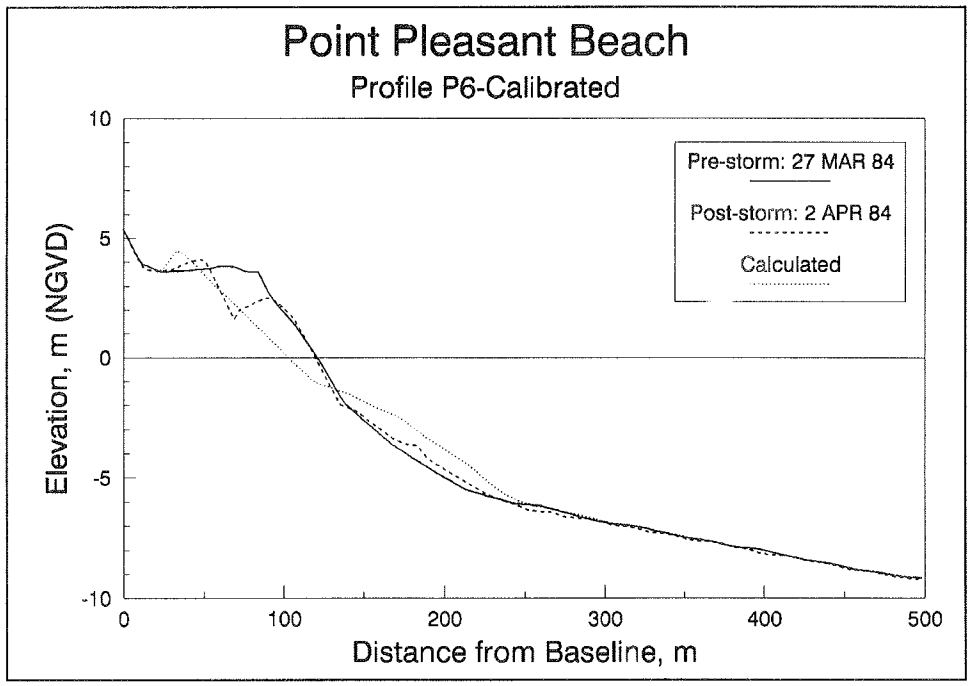

Figure B62. Result of calibrated simulation of the March 1984 storm for profile P6, Point Pleasant Beach, NJ (model calibrated to case M5)

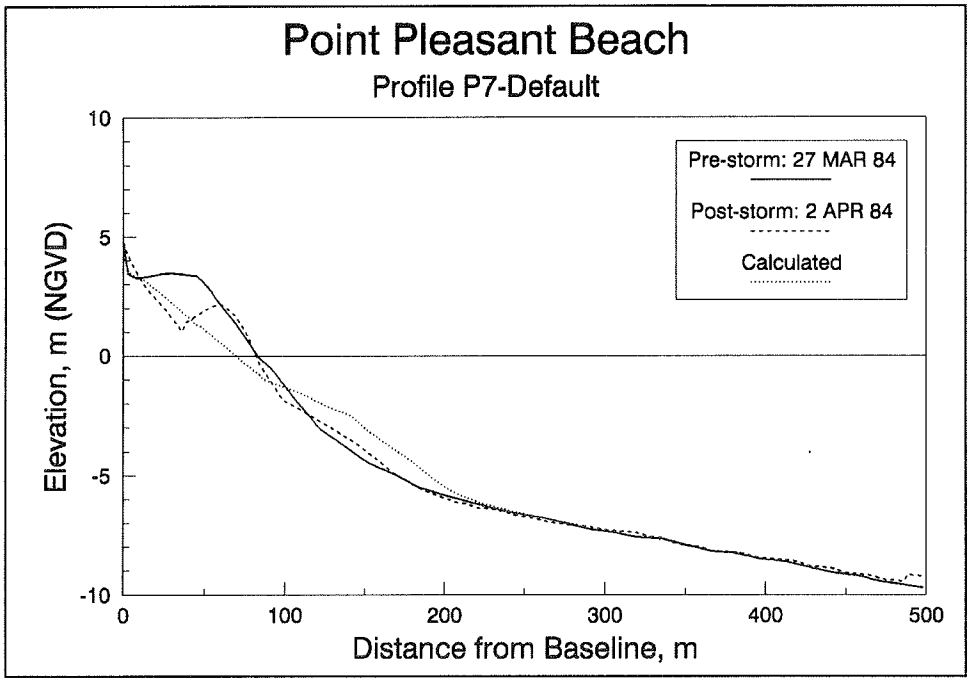

Figure B63. Result of default simulation of the March 1984 storm for profile P7, Point Pleasant Beach, NJ

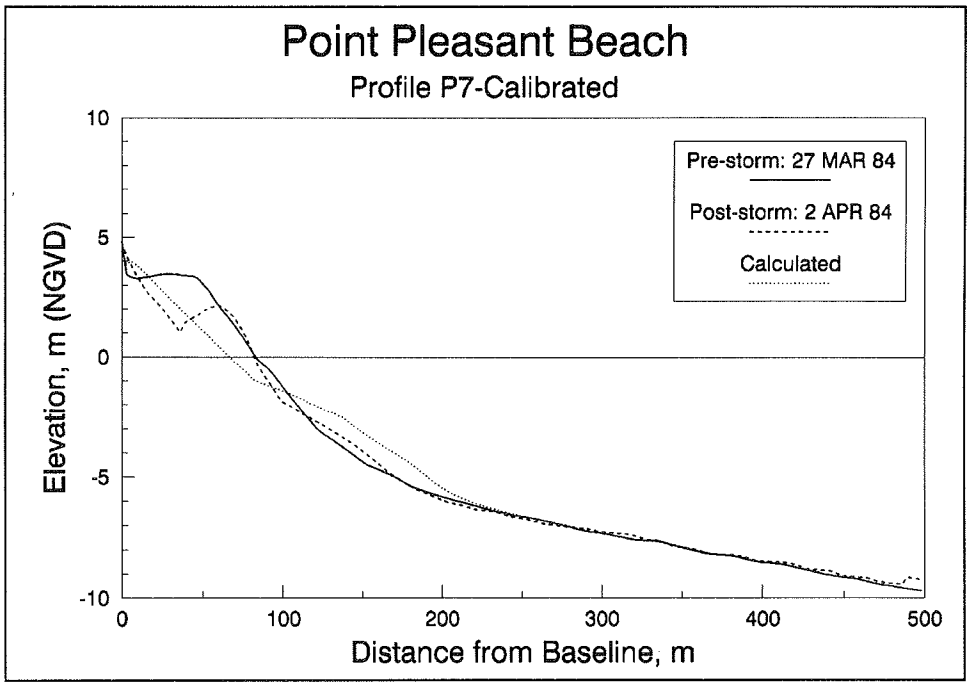

Figure B64. Result of calibrated simulation of the March 1984 storm for profile P7, Point Pleasant Beach, NJ (model calibrated to case M5)

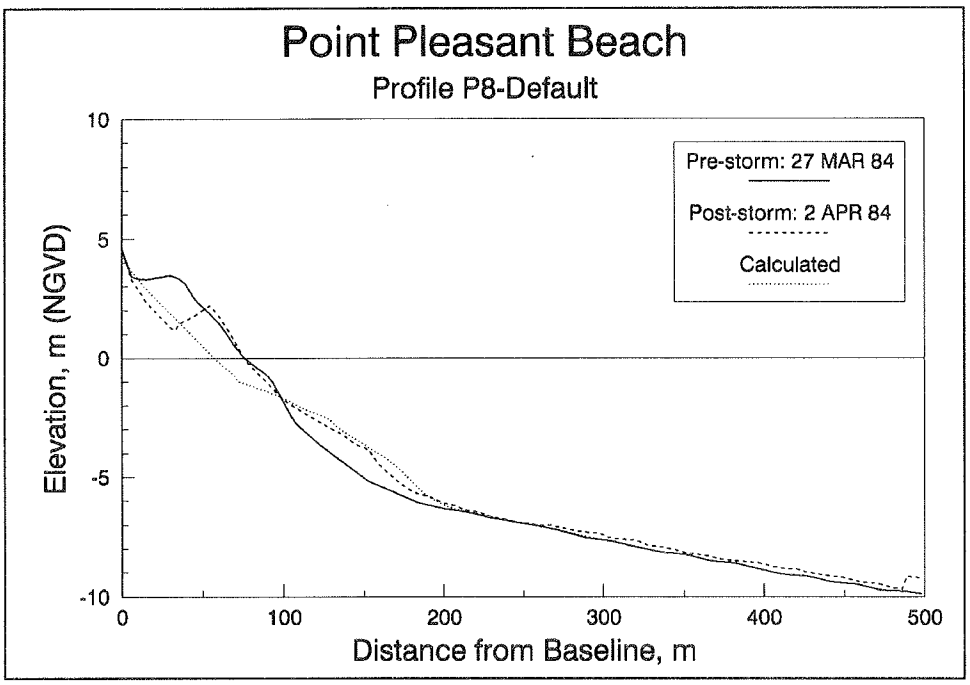

Figure B65. Result of default simulation of the March 1984 storm for profile P8, Point Pleasant Beach, NJ

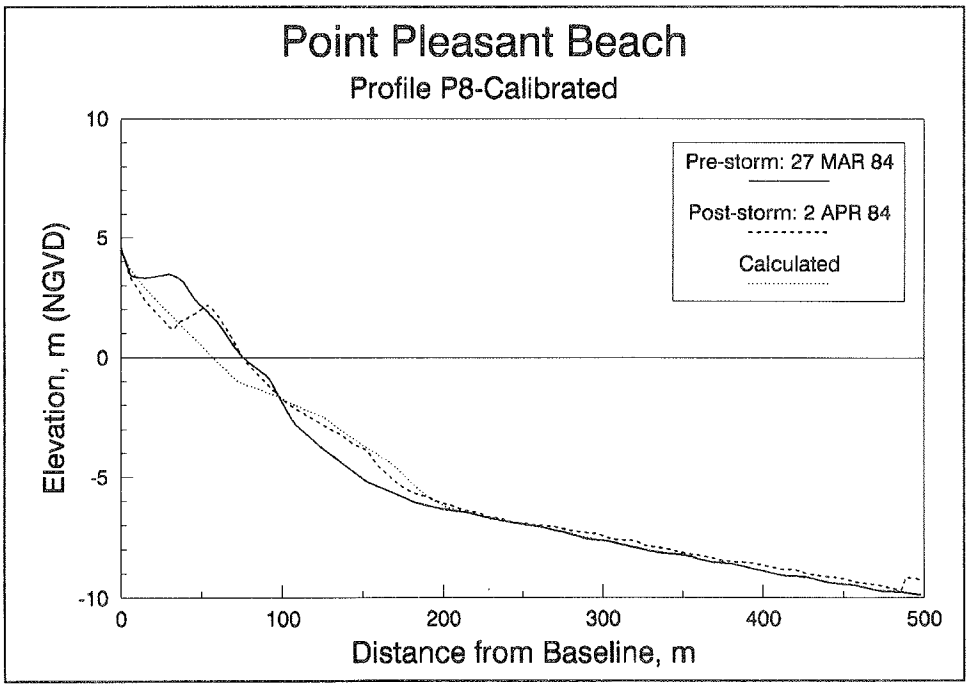

Figure B66. Result of calibrated simulation of the March 1984 storm for profile P8, Point Pleasant Beach, NJ (model calibrated to case M5)

Dewey Beach and Rehoboth Beach, DE

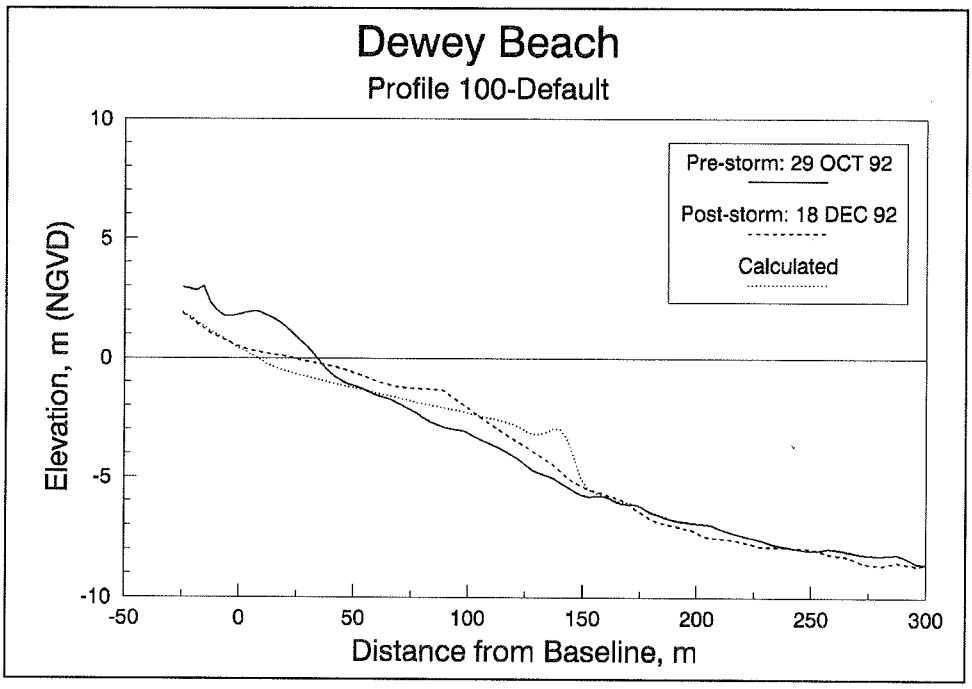

Figure B67. Result of default simulation of the December 1992 storm for profile 100, Dewey Beach, DE

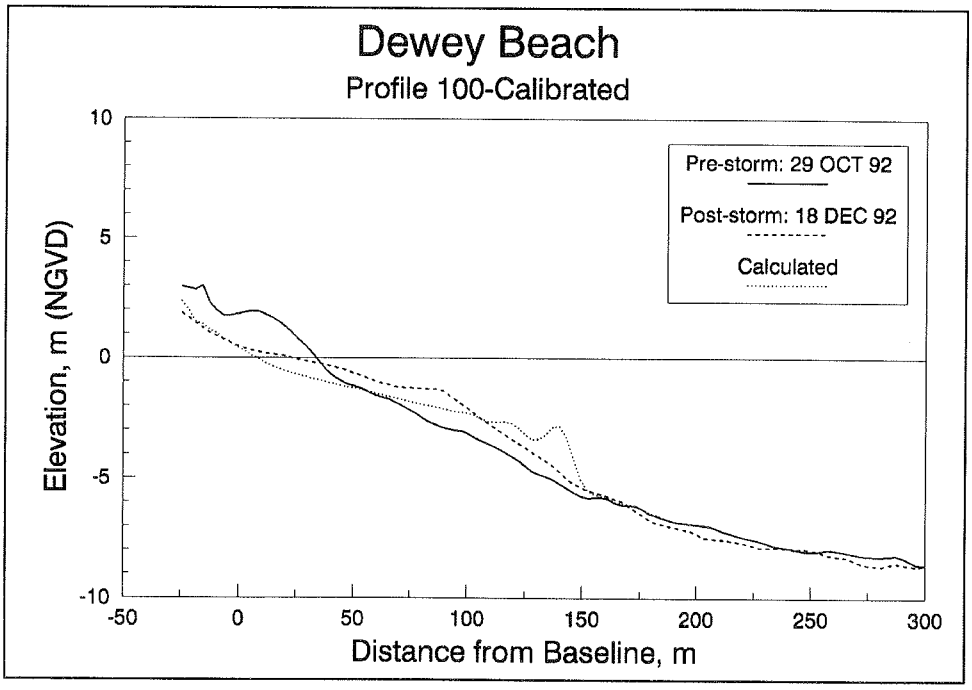

Figure B68. Result of calibrated simulation of the December 1992 storm for profile 100, Dewey Beach, DE (model calibrated to Dewey Beach case 140)

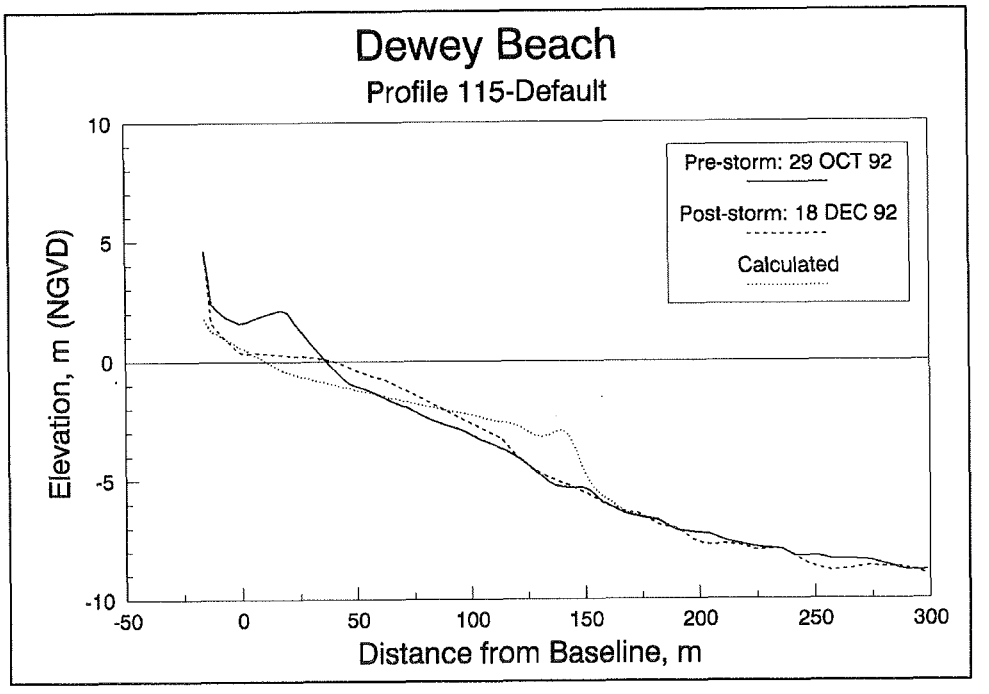

Figure B69. Result of default simulation of the December 1992 storm for profile 115, Dewey Beach, DE

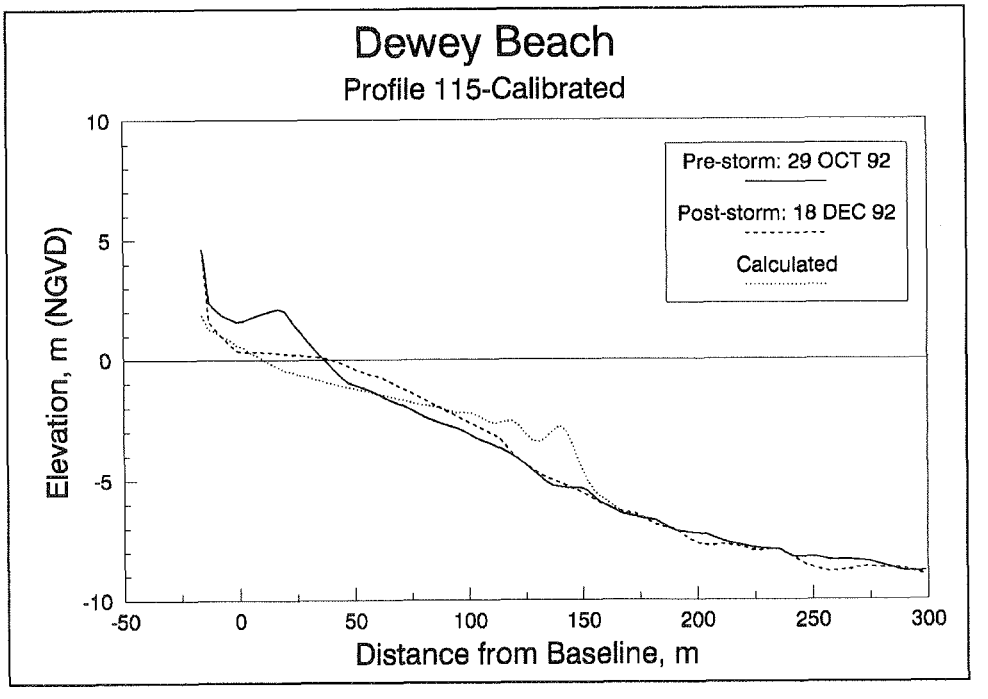

Figure B70. Result of calibrated simulation of the December 1992 storm for profile 115, Dewey Beach, DE (model calibrated to Dewey Beach case 140)

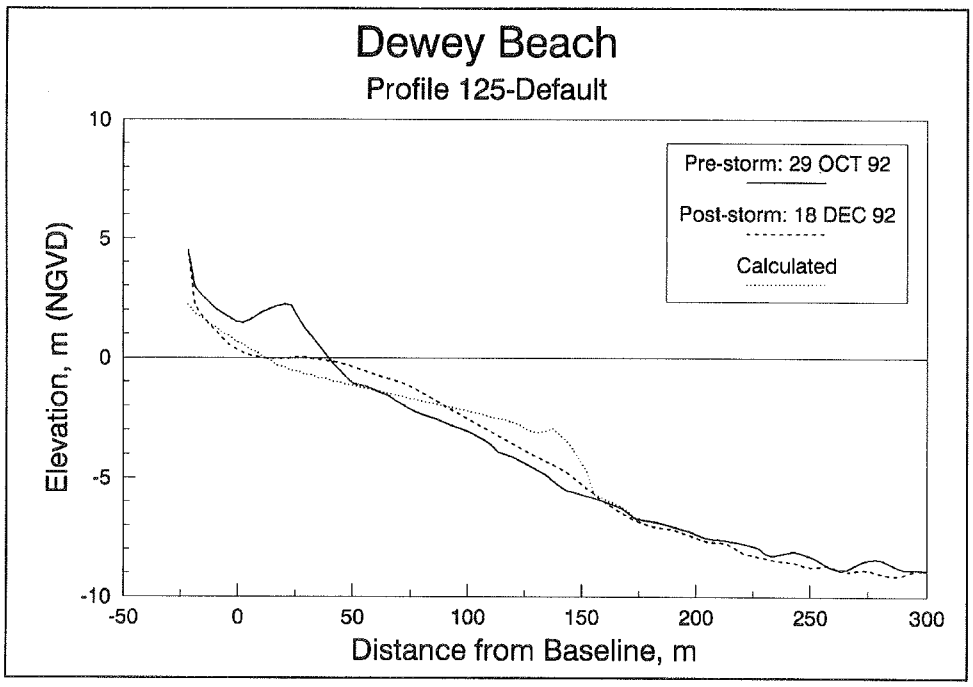

Figure B71. Result of default simulation of the December 1992 storm for profile 125, Dewey Beach, DE

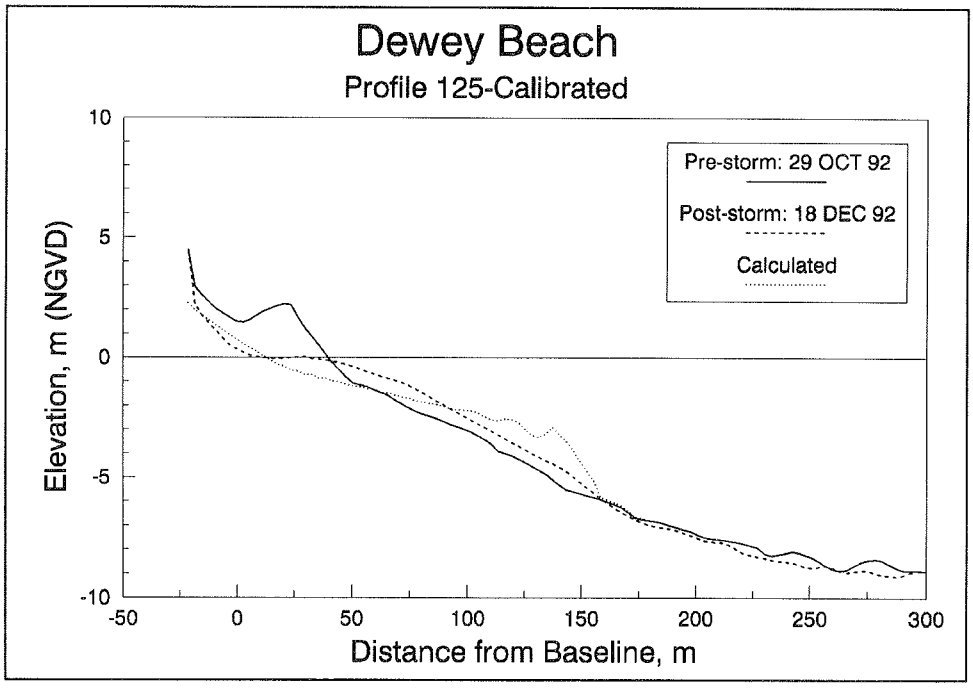

Figure B72. Result of calibrated simulation of the December 1992 storm for profile 125, Dewey Beach, DE (model calibrated to Dewey Beach case 140)

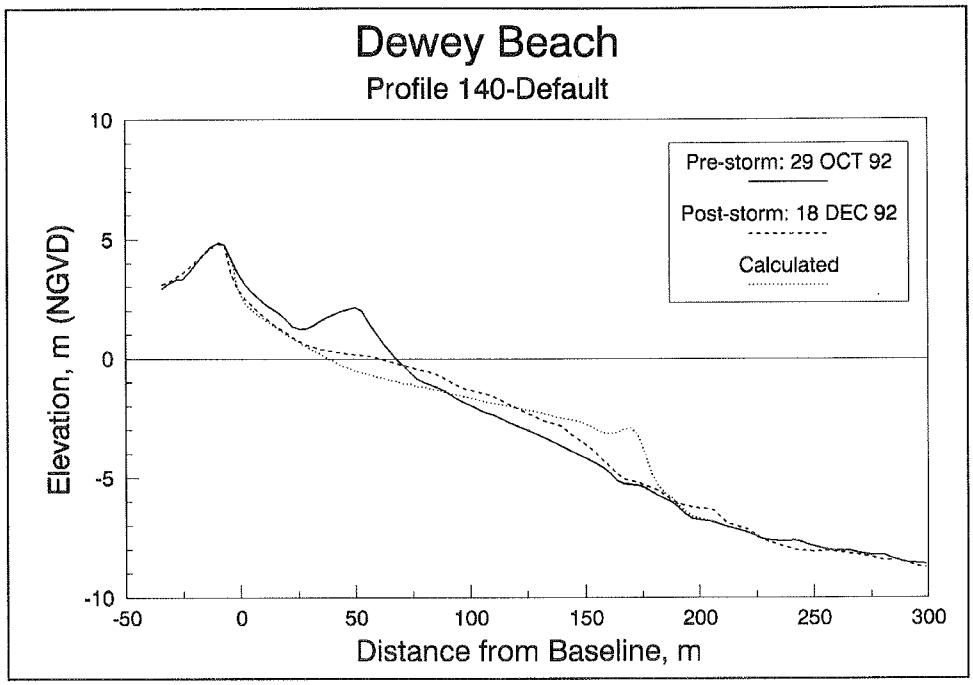

Figure B73. Result of default simulation of the December 1992 storm for profile 140, Dewey Beach, DE

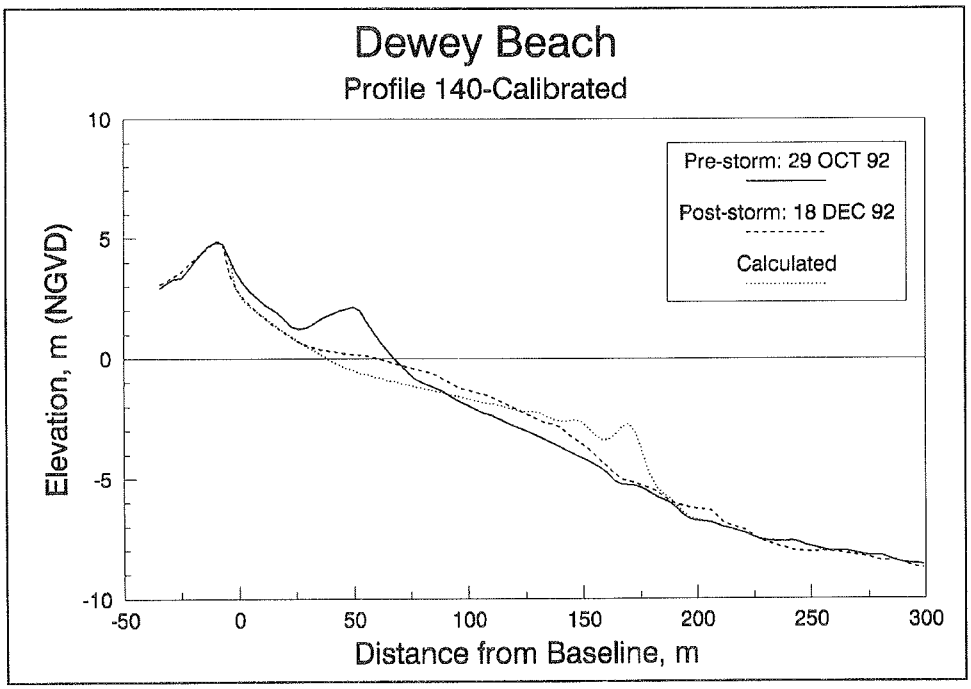

Figure B74. Result of calibrated simulation of the December 1992 storm for profile 140, Dewey Beach, DE (model calibrated to Dewey Beach case 140)

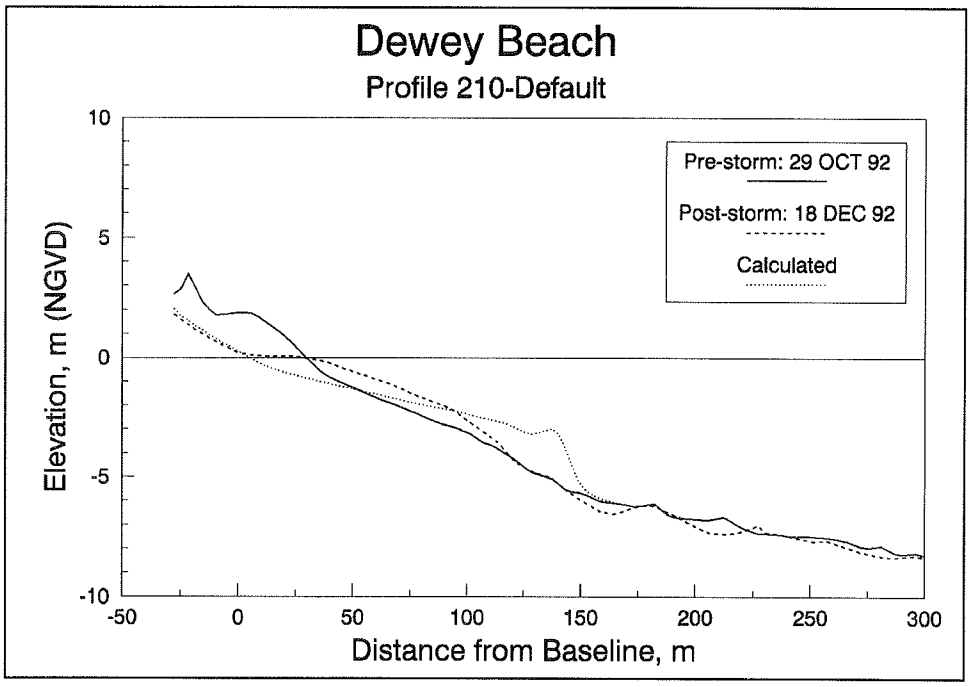

Figure B75. Result of default simulation of the December 1992 storm for profile 210, Dewey Beach, DE

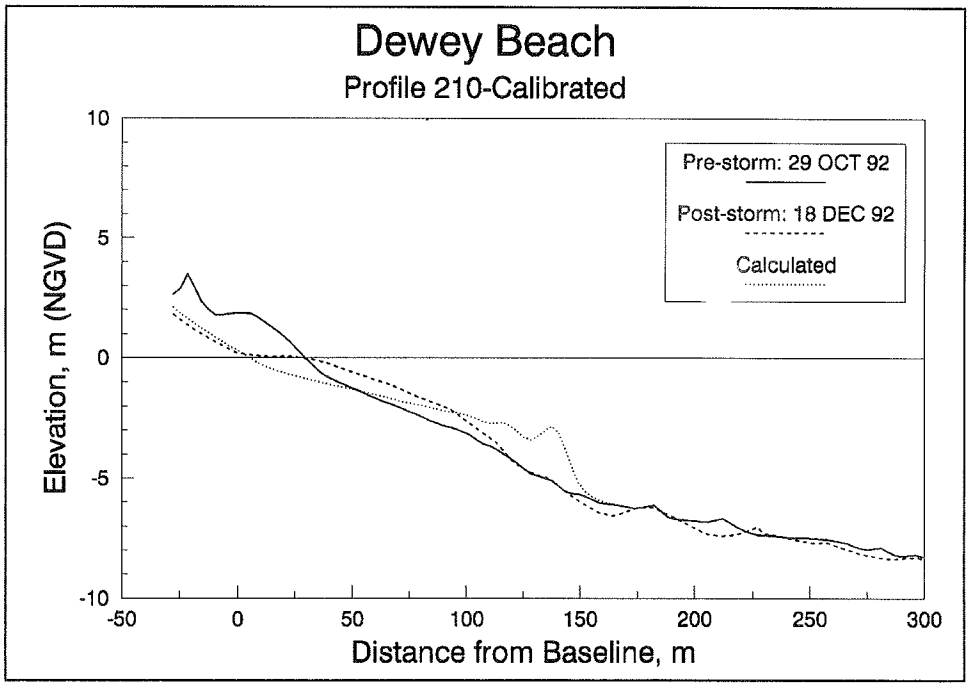

Figure B76. Result of calibrated simulation of the December 1992 storm for profile 210, Dewey Beach, DE (model calibrated to Dewey Beach case 140)

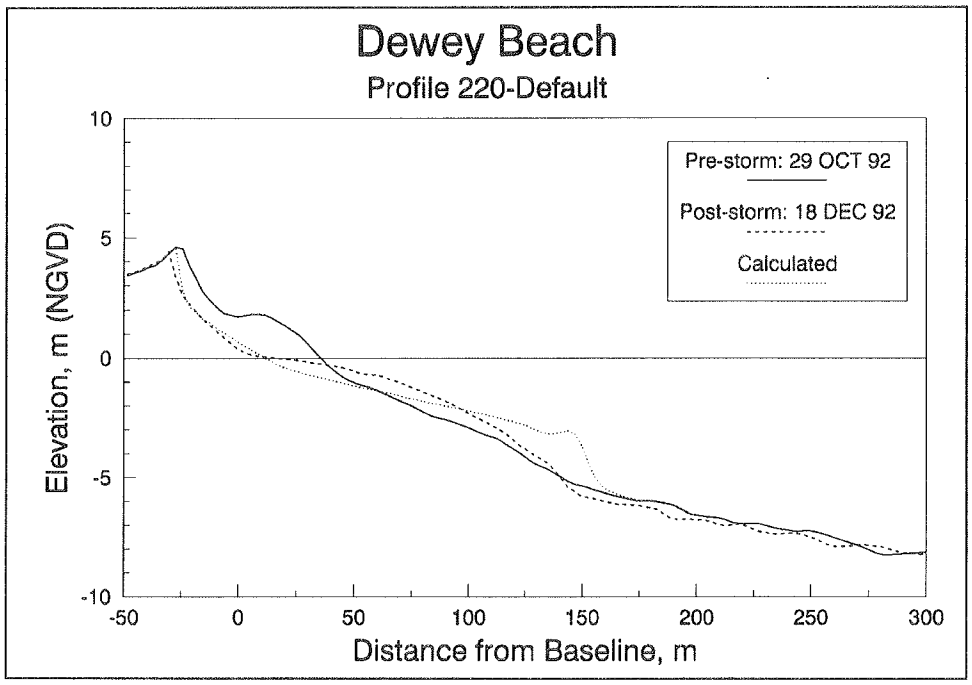

Figure B77. Result of default simulation of the December 1992 storm for profile 220, Dewey Beach, DE

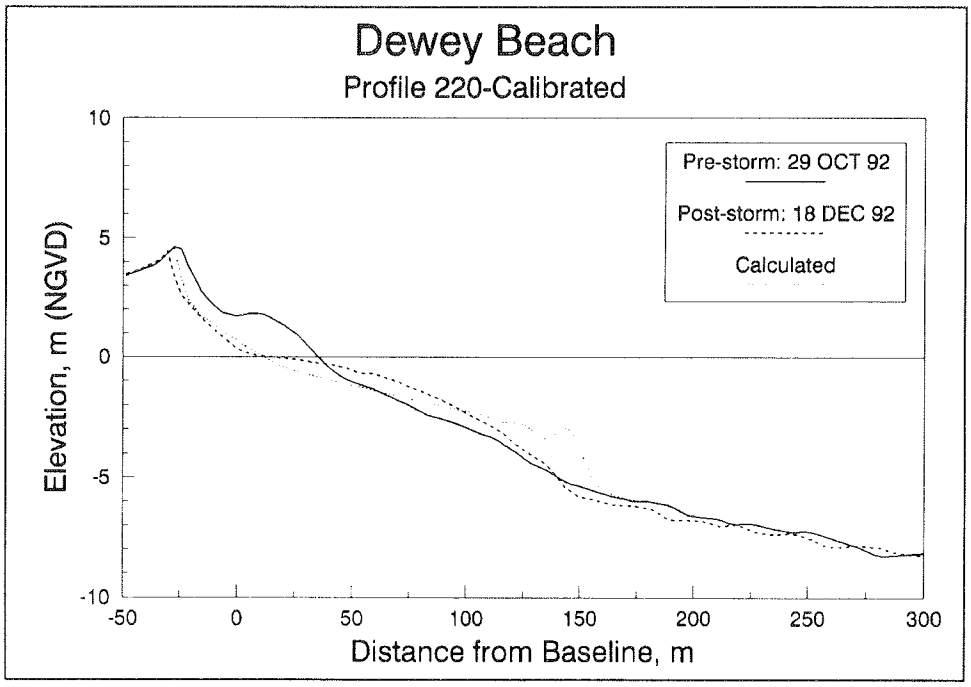

Figure B78. Result of calibrated simulation of the December 1992 storm for profile 220, Dewey Beach, DE (model calibrated to Dewey Beach case 140)

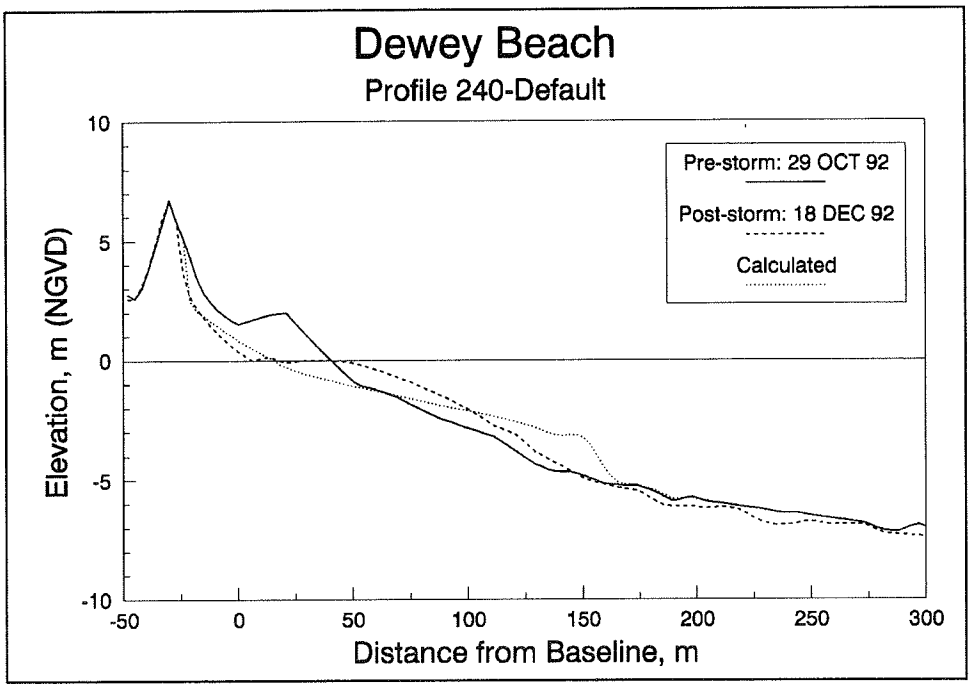

Figure B79. Result of default simulation of the December 1992 storm for profile 240, Dewey Beach, DE

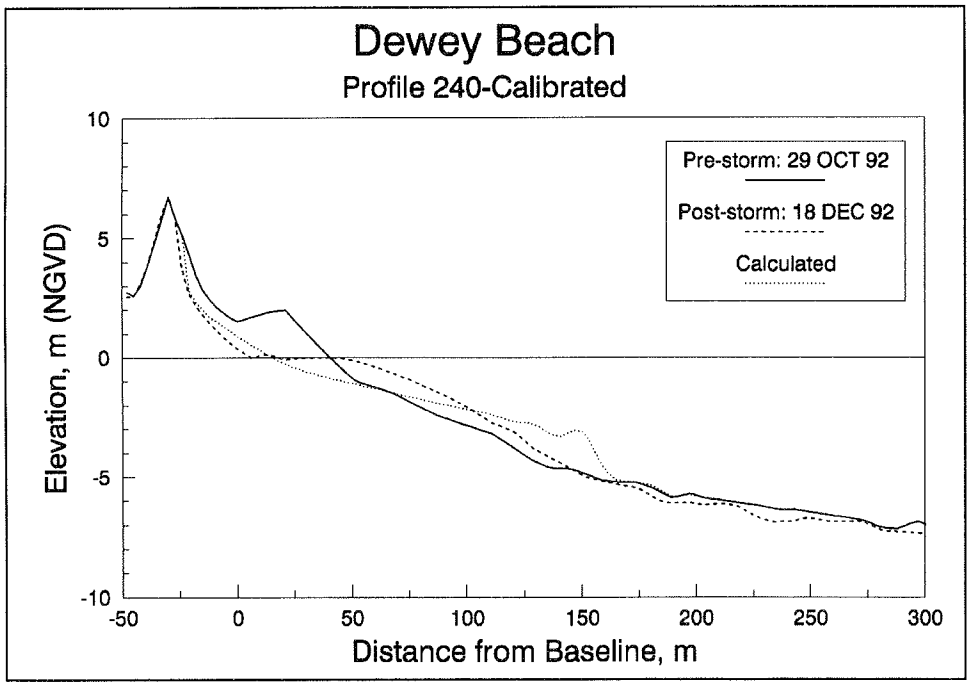

Figure B80. Result of calibrated simulation of the December 1992 storm for profile 240, Dewey Beach, DE (model calibrated to Dewey Beach case 140)

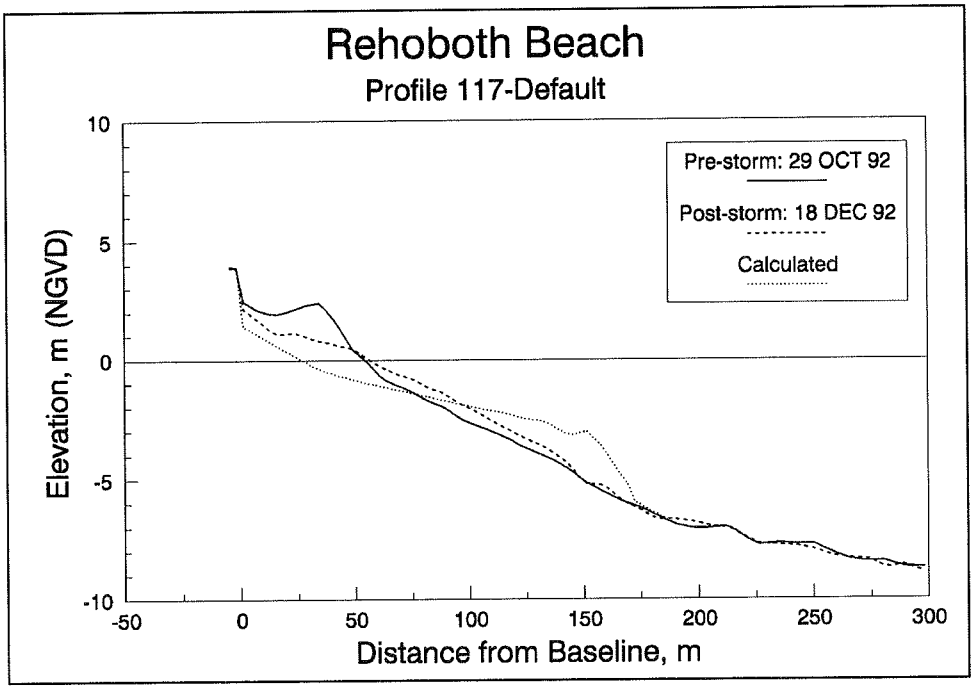

Figure B81. Result of default simulation of the December 1992 storm for profile 117, Rehoboth Beach, DE

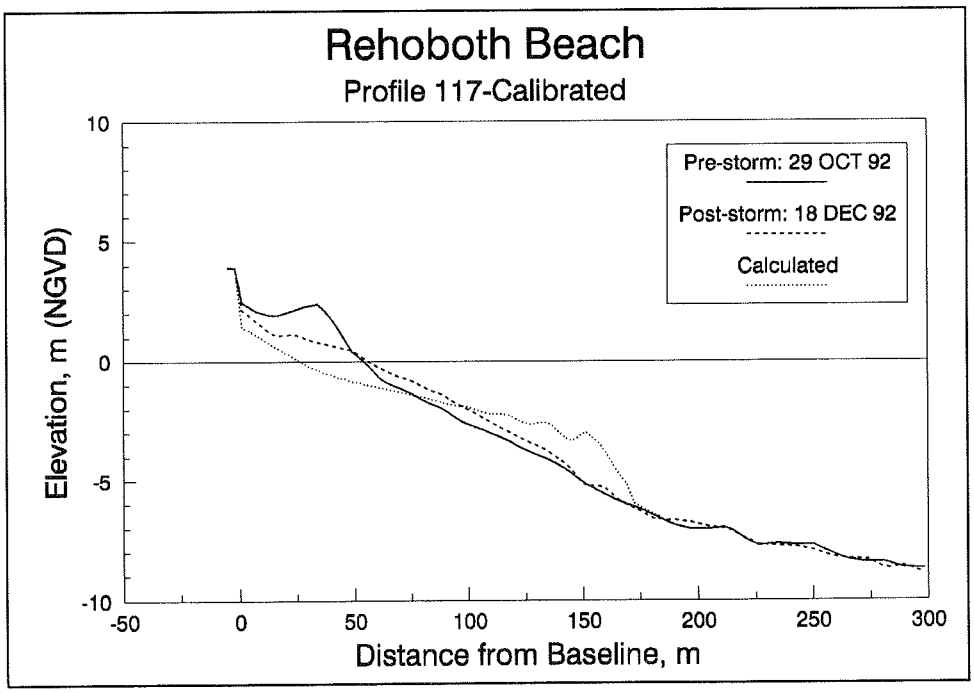

Figure B82. Result of calibrated simulation of the December 1992 storm for profile 117, Rehoboth Beach, DE (model calibrated to Dewey Beach case 140)

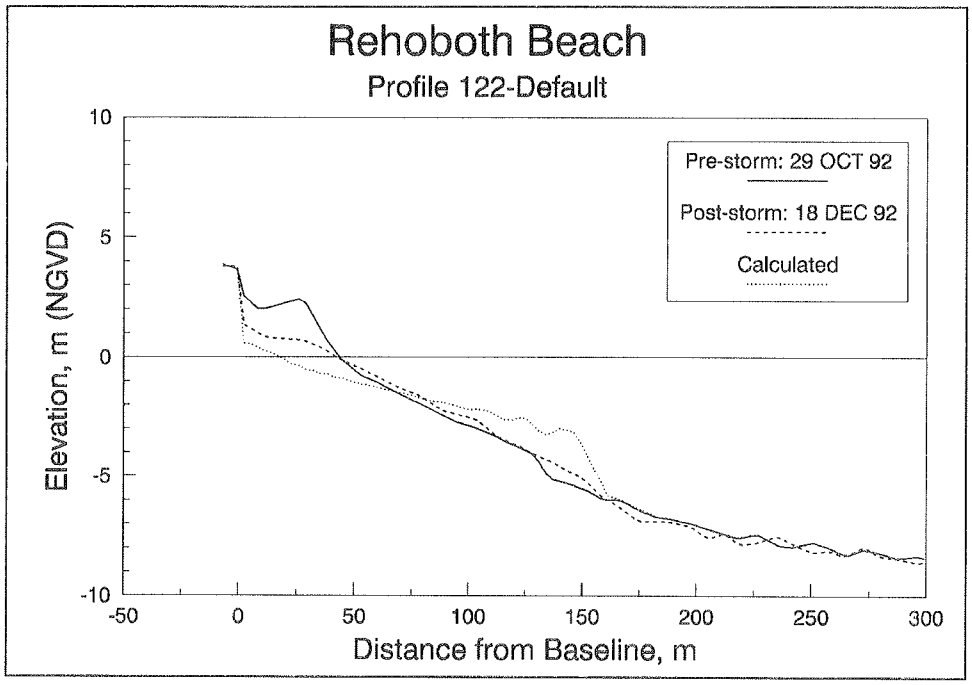

Figure B83. Result of default simulation of the December 1992 storm for profile 122, Rehoboth Beach, DE

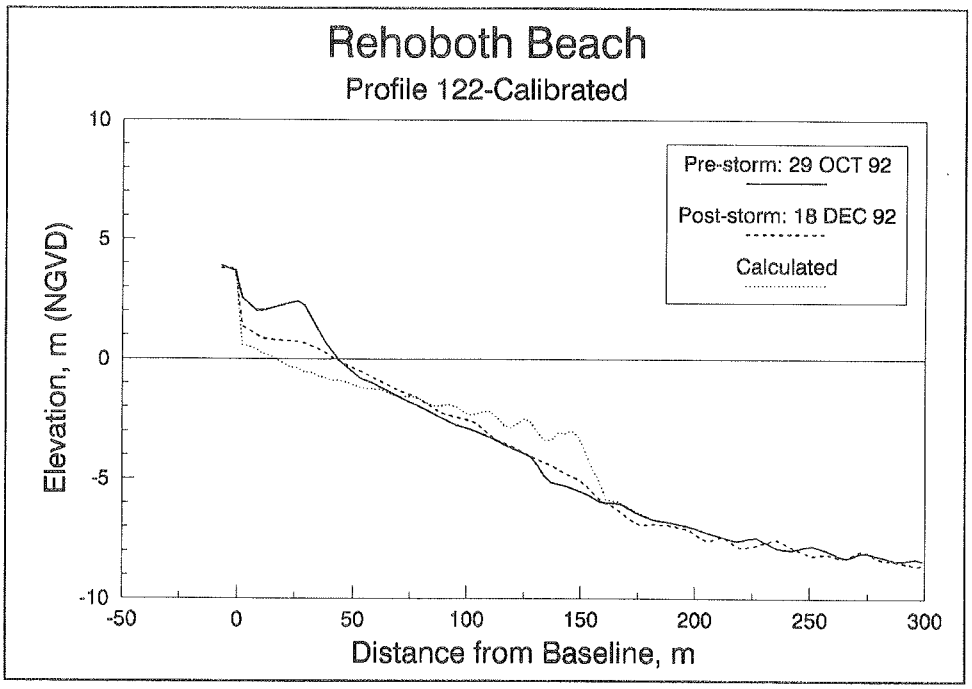

Figure B84. Result of calibrated simulation of the December 1992 storm for profile 122, Rehoboth Beach, DE (model calibrated to Dewey Beach case 140)

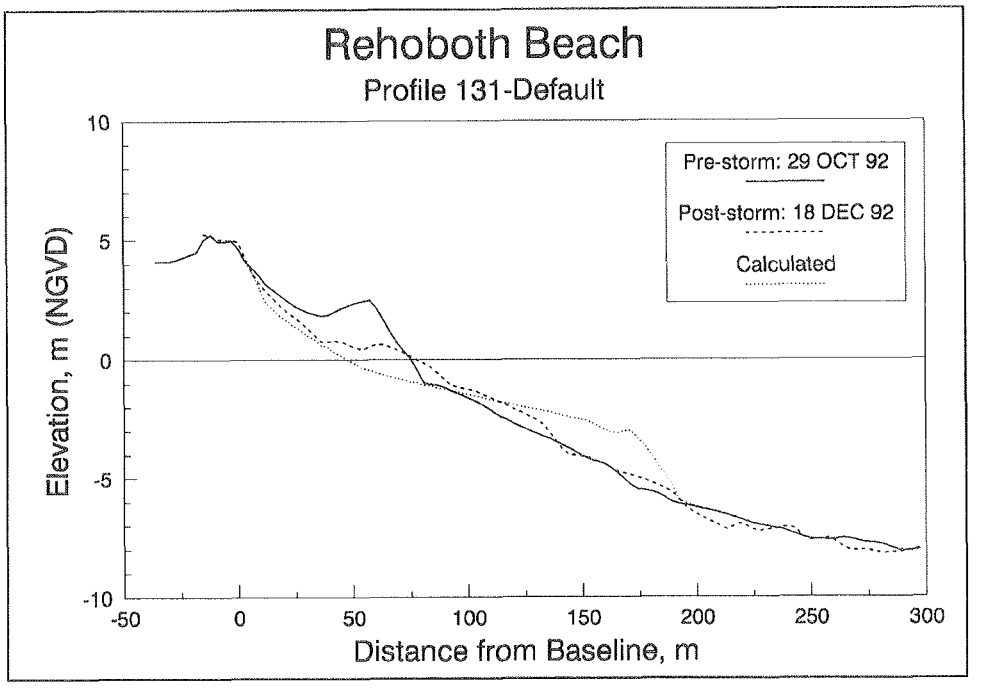

Figure B85. Result of default simulation of the December 1992 storm for profile 131, Rehoboth Beach, DE

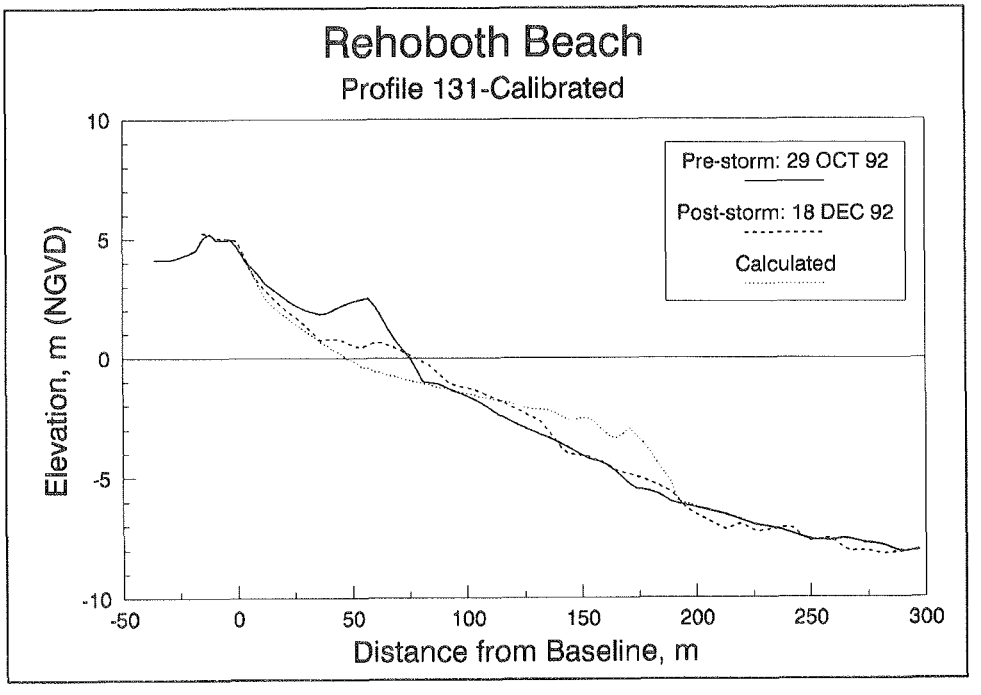

Figure B86. Result of calibrated simulation of the December 1992 storm for profile 131, Rehoboth Beach, DE (model calibrated to Dewey Beach case 140)

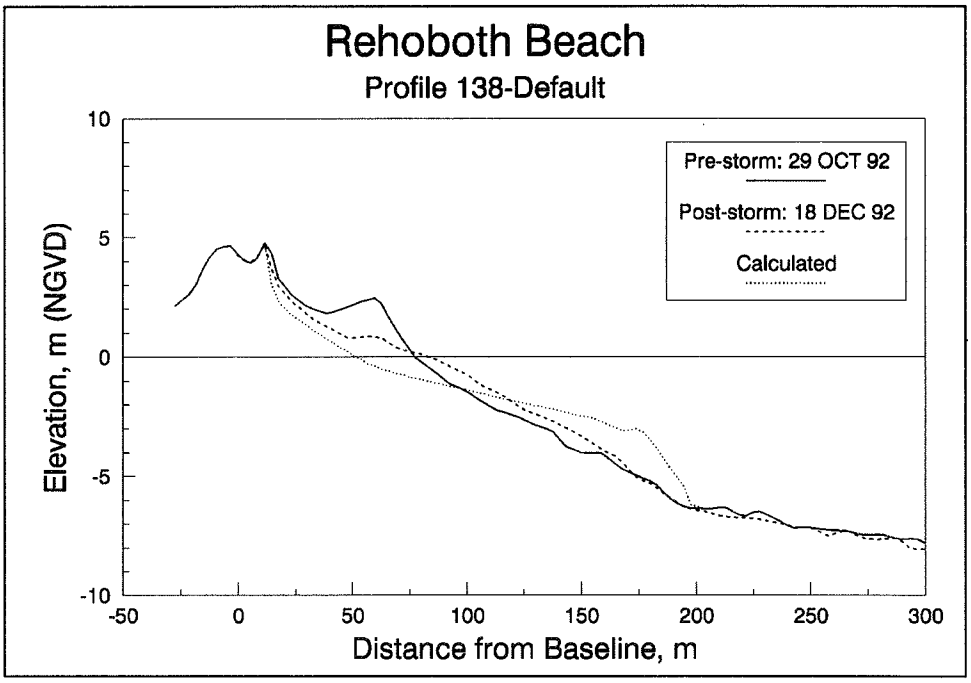

Figure B87. Result of default simulation of the December 1992 storm for profile 138, Rehoboth Beach, DE

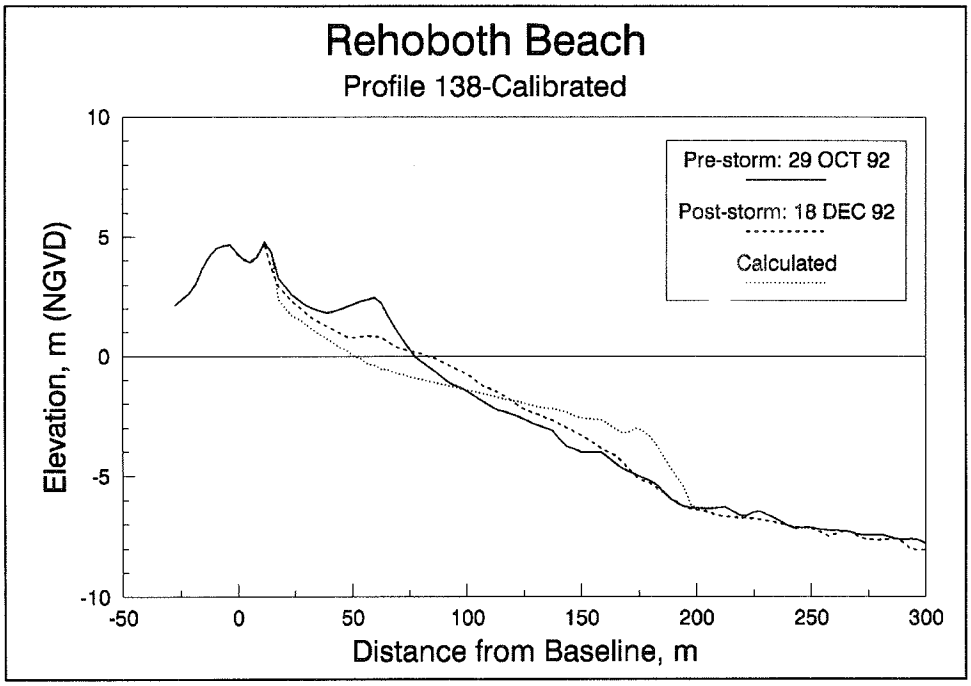

Figure B88. Result of calibrated simulation of the December 1992 storm for profile 138, Rehoboth Beach, DE (model calibrated to Dewey Beach case 140)

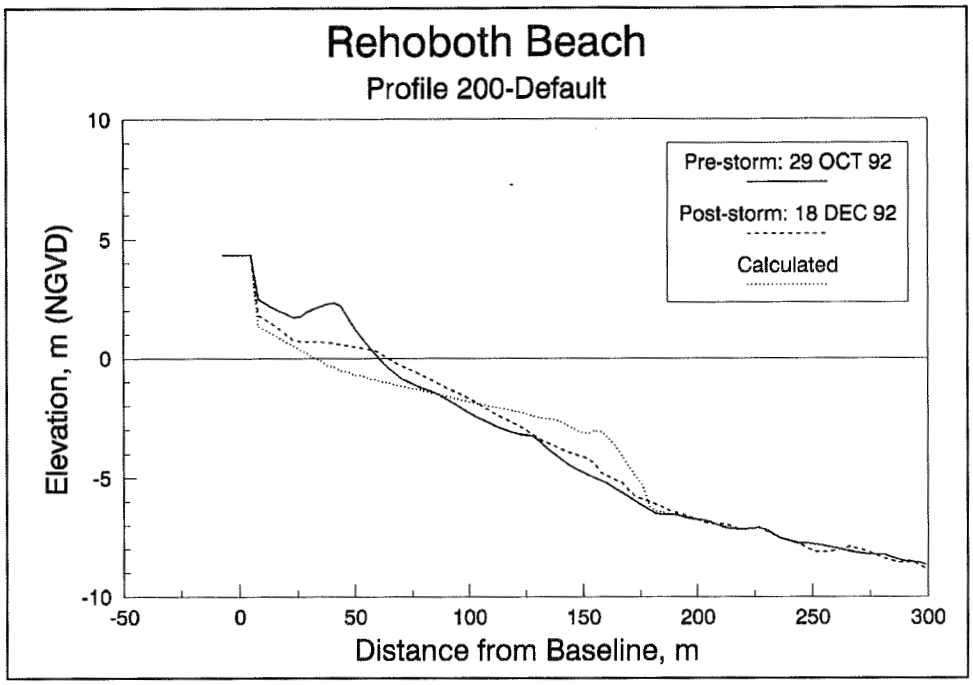

Figure B89. Result of default simulation of the December 1992 storm for profile 200, Rehoboth Beach, DE

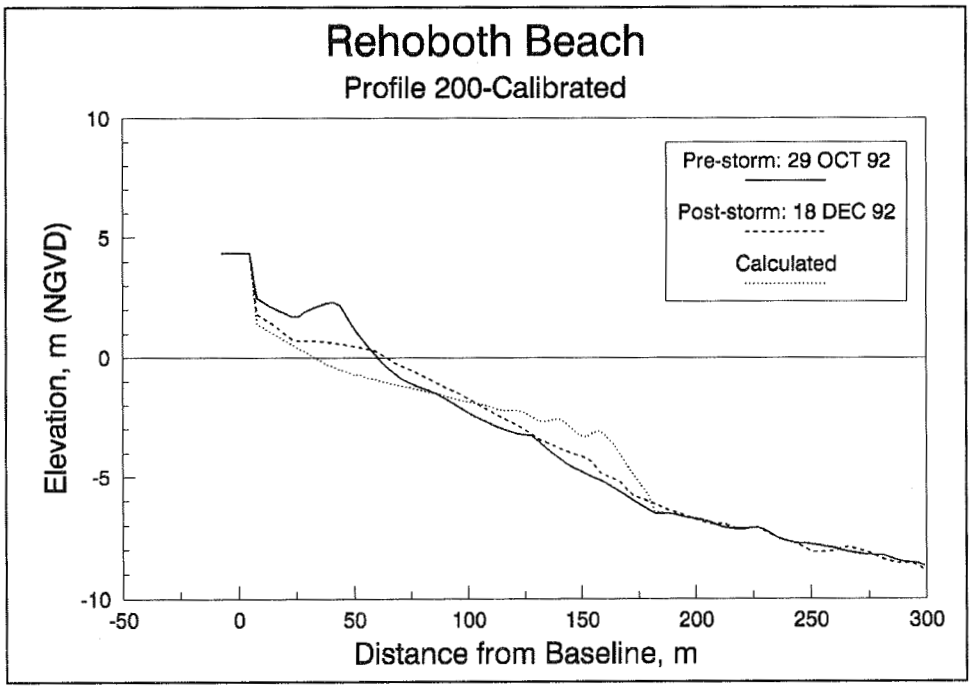

Figure B90. Result of calibrated simulation of the December 1992 storm for profile 200, Rehoboth Beach, DE (model calibrated to Dewey Beach case 140)

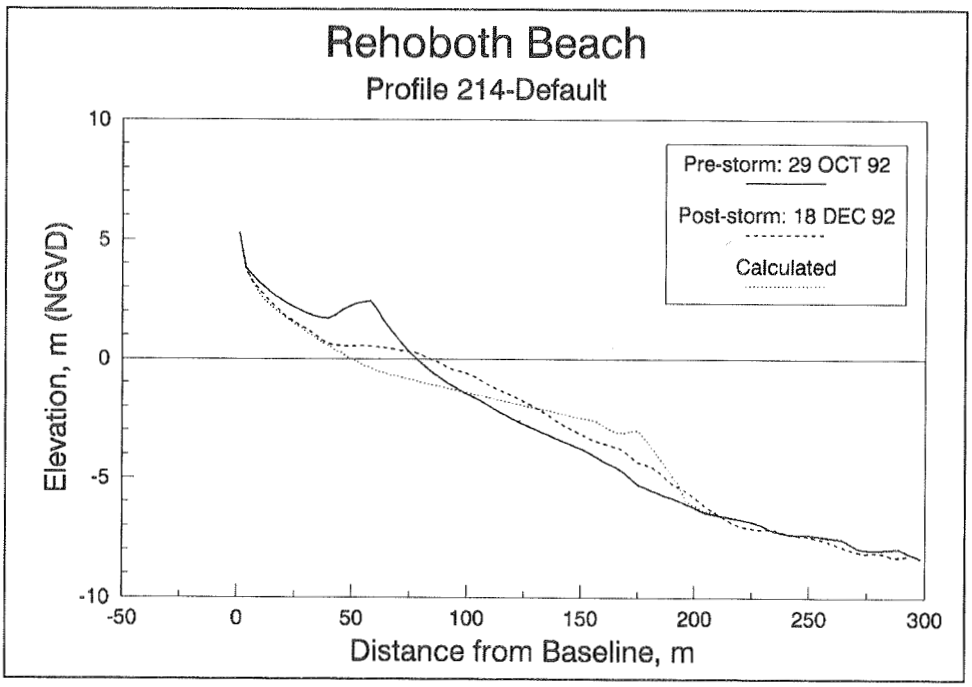

Figure B91. Result of default simulation of the December 1992 storm for profile 214, Rehoboth Beach, DE

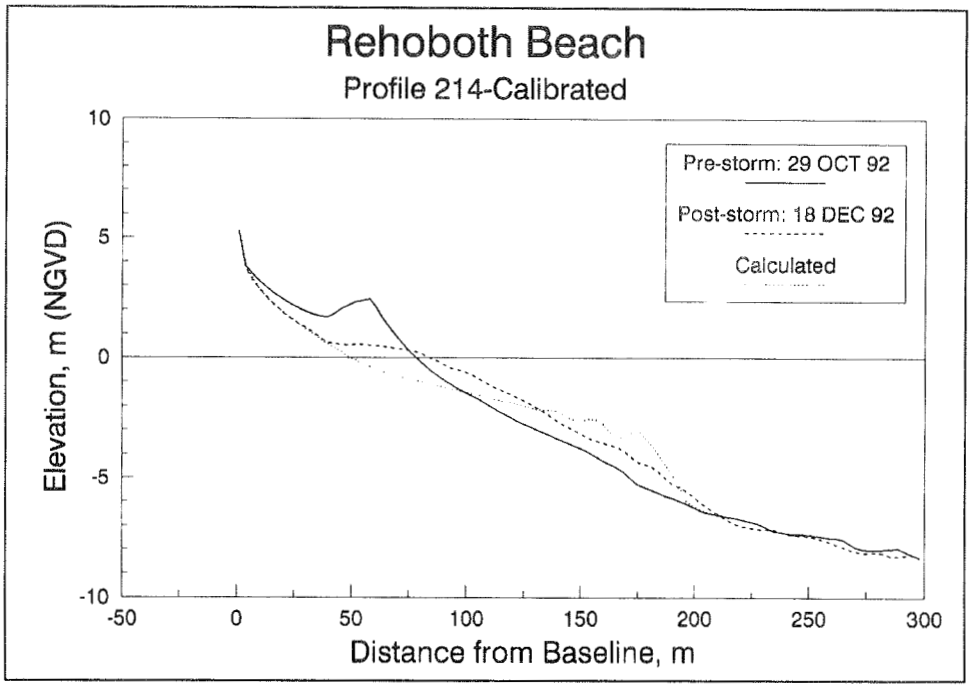

Figure B92. Result of calibrated simulation of the December 1992 storm for profile 214, Rehoboth Beach, DE (model calibrated to Dewey Beach case 140)

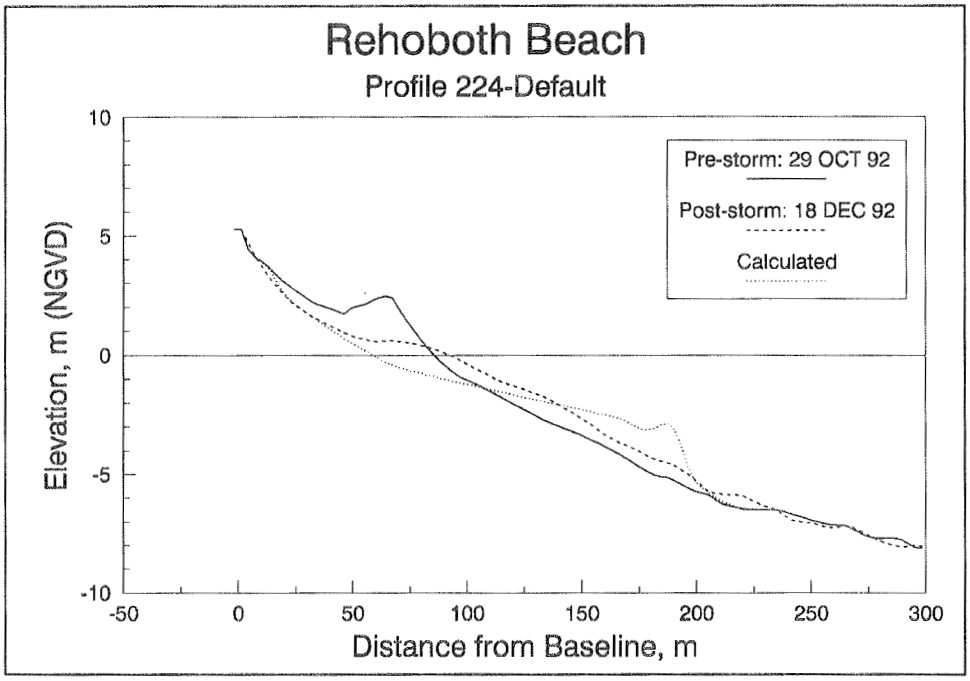

Figure B93. Result of default simulation of the December 1992 storm for profile 224, Rehoboth Beach, DE

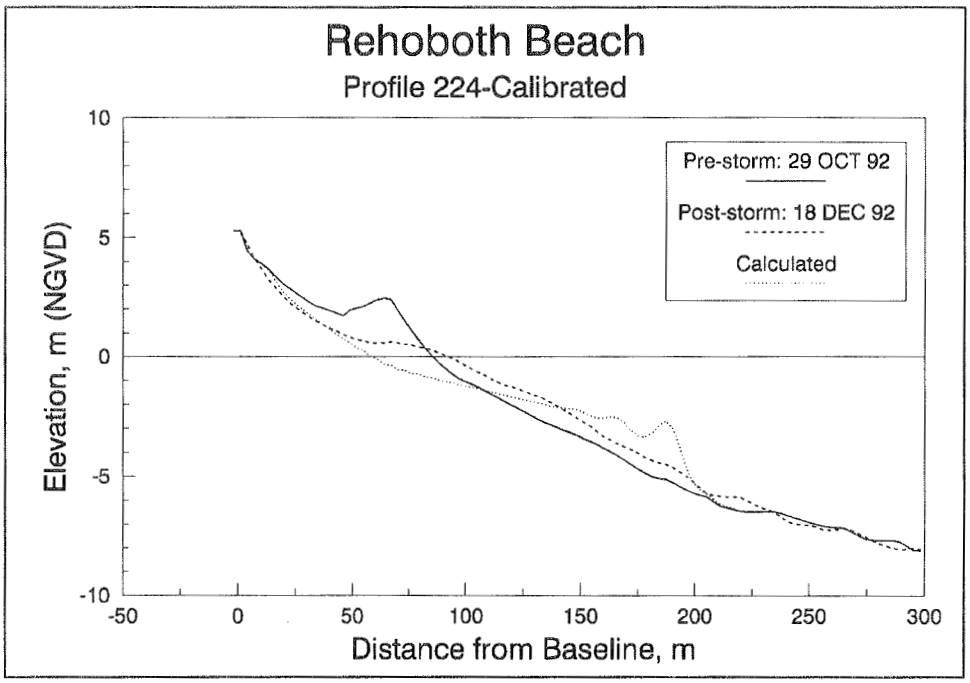

Figure B94. Result of calibrated simulation of the December 1992 storm for profile 224, Rehoboth Beach, DE (model calibrated to Dewey Beach case 140)

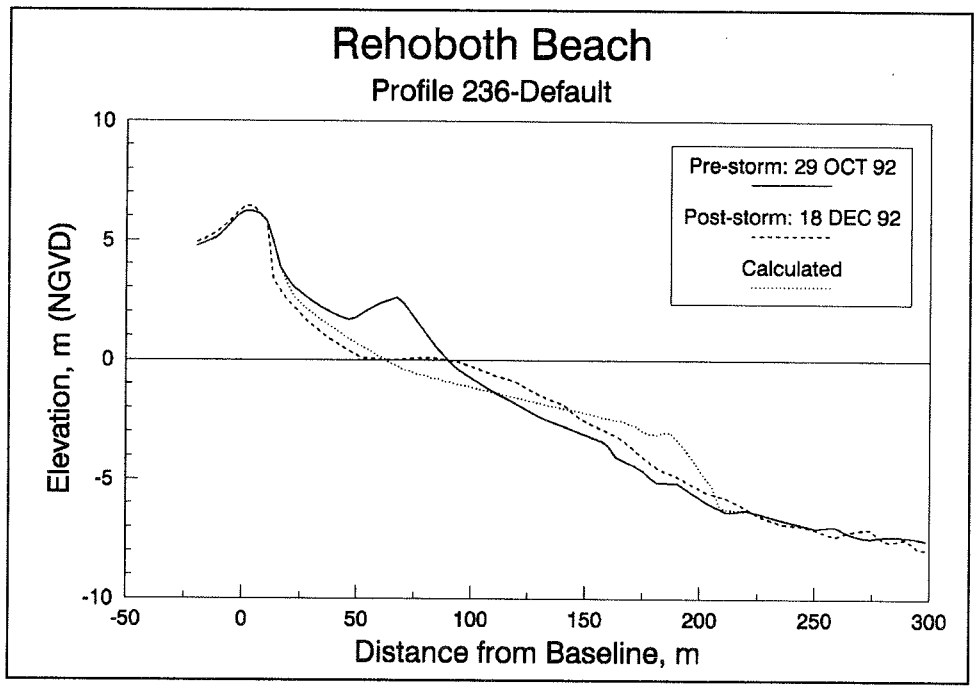

Figure B95. Result of default simulation of the December 1992 storm for profile 236, Rehoboth Beach, DE

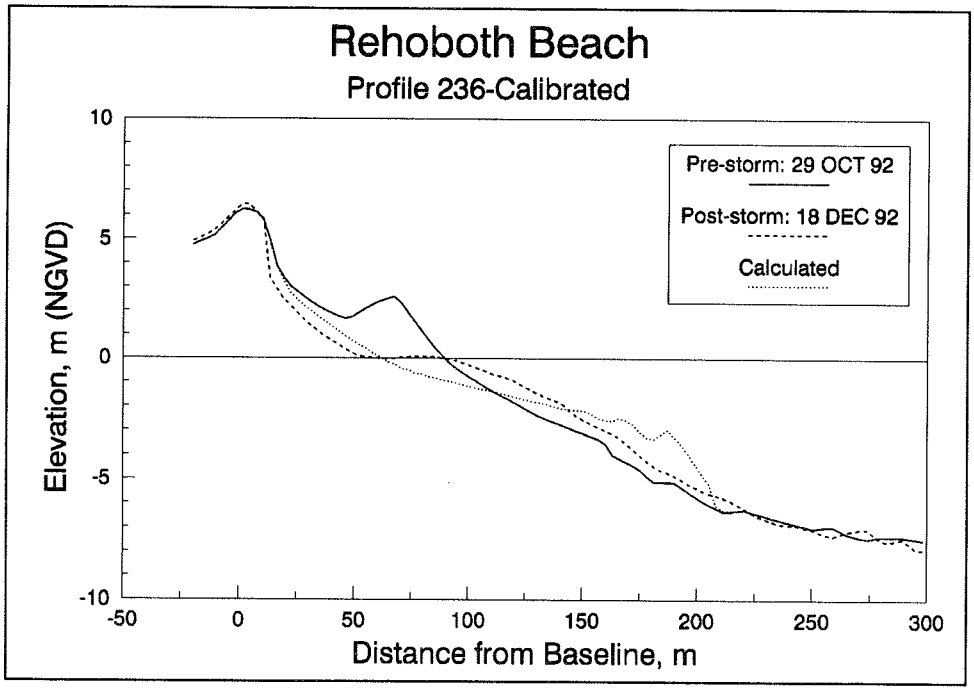

Figure B96. Result of calibrated simulation of the December 1992 storm for profile 236, Rehoboth Beach, DE (model calibrated to Dewey Beach case 140)

Debidue Beach and Myrtle Beach, SC

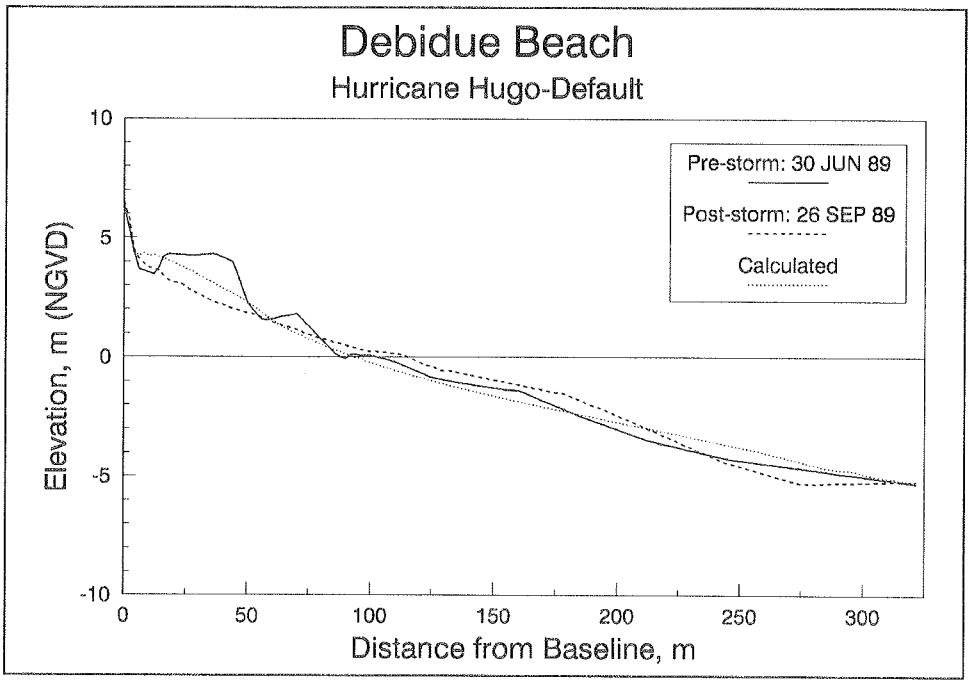

Figure 97. Result of default simulation of Hurricane Hugo, Debidue Beach, SC

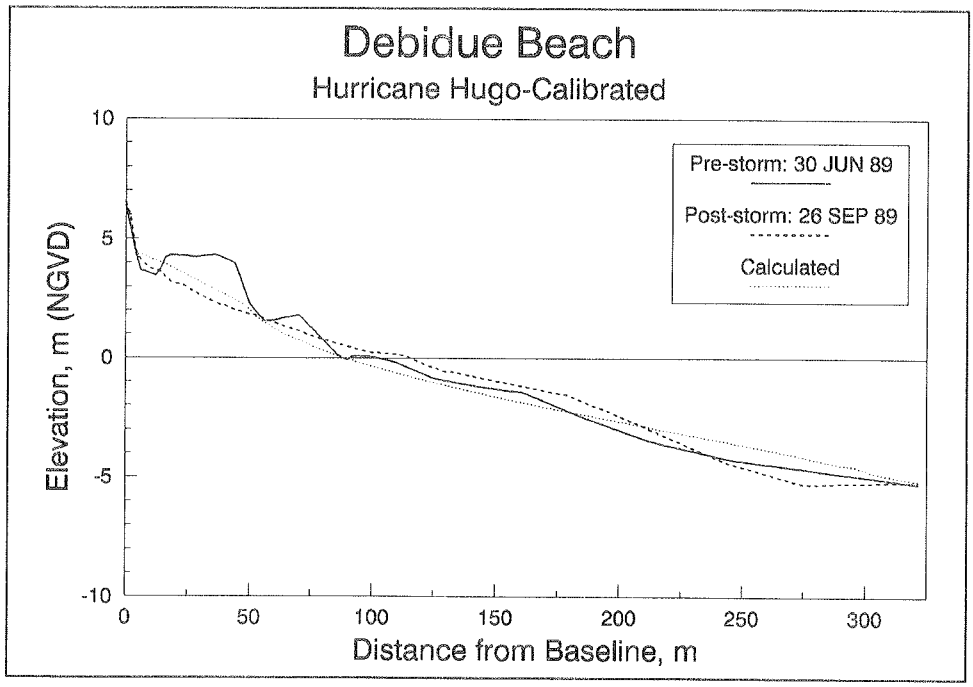

Figure 98. Result of calibrated simulation of Hurricane Hugo, Debidue Beach, SC

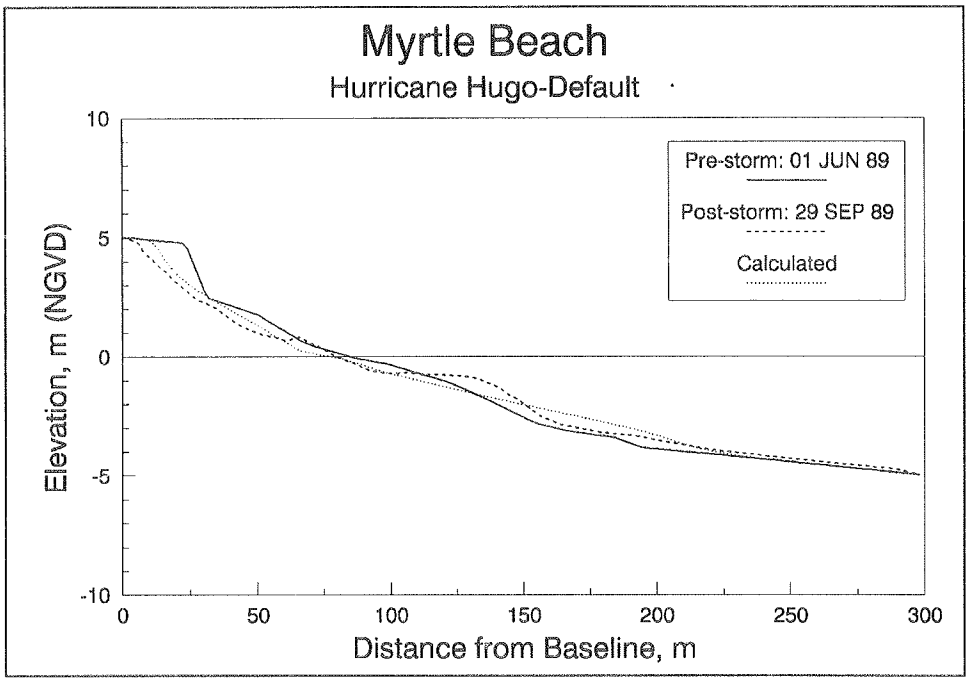

Figure 99. Result of default simulation of Hurricane Hugo, Myrtle Beach, SC

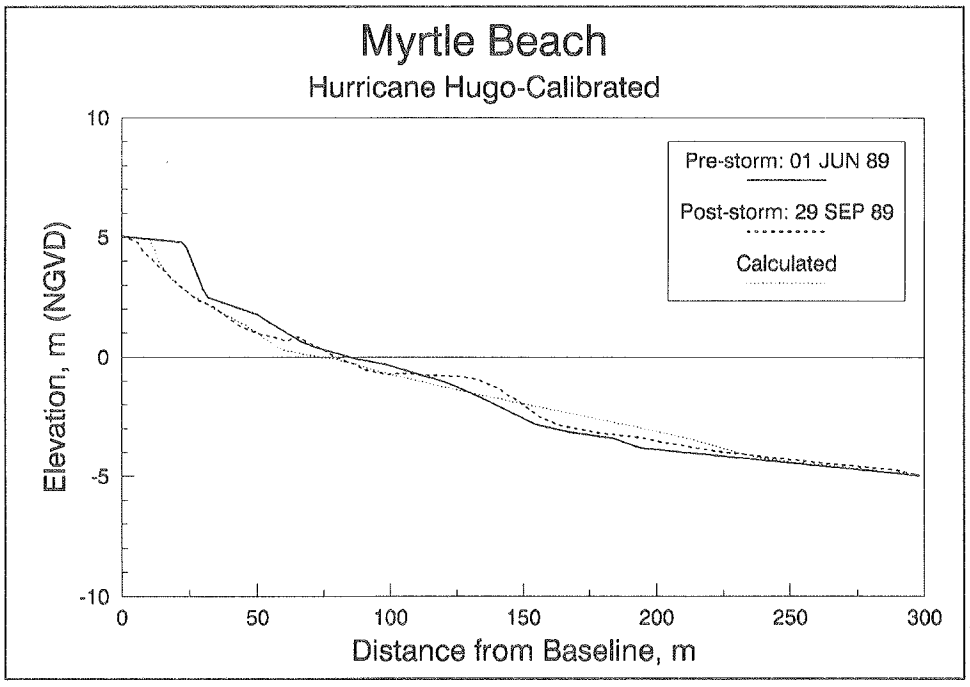

Figure 100. Result of calibrated simulation of Hurricane Hugo, Myrtle Beach, SC

Appendix C
Notation

B_1	Empirical coefficient
B_2	Empirical coefficient
B_3	Empirical coefficient
B_*	Empirical coefficient
C	Wave phase speed
C_D	Wind drag coefficient
C_g	Wave group speed
C_{go}	Wave group speed in deep water
C_{goff}	Wave group speed at x_{off}
C_{gsm}	Wave group speed at x_{sm}
C_o	Wave phase speed in deep water
d	Total water depth
d_{dc}	Depth of bore at dune crest
d_s	Water depth at x_s
d_{sm}	Smallest depth seaward of studied point
D	Wave energy dissipation per unit water volume
D_{eq}	Equilibrium wave energy dissipation per unit water volume
D_i	Wave energy dissipation per unit water volume of individual wave i
D_{50}	Median sediment grain size
DFS	Depth of the foreshore
f	Friction coefficient
f_s	Ratio of significant wave height to rms wave height for unbroken waves

f_{slope}	Ratio of local beach slope to representative foreshore slope
F_i	Energy flux of individual wave i
F_{rms}	Energy flux based on rms wave height
$F_{rms,o}$	Energy flux based on rms wave height at x_o
F_s	Energy flux based on significant wave height
F_{st}	Stable energy flux
F_{stab}	Stable energy flux based on rms wave height
F_{stabs}	Stable energy flux based on significant wave height
$F_{stab,o}$	Stable energy flux based on rms wave height at x_o
$F()$	Wave height distribution function
g	Acceleration of gravity
h	Still-water depth
H	Wave height
H_b	Breaking wave height
H_{bo}	Breaking wave height transformed to deep water
H_i	Wave height of individual wave i
H_m	rms wave height of broken waves
H_n	rms wave height of nonbroken waves
H_o	Deepwater wave height
H_{oc}	Critical deepwater wave height separating erosion and accretion
H_{off}	rms wave height at x_{off}
H_r	rms wave height of reformed waves
H_{rms}	rms wave height
H_{rmso}	Deepwater rms wave height
H_s	Significant wave height
H_{st}	Stable wave height
H_t	Threshold wave height greater than 2/3 of unbroken waves
H_u	rms wave height of unbroken waves
H_{us}	Significant wave height of unbroken waves
H_x	rms wave height ignoring wave breaking
H_{xsm}	rms wave height at x_{sm} ignoring wave breaking

i	Integer number
j	Integer number
K	Sand transport rate coefficient
L	Wavelength
L_o	Deepwater wavelength
m_*	Empirical coefficient
m	Number of broken waves
m_a	Number of broken waves which are accretionary
m_e	Number of broken waves which are erosional
m_{fs}	Constant foreshore slope
M	Transport direction coefficient
n	Number of nonbroken waves
n_s	Number of grid cells shoreward of studied point
N	Number of waves
N_p	Number of points across profile
$p()$	Probability density of wave height distribution
q	Cross-shore transport rate
q_b	Transport rate at wave breakpoint
q_{bi}	Transport rate at wave breakpoint for individual wave i
q_{bj}	Transport rate at wave breakpoint located at cell j
q_{dc}	Transport rate at dune crest
q_i	Transport rate for individual wave i
q_p	Transport rate at wave plunge point
q_s	Transport rate at shoreward boundary of surf zone
r	Number of reformed waves
Res	Residual parameter
RMS	rms difference between measured and calculated profiles
S_{xx}	Cross-shore component of radiation stress
T	Wave period
T_p	Wave period
u	Number of unbroken waves
u_b	Velocity of bore front

u_{bs}	Velocity of bore at x_s
u_{dc}	Velocity of bore at dune crest
u_s	Time-averaged velocity in the swash
V_r	Profile volume above still-water level traversed by runup
w	Sediment fall speed
W	Wind velocity
x	Cross-shore coordinate
x_b	Location of wave breakpoint
x_{bi}	Location of wave breakpoint for individual wave i
x_{bj}	Location of wave breakpoint at cell j
x_{dc}	Location of dune crest
x_o	Location where wave re-formation starts
x_{off}	Offshore location where wave breaking is negligible
x_p	Location of wave plunge point
x_r	Location of runup limit
x_{r*}	Location of runup limit on hypothetical constant foreshore slope
x_s	Location of shoreward boundary of surf zone
x_{sm}	Location of smallest depth seaward of studied point
x_{swl}	Location where still-water level intersects beach profile
y_c	Calculated final profile elevation
y_i	Initial profile elevation
y_m	Measured final profile elevation
Z_R	Limit of runup
α	Fraction of broken waves
α_{sm}	Fraction of broken waves at x_{sm}
α_o	Fraction of broken waves at x_o
β	Fraction of unbroken waves
$\tan\beta_l$	Local beach slope
$\tan\beta_o$	Representative foreshore slope
$\tan\beta_s$	Beach slope at x_s
γ_b	Ratio between wave height and water depth at breaking

Γ	Stable wave height coefficient
δ_a	Fraction of broken waves which are accretionary
δ_e	Fraction of broken waves which are erosional
$\Delta\alpha_j$	Increase in fraction of broken waves at cell j
Δh	Elevation difference between center of bore at x_s and studied point on foreshore
ϵ	Slope-related transport coefficient
η	Wave setup and water level displacement
θ	Wave angle
θ_{off}	Wave angle at x_{off}
θ_{sm}	Wave angle at x_{sm}
κ	Wave energy decay coefficient
λ	Wave re-formation coefficient
λ_i	Transport rate decay coefficient for individual wave i
λ_j	Transport rate decay coefficient for wave with breakpoint at cell j
λ_1	Transport rate decay coefficient seaward of wave breaking
λ_2	Transport rate decay coefficient in breaker transition zone
μ	Fraction of re-formed waves
μ_o	Fraction of re-formed waves at x_o
ξ	Transport direction function for random waves
ρ	Density of water
ρ_a	Density of air
τ_b	Time-averaged bottom shear stress
φ	Wind direction

REPORT DOCUMENTATION PAGE

Form Approved
OMB No. 0704-0188

1. AGENCY USE ONLY *(Leave blank)*	2. REPORT DATE	3. REPORT TYPE AND DATES COVERED
	April 1996	Report 4 of a series

4. TITLE AND SUBTITLE
SBEACH: Numerical Model for Simulating Storm-Induced Beach Change; Report 4, Cross-Shore Transport Under Random Waves and Model Validation with SUPERTANK and Field Data

5. FUNDING NUMBERS
Work Unit 32530

6. AUTHOR(S)
Randall A. Wise, S. Jarrell Smith, Magnus Larson

7. PERFORMING ORGANIZATION NAME(S) AND ADDRESS(ES)
U.S. Army Engineer Waterways Experiment Station
3909 Halls Ferry Road, Vicksburg, MS 39180-6199;
Depart of Water Resources Engineering, Lund Institute of Technology
University of Lund, Box 118, Lund, Sweden S-221 00

8. PERFORMING ORGANIZATION REPORT NUMBER
Technical Report CERC-89-9

9. SPONSORING/MONITORING AGENCY NAME(S) AND ADDRESS(ES)
U.S. Army Corps of Engineers
Washington, DC 20314-1000

10. SPONSORING/MONITORING AGENCY REPORT NUMBER

11. SUPPLEMENTARY NOTES
Available from National Technical Information Service, 5285 Port Royal Road, Springfield, VA 22161.

12a. DISTRIBUTION/AVAILABILITY STATEMENT
Approved for public release; distribution is unlimited.

12b. DISTRIBUTION CODE

13. ABSTRACT ***(Maximum 200 words)***

Beach erode and accrete in response to varying waves, water levels, and currents in the nearshore zone. During storms beach and dune erosion can occur quickly, causing shoreline recession and damage to property and upland resources. Hence, protection of upland infrastructure is a primary concern of coastal engineering. Beach nourishment is a preferred method of providing such protection, and many beach-fill projects have been designed and constructed in recent years. Design of such fills requires an understanding of and the capability to predict sediment transport processes that control beach response to storms. Numerical modeling of beach evolution can be applied to assist in project design. Numerical models provide a framework for predicting project response, objectively evaluating design alternatives and analyzing data to develop an understanding of coastal processes. The Storm-induced BEAch CHange (SBEACH) numerical model is an engineering tool for simulating beach profile evolution in response to storms. This report, the fourth in a series describing the development of SBEACH, describes recent model enhancements developed to improve calculation of sediment transport under random waves. A comprehensive evaluation of model capabilities in predicting beach and dune erosion is presented using high-quality laboratory and field data of beach profile change.

14. SUBJECT TERMS

Beach erosion	Dune overwash	Numerical models
Cross-shore sand transport	Erosion	Random waves
Dune erosion	Model validation	Storm erosion

15. NUMBER OF PAGES
266

16. PRICE CODE

17. SECURITY CLASSIFICATION OF REPORT	18. SECURITY CLASSIFICATION OF THIS PAGE	19. SECURITY CLASSIFICATION OF ABSTRACT	20. LIMITATION OF ABSTRACT
UNCLASSIFIED	UNCLASSIFIED		